

# **Synthetic Biotechnology to Engineer Myxopyronin Production**

Dissertation  
zur Erlangung des Grades  
des Doktors der Naturwissenschaften  
der Naturwissenschaftlich-Technischen Fakultät III  
Chemie, Pharmazie, Bio- und Werkstoffwissenschaften  
der Universität des Saarlandes

von

**Hilda Sucipto**

Saarbrücken

2015

Tag des Kolloquiums: 25. November 2015

Dekan: Prof. Dr.–Ing. Dirk Bähre

Berichterstatter: Prof. Dr. Rolf Müller  
Prof. Dr. Rolf W. Hartmann

Vorsitz: Prof. Dr. Andriy Luzhetskyy

Akad. Mitarbeiter: Dr. Jens Neunzig

---

Die vorliegende Arbeit wurde von Oktober 2011 bis Juni 2015 unter Anleitung von Herrn Prof. Dr. Rolf Müller am Helmholtz-Institut für Pharmazeutische Forschung Saarland (HIPS) angefertigt.

*May I always be humble and always learn*

*May all beings be happy*

---

## Acknowledgment

First of all, I would like to thank Prof. Rolf Müller for his supervision during my PhD in his group. I am grateful for the opportunity that he offered after my short summer internship in 2010. It has been a pleasure to work in such a great research environment in Helmholtz Center for Infection Research (HZI) especially at the Department Microbial Natural Products.

I would like to thank Prof. Rolf W. Hartmann for being my second supervisor and for reviewing my dissertation. I am also thankful to have Jan Henning Sahner (DDOP) as my collaborator and have a successful team works.

I owe my deepest gratitude to my tutor Dr. Silke Wenzel who taught me and shared with me a lot of skills about molecular biology. Her outstanding skills and interesting ideas/design always inspire me for the experiments and research. Thank you for many advices and guidance for my career and personal developments.

I would like to thank the all of the former and current group members especially Katrin Jungmann, Lena Etzbach, and Ullrich Scheid for being great companions during these four years in the group. Thank you also to Dr. Thomas Hoffmann, Michael Hoffmann, and Eva Luxenberger for their helpful analytical expertise. Thank you for a great collaboration with Dr. Jesko Koehnke. Thank you to Dr. Alberto Plaza and Dr. Kirsten Harmrolfs for the NMR discussions. I also would like to thank Dr. Nestor Zaburannyi for many things during the project.

Thank you to Dr. Suvd Nadmid, Sara Andes, and Dr. Louise Kjaerulff for sharing many days and things with me. Also thank you to my friends Charles and Elline for many enjoyable years.

Lastly, I do not have many words that will fully express my gratitude to my parents, sister, and brother with their families for their continuous support during my stay abroad for the last eight years.

Hilda Sucipto

Saarbrücken, 3<sup>rd</sup> August 2015

## Abstract

Myxobacteria produce a broad range of anti-infectives that contain novel scaffolds and exhibit promising bioactivities. These features make myxobacterial secondary metabolites an interesting target for scientific research and clinical application. The present thesis deals with myxopyronins from *Myxococcus fulvus* Mx f50 which target a novel binding site at the bacterial RNA polymerase “switch region”. Due to their insufficient physicochemical and pharmacokinetic properties for direct clinical drug usage, this work aims to exploit and optimize this compound family through biotechnological approaches.

Genetic tools for the myxopyronin producer were established to facilitate the identification and elucidation of the myxopyronin biosynthetic gene cluster through directed mutagenesis. Detailed biochemical and structural characterization of the key enzyme responsible for  $\alpha$ -pyrone ring formation provided valuable insights into the reaction mechanism and structural requirements of modified polyketide chain substrates. Furthermore, mutasynthesis approaches at different stages of the biosynthesis allowed the generation of novel myxopyronin analogues. In order to improve productivity, a heterologous expression system for myxopyronin production was achieved in *Myxococcus xanthus* DK1622 at promising yields. The obtained results provide various platforms for further pathway engineering to generate myxopyronin analogues with improved pharmaceutical properties.

---

## Zusammenfassung

Myxobakterien produzieren ein breites Spektrum an Anti-Infektiva mit neuen Grundgerüsten und vielversprechenden Bioaktivitäten. Diese Eigenschaften machen myxobakterielle Sekundärmetabolite zu interessanten Zielstrukturen für die Forschung und klinische Anwendungen. Die vorliegende Arbeit beschäftigt sich mit Myxopyroninen aus *Myxococcus fulvus* Mx f50, die an eine neue Stelle, die „switch region“, der RNA-Polymerase binden. Da ihre physikochemischen und pharmakokinetischen Eigenschaften keine direkte klinische Anwendung erlauben, zielt diese Arbeit darauf ab, über biotechnologische Ansätze die Naturstoff-Familie zu optimieren und weiter auszunutzen.

Es wurden genetische Verfahren für den Myxopyronin-Produzenten etabliert, um den Myxopyronin-Biosynthesegencluster mittels gerichteter Mutagenese zu identifizieren und charakterisieren. Detaillierte Studien zur Biochemie und Struktur des an der  $\alpha$ -Pyronring-Biosynthese beteiligten Schlüsselenzyms lieferten wertvolle Einblicke in den Reaktionsmechanismus und die Strukturanforderungen modifizierter Polyketidketten-Substrate. Zudem gelang es über Mutasynthese-Experimente auf verschiedenen Stadien der Biosynthese neue Myxopyronin-Analoga zu generieren. Zur Produktionsverbesserung wurde ein heterologes Expressionssystem in *Myxococcus xanthus* DK1622 mit vielversprechenden Ausbeuten etabliert. Die erzielten Ergebnisse bieten verschiedene Plattformen zur Manipulation der Biosynthese, um Myxopyronin-Analoga mit verbesserten pharmazeutischen Eigenschaften herzustellen.

## Vorveröffentlichungen der Dissertation

Teile dieser Arbeit wurden vorab mit Genehmigung der Naturwissenschaftlich-Technischen Fakultät III, vertreten durch den Mentor der Arbeit, in folgenden Beiträgen veröffentlicht oder sind derzeit in Vorbereitung zur Veröffentlichung:

### Publications

**H. Sucipto\***, J. H. Sahner\*, E. Prusov, S. C. Wenzel, R. W. Hartmann, J. Koehnke, and R. Müller, *Chem. Sci.*, **2015**, 6, 5076-5085.

J. H. Sahner\*, **H. Sucipto\***, S. C. Wenzel, M. Groh, R. W. Hartmann and R. Müller, *ChemBioChem*, **2015**, 16, 946–953.

**H. Sucipto**, S. C. Wenzel and R. Müller, *ChemBioChem*, **2013**, 14, 1581–1589.

(\*:Authors contributed equally to the work)

### Conference Contributions (Poster and Oral Presentations)

**H. Sucipto**, S. C. Wenzel and R. Müller. Characterization and engineering of myxopyronin biosynthesis. **Oral Presentation** VAAM International Workshop 2014 on the "Biology of Natural Product-Producing Microorganisms", 2014: Dresden, Germany.

**H. Sucipto**, S. C. Wenzel and R. Müller. Characterization and engineering of myxopyronin biosynthesis. **Poster Presentation**, 1<sup>st</sup> European Conference on Natural Products, 2013: Frankfurt, Germany.

**H. Sucipto**, J. H. Sahner, S. C. Wenzel, M. Groh, R. W. Hartmann and R. Müller. Characterization and engineering of myxopyronin biosynthesis. **Poster Presentation**, 3<sup>rd</sup> International HIPS Symposium, 2013: Saarbrücken, Germany.

**H. Sucipto**, S. C. Wenzel and R. Müller. Characterization and engineering of myxopyronin biosynthesis. **Oral presentation**, Summer Symposium of Interdisciplinary Graduate School, 2013: Saarbrücken, Germany.



## Table of Contents

<b>Acknowledgment</b>	<b>V</b>
<b>Abstract</b>	<b>VI</b>
<b>Zusammenfassung</b>	<b>VII</b>
<b>Vorveröffentlichungen der Dissertation</b>	<b>VIII</b>
<b>1 Introduction</b>	<b>1</b>
1.1 Natural Products the Source of Novel Anti-Infectives	1
1.2 The Potential of Myxobacteria as Producers of Anti-Infectives	3
1.3 Microbial Natural Product Assembly Lines	7
1.4 Engineering Myxobacterial Natural Product Biosynthesis	12
1.5 Outline of the Present Work	18
1.6 References	21
<b>2 Molecular Basis of Myxopyronin Biosynthesis</b>	<b>30</b>
2.1 Abstract	30
2.2 Introduction	30
2.3 Results and Discussion	32
2.3.1 Identification of the myxopyronin biosynthetic gene cluster	32
2.3.2 Comparison of the myxopyronin biosynthetic pathway with that of corallopyronin	33
2.3.3 MxnL and MxnM are not essential for myxopyronin biosynthesis	38
2.3.4 Unexpected myxopyronin A derivative from $\beta$ -branching cassette deletion	40
2.3.5 <i>O</i> -methylation by MxnH is essential for myxopyronin biosynthesis	42
2.4 Conclusion	43
2.5 Experimental Section	43
2.6 Supporting Information	47
2.7 References	64
2.7.1 References for Main Text	64
2.7.2 References for Supporting Information	65
<b>3 <i>In Vitro</i> Reconstitution of <math>\alpha</math>-Pyrone Ring Formation in Myxopyronin Biosynthesis</b>	<b>68</b>
3.1 Abstract	68
3.2 Introduction	68

---

3.3	Results and Discussion	71
3.3.1	MxnB is Responsible for $\alpha$ -Pyrone Ring Formation in Myxopyronins	71
3.3.2	Overall Structure of MxnB	74
3.3.3	Initial Biochemical Characterization of MxnB	77
3.3.4	Biochemical Insights into $\alpha$ -Pyrone Ring Formation	79
3.3.5	Mechanism Proposal	81
3.4	Conclusion	84
3.5	Experimental Section	84
3.6	Supporting Information	91
3.7	Supplementary Results	92
3.8	References	109
3.8.1	References for Main Text	109
3.8.2	References for Supporting Information	110
<b>4</b>	<b>Mutasynthesis Studies on Myxopyronin</b>	<b>114</b>
4.1	Abstract	114
4.2	Introduction	114
4.3	Results and Discussion	117
4.4	Conclusion	125
4.5	Experimental Section	126
4.6	Supporting Information	130
4.7	References	134
4.7.1	References for Main Text	134
4.7.2	References for Supporting Information	135
<b>5</b>	<b>Heterologous Production of Myxopyronin</b>	<b>138</b>
5.1	Introduction	138
5.2	Result and Discussion	139
5.2.1	Reconstitution of the complete myxopyronin gene cluster	139
5.2.2	Heterologous Expression of the Myxopyronin Gene Cluster in <i>M. xanthus</i>	144
5.2.3	Genetic Modification of the Myxopyronin Heterologous Expression System	147
5.3	Conclusions and Perspectives	148
5.4	Experimental Section	150
5.5	Supporting Information	155

---

5.6	References	160
<b>6</b>	<b>Discussion and Perspectives</b>	<b>165</b>
6.1	General Scope of the Present Work	165
6.2	Myxopyronin biosynthesis in <i>Myxococcus fulvus</i> Mx f50	165
6.2.1	An unexpected myxopyronin A derivative from $\beta$ -branching cassette deletion	167
6.2.2	The importance of MxnH for <i>O</i> -methylation in myxopyronin biosynthesis	169
6.3	$\alpha$ -Pyrone ring formation during polyketide biosynthesis – in depth studies on myxopyronin	172
6.4	Expanding the chemical space of $\alpha$ -pyrone antibiotics – Mutasynthesis approach towards novel myxopyronin analogues	176
6.5	Heterologous expression of complex natural product biosynthetic pathways – myxopyronin production in the myxobacterial model strain <i>M. xanthus</i>	181
6.6	Concluding Remarks and Future Directions	186
6.7	References	190



# 1 Introduction

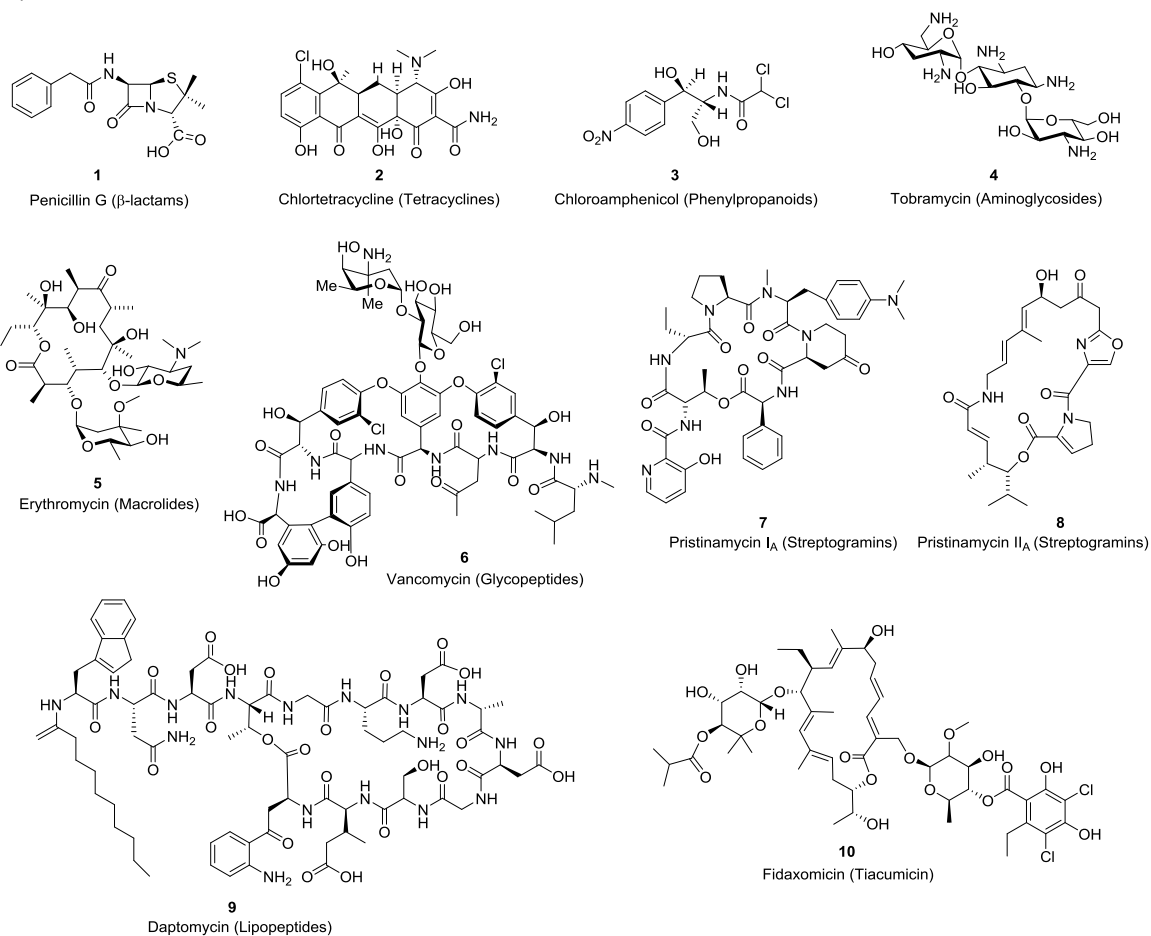
## 1.1 Natural Products the Source of Novel Anti-Infectives

Infectious disease is one of the main leading cause of deaths worldwide.<sup>1</sup> The widespread use of anti-infective drugs over several decades has improved human life expectancy. Unfortunately, antibiotics are also vastly misused in both humans and food-producing animals in a fashion that favours the selection and spread of resistant bacteria.<sup>2-4</sup> Antimicrobial resistance has made drugs, which were previously effective to treat infections caused by bacteria, fungi, viruses and parasites, are no longer competent to cure them. This rapid development and spreading of antimicrobial resistance has then made human beings vulnerable to re-occurring and new infectious diseases.<sup>5</sup> Thus, one approach to address the resistance to these anti-infectives is to find new sources for drug discovery.

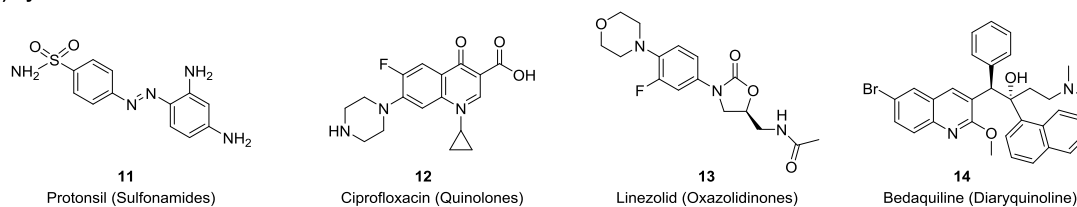
Throughout history, Nature has been used as a source of medicines to treat a broad spectrum of diseases. Progress in scientific knowledge led to the discovery of biologically active compounds, commonly referred to as natural products (NPs). NPs produced by bacteria, fungi, and plants have been a prolific source for drug discovery and development.<sup>6</sup> Not only have NPs shown impressive structural diversity and complexity hardly possible to make by organic synthesis, but they also display complex mechanisms of action that are very difficult to achieve by human rational design.<sup>7</sup>

The discovery of penicillins from fungi started the way for the 'golden era' of antibiotic discovery from microbes (1945-1960) during which most of the chemical classes of antibiotics now in clinical use were first characterized (Fig. 1). Nevertheless, there was a significant gap between the introduction of quinolones in 1962 and the next new structural classes of antibiotics such as the oxazolidinones (linezolid, 2000) and the lipopeptides (daptomycin, 2003). Resistant bacteria against linezolid and daptomycin are readily developed in only a few years after their first clinical use.<sup>8,9</sup> Indeed, many years later, other new classes of antibiotics, fidaxomicin was approved in 2011 and synthetic bedaquiline in 2012 (Fig. 1).<sup>10</sup> Inevitably, the introduction of a new drug for clinical use is always followed by survival of the small fraction of a bacterial population that have acquired a resistance mechanism. Furthermore, all these new antibiotic classes are limited to the treatment of infections by Gram-positive bacteria while anti-infectives against Gram-negatives are urgently required. However, despite the need of novel, effective, and safe anti-infectives, the rate of discovery and development has lagged far behind the rate of resistance development. No other resource has returned as much lead generation value to drug discovery as have secondary metabolites derived from microbes and plants.<sup>11</sup>

## A) Natural Products



## B) Synthetic Products



## C) Timeline of Antibiotic Drug Discovery

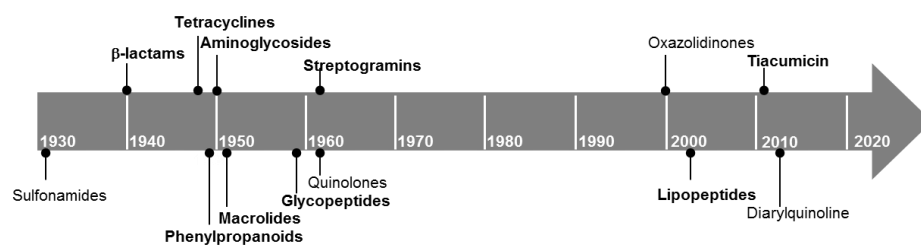


**Figure 1** Structures and discovery timeline of antibiotics in clinical use. A) Naturally and B) Synthetically derived antibiotics, in bracket is the compound class; C) timeline of antibiotics drug discovery, in bold are microbe-derived antibiotics.

Therefore, the urgent need to find new drugs has become a major driving force for the scientific community to keep exploring natural products, as the most promising source of the future antibiotics, to overcome the above mentioned situations regarding antibiotics.

## 1.2 The Potential of Myxobacteria as Producers of Anti-Infectives

Since the golden era of antibiotics, the majority of anti-infective compound classes in use today have been isolated from a limited number of taxonomic groups, mainly from soil actinobacteria and fungi. However, in the last decades, Gram-negative myxobacteria have been featured as prominent producers of structurally diverse microbial secondary metabolites.<sup>12–14</sup> Secondary metabolites, including antibiotics, are regarded as natural products produced by living organisms and often used against competitors or predators.<sup>15</sup>

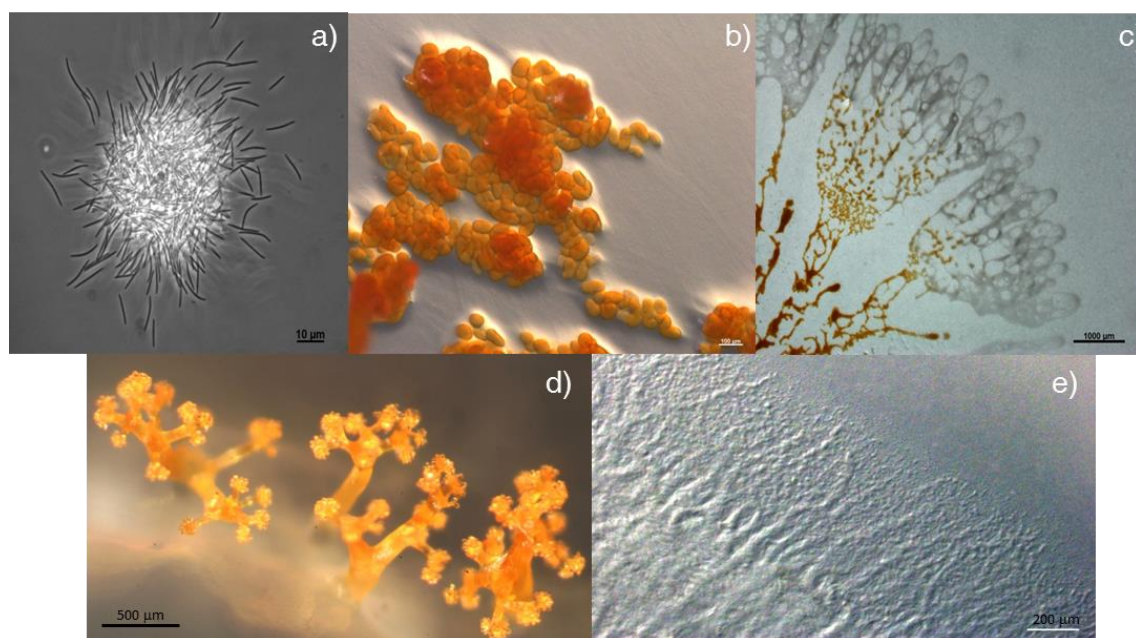


**Figure 2.** Different stages of the myxobacterial life cycle. (a) vegetative cells of *Cystobacter* sp.; (b) fruiting bodies of *Cystobacter* sp.; (c) fruiting bodies and swarming colony of *Sorangium cellulosum* Soce 1875 on agar; (d) fruiting body of *Chondromyces crocatus*; (e) swarm colony edge of *Myxococcus xanthus* sp on agar showing ripples and flare-like pattern. (a), (b), pictured in phase-contrast and (c), (d), and (e) in stereophotomicrograph (pictures: Ronald O. Garcia)

Myxobacteria belong to the group of  $\delta$ -proteobacteria and are distinguished from other bacteria by unique features.<sup>16–18</sup> They move by gliding or creeping, and under starvation conditions they produce fruiting bodies in which the vegetative cells convert into dormant, resistant myxospores (Fig. 2). Myxobacteria have a unique ability not only to degrade an array of biological macromolecules as food source, but also they possess predatory behavior against bacteria and fungi.<sup>19</sup>

In the last three decades, myxobacteria have been established as potent producers of novel compounds yielding more than 100 natural products and approximately 600 additional structural derivatives.<sup>14,20,21</sup> In particular, many of these compounds exhibit rarely observed or wholly novel mode of actions, which makes myxobacteria a promising source of anti-infective drugs.<sup>22,23</sup> Traditionally, antibiotics have been classified for their ability to kill bacteria (bactericidal activity) or inhibit growth (bacteriostatic activity). They achieve this by interfering with the essential bacterial functions such as cell wall synthesis, DNA replication, RNA transcription and protein synthesis that are indispensable for the growth.<sup>24</sup> Even though it is obvious that antibiotics directed at cellular viability have been highly effective, these modes of action inflict selective pressure that stimulates the growth of antibiotic-resistant strains. Therefore, in addition to the compounds that act by targeting *in vitro* cell growth, it is important to develop anti-infectives that have novel mode of actions. Several isolated myxobacterial compounds present novel structural scaffolds or unique modes of action,<sup>22</sup> such as the cystobactamids **15** (DNA topoisomerase II inhibitor),<sup>25</sup> aetheramides **16** (HIV inhibitor),<sup>26</sup> ambruticin **17** (anti-fungal),<sup>27</sup> and argyirin **18** (inhibitor of elongation factor G),<sup>28,29</sup> (Fig.3).

Studies on the  $\alpha$ -pyrone antibiotics myxopyronin A **19**<sup>30</sup> or coralopyronin A **20**,<sup>31</sup> and the macrolactone ripostatin **21**,<sup>32</sup> revealed their novel target site at the RNA polymerase (RNAP).<sup>33,34</sup> RNAP catalyzes the DNA-dependent synthesis of RNA. This enzyme is essential for bacterial growth and survival. RNAP subunit sequences are highly conserved among Gram-negative and Gram-positive bacteria permitting broad-spectrum antibacterial therapy and exhibits major structural differences from eukaryotic RNAP allowing therapeutic selectivity.<sup>35,36</sup>

Selective bacterial RNAP inhibition is the basis for antibiotic treatment of tuberculosis (TB), the most widespread and persistent bacterial infection.<sup>37</sup> In 2013, there were approximately 9 million new TB cases and 1.5 million TB deaths reported.<sup>38</sup> The rifamycins (rifampicin **22**, rifapentine, and rifabutin) have been in use as the first-line anti-TB therapy in combination with other agents (e.g. isoniazid, pyrazinamide) since the 1960s.<sup>38,39</sup> However, their efficiency and versatility is becoming limited by the rapid emergence of multi-resistant variants of *Mycobacterium tuberculosis* (MDR-TB and XDR-TB). This high-level resistance to rifampicin can be caused by a single mutation in *rpoB*, the gene that encodes for the RNAP  $\beta$ -subunit.<sup>40</sup> These mutations change amino acids in or surrounding the Rif-binding pocket, which cause a drastic decrease in the antibacterial activity.<sup>41</sup> Therefore, antibiotics that have the same ability to inhibit bacterial RNAP as rifamycins do, but inhibit the bacterial RNAP through binding sites that are distinct from the rifamycins binding site,



are urgently needed not only for anti-TB development but also for developing broad spectrum anti-infectives.

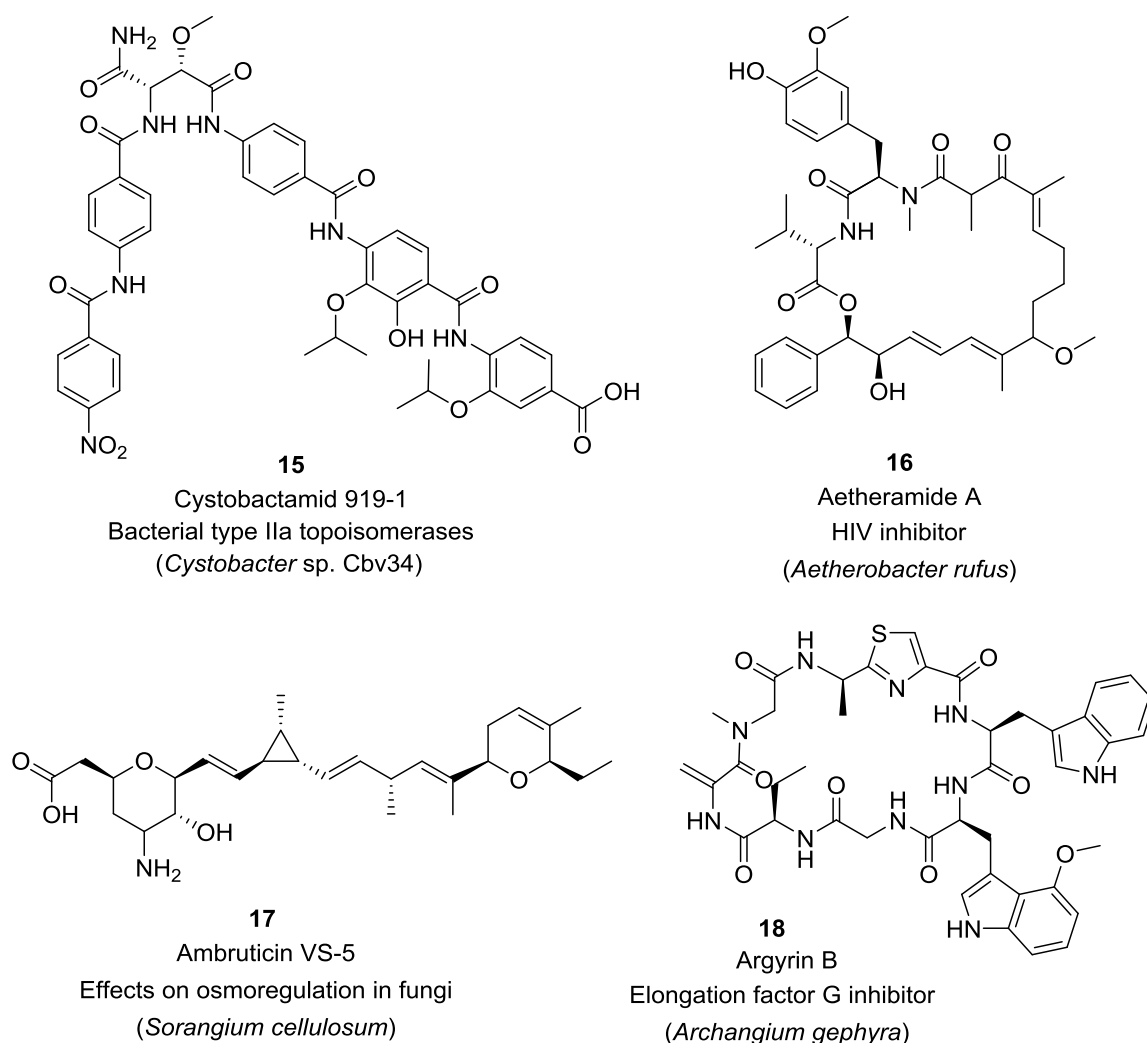


**Figure 3.** Myxobacterial anti-infectives. The structure, name, mode of action or target, and producer organism are given.

In 2008, the structure determination of *Thermus thermophilus* RNA polymerase (RNAP) holoenzyme in complex with the myxobacterial  $\alpha$ -pyrones myxopyronin A **19**<sup>30</sup> and coralopyronin A **20**,<sup>31</sup> or the macrolactone ripostatin **21**,<sup>32</sup> have revealed a novel target site in RNAP, called the switch region (Fig. 4).<sup>33</sup> The switch region is a hinge that mediates opening and closing of the RNAP active center cleft. The binding of those three compounds to the RNAP switch region will then prevent interaction of RNAP with promoter DNA, probably by preventing opening of the clamp to permit entry of promoter DNA during transcription initiation.<sup>33</sup> The amino acid residues involved in the interaction of those three compounds in

the switch region of RNAP are remote from the binding site of rifampicin, which explains the absence of cross-resistance between the antibiotics (Fig. 4).

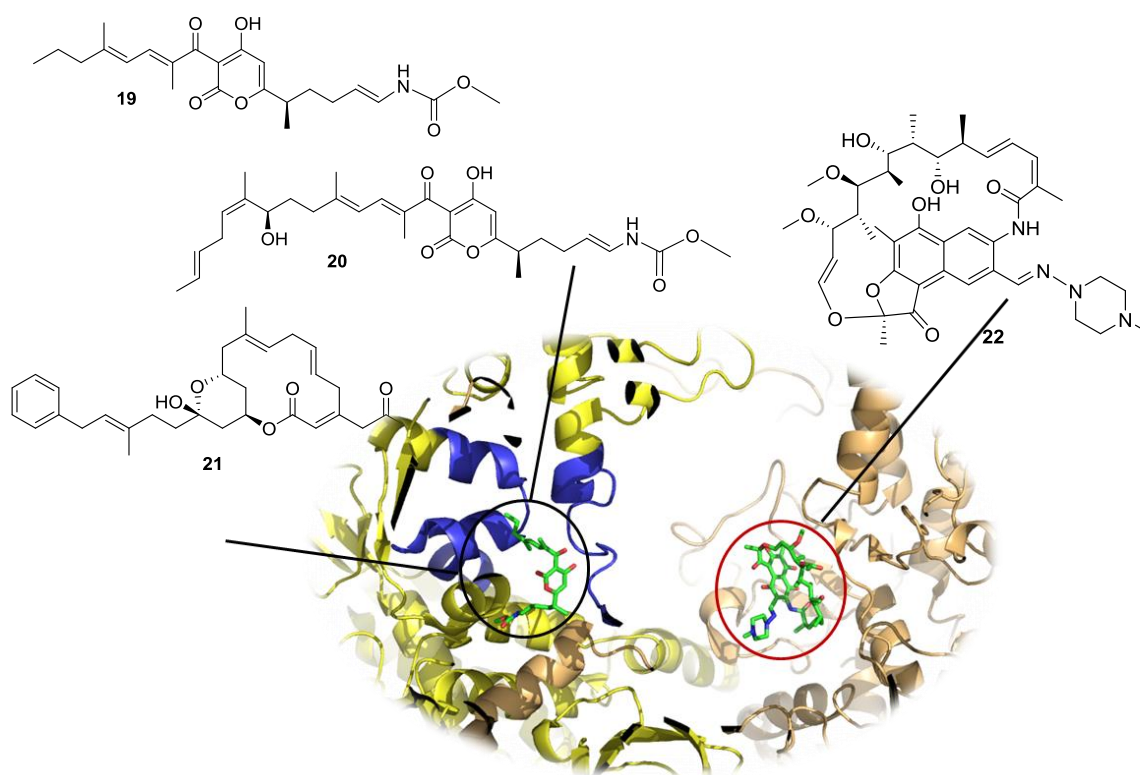


**Figure 4.** Structural basis of RNA transcription inhibition by myxopyronin A **19**, coralloyronin A **20**, and ripostatin A **21** at the switch region of RNAP (blue ribbon, black circle) from *Thermus thermophilus* (yellow ribbon, PDB: 3DXJ) and binding site of rifampicin **22** (red circle) to RNAP from *Escherichia coli* (golden ribbon, PDB: 4KMU). Superposition is performed using Pymol V 1.7.4 (crystal figure: Jesko Koehnke).

Further structural studies using dMyx (a desmethyl derivative of myxopyronin B) complexed with *T. thermophilus* RNAP holoenzyme also showed that dMyx binds to a pocket deep inside the RNAP clamp head domain, which interacts with the DNA template in the transcription bubble.<sup>42</sup> Although myxopyronin and coralloyronin have similar structures, they show differences in their inhibitory mechanisms. Myxopyronin is not able to completely block the RNA formation, which relates to the longer alkyl chain of coralloyronin.<sup>31</sup> Nonetheless, myxopyronin shows better minimal inhibitory concentration (MIC) values against several pathogens such as *M. tuberculosis*, *Enterococcus faecalis*, and *Staphylococcus aureus*.<sup>34</sup> Altogether, these properties show that these three myxobacterial compounds are promising candidates for development of broad-spectrum antibacterial therapeutics agents and indicate that myxobacteria are indeed a rich source for novel anti-infectives discovery.

In parallel with continuous isolation and characterization of myxobacterial compounds, the information on the biosynthetic potential of myxobacteria has also been

increasingly collected from genome sequence projects. This information regarding the genetic basis of natural product formation in myxobacteria revealed that their genetic potential for the production of novel anti-infectives is far from exhausted.<sup>20</sup> Thus, there is definitely much more biosynthetic potential to be explored, and the prospects for imminent natural product research with myxobacteria are very promising.

### 1.3 Microbial Natural Product Assembly Lines

Microorganisms utilize complex biosynthetic machineries to produce structurally diverse natural products. Two major classes of natural products are constituted by multimodular megasynthase systems called polyketide synthases (PKS) or non-ribosomal peptide synthetases (NRPS), or hybrids of both systems.<sup>43,44</sup> Understanding the mechanism involved in the biosynthesis of PKS, NRPS or hybrid systems is required for optimizing product yields and for manipulation of the biosynthetic pathways to achieve structural modification of secondary metabolites.

Although PKS and NRPS employ different building blocks, both systems share similarities in their modular architecture of various catalytic domains and assembly-like mechanisms. Each module usually incorporates one building block into the growing ketide or peptide chain and passes the elongated product on to a downstream module, with that the growing chain is shuttled from the beginning of the enzyme-complex to the end. The process is linear and resembles an assembly line which led to the term called “molecular assembly line”.<sup>45</sup> The order of catalytic modules in the biosynthetic complex is closely reflected in the chromosomal order of the underlying genes – a property known as the “collinearity rule” which then permits the prediction of the product based on the order of catalytic modules and vice versa.<sup>46,47</sup> One module consists of several domains and every domain is responsible for a single reaction step.<sup>48</sup> Essentially, a module catalyzes a full round of monomer selection, attachment, and coupling (C-C bond formation in PKS and C-N bond formation in NRPS).<sup>44</sup> In PKS assembly lines, the monomers are acyl-coenzyme A (acyl-CoA) precursors while the NRPs are assembled by proteinogenic amino acids, nonproteinogenic amino acids, and aryl acids.<sup>44</sup> The compatible biosynthetic logic of PKS and NRPS allows growing polyketide chains to be transferred across a PKS-NRPS interface to switch from incorporating acyl-CoA monomers to amino acid monomers, and vice versa.<sup>44</sup>

The biosynthetic mechanism of polyketide biosynthesis is similar to fatty acid biosynthesis.<sup>43,49</sup> In principal, they are constructed by repetitive decarboxylative Claisen thioester condensation which involves three essential domains: an acyltransferase (AT) domain for extender unit selection and loading, a carrier protein (CP) domain to covalently

bind the extender unit, and a  $\beta$ -ketoacylsynthase (KS) domain, which performs a decarboxylative Claisen thioester condensation of the extender unit (generally malonyl-CoA or methylmalonyl-CoA) with the acyl thioester intermediate from the upstream module (Fig. 5).

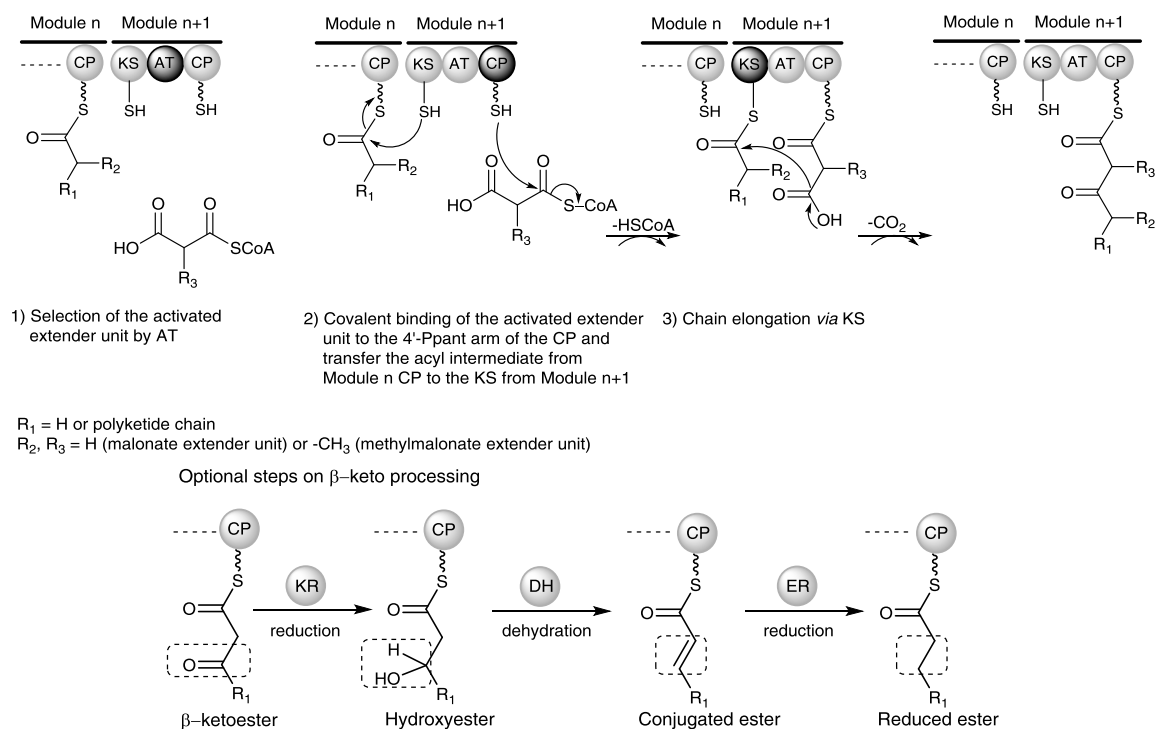


**Figure 5.** Polyketide chain extension and optional steps on  $\beta$ -keto processing. The elimination of water can result either in *E* or *Z* configuration at the conjugated ester.

The inactive CP protein (apo-CP) requires a posttranslational activation to allow covalent binding of precursors or intermediates. In this process, the 4'-phosphopantetheine (PPant) prosthetic group of CoA is transferred to the serine active site residue of the CP by a phosphopantetheinyl transferase (PPTase) resulting in the catalytically active CP form (holo-CP).<sup>50</sup> A free thiol group at the end of this PPant-arm serves as an anchor for the growing chain and is often described as a “swinging arm” in the CP.<sup>51</sup> This “swinging arm” is able to channel the intermediates through all the various catalytic sites on the PKS/NRPS/Fatty acid synthase (FAS). At the terminus of the assembly lines, the module usually contains a thioesterase (TE) domain, which catalyzes the release of the growing chain from the enzyme either as linear polyketide by hydrolysis or as cyclized lactone ring.<sup>52</sup>

The significant difference between PKS and FAS is that in fatty acid biosynthesis, after every chain elongation using malonyl-CoA as extender unit, the resulting  $\beta$ -keto group is always fully reduced<sup>53</sup> in a stepwise process catalyzed by three additional domain

activities: A ketoreductase (KR) domain reduce the  $\beta$ -keto function to a hydroxyl group, a dehydratase (DH) domain performs elimination of water (dehydration) to form a conjugated ester, which is then reduced by an enoyl reductase (ER) domain to generate a fully saturated acyl chain intermediate. In PKS, not only there is a broader range of building blocks than acetyl-CoA or malonyl-CoA, but also the full reductive cycle by KR, DH, and ER is optional (Fig. 5). These three steps can be skipped (partially or altogether) before the next round of elongation, thus allowing the synthesis of a wide variety of complex polyketides.

A typical PKS elongation domain comprises minimally AT, CP, and KS domains. Similarly, three domains are necessary as the basic machinery of an NRPS elongation module: an adenylation (A) domain responsible for amino acid recognition and activation, a CP or thiolation (T) domain to which the activated amino acid is covalently attached as thioester, and a condensation (C) domain that catalyzes the peptide bond formation. In summary, the core domains of PKS (KS, AT, CP) have similar counterparts in NRPS (C, A, CP) which catalyze three main steps as explained above.<sup>44</sup> The specificity of A domains towards the amino acids play an important role in the peptide sequence of the final natural product and the biological activity as well. The crystallization and structural analysis of a prototype A domain with its amino acid substrate and ATP revealed the structural basis of substrate recognition and activation<sup>54</sup> In combination with primary sequence alignment analyses to other A domains, 8-10 amino acids within the substrate binding pocket could be identified. These residues can be defined as specificity-conferring code for substrate prediction of NRPSs.<sup>55</sup> The ability to produce a wide range of compounds with high structural diversity is further increased by the presence of additional optional catalytic and modifying enzymes catalyzing reactions such as epimerization, hydroxylation, methylation, isomerization, and halogenation.<sup>56</sup>

The structural and catalytic similarities between PKSs and NRPSs allow a conception that these modular enzymatic systems, termed hybrid PKS/NRPS system, can closely cooperate to produce natural products. Indeed, the advances in cloning and characterization of biosynthetic gene clusters for naturally produced polyketides/peptides metabolites have provided clear evidence for the existence of hybrid PKS/NRPS systems.<sup>57-60</sup> The secondary metabolites produced by myxobacteria are also often derived from PKS/NRPS megasynthetase hybrid systems<sup>61,62</sup> such as ambruticin **17**<sup>63</sup>, myxopyronin **19**<sup>64</sup>, coralopyronin **20**<sup>65</sup>, and myxalamids A–D **23–26**<sup>66</sup>.

Myxalamids are produced by *M. xanthus* DK1622 and *S. aurantiaca* Sga15.<sup>67,68</sup> They are potent inhibitors of the eukaryotic electron transfer chain and one of the first PKS/NRPS hybrid compounds reported from myxobacteria in 2000s.<sup>66,68</sup> The myxalamid assembly line

features a promiscuous loading AT ( $AT_L$ ) module which accepts CoA esters of different short-chain carboxylic acid starter units (2-methyl-butryl-CoA, isobutyryl-CoA, propionyl-CoA, and acetyl-CoA) resulting in the production of myxalamids A–D (**23–26**), respectively (Fig. 6). It is suggested that after the  $AT_L$  loads the starter unit, the second AT from MxaF loads methylmalonate, which is used for the first chain extension step. MxaEDC contain five PKS modules required for chain extension using methylmalonyl-CoA or malonyl-CoA. A different set of domains in each module gives various degrees of  $\beta$ -keto processing (Fig. 6).

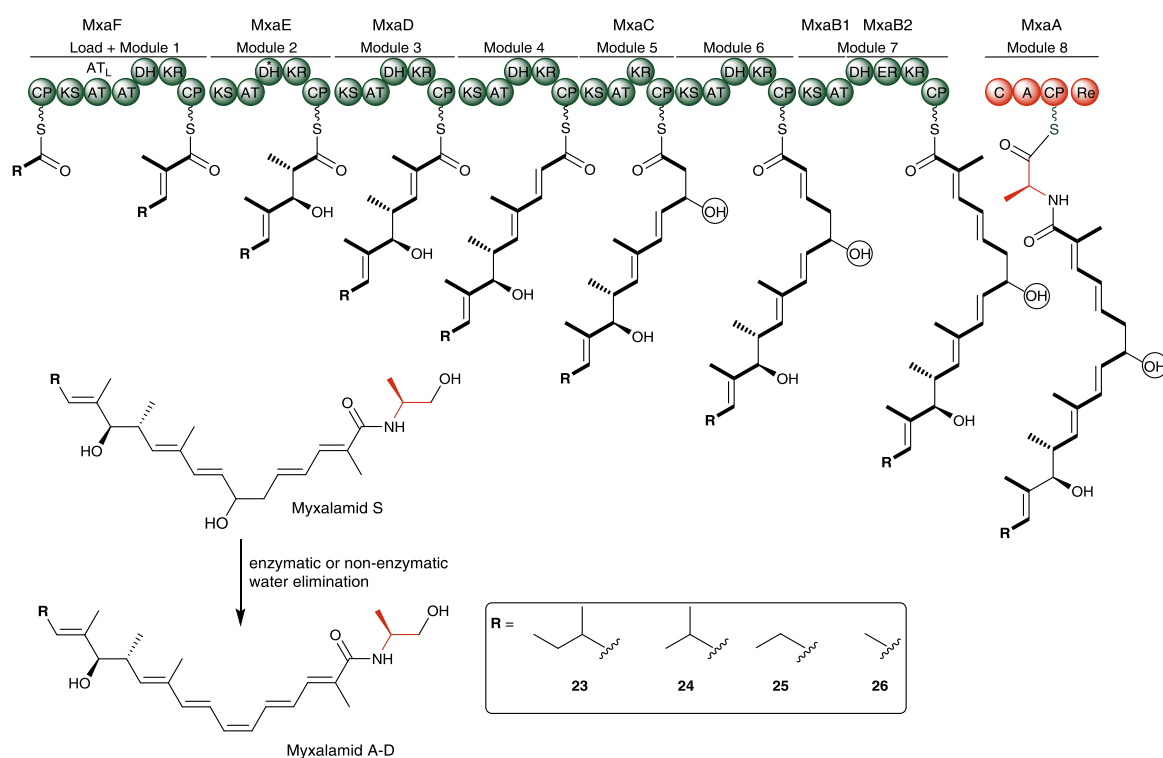


**Figure 6.** Myxalamid PKS/NRPS hybrid assembly line adapted from Silakowski et al.<sup>31</sup> **23 – 26:** myxalamid A–D. KS: ketosynthase, AT: acyltransferase, CP: carrier protein, KR: ketoreductase, DH: dehydratase, ER: enoylreductase, C: condensation, A: adenylation, Re: reductase, \*: presumably inactive domain. Green circles represent PKS domains, red circles represent NRPS domains, the carbon skeleton of starter unit and extender units are marked in bold. The circled OH group showed myxalamid S

According to the observed polyketide structure it seems that the DH domain from subunit MxaE is not involved in the reduction cycle of the module 2 ketide intermediate. Further on, the growing chain is then extended by splitting module 7 which is encoded on two separate proteins MxaB1 and MxaB2. Finally the assembled polyketide is extended via the NRPS subunit MxaA (module 8) to incorporate alanine.

Normally, assembly lines harbor a terminal domain to release the fully matured chain which in most cases is performed by a thioesterase (TE) domain for hydrolyzation of the

linear chain or macrocyclization. Myxalamid assembly line employs an unusual chain release mechanism where a reductase domain (Re) is assumed to perform the reductive release of the hybrid polyketide/peptide chain, giving rise to a linear aldehyde which is further reduced to obtain the final compound containing terminal 2-amino-propanol (alaninol). Furthermore, myxalamid S might be produced first and undergo water elimination either enzymatically or non-enzymatically giving rise to the conjugated pentadiene in the myxalamids A-D (Fig. 6). In general, the enormous variety of secondary metabolites that we observe today is the result of different domain arrangements and specificities as well as the action of various tailoring enzymes in post assembly modifications.

The textbook model of PKSs was extensively studied from the erythromycin PKS and other synthases present in filamentous actinomycetes.<sup>69</sup> However, the increasing interest in the secondary metabolites produced by bacteria from various taxa and habitats resulted in the unexpected discovery of a distinct multimodular PKS type. Each module in this multimodular PKS system lacks the AT domain and receives its acyl building block by an iteratively operating free-standing AT.<sup>70</sup> To distinguish the two PKS types, the term “*trans*-AT PKS” and “*cis*-AT PKS” were introduced for synthases with free-standing and integrated ATs, respectively (Fig.7).<sup>71</sup>

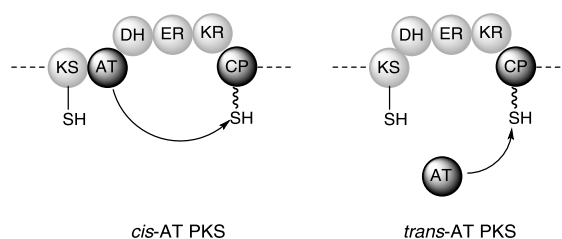


**Figure 7.** Domain organization of *cis*-AT (left) and *trans*-AT (right) PKS.

The *trans*-AT PKS system was first reported from pederin (produced by bacterial symbiont of *Paederus* beetles)<sup>70</sup> and the first *in vitro* study of this discrete AT was performed for LnmG in leinamycin biosynthesis which showed that this AT loads malonyl-CoA in *trans* to all six CP domains from the PKS modules of LnmIJ.<sup>72</sup> Phylogenetic studies suggest that *cis*- and *trans*-AT PKS multimodularity emerged by different evolutionary pathways. The *cis*-AT system is mainly derived from gene duplication of individual modules, followed by diversification of the domain sets.<sup>73</sup> In contrast, *trans*-AT PKS genes are DNA mosaics assembled from multiple gene segments *via* comprehensive horizontal gene transfer between bacteria.<sup>74</sup> The factor that triggered such distinct evolutionary pathways remains unclear. It is

noteworthy that both routes, producing similar enzymes architectures and similar metabolites outcome, contribute to the complexity of natural product evolution.

*Trans*-AT PKSs harbour many different domains that are thought to exclusively exist in these systems and their modules can be split at unusual positions even though the first example of splitting modules were actually reported in *cis*-AT PKS system from myxalamid. Furthermore, some domains are also often found unused, skipped or even used iteratively.<sup>47</sup> This results in many more module variations compared to the *cis*-AT systems. These entire peculiarities make the colinearity rule often not applicable. However, it was shown that a prediction of the product can be achieved, relying on the KS domains. Contrary to the *cis*-AT where KS have relaxed substrate specificities, the substrate specificity in *trans*-AT systems is quite limited and correlates with KS sequence.<sup>74</sup> Utilizing this correlation, product predictions can be deduced from the gene cluster.<sup>75,76</sup>

A further distinct feature from *trans*-AT PKS is the presence of more complex variations at the  $\beta$ -keto position called  $\beta$ -branching. Compared to the nucleophilic  $\alpha$ -position, the  $\beta$ -position is electrophilic and therefore requires a nucleophilic alkyl source for methylation.<sup>77</sup> The resulting  $\beta$ -branch is less common than branching at the  $\alpha$ -position and is predominantly observed in the *trans*-AT PKS even though not exclusively.<sup>47,77</sup> Today, the *trans*-AT PKS derived compounds are increasingly discovered from different microorganisms,<sup>47,78</sup> including compounds from myxobacteria such as myxovirescins **27**<sup>79</sup>, disorazols **28**<sup>80</sup>, etnangien **29**<sup>81</sup>, chivosazols **30**<sup>82</sup>, sorangicin **31**<sup>83</sup>, corallopironins **20**<sup>84</sup>, myxopyronin **19**<sup>64</sup> (Fig. 8).

## 1.4 Engineering Myxobacterial Natural Product Biosynthesis

Natural products are often produced in low quantity which hampers further studies to develop them as lead compounds. This problem may be addressed by chemical synthesis or classical strain improvement. However, as natural products generally contain many stereocenters and high structural complexity, total synthesis – if feasible at all – is often a very laborious and a time-consuming task. Classical strain improvement also has disadvantages, being a time-consuming and undirected process, in which several rounds of mutagenesis and subsequent screening of the resulting mutants need to be performed in order to get the improved strain. Fortunately, in the past two decades, the significant developments in genomic technology have been greatly facilitating the discovery of biosynthetic gene clusters responsible for synthesizing the compounds of interest. This DNA sequence information creates the platform for genetic engineering of natural product biosynthetic pathways, with the aim of improving productions yields or producing novel derivatives.



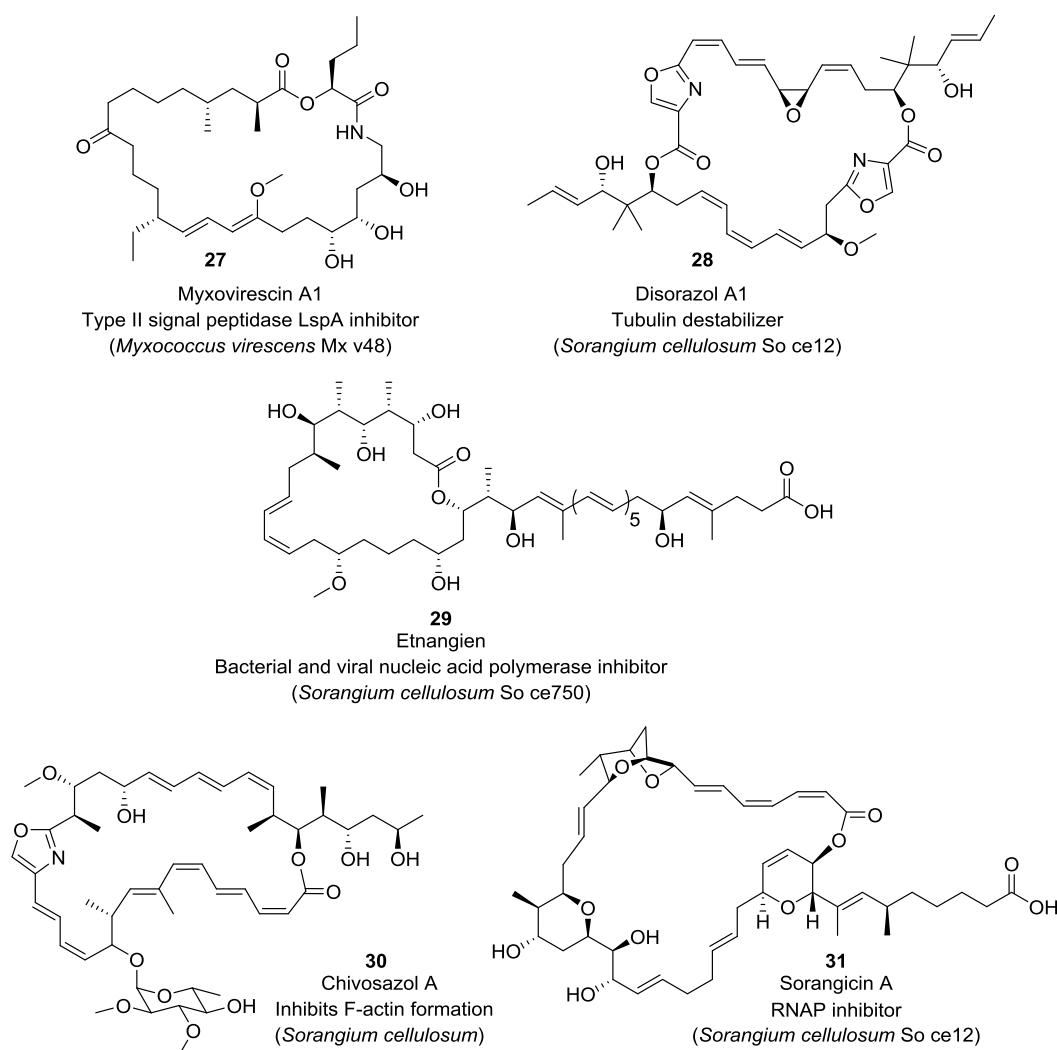


**Figure 8.** Myxobacterial *trans*-AT PKS compounds. The structure, name, mechanism of action, and producer organisms are given.

Most of secondary metabolites biosynthetic gene clusters derived from myxobacteria possess modular, multifunctional PKS and/or NRPS.<sup>62</sup> For manipulating these enzymes by exchange, insertion, deletion or site-directed mutagenesis of catalytic domains or whole complete modules, it is necessary to modify the original strain's chromosome, which is usually performed through double crossover recombination. However, genetic manipulation of procedures, especially markerless mutations, for myxobacteria are often difficult to establish. Therefore, pathway engineering has often been limited to the inactivation of polyketide/non-ribosomal peptide scaffold modifying genes (such as methyltransferases, P450s, hydrolases, and chlorinases) through single crossover experiments conducted in only a few amenable myxobacterial strains.

A few examples of this strategy include the inactivation of gene involved in ambruticin<sup>63</sup> and spirangien<sup>85</sup> biosynthesis in *S. cellulosum*, as well as ajudazol,<sup>86</sup> chondramide,<sup>87</sup> and thuggacin<sup>88</sup> biosynthesis in *C. crocatus* which lead to the formation of several derivatives. However, this type of pathway engineering only focuses on the mutagenesis of post-PKS/NRPS processing enzymes and therefore it did not introduce alterations into the polyketide/peptide backbones of the compounds. To accomplish such alterations, modification at the PKS and NRPS encoding genes themselves are necessary and require markerless mutations. Unfortunately, the techniques for this type of modification are limited and poorly established in myxobacteria.

In order to facilitate biosynthetic pathway engineering, it is therefore highly desirable to transfer the natural product's biosynthetic pathways into well-characterized host organism, an approach called 'heterologous expression'.<sup>89-92</sup> Before transferring the biosynthetic gene cluster of interest to the heterologous host, the complete set of biosynthetic genes needs to be subcloned. This can be achieved either by the generation of a cosmid library or by direct subcloning of the target region from genomic DNA using advanced cloning technologies such as Red/ET recombination (Fig. 9).<sup>93-96</sup> Red/ET recombination is performed in *E. coli* and is independent of the location of restriction sites and the size of the DNA fragments.<sup>93,95</sup> The viability of this strategy to establish heterologous production platforms for myxobacterial compounds has been exemplified by the successful heterologous expression of myxochromide S<sup>97</sup>, myxothiazol<sup>98</sup>, and tubulyisin<sup>99</sup> pathways from their native producer to heterologous hosts such as *Streptomyces coelicolor*, *Myxococcus xanthus*, *Pseudomonas putida*, *Burkholderia glumae*.

Selection of the heterologous host is usually based on its system compatibility for the production of the compound. For example, it ideally should carry the cellular machinery required for successful protein production and retained activity. Sometimes a certain modification is also necessary to be performed on the host strain to accommodate the natural product of interest e.g. introduction of methylmalonyl-CoA biosynthetic pathway to *Pseudomonas putida* to allow myxothiazol production.<sup>100</sup> It is also important that the GC content of the incoming genes and the host genomes are similar since the codon usage is usually essential for efficient expression.<sup>91,92</sup> *Myxococcus xanthus* DK1622 is often used as the first choice of heterologous host for producing myxobacterial compounds as it is a relatively fast growing and phylogenetically related myxobacterium (high GC content, preferential codon usage).

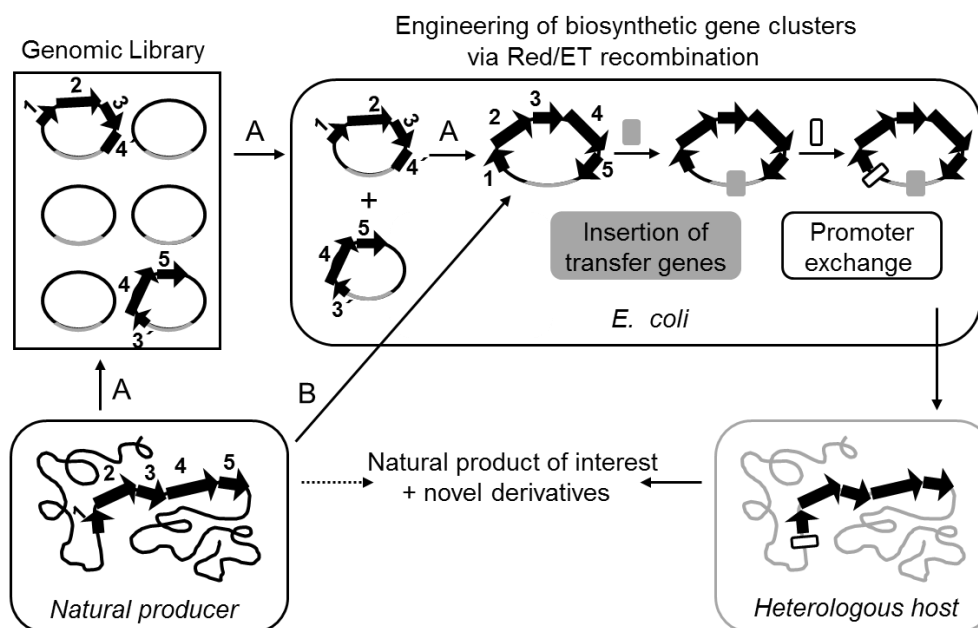


**Figure 9.** General strategy for the cloning and heterologous expression of complex natural product biosynthetic gene clusters. The entire pathway can be subcloned using two approaches: A) Generation of a genomic library, screening for constructs harboring overlapping parts of the gene cluster and stitching them onto one physical entity *via* Red/ET or B) By direct subcloning from genomic DNA using Red/ET-based methods. Further Red/ET-mediated engineering steps then yield the final expression construct, which can be transferred into an appropriate host for heterologous expression.

Once a robust heterologous expression system is established, combination of heterologous expression with the rational genetic engineering of biosynthetic gene clusters will set up an important basis for the combinatorial biosynthesis and molecular engineering approach to obtain new compounds.<sup>92</sup> Rational genetic engineering can be conducted by domain or tailoring enzyme engineering (point mutations, deletions, insertions, swapping). This has been exemplified by successful genetic manipulation of epothilone PKS/NRPS megasynthetase from *S. cellulosum* into heterologous host *S. coelicolor* and *M. xanthus*.<sup>101,102</sup> Deletion of *epoK* (epoxidase) resulted in higher amounts of epothilone D and a new derivative (10, 11-didehydro-epothilone D) in the new host strains.<sup>103,104</sup> Inactivation of reductive domains in different PKS modules (the DH, ER domain in module 5 and KR domain in module 4 and 6) resulted in the accumulation of previously identified by products and generation of novel analogues.<sup>105–107</sup> These experiments demonstrate the feasibility of using heterologous expression to modify myxobacterial PKS/NRPS megasynthetases to generate novel secondary metabolites analogues. For various strains pathway engineering are often not feasible and for many strains genetic modification is only limitedly available, therefore domain or tailoring enzyme engineering could be straightforwardly achieved in *E. coli* for instance by Red/ET recombineering technology before transferring to heterologous host.

The linear correlation between the catalytic units of a PKS and the product structure makes it possible to produce novel compounds with altered structures. There are two further common methods used to generate novel structural diversity via incorporation of unnatural building blocks (mutasynthons) namely precursor directed biosynthesis (PDB) and mutasynthesis. In PDB, the growth medium is supplemented with a compound used competitively as building block for the biosynthetic assembly (Fig. 10 c). Because of the structural similarity between the natural building block and the supplemented building block, the wild type strains are likely to accept the non-natural building block as substrate for the assembly line. Therefore, PDB experiment will obtain two metabolites: wild-type compound and its analogue as exemplified by feeding the producer strain of chondramide, *Chondromyces crocatus*, with fluorinated tryptophan extender units obtaining chondramide and its derivative fluorochondramide A.<sup>87</sup> However, in PDB experiments, the mutasynthons are often not able to efficiently compete with the natural building block, resulting in very low yield or even no production of the expected analogue.

To increase the chance of producing unnatural secondary metabolites, a combination of genetic engineering and feeding, termed mutasynthesis, was developed. In mutasynthesis approaches, a rational engineering of the biosynthetic pathway is applied. The strains are constructed in a way that the production of the natural precursor at certain stage is blocked, thus the resulting mutant strains are not able to produce the native compound anymore (Fig. 10b).<sup>108–110</sup> When they are supplied with mutasynthons, the mutant strains will be expected to incorporate them to produce structural analogues (Fig. 10 d). Compared to PDB, the microbes have no alternative but to use the surrogate substrate to start the assembly process.

The mutasynthesis approach has been successfully applied for generating myxobacterial compound analogues from the myxalamid biosynthetic pathway shown in Figure 6. As explained above, the myxalamid gene cluster AT<sub>L</sub> accepts a range of starter units resulting in myxalamid A–D **23**– **26** (Fig. 6, Fig. 11). Using this advantage, the PDB approach may lead to successful production of analogues. However, the mixture of native myxalamids and analogues may complicate the isolation of new analogues, and therefore the mutagenesis approach is preferred. In order to reduce the production of the natural myxalamids, branched-chain ketoacid dehydrogenase (*bkd*) mutants of the *M. xanthus* or *S. aurantiaca* were generated.<sup>111,112</sup> Bkd is responsible for the degradation of the branched-chain amino acids isoleucine and valine to 2-methyl-butyryl-CoA and isobutyryl-CoA, the starter units of **23** and **24**, respectively.

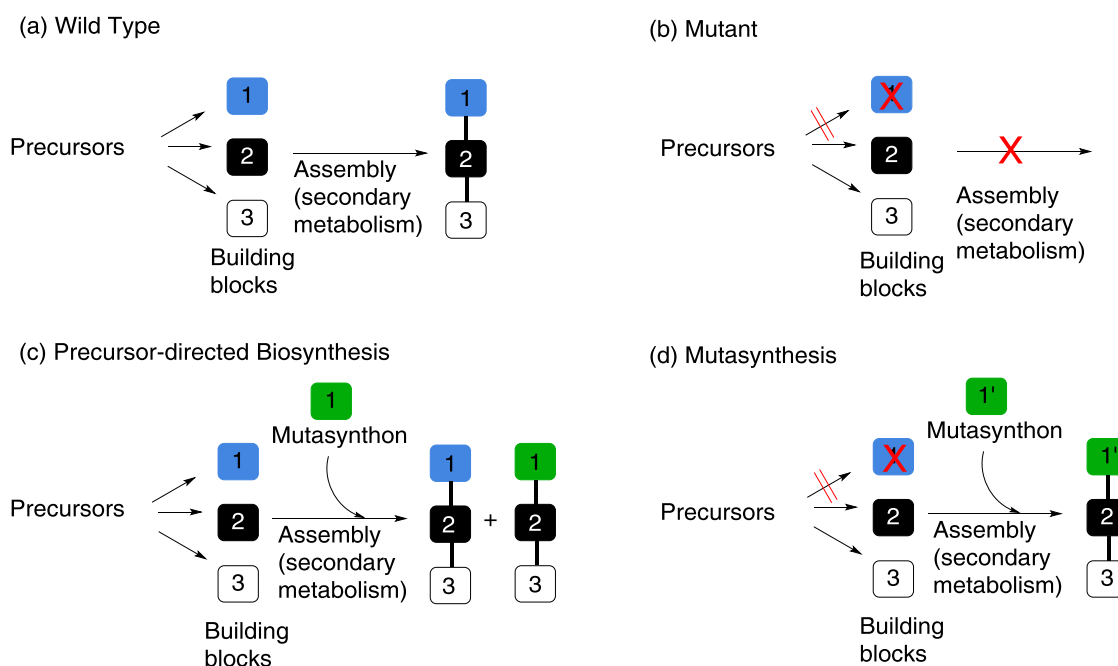


**Figure 10.** Schematic illustration of precursor-directed biosynthesis (PDB) and mutasynthesis (MBS). (a) Natural product biosynthesis by the wild type strain; (b) Biosynthesis is abolished by mutating the pathway at a crucial step (e.g. the assembly of a starter unit); (c) Precursor-directed biosynthesis: the culture medium is supplemented with an analogue of a natural building block (mutasynthon), which competes for incorporation into the natural product. Both native and modified products are usually obtained; (d) Mutasynthesis: biosynthesis by the non-producing mutant strain is reactivated by addition of mutasynthons. Only novel analogues are produced. Precursors may come from primary or secondary metabolisms.

Various non-natural carboxylic acids were then fed to the *bkd* mutants resulting in nine novel myxalamid analogues **32–40** (Fig. 11).<sup>113</sup> The biosynthetic machinery in *M. xanthus* was more flexible (resulting in **32–40**) than that in *S. aurantiaca* (resulting in **37–39**). This flexibility is in agreement with the fact that *M. xanthus* utilizes a larger starter unit to produce **23** as the major product, while *S. aurantiaca* uses a smaller starter unit to produce **24** as the major product. This successful mutasynthesis experiment in myxobacteria has become a proof of concept and has opened opportunities to apply the approach to other myxobacterial biosynthetic pathways. However, mutasynthesis approaches have not been widely applied for myxobacterial pathways yet due to the difficulties in mutant generation. Therefore, establishment of a heterologous expression platform would open various possibilities for pathway engineering including the construction of blocked mutants for mutasynthesis approaches.

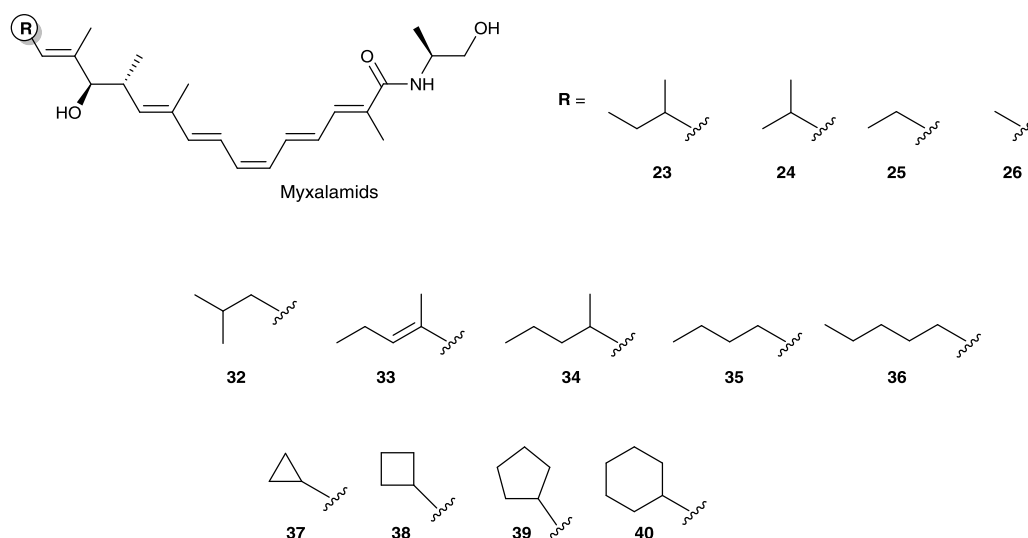


**Figure 11.** Myxalamids A–D (23–26) and its derivatives produced by a mutasynthesis approach (32–40). R represents the starting unit and marks the stage where the native precursor supply was blocked by *bkd* mutations.

## 1.5 Outline of the Present Work

The present thesis focuses on a promising anti-infective compound family from myxobacteria, myxopyronins, which were recently shown to target the bacterial RNA polymerase (RNAP) at an intriguing new binding site, the so called “switch region” (Fig. 4).<sup>33</sup> Due to the different binding mode compared to clinically used RNAP inhibitors, myxopyronins are expected to overcome existent resistances.<sup>33,42</sup> However, although the natural myxopyronin derivative was shown to be highly active in *in vitro* assays, it may not be used directly as a clinical drug due to its insufficient physicochemical and pharmacokinetic properties.<sup>37,114</sup> In a collaborative effort with the department “Drug Design and Optimization” at the Helmholtz-Institute for Pharmaceutical Research Saarland (HIPS) we intended to develop novel druggable derivatives of myxopyronin. The overall aim of the present thesis within this project was to establish biotechnological approaches to further exploit this compound family, which is naturally produced by the myxobacterium *Myxococcus fulvus* Mx f50 (Fig. 12).<sup>30</sup>

The identification and characterization of the myxopyronin biosynthetic pathway was the primary goal of this work (see Chapter 2) as it represents a prerequisite for rational engineering and optimization of the biotechnological production. Based on shotgun genome sequence data of *M. fulvus* Mx f50 a ~53 kb gene cluster involved in myxopyronin biosynthesis was identified and verified via gene deletion experiments after developing a suitable strain mutagenesis procedure. Detailed *in silico* analysis of the encoded

multimodular megasynthase led to a model for myxopyronin biosynthesis, which explains the observed structural differences compared to the highly related  $\alpha$ -pyrone antibiotic corallopyronin produced by the myxobacterium *Corallocooccus coralloides*.<sup>31,65</sup> In order to generate first myxopyronin derivatives, several gene deletion experiments were performed via a developed markerless mutagenesis procedure, but the access towards novel derivatives using this approach turned out to be very limited. Therefore, we intended to evaluate alternative approaches to generate myxopyronin analogs *via* the incorporation of unnatural precursors and to perform more detailed studies on the biosynthesis and substrate requirements.

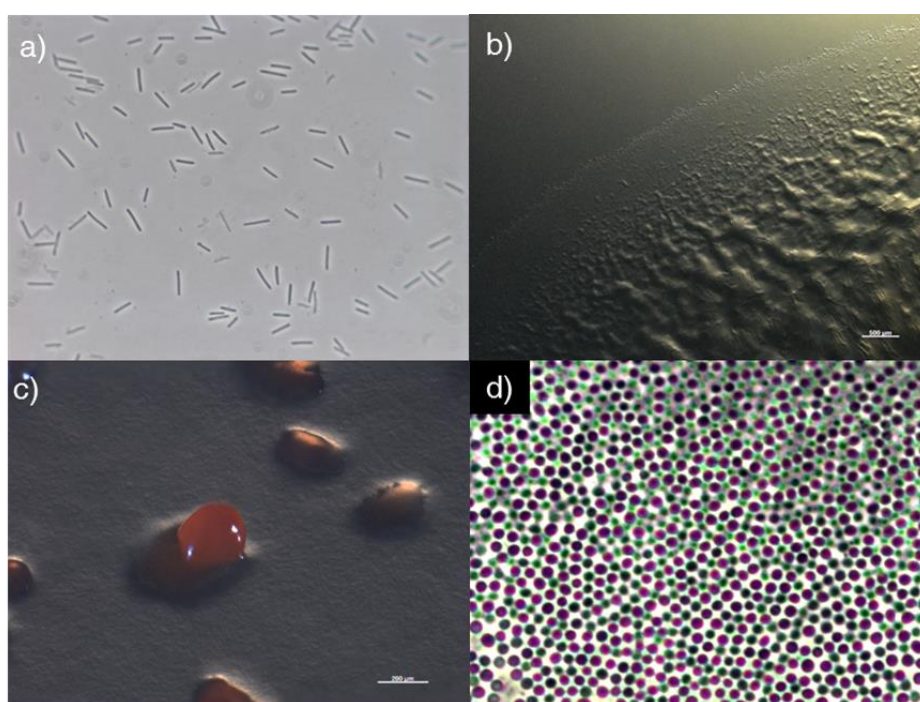


**Figure 12.** Different stages of the *Myxococcus fulvus* Mx f50 life cycle. (a) vegetative cells, (b) swarming colony, (c) fruiting bodies, and (d) myxospores (pictures: Ronald O. Garcia)

Myxopyronins are assembled from two polyketide chains, respectively a western and an eastern chain (Fig.13). The condensation of both chain intermediates reveals the typical  $\alpha$ -pyrone ring structure and represents a key step during the biosynthesis of myxopyronin and the structurally related corallopyronin. *In silico* analysis predicted that a stand-alone ketosynthase MxnB is responsible for catalyzing this reaction. To gain deeper insights in the biochemistry of this crucial step detailed *in vitro* studies were performed (see Chapter 3). Based on a series of enzyme assays using different sets of chemically activated or enzyme-bound polyketide chain substrates the MxnB reaction mechanism could be characterized in

detail. The study was supported by structural analysis of MxnB, which was performed in collaboration with the HIPS Junior Research Group “Structural Biology of Biosynthetic Enzymes”. The established *in vitro* condensation reaction allowed for generation of novel derivatives in analytical amounts and provided valuable insights into the reaction mechanism and structural requirements of modified polyketide chain substrates.

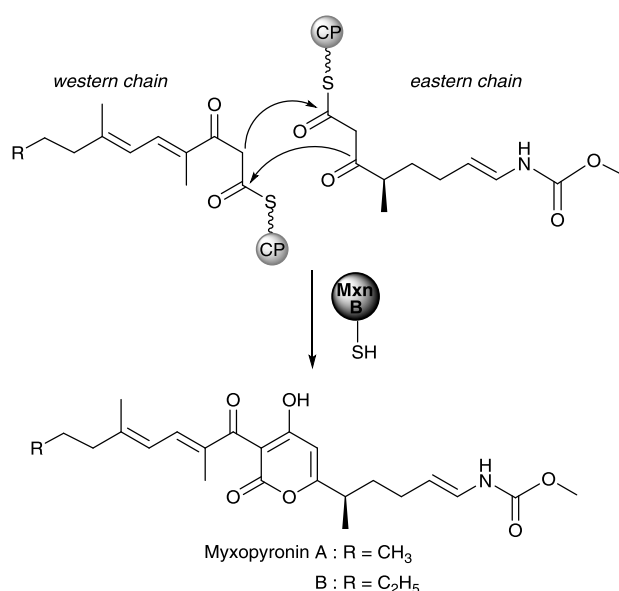


**Figure 13.** Schematic illustration of the condensation catalyzed by the putative ketosynthase MxnB to form the  $\alpha$ -pyrone ring structure from western and eastern polyketide chain substrates.

As it would be highly desirable to provide fermentation-based procedures for the production of novel myxopyronin analogs we aimed to develop a functional mutasynthesis system (see Chapter 4). As initial structure-activity relationship (SAR) studies revealed that in general the western chain provides a broader scope for structural variations to increase the inhibitory effect on RNAP,<sup>115</sup> we focused our studies on this half site of the molecule. Using genetic tools previously established for the native myxopyronin producer strain several mutants were constructed to block (or at least significantly reduce) native western chain assembly at different stages. A series of feeding studies with different western chain mutasynthons provided by our collaboration partner were carried out resulting in the production of novel myxopyronin analogues. Intriguingly, most of the synthesized mutasynthons were successfully incorporated indicating a broad western chain substrate tolerance in the final condensation reaction under *in vivo* conditions. However, productivity was too low to allow full characterization of the products and thus clearly has to be improved to provide an efficient production platform for novel myxopyronin analogs.



One option to improve productivity is to switch the production strain, which motivated us to establish a heterologous expression system in a related host strain (see Chapter 5). After subcloning chromosomal fragments from the native producer, the 57 kb myxopyronin biosynthetic gene cluster was reconstituted and engineered by applying the Red/ET recombineering technology.<sup>95</sup> Successful heterologous expression in the myxobacterial model strain *Myxococcus xanthus* DK1622 at promising production yields opens up many opportunities for further pathway engineering to generate novel myxopyronin analogues, e.g. via mutasynthesis which turned out to be inefficient in the natural producer strain.

The results achieved in the present thesis built the basis for a patent application on the production of myxopyronin and its derivatives (Sucipto et al., PCT/EP2014/059677) and resulted in three publications (Chapters 2-4). The studies on the heterologous expression of the entire myxopyronin pathway reported in Chapter 5 are planned to be published soon.

## 1.6 References

1. *Reducing risks, promoting healthy life. The world health report 2002* (World Health Organization (WHO), Geneva, 2002).
2. Wegener, H. C. Antibiotics in animal feed and their role in resistance development, *Curr. Opin. Microbiol.* **6**, 439–445 (2003).
3. DeLeo, F. R. & Chambers, H. F. Reemergence of antibiotic-resistant *Staphylococcus aureus* in the genomics era, *J. Clin. Invest.* **119**, 2464–2474 (2009).
4. Freire-Moran, L. et al. Critical shortage of new antibiotics in development against multidrug-resistant bacteria-Time to react is now, *Drug Resist. Updat.* **14**, 118–124 (2011).
5. Cooper, M. A. & Shlaes, D. Fix the antibiotics pipeline, *Nature* **472**, 32 (2011).
6. Newman, D. J. & Cragg, G. M. Natural products as sources of new drugs over the 30 years from 1981 to 2010, *J. Nat. Prod.* **75**, 311–335 (2012).
7. Butler, M. S. The role of natural product chemistry in drug discovery, *J. Nat. Prod.* **67**, 2141–2153 (2004).
8. Hayden, M. K. et al. Development of daptomycin resistance in vivo in methicillin-resistant *Staphylococcus aureus*, *J. Clin. Microbiol.* **43**, 5285–5287 (2005).
9. Gu, B. Kelesidis, T. Tsiodras, S. Hindler, J. & Humphries, R. M. The emerging problem of linezolid-resistant *Staphylococcus*, *J. Antimicrob. Chemother* **68**, 4–11 (2013).
10. Butler, M. S. Blaskovich, M. A. & Cooper, M. A. Antibiotics in the clinical pipeline in 2013, *J. Antibiot* **66**, 571–591 (2013).
11. Koehn, F. E. Biosynthetic medicinal chemistry of natural product drugs, *Med. Chem. Commun.* **3**, 854–865 (2012).

12. Gerth, K. Pradella, S. Perlova, O. Beyer, S. & Müller, R. Myxobacteria: proficient producers of novel natural products with various biological activities - past and future biotechnological aspects with the focus on the genus *Sorangium*, *J. Biotechnol.* **106**, 233–253 (2003).
13. Bode, H. B. & Müller, R. in *Myxobacteria: Multicellularity and differentiation*, edited by D. Whitworth (ASM Press, Chicago, 2007), pp. 259–282.
14. Reichenbach, H. Myxobacteria, producers of novel bioactive substances, *J. Ind. Microbiol. Biotechnol.* **27**, 149–156 (2001).
15. Demain, A. L. & Fang, A. The natural functions of secondary metabolites, *Adv. Biochem. Eng. Biotechnol.* **69**, 1–39 (2000).
16. Dworkin, M. in *Prokaryotic Development*, edited by Y. Brun & L. Shimkets (ASM Press, Washington, DC, 2000), pp. 221–242.
17. Dawid, W. Biology and global distribution of myxobacteria in soils, *FEMS Microbiol. Rev.* **24**, 403–427 (2000).
18. M. Dworkin, S. Falkow, E. Rosenberg, K. Schleifer & E. Stackebrandt (eds.). *The Prokaryotes* (Springer Verlag, New York, 2006).
19. Reichenbach, H. Gerth, K. Irschik, H. & Kunze, B. Myxobacteria: a source of new antibiotics, *Trends Biotechnol.* **6**, 115–121 (1988).
20. Wenzel, S. C. & Müller, R. The biosynthetic potential of myxobacteria and their impact on drug discovery, *Curr. Opin. Drug Discov. Devel.* **12**, 220–230 (2009).
21. Plaza, A. & Müller, R. in *Natural Products*, edited by A. Osbourn, R. J. Goss & G. T. Carter (John Wiley & Sons, Inc, Hoboken, NJ, USA, 2014), pp. 103–124.
22. Weissman, K. J. & Müller, R. Myxobacterial secondary metabolites: bioactivities and modes-of-action, *Nat. Prod. Rep.* **27**, 1276–1295 (2010).
23. Schäberle, T. F. Lohr, F. Schmitz, A. & König, G. M. Antibiotics from myxobacteria, *Nat. Prod. Rep.* **31**, 953–972 (2014).
24. Clatworthy, A. E. Pierson, E. & Hung, D. T. Targeting virulence: a new paradigm for antimicrobial therapy, *Nat. Chem. Biol.* **3**, 541–548 (2007).
25. Baumann, S. *et al.* Cystobactamids: myxobacterial topoisomerase inhibitors exhibiting potent antibacterial activity, *Angewandte Chemie (International ed. in English)* **53**, 14605–14609 (2014).
26. Plaza, A. *et al.* Aetheramides A and B, potent HIV-inhibitory depsipeptides from a myxobacterium of the new genus "Aetherobacter", *Org. Lett.* **14**, 2854–2857 (2012).
27. Knauth, P. & Reichenbach, H. On the mechanism of action of the myxobacterial fungicide ambruticin, *J. Antibiot.* **53**, 1182–1190 (2000).
28. Bielecki, P. *et al.* Mutation in elongation factor G confers resistance to the antibiotic argyirin in the opportunistic pathogen *Pseudomonas aeruginosa*, *ChemBioChem* **13**, 2339–2345 (2012).
29. Nyfeler, B. *et al.* Identification of elongation factor G as the conserved cellular target of argyirin B, *PLoS ONE* **7**, e42657 (2012).
30. Irschik, H. Gerth, K. Höfle, G. Kohl, W. & Reichenbach, H. The myxopyronins, new inhibitors of bacterial RNA synthesis from *Myxococcus fulvus* (Myxobacterales), *J. Antibiot.* **36**, 1651–1658 (1983).

31. Irschik, H. Jansen, R. Höfle, G. Gerth, K. & Reichenbach, H. The coralopyronins, new inhibitors of bacterial RNA synthesis from Myxobacteria, *J. Antibiot.* **38**, 145–152 (1985).
32. Irschik, H. Augustiniak, H. Gerth, K. Höfle, G. & Reichenbach, H. The ripostatins, novel inhibitors of eubacterial RNA polymerase isolated from myxobacteria, *J. Antibiot.* **48**, 787–792 (1995).
33. Mukhopadhyay, J. *et al.* The RNA polymerase "switch region" is a target of inhibitors, *Cell* **135**, 295–307 (2008).
34. Srivastava, A. *et al.* New target for inhibition of bacterial RNA polymerase: 'switch region', *Curr. Opin. Microbiol.* **14**, 532–543 (2011).
35. Chopra, I. Bacterial RNA polymerase: a promising target for the discovery of new antimicrobial agents, *Curr. Opin. Invest. Drugs* **8**, 600–607 (2007).
36. Darst, S. A. New inhibitors targeting bacterial RNA polymerase, *Trends Biochem. Sci.* **29**, 159–160 (2004).
37. Haebich, D. & von, N. F. Lost in transcription--inhibition of RNA polymerase, *Angew. Chem. Int. Ed. Engl.* **48**, 3397–3400 (2009).
38. World Health Organization (ed.). *Global Tuberculosis Report 2014* (World Health Organization, France, 2014).
39. Nakamura, Y. Osawa, T. & Yura, T. Intragenic localization of amber and temperature-sensitive rpoD mutations affecting RNA polymerase sigma factor of Escherichia coli, *Mol. Gen. Genet.* **189**, 193–198 (1983).
40. Ozoline, O. N. Uteshev, T. A. Masulis, I. S. & Kamzolova, S. G. Interaction of bacterial RNA-polymerase with two different promoters of phage T7 DNA. Conformational analysis, *Biochim. Biophys. Acta* **1172**, 251–261 (1993).
41. Campbell, E. A. *et al.* Structural mechanism for rifampicin inhibition of bacterial RNA polymerase, *Cell* **104**, 901–912 (2001).
42. Belogurov, G. A. *et al.* Transcription inactivation through local refolding of the RNA polymerase structure, *Nature* (2008).
43. Hertweck, C. The biosynthetic logic of polyketide diversity, *Angew. Chem. Int. Ed. Engl.* **48**, 4688–4716 (2009).
44. Fischbach, M. A. & Walsh, C. T. Assembly-line enzymology for polyketide and nonribosomal Peptide antibiotics: logic, machinery, and mechanisms, *Chem. Rev.* **106**, 3468–3496 (2006).
45. Walsh, C. T. & Fischbach, M. A. Natural Products Version 2.0: Connecting Genes to Molecules, *J. Am. Chem. Soc.* **132**, 2469–2493 (2010).
46. Minowa, Y. Araki, M. & Kanehisa, M. Comprehensive analysis of distinctive polyketide and nonribosomal peptide structural motifs encoded in microbial genomes, *J. Mol. Biol.* **368**, 1500–1517 (2007).
47. Piel, J. Biosynthesis of polyketides by trans-AT polyketide synthases, *Nat. Prod. Rep.* **27**, 996–1047 (2010).
48. Keating, T. A. & Walsh, C. T. Initiation, elongation, and termination strategies in polyketide and polypeptide antibiotic biosynthesis, *Curr. Opin. Chem. Biol.* **3**, 598–606 (1999).

49. Weissman, K. J. & Müller, R. Protein-protein interactions in multienzyme megasynthetases, *ChemBioChem* **9**, 826–848 (2008).
50. Lambalot, R. H. *et al.* A new enzyme superfamily - the phosphopantetheinyl transferases, *Chem. Biol.* **3**, 923–936 (1996).
51. Perham, R. N. Swinging arms and swinging domains in multifunctional enzymes: catalytic machines for multistep reactions, *Annu Rev Biochem* **69**, 961–1004 (2000).
52. Kohli, R. M. & Walsh, C. T. Enzymology of acyl chain macrocyclization in natural product biosynthesis, *Chem. Commun. (Camb.)*, 297–307 (2003).
53. Staunton, J. & Weissman, K. J. Polyketide biosynthesis: a millennium review, *Nat. Prod. Rep.* **18**, 380–416 (2001).
54. Conti, E. Stachelhaus, T. Marahiel, M. A. & Brick, P. Structural basis for the activation of phenylalanine in the non-ribosomal biosynthesis of gramicidin S, *EMBO J.* **16**, 4174–4183 (1997).
55. Stachelhaus, T. Mootz, H. D. & Marahiel, M. A. The specificity-conferring code of adenylation domains in nonribosomal peptide synthetases, *Chem. Biol.* **6**, 493–505 (1999).
56. Walsh, C. T. *et al.* Tailoring enzymes that modify nonribosomal peptides during and after chain elongation on NRPS assembly lines, *Curr. Opin. Chem. Biol.* **5**, 525–534 (2001).
57. Weinig, S. Hecht, H. J. Mahmud, T. & Müller, R. Melithiazol biosynthesis: further insights into myxobacterial PKS/NRPS systems and evidence for a new subclass of methyl transferases, *Chem. Biol.* **10**, 939–952 (2003).
58. Du, L. H. Sanchez, C. & Shen, B. Hybrid peptide-polyketide natural products: biosynthesis and prospects toward engineering novel molecules, *Metab. Eng.* **3**, 78–95 (2001).
59. Silakowski, B. *et al.* New lessons for combinatorial biosynthesis from myxobacteria: the myxothiazol biosynthetic gene cluster of *Stigmatella aurantiaca* DW4/3-1, *J. Biol. Chem.* **274**, 37391–37399 (1999).
60. Silakowski, B. Kunze, B. & Müller, R. Multiple hybrid polyketide synthase/non-ribosomal peptide synthetase gene clusters in the myxobacterium *Stigmatella aurantiaca*, *Gene* **275**, 233–240 (2001).
61. Wenzel, S. C. & Müller, R. in *Comprehensive Natural Products Chemistry II, Vol 2: Structural Diversity II - Secondary Metabolite Sources, Evolution and Selected Molecular Structures*, edited by B. Moore (Elsevier, Oxford, 2010), pp. 189–222.
62. Wenzel, S. C. & Müller, R. Myxobacterial natural product assembly lines: fascinating examples of curious biochemistry, *Nat. Prod. Rep.* **24**, 1211–1224 (2007).
63. Julien, B. Tian, Z. Q. Reid, R. & Reeves, C. D. Analysis of the ambruticin and jerangolid gene clusters of *Sorangium cellulosum* reveals unusual mechanisms of polyketide biosynthesis, *Chem. Biol.* **13**, 1277–1286 (2006).
64. Sucipto, H. Wenzel, S. C. & Müller, R. Exploring chemical diversity of a-pyrone antibiotics: molecular basis of myxopyronin biosynthesis, *ChemBioChem* **14**, 1581–1589 (2013).
65. Erol, Ö. *et al.* Biosynthesis of the myxobacterial antibiotic coralopyronin A, *ChemBioChem* **11**, 1235–1265 (2010).

66. Silakowski, B. Nordsiek, G. Kunze, B. Blöcker, H. & Müller, R. Novel features in a combined polyketide synthase/non-ribosomal peptide synthetase: The myxalamid biosynthetic gene cluster of the myxobacterium *Stigmatella aurantiaca* Sga15, *Chem. Biol.* **8**, 59–69 (2001).
67. Beyer, S. Kunze, B. Silakowski, B. & Müller, R. Metabolic diversity in myxobacteria: identification of the myxalamid and the stigmatellin biosynthetic gene cluster of *Stigmatella aurantiaca* Sg a15 and a combined polyketide-(poly)peptide gene cluster from the epothilone producing strain *Sorangium cellulosum* So ce90, *Biochim. Biophys. Acta* **1445**, 185–195 (1999).
68. Gerth, K. *et al.* The myxalamids, new antibiotics from *Myxococcus xanthus* (Myxobacteriales). I. Production, physico-chemical and biological properties, and mechanism of action, *J. Antibiot.* **36**, 1150–1156 (1983).
69. Khosla, C. Tang, Y. Chen, A. Y. Schnarr, N. A. & Cane, D. E. Structure and mechanism of the 6-deoxyerythronolide B synthase, *Annu. Rev. Biochem.* **76**, 195–221 (2007).
70. Piel, J. A polyketide synthase-peptide synthetase gene cluster from an uncultured bacterial symbiont of Paederus beetles, *Proc. Natl. Acad. Sci.* **99**, 14002–14007 (2002).
71. Piel, J. Hui, D. Fusetani, N. & Matsunaga, S. Targeting modular polyketide synthases with iteratively acting acyltransferases from metagenomes of uncultured bacterial consortia, *Environ. Microbiol.* **6**, 921–927 (2003).
72. Cheng, Y. Q. Tang, G. L. & Shen, B. Type I polyketide synthase requiring a discrete acyltransferase for polyketide biosynthesis, *Proc. Natl. Acad. Sci. USA* **100**, 3149–3154 (2003).
73. Jenke-Kodama, H. Borner, T. & Dittmann, E. Natural biocombinatorics in the polyketide synthase genes of the actinobacterium *Streptomyces avermitilis*, *PLoS Comput. Biol.* **2**, 1210–1218 (2006).
74. Nguyen, T. *et al.* Exploiting the mosaic structure of trans-acyltransferase polyketide synthases for natural product discovery and pathway dissection, *Nat. Biotechnol.* **26**, 225–233 (2008).
75. Jenner, M. *et al.* Substrate Specificity in Ketosynthase Domains from trans-AT Polyketide Synthases, *Angew. Chem. Int. Ed. Engl.* **52**, 1143–1147 (2013).
76. Kohlhaas, C. *et al.* Amino acid-accepting ketosynthase domain from a trans-AT polyketide synthase exhibits high selectivity for predicted intermediate, *Chem. Sci.* **4**, 3212 (2013).
77. Calderone, C. T. Isoprenoid-like alkylations in polyketide biosynthesis, *Nat. Prod. Rep.* **25**, 845–853 (2008).
78. Musiol, E. M. & Weber, T. Discrete acyltransferases involved in polyketide biosynthesis, *Med. Chem. Commun.* **3**, 871–886 (2012).
79. Simunovic, V. *et al.* Myxovirescin biosynthesis is directed by hybrid polyketide synthases/nonribosomal peptide synthetase, 3-hydroxy-3-methylglutaryl CoA synthases and trans-acting acyltransferases, *ChemBioChem* **7**, 1206–1220 (2006).
80. Kopp, M. Irschik, H. Pradella, S. & Müller, R. Production of the tubulin destabilizer disorazol in *Sorangium cellulosum*: biosynthetic machinery and regulatory genes, *ChemBioChem* **6**, 1277–1286 (2005).
81. Irschik, H. *et al.* Etnangien, a macrolide-polyene antibiotic from *Sorangium cellulosum* that inhibits nucleic acid polymerases, *J. Nat. Prod.* **70**, 1060–1063 (2007).

82. Perlova, O. Gerth, K. Hans, A. Kaiser, O. & Müller, R. Identification and analysis of the chivosazol biosynthetic gene cluster from the myxobacterial model strain *Sorangium cellulosum* So ce56, *J. Biotechnol.* **121**, 174–191 (2006).
83. Irschik, H. *et al.* Analysis of the sorangicin gene cluster reinforces the utility of a combined phylogenetic/retrobiosynthetic analysis for deciphering natural product assembly by trans-AT PKS, *ChemBioChem* **11**, 1840–1849 (2010).
84. Li, Y. Weissman, K. J. & Müller, R. Insights into multienzyme docking in hybrid PKS-NRPS megasynthetases revealed by heterologous expression and genetic engineering, *ChemBioChem* **11**, 1069–1075 (2010).
85. Frank, B. *et al.* Spiroketal polyketide formation in *Sorangium*: Identification and analysis of the biosynthetic gene cluster for the highly cytotoxic spirangienes, *Chem. Biol.* **14**, 221–233 (2007).
86. Buntin, K. *et al.* Production of the antifungal isochromanone ajudazols A and B in *Chondromyces crocatus* Cm c5: biosynthetic machinery and cytochrome P450 modifications, *Angew. Chem. Int. Ed. Engl.* **47**, 4595–4599 (2008).
87. Rachid, S. *et al.* Molecular and biochemical studies of chondramide formation - highly cytotoxic natural products from *Chondromyces crocatus* Cm c5, *Chem. Biol.* **14**, 667–681 (2006).
88. Buntin, K. *et al.* Biosynthesis of thuggacins in myxobacteria: comparative cluster analysis reveals basis for natural product structural diversity, *Chem. Biol.* **17**, 342–356 (2010).
89. Pfeifer, B. A. & Khosla, C. Biosynthesis of polyketides in heterologous hosts, *Microbiol. Mol. Biol. Rev.* **65**, 106–118 (2001).
90. Fujii, I. Heterologous expression systems for polyketide synthases, *Nat. Prod. Rep.* **26**, 155–169 (2009).
91. Wenzel, S. C. & Müller, R. Recent developments towards the heterologous expression of complex bacterial natural product biosynthetic pathways, *Curr. Opin. Biotechnol.* **16**, 594–606 (2005).
92. Ongley, S. Bian, X. Neilan, B. A. & Müller, R. Recent advances in the heterologous expression of microbial natural product biosynthetic pathways, *Nat. Prod. Rep.* **30**, 1121–1138 (2013).
93. Zhang, Y. Muyrers, J. P. P. Testa, G. & Stewart, A. F. DNA cloning by homologous recombination in *Escherichia coli*, *Nat. Biotechnol.* **18**, 1314–1317 (2000).
94. Zhang, Y. Buchholz, F. Muyrers, J. P. & Stewart, F. A. A new logic for DNA engineering using recombination in *Escherichia coli*, *Nat. Genet.* **20**, 123–128 (1998).
95. Muyrers, J. P. P. Zhang, Y. & Stewart, A. F. Techniques: Recombinogenic engineering - new options for cloning and manipulating DNA, *Trends Biochem. Sci.* **26**, 325–331 (2001).
96. Fu, J. *et al.* Full-length RecE enhances linear-linear homologous recombination and facilitates direct cloning for bioprospecting, *Nat. Biotechnol.* **30**, 440–446 (2012).
97. Wenzel, S. C. *et al.* Heterologous expression of a myxobacterial natural products assembly line in pseudomonads via red/ET recombineering, *Chem. Biol.* **12**, 349–356 (2005).
98. Perlova, O. *et al.* Reconstitution of myxothiazol biosynthetic gene cluster by Red/ET recombination and heterologous expression in *Myxococcus xanthus*, *Appl. Environ. Microbiol.* **72**, 7485–7494 (2006).

99. Chai, Y. *et al.* Heterologous expression and genetic engineering of the tubulysin biosynthetic gene cluster using Red/ET recombineering and inactivation mutagenesis, *Chem. Biol.* **19**, 361–371 (2012).
100. Gross, F. *et al.* Metabolic engineering of *Pseudomonas putida* for methylmalonyl-CoA biosynthesis to enable complex heterologous secondary metabolite formation, *Chem. Biol.* **13**, 1253–1264 (2006).
101. Julien, B. & Shah, S. Heterologous expression of epothilone biosynthetic genes in *Myxococcus xanthus*, *Antimicrob. Agents Chemother.* **46**, 2772–2778 (2002).
102. Tang, L. *et al.* Cloning and heterologous expression of the epothilone gene cluster, *Science* **287**, 640–642 (2000).
103. Arslanian, R. L. *et al.* A new cytotoxic epothilone from modified polyketide synthases heterologously expressed in *Myxococcus xanthus*, *J. Nat. Prod.* **65**, 1061–1064 (2002).
104. Arslanian, R. L. *et al.* Large-scale isolation and crystallization of epothilone D from *Myxococcus xanthus* cultures, *J. Nat. Prod.* **65**, 570–572 (2002).
105. Tang, L. *et al.* Elucidating the mechanism of cis double bond formation in epothilone biosynthesis, *J. Am. Chem. Soc.* **126**, 46–47 (2004).
106. Tang, L. *et al.* Generation of new epothilones by genetic engineering of a polyketide synthase in *Myxococcus xanthus*, *J. Antibiot.* **58**, 178–184 (2005).
107. Starks, C. M. Zhou, Y. Q. Liu, F. H. & Licari, P. J. Isolation and characterization of new epothilone analogues from recombinant *Myxococcus xanthus* fermentations, *J. Nat. Prod.* **66**, 1313–1317 (2003).
108. Rinehart, K. L. Mutasythesis of new antibiotics, *Pure Appl. Chem.* **49**, 1361–1384 (1977).
109. Weist, S. & Süssmuth, R. D. Mutational biosynthesis—a tool for the generation of structural diversity in the biosynthesis of antibiotics, *Appl. Microbiol. Biotechnol.* **68**, 141–150 (2005).
110. Weissman, K. J. Mutasythesis - uniting chemistry and genetics for drug discovery, *Trends Biotechnol.* **25**, 139–142 (2007).
111. Bode, H. B. *et al.* 3-Hydroxy-3-methylglutaryl-coenzyme A (CoA) synthase is involved in the biosynthesis of isovaleryl-CoA in the myxobacterium *Myxococcus xanthus* during fruiting body formation, *J. Bacteriol.* **188**, 6524–6528 (2006).
112. Mahmud, T. *et al.* A novel biosynthetic pathway to isovaleryl-CoA in myxobacteria: The involvement of the mevalonate pathway, *ChemBioChem* **6**, 322–330 (2005).
113. Bode, H. B. *et al.* Mutasythesis-derived myxalamids and origin of the isobutyryl-CoA starter unit of myxalamid B, *ChemBioChem* **8**, 2139–2144 (2007).
114. O'Shea, R. & Moser, H. E. Physicochemical properties of antibacterial compounds: implications for drug discovery, *J. Med. Chem.* **51**, 2871–2878 (2008).
115. Lira, R. *et al.* Syntheses of novel myxopyronin B analogs as potential inhibitors of bacterial RNA polymerase, *Bioorg. Med. Chem. Lett.* **17**, 6797–6800 (2007).





---

## Chapter 2

# Exploring Chemical Diversity of $\alpha$ -Pyrone Antibiotics: Molecular Basis of Myxopyronin Biosynthesis

*Hilda Sucipto, Silke C. Wenzel, Rolf Müller*

*ChemBioChem*, **2013**, 14, 1581–1589

DOI: 10.1002/cbic.201300289

Published online: 26.08.2013

## 2 Molecular Basis of Myxopyronin Biosynthesis

### 2.1 Abstract

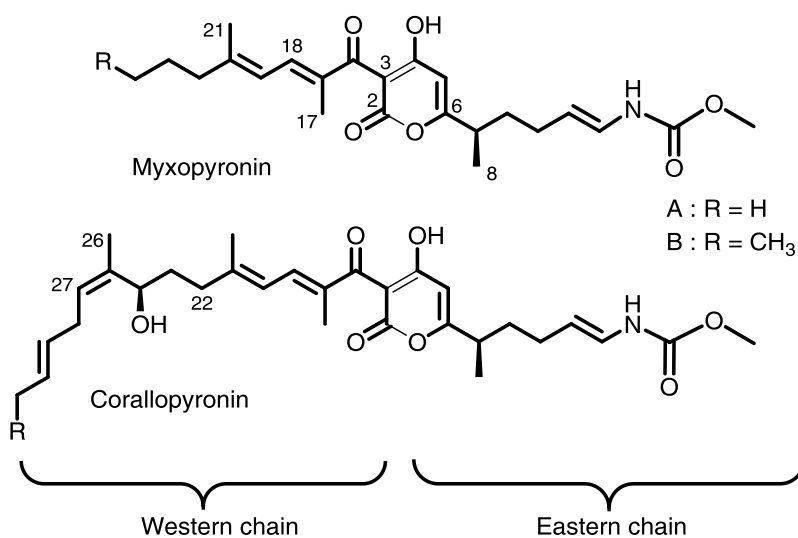
Myxopyronins and corallopyronins are structurally related  $\alpha$ -pyrone antibiotics from myxobacteria. They are thought to represent a highly promising compound class for the development of broad-spectrum antibacterial therapeutic agents, because of their ability to inhibit RNA polymerase through interaction with the "switch region", a recently identified novel drug target. Here we describe the identification and characterization of the myxopyronin biosynthetic pathway from *Mycrococcus fulvus* Mx f50. A detailed comparison with the recently identified corallopyronin biosynthetic pathway revealed the genetic and biochemical basis, thus explaining the observed structural differences between the two natural product families. Directed mutagenesis procedures for *M. fulvus* Mx f50 were developed to enable functional studies and pathway modifications. Our work provided new insights into myxopyronin biosynthesis and led to the production of a novel and unexpected myxopyronin derivative.

### 2.2 Introduction

Because of rapidly emerging antibiotic resistances, human beings have become more vulnerable to re-occurring and new infectious diseases.<sup>[1]</sup> For the last decades, serious health threats in this field keep forcing us to identify new alternative and more effective antibiotics. However, success rates in the field of antibiotic development have continuously decreased.<sup>[1]</sup> Importantly, natural products continue to play the major role as a promising source of drug discovery and development.<sup>[2]</sup> Not only have natural products shown remarkable structural diversity and complexity difficult to find using synthetic compounds, but also they exhibit complex mechanisms of action hardly possible to achieve by rational design. Furthermore, millions of years of evolution have optimized antibiotics from microorganisms regarding affinity and specificity to their targets.<sup>[3]</sup> Recently, a novel drug target termed "switch region" has been located on bacterial RNA polymerase (RNAP) based on its interaction with three antibiotics myxopyronin, corallopyronin and ripostatin.<sup>[4]</sup> These substances therefore show a different target site and mechanism of inhibition compared to known RNAP inhibitors, thus they are regarded as highly promising compound classes for the development of broad-spectrum antibacterial therapeutic agents.<sup>[4;5]</sup>

The  $\alpha$ -pyrone antibiotics myxopyronin<sup>[6]</sup> with its structurally related compound corallopyronin<sup>[7]</sup> (Scheme 1) and the macrolactone ripostatin<sup>[8]</sup> are all produced by myxobacteria,

Gram-negative soil bacteria that have been established as proficient source for novel natural products over the last decades.<sup>[9]</sup> Complex biosynthetic machineries and regulatory networks are usually involved in the production of such so-called secondary metabolites posing several challenges for biosynthetic engineering approaches. Identification of the corresponding biosynthetic pathways, studies on the underlying biochemistry and appropriate genetic tools are required to rationally improve structures and boost production yields of secondary metabolites in general. Recently, a hybrid polyketide synthase (PKS)/nonribosomal peptide synthetase (NRPS) system was reported to be involved in the biosynthesis of corallopyronin in *Coralloccoccus coralloides*.<sup>[10]</sup>



**Scheme 1.** Myxopyronin and corallopyronin

Such multimodular mega-synthetases catalyze the stepwise assembly of simple precursors (activated short-chain carboxylic acids or amino acids) by using a distinct set of catalytic domains bundled into so-called modules each incorporating one specific biosynthetic unit into the growing polyketide/peptide chain.<sup>[11]</sup> After the last elongation step the biosynthetic intermediate is usually released from the enzyme complex in linear, cyclic or branched-cyclic form by simple hydrolysis or intramolecular macrocyclization. The biosynthesis of  $\alpha$ -pyrone antibiotics seems to involve an unusual condensation of two linear polyketide (or peptide) chains, the “eastern” and “western” chains of the molecule (Scheme 1). These have been proposed to be generated on two distinct multimodular assembly lines, based on detailed *in silico* analysis of the putative corallopyronin pathway genes from *C. coralloides* as well as on feeding studies, to

reveal the biosynthetic origin of this compound class.<sup>[10, 12]</sup> However, as no genetic manipulation has been reported for the corallopyronin producer, no functional *in vivo* studies on the presumed biosynthetic gene cluster have been published.

Here we describe the pathway identification and characterization of the  $\alpha$ -pyrone antibiotic myxopyronin from *Myxococcus fulvus* Mx f50. A detailed comparison with the putative corallopyronin pathway revealed the genetic basis leading to the chemical diversity observed in the western chains of both molecules. The establishment of genetic tools for the myxopyronin producer allowed us to perform several gene deletion experiments for functional studies and to produce an unexpected novel derivative. Our studies provide further insights into the biosynthesis of  $\alpha$ -pyrone antibiotics and will serve as important basis to establish production platforms for this compound class by biosynthetic engineering.

## 2.3 Results and Discussion

### 2.3.1 Identification of the myxopyronin biosynthetic gene cluster

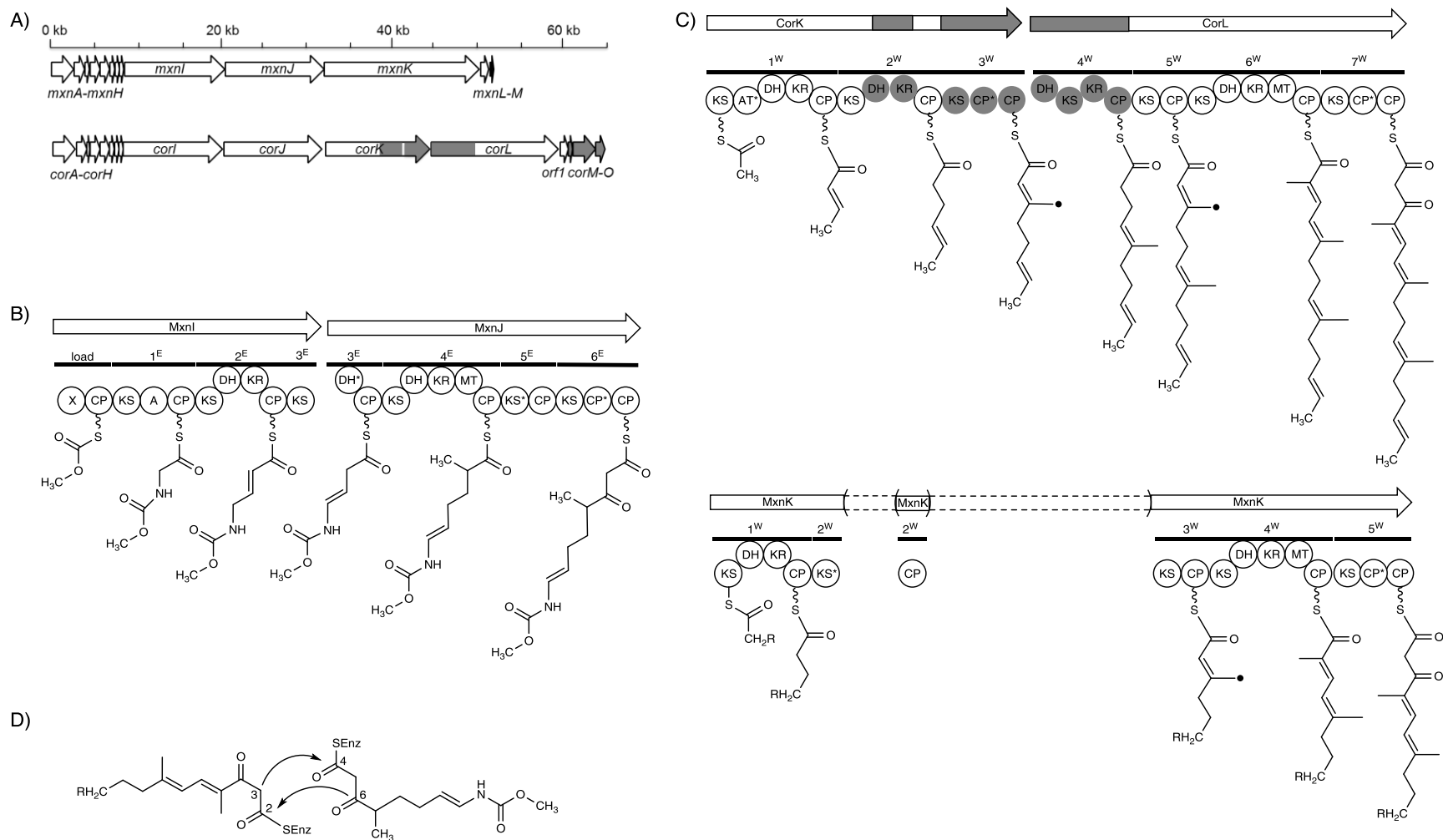
To identify the myxopyronin biosynthetic pathway in *M. fulvus* Mx f50, shotgun genome sequence data were generated by using the Illumina HiSeq sequencing system. The 578 sequence contigs and 235 sequence scaffolds (spanning ~11.2 Mbp) were screened for gene loci encoding putative PKS/NRPS pathways with high similarity to the putative corallopyronin biosynthetic pathway.<sup>[10]</sup> A corresponding genomic region was identified, and the sequence of the proposed myxopyronin biosynthetic gene cluster was completely deciphered by manual gap closing, through PCR and subsequent sequencing. After establishing and applying a directed mutagenesis procedure for *M. fulvus* Mx f50, the putative PKS/NRPS-encoding gene *mxnI* was inactivated, to verify the involvement of the identified gene locus in myxopyronin biosynthesis. As expected, myxopyronin production was completely abolished in the mutant (Mx f50::*mxnI*), thus implying that *mxnI* is essential for myxopyronin biosynthesis, although polar effects on downstream genes (*mxnJ-M*), which are most likely also affected by *mxnI* inactivation, could also result in this phenotype (Scheme 2A). In addition, a markerless gene-deletion procedure was developed for *M. fulvus* Mx f50, to perform functional studies on selective pathway genes, as explained below. A summary of all mutants generated in this work and their corresponding phenotypes is given in Table S1 in the Supporting Information. The identified myxopyronin biosynthetic gene cluster is 53 kb in length, with a high overall GC content (68.3%, typical for myxobacteria).<sup>[13]</sup> Bioinformatic analysis revealed 13 open reading frames (ORFs), designated *mxnA-M*; all are

transcribed in the same direction and are assumed to represent a single transcription unit (Scheme 2A).

### 2.3.2 Comparison of the myxopyronin biosynthetic pathway with that of corallopyronin

As expected, most of the proteins encoded in the myxopyronin (*mxn*) biosynthetic gene cluster show high homology (70-94 % similarity) to proteins from the recently postulated corallopyronin (*cor*) biosynthetic pathway (Table 1).<sup>[10]</sup> However, there are significant differences between these pathways; these are (at least in part) in accordance with the structural differences observed between the myxopyronin/corallopyronin scaffolds. Although the eastern chains are identical, the myxopyronin western chain is considerably shorter than that in the corallopyronin structure. As discussed in more detail below, this structural difference can be explained by various constituents of the western chain assembly lines (MxnK versus CorK/CorL), and the presence of additional modifying genes (CorN, CorO) in the corallopyronin biosynthetic pathway. The myxopyronin/corallopyronin assembly lines belong to the growing class of *trans*-AT PKS systems that lack integrated acyltransferase (AT) domains,<sup>[14-16]</sup> but instead exhibit discrete, free-standing AT-activity (MxnA/CorA). In addition to a malonyl-CoA-specific AT domain, MxnA/CorA exhibit enoylreductase (ER) activity, which is also absent in the modular PKS subunits. Similar arrangements are also found in other *trans*-AT PKS pathways as reviewed recently.<sup>[15, 17]</sup>

In general, myxopyronin and corallopyronin biosynthesis can be divided into three major steps: 1) eastern chain assembly, 2) western chain assembly, and 3) chain condensation, thereby giving rise to formation of the pyrone moiety (Scheme 2B-D). The myxopyronin and corallopyronin eastern chains are structurally identical (Scheme 1), and, as expected, the identified assembly lines (MxnI/MxnJ and CorI/CorJ) show high similarities. Feeding studies with the corallopyronin producer have shown that the starter unit originates from bicarbonate, and that likely a bicarbonate-dependent ATPase activity from primary metabolism is involved in its activation.<sup>[10]</sup>



**Scheme 2.** A) Myxopyronin and corallopyronin biosynthetic gene clusters, B) Eastern chain assembly line, C) Myxopyronin and corallopyronin western chain assembly lines, D) Chain condensation and formation of the pyrone moiety. CP: carrier protein; DH: dehydratase domain; ER: enoylreductase domain; KR: ketoreductase domain; KS: ketosynthase domain; MT: methyltransferase domain; X: putative inactive KR or truncated phosphoglucumutase/phosphomannomutase domain. The CP\*, DH\*, and KS\* domains are assumed to be inactive. Black circles mark the carbons introduced by the  $\beta$ -branching cassette. Unique genes or gene fragments are highlighted for the corallopyronin (gray) and myxopyronin (black) biosynthetic pathways.

The resulting (highly labile) carboxyphosphate intermediate would allow subsequent attachment to the carrier protein (CP) domain of the loading module, to start eastern chain biosynthesis (Scheme 2B). It is interesting to note that a putative N-terminal domain (X) in MxnI might represent an inactive ketoreductase (KR) domain (as also postulated for CorI), but we found that it also exhibits very weak similarity to a truncated phosphoglucomutase/phosphomannomutase, alpha, beta/alpha domain II (PGM PMM II). We speculate that this domain is involved in activation/modification of the proposed bicarbonate starter by phosphoryl group transfer. However, the eastern chain assembly mostly proceeds by incorporation of a glycine and three malonyl-CoA extender units mostly according to textbook biosynthetic logic but also involving several exceptions typical for *trans*-AT PKS systems.<sup>[15]</sup> These include the presence of an unusual mixed PKS/NRPS module (module 1<sup>E</sup>: KS-A-CP; KS: ketosynthase, A: adenylation domain) for the incorporation of glycine, and a "split module" (module 3<sup>E</sup>: KS, DH\*-CP; <sup>E</sup>: modules from the eastern chain assembly line (as shown in Scheme 2), \*: domains that are supposed to be inactive, DH: dehydratase), which is most likely not involved in chain elongation. However, the DH\* domain might catalyze the double-bond shift from the  $\alpha,\beta$  to the  $\beta,\gamma$  position, as was described in rhizoxin biosynthesis for RhiE, which shows a similar "split module" arrangement.<sup>[18]</sup> The following module, module 4<sup>E</sup>, lacks the ER activity required to complete the reduction cycle, which might be provided by MxnA in *trans*, as discussed above. The next module is assumed not to be involved in chain elongation because it contains a mutated ketosynthase domain (module 5<sup>E</sup>: KS\*-CP); it should not be able to catalyze a condensation reaction. Another deviation from textbook biochemistry is the presence of *tandem*-CP domains within the last module (module 6<sup>E</sup>: KS-CP\*-CP; CP\* seems to be inactive), which incorporates the third malonyl-CoA extender to generate the final eastern chain  $\beta$ -keto intermediate. The terminal carboxy moiety is assumed to be methylated by the putative carboxy methyltransferase (MxnH/CorH) encoded in each pathway. This modification would increase the stability of the starter unit as well as of eastern chain assembly line intermediates, and therefore likely takes place at an early stage of eastern chain biosynthesis.

In contrast to the eastern chains, the western chains of myxopyronins and coralopyronins show significant structural differences (Scheme 1). This is reflected in the domain arrangements of the corresponding western chain assembly lines. A single pentamodular subunit, MxnK, is found in the myxopyronin pathway; in contrast, a heptamodular dual subunit system, CorK/CorL, is found for coralopyronin western chain formation (Scheme 2C).

**Table 1.** Proposed function of the proteins involved in myxopyronin biosynthesis and homologues from the related corallopyronin biosynthetic pathway.

Myxopyronin protein (amino acids)	Corallopyronin protein (amino acids)	Homology between Mxn and Cor proteins Identity/Similarity [%]	Putative function [Catalytic domains]
MxnA (798)	CorA (763)	77/86	acyltransferase – enoylreductase [AT-ER]
MxnB (335)	CorB (335)	84/94	ketosynthase [KS]
MxnC (83)	CorC (83)	76/90	acyl carrier protein [CP]
MxnD (423)	CorD (423)	74/83	ketosynthase [KS]
MxnE (410)	CorE (410)	82/92	hydroxymethylglutaryl-CoA (HMG-CoA) synthase
MxnF (253)	CorF (261)	75/83	enoyl-CoA hydratase/isomerase [ECH]
MxnG (254)	CorG (254)	83/92	enoyl-CoA hydratase/isomerase [ECH]
MxnH (286)	CorH (286)	86/93	carboxyl-methyltransferase [MT]
MxnI (3906)	CorI (3883)	71/80	hybrid polyketide synthase (PKS, <i>trans</i> -AT type) /nonribosomal peptide synthetase (NRPS) [PM-CP-KS-A-CP-KS-DH-KR-CP-KS]
MxnJ (3862)	CorJ (3817)	70/80	polyketide synthase (PKS, <i>trans</i> -AT type) [DH-CP-KS-DH-KR-MT-CP-KS-CP-KS-CP-CP]
MxnK (6045)	CorK (4068)	70/78	polyketide synthase (PKS, <i>trans</i> -AT type)
	CorL (4981)	68/78	[KS-DH-KR-CP-KS-CP-KS-CP-KS-DH-KR-MT-CP-KS-CP-CP]
MxnL (582)	Orf1 (573)	75/86	hypothetical protein (SorT)
MxnM (326)	Not found	-	acyltransferase
Not found	CorM (240)	-	thioesterase
Not found	CorN (724)	-	enoyl CoA hydratase
Not found	CorO (449)	-	cytochrome P450

Domain abbreviations as in Scheme 2.

Sequence alignment of the two western chain assembly lines revealed that modules 3<sup>W</sup> and 4<sup>W</sup> of CorK/CorL are absent in MxnK, which also lacks the reductive domains (DH-KR) in module 2<sup>W</sup>. The assembly is most likely initiated with an acetyl-CoA (myxopyronin A) or propionyl-CoA (myxopyronin B) starter unit, which is assumed to be directly loaded onto the N-terminal KS domain of module 1<sup>W</sup>, as no typical loading module could be identified. After elongation with the



first malonyl-CoA extender unit, the resulting  $\beta$ -keto intermediate is then fully reduced, for which the final reduction step is again likely catalyzed in *trans* by MxnA. The KS domain of the next module (module 2<sup>W</sup>: KS\*-CP) seems to be inactive, and is therefore not involved in chain elongation. The downstream modules (modules 3<sup>W</sup>, 4<sup>W</sup>, 5<sup>W</sup>) incorporate three additional malonyl-CoA extender units (according to textbook polyketide chemistry) to generate the final western chain  $\beta$ -keto intermediate. Chain elongation on module 3<sup>W</sup> includes  $\beta$ -branching, which is another feature typical for *trans*-AT PKS systems<sup>[15, 19]</sup> and results in a methyl group at C-20. The genes for this modification show the typical cluster organization (*mxnCDEFG*), as also observed in the corallopyronin biosynthetic pathway (*corCDEFG*). They encode an acyl carrier protein (CP; MxnC) to load malonyl-CoA, which is subsequently decarboxylated by a mutated, nonelongating ketosynthase (MxnD). Aldol addition of the generated acetate unit to the biosynthetic intermediate bound to module 3<sup>W</sup> is catalyzed by the 3-hydroxy-3-methylglutaryl-CoA (HMG-CoA) synthase homologue (MxnE). The resulting product then undergoes dehydration and decarboxylation by two enoyl-CoA hydratase (ECH) homologues (MxnF and MxnG). Based on sequence comparison with the functionally characterized homologues CurE and CurF, we assume that MxnF and MxnG are involved in dehydration and decarboxylation, respectively (Scheme S1).<sup>[20]</sup> It is interesting to note that a second  $\beta$ -branch is introduced into the corallopyronin western chain (C-26 in addition to C-21), whereas the shorter myxopyronin chain contains only one such  $\beta$ -branch (C-21). Furthermore, corallopyronin western chain biosynthesis includes a double bond isomerization (from position  $\Delta^{24,25}$  to  $\Delta^{25,27}$ ), which is likely catalyzed by CorN. A further hydroxylation at C-24 is probably introduced by the putative cytochrome P450 CorO. CorN and CorO enzyme activities are not required and are not encoded in the myxopyronin biosynthetic pathway.

In the last stage of the biosynthesis, the eastern and western chain  $\beta$ -keto intermediates are released from the PKS complex and undergo condensation to form the characteristic pyrone ring (Scheme 2D). We assume that the discrete ketosynthase (MxnB/CorB) is involved in this transformation. For corallopyronin, it was speculated that an additional thioesterase (TE) activity, catalyzed by CorM, is involved in this process, by cleaving the intermediate from CorL--PKS and building the lactone moiety.<sup>[10]</sup> As no CorM homologue is encoded within the myxopyronin pathway we postulate that MxnB should be sufficient for pyrone ring formation. This is consistent with a recent study by Leadlay and co-workers, who showed in vitro formation of a tetronate polyketide in the presence of RkD (a FabH-like 3-oxoacyl-(acyl carrier protein) synthase III) and acyl-carrier-protein-bound substrates.<sup>[21]</sup> However, from the in silico analysis

we cannot completely exclude the involvement of the hypothetical protein MxnL in the final chain release and condensation steps. MxnL and its homologue from *cor* pathway (Orf1) show very weak similarity to a hypothetical protein from the sorangicin pathway, SorT, for which a possible role in chain release from the PKS complex was speculated. The last gene in the *mxn* pathway encodes a putative acyltransferase, MxnM, which has no counterpart in the coralopyronin pathway. Therefore, MxnM as well as the hypothetical protein MxnL represented interesting candidates for functional studies (described in the next section).

### 2.3.3 MxnL and MxnM are not essential for myxopyronin biosynthesis

The presence of the hypothetical protein MxnL and the putative acyltransferase MxnM (with no obvious roles in myxopyronin biosynthesis) motivated us to perform functional studies through gene deletion experiments. Genetic tools and mutagenesis protocols for myxobacteria are rather limited, not widely applicable, and usually have to be established for each strain individually.<sup>[22]</sup> To develop a markerless gene-deletion procedure for the myxopyronin producer *M. fulvus* Mx f50 we made use of the *sacB* counterselection method, which has been successfully applied in the myxobacterial model strain *Myxococcus xanthus*.<sup>[23]</sup> Appropriate procedures for efficient DNA transfer were evaluated, to establish a robust genetic system for markerless gene deletion in *M. fulvus* Mx f50; this was used to generate five gene-deletion mutants, as described below (Figure 1). The genotypes of all mutants were confirmed by PCR or Southern blot analysis (see the Supporting Information).

The *mxnL* gene was excised from the chromosome, and the obtained mutant strain, *M. fulvus* Mx f50 $\Delta$ pHSU-mxn20 ( $\Delta$ *mxnL*), was analyzed, in parallel with the wild-type strain, for myxopyronin production. Interestingly, comparable myxopyronin production levels were detected (Figure S8), thus indicating that MxnL is not essential—indeed, not even promotional—for myxopyronin biosynthesis, in terms of production yield under the tested conditions. However, we cannot exclude that possible MxnL deficits might be complemented by enzymes encoded elsewhere in the genome. Significant bottlenecks in other stages of the production line or a minimal positive impact of MxnL in the wild-type strain under the tested production conditions (e.g., due to low *mxnL* expression levels) might also explain the absence of detectable effects upon *mxnL* deletion.

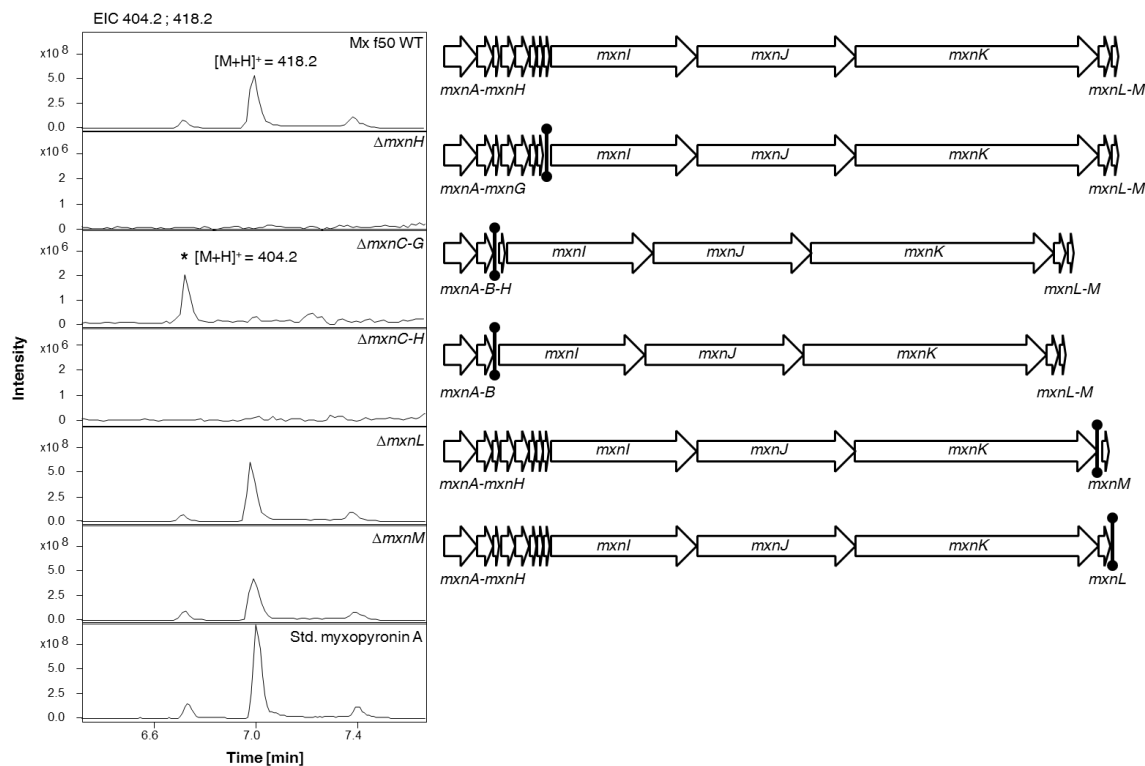


**Figure 1.** HPLC-MS chromatograms for myxopyronin gene cluster variants. Culture extracts of *M. fulvus* Mx f50 (Mx f50 WT) and the deletion mutants of *M. fulvus* Mxf50ΔpHSU-mxn23 ( $\Delta mxnH$ ), *M. fulvus* Mxf50ΔpHSU-mxn21 ( $\Delta mxnC-G$ ), *M. fulvus* Mxf50ΔpHSU-mxn22 ( $\Delta mxnC-H$ ), *M. fulvus* Mxf50ΔpHSU-mxn20 ( $\Delta mxnL$ ), *M. fulvus* Mxf50ΔpHSU-mxn34 ( $\Delta mxnM$ ) were analyzed in comparison with an authentic reference (standard myxopyronin A). In  $\Delta mxnH$ ,  $\Delta mxnC-G$ , and  $\Delta mxnC-H$  no myxopyronin A was detected. Asterisk shows the peak of the novel myxopyronin derivative identified in the  $\Delta mxnC-G$  mutant. Vertical symbols (●—●) show the position of deleted genes in the variants.

Another interesting candidate for functional studies was MxnM, a putative discrete acyltransferase (AT) with no homologue in the coralopyronin biosynthetic pathway. Whereas the MxnA AT activity was proposed to load the PKS with malonyl units, the function of the second AT copy (MxnM) was unclear. A recent study by Piel and co-workers described a proofreading function for such "additional" AT copies (to remove aberrant acyl units from blocked trans-AT PKS modules), and a novel group of editing acyl hydrolases (AHs) was discovered.<sup>[24]</sup> These studies were carried out with PedC from the pederin pathway from a *Pseudomonas* sp. Symbiont of *Paederus fuscipes* beetles, and, interestingly, MxnM falls into the same clade in phylogenetic analysis (Figure S7). Another member of this "AT2 clade" is MmpC-AT<sub>1</sub> from the mupirocin pathway *Pseudomonas fluorescens*; a negative effect on overall production yield was shown upon deletion of the AT<sub>1</sub>-encoding fragment of the *mmpC*.<sup>[25, 26]</sup> Production titers in the mutant strain were around 13.5% of wild-type. Although an unfavorable effect on the malonyl loading ability of AT MmpC-AT<sub>2</sub> could not be excluded (due to the

disruption of the bifunctional MmpC-AT1-AT2 protein), the observed negative impact on production yield also supports a proof-reading function for MmpC-AT<sub>1</sub>. In light of these results, we considered that MxnM might represent an editing acyltransferase-like protein that positively influences the overall productivity of the myxopyronin PKS and/or plays a role in chain release during final pyrone ring formation. As the corallopyronin pathway lacks an MxnM homologue, we further speculated that MxnM might be specific for the significantly different western chain assembly line, or that the productivity of the corallopyronin pathway is lower because of the absence of such an editing AT. To study the impact of *mxnM* on myxopyronin production, the gene was deleted to yield the mutant strain *M. fulvus* Mx f50ΔpHSU-mxn34 ( $\Delta$ *mxnM*). Analysis of products revealed no obvious effects on yield (Figure S8) relative to the wild-type, thus suggesting that MxnM is neither essential nor beneficial for myxopyronin production under the tested conditions. Again, we cannot exclude complementation by other enzymes (encoded elsewhere in the genome) or crucial bottlenecks in other stages of the production that might mask "beneficial factors", such as proofreading. In addition, it is possible that MxnM does not mediate strong activity in the wild-type strain (e.g., due to low expression levels), so its deletion showed no detectable effect. Overall, the presence of MxnM might be useful, but is not essential for myxopyronin biosynthesis. For forthcoming studies, it would be interesting to investigate whether overexpression of MxnM in the myxopyronin producer (and also in the corallopyronin producer) boosts production yield.

### 2.3.4 Unexpected myxopyronin A derivative from $\beta$ -branching cassette deletion

In order to generate modified myxopyronin derivatives we aimed to delete the entire  $\beta$ -branching cassette *mxnCDEFG* by using the markerless mutagenesis procedure established in this study. Production in the mutant strain, *M. fulvus* Mx f50ΔpHSU-mxn21 ( $\Delta$ *mxnC--G*), was compared with wild-type. As expected, HPLC-MS analysis of the extracts revealed no production of the native derivatives myxopyronin A or B in the  $\Delta$ *mxnC--G* mutant, but a novel myxopyronin derivative was detected. The high-resolution mass spectrum (HRMS) displayed an  $[M+H]^+$  peak at  $m/z$  404.2065 (calcd for C<sub>22</sub>H<sub>30</sub>O<sub>6</sub>N: 404.2067;  $\Delta$  -0.5 ppm) which is 14 amu lower than for myxopyronin A and consistent with the molecular formula C<sub>22</sub>H<sub>29</sub>O<sub>6</sub>N. In order to confirm the structure of this novel derivative, 0.35 mg was purified from 10 L culture and subjected to NMR analysis (Table S4 and Figures S1-S4). <sup>1</sup>H NMR and HSQC spectra of the isolated compound show the absence of the Me-21  $\beta$ -branch (compared to myxopyronin A). Detailed analysis of the

2D NMR data allowed us to determine it as a 21-desmethyl analogue of myxopyronin A (Figure 2).

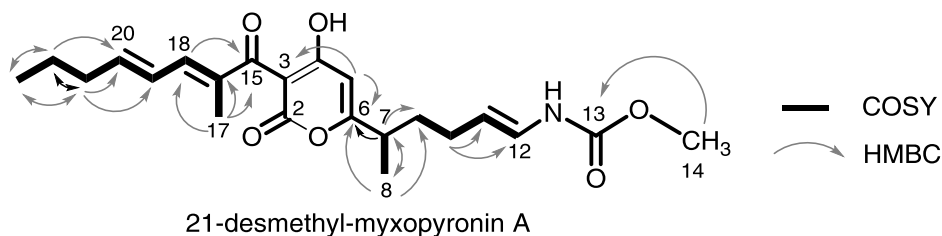


**Figure 2.** Key correlations of HMBC and COSY of 21-desmethyl-myxopyronin A isolated from *M. fulvus* Mxf50ΔpHSU-mxn21 ( $\Delta$ mxnC-G).

In particular, uninterrupted COSY correlations from the olefinic proton at  $\delta=6.93$  ppm (H-18) to the methyl protons  $\delta=0.93$  ppm (Me-23) and HMBC correlations from the methyl vinyl protons at  $\delta=1.93$  ppm (Me-17) to the carbon resonances at  $\delta=201.0$  (C-15), 136.7 (C-16), and 141.5 ppm (C-18) confirmed its structure. Subsequent studies on its biological activity against a small panel of microorganisms revealed that the 21-desmethyl derivative was less active than myxopyronin A (Table S3).

However, the structure of 21-desmethyl-myxopyronin A did not completely correlate with the structural variation expected from this genetic modification. In fact, removal of the  $\beta$ -branching machinery should have resulted in retention an unmodified C-20 carbonyl functionality instead of the observed  $\Delta^{19,20}$  double bond. This reduction can be explained by downstream KR and DH activities by module 4<sup>W</sup>, which might act on both the C-18  $\beta$ -carbonyl and the C-20 O-carbonyl functionality of the biosynthetic intermediate. However, the production yield of the novel derivative was about fiftyfold lower than that of native myxopyronin in the wild-type strain; not even trace amounts of the originally expected derivative (retained C-20 carbonyl functionality) could be detected. If we exclude general negative effects on gene expression in the modified *mxn* biosynthetic operon ( $\Delta$ mxnC--G), these results might be explained by two scenarios: 1) the conjugated olefinic system might be essential for pyrone ring formation, and C-20 carbonyl intermediates bound to 5<sup>W</sup>-CP are not processed further, or 2) O-carbonyl reduction on module 4<sup>W</sup> is highly efficient, but because of the lack of the C-21  $\beta$ -branch, the overall productivity of the condensation step is significantly decreased. Future studies on the final condensation reaction, especially on substrate specificity of the involved enzymes(s) (most likely MxnB), should provide deeper insights into this crucial biosynthetic step.

### 2.3.5 O-methylation by MxnH is essential for myxopyronin biosynthesis

The successful biosynthetic engineering of the  $\beta$ -branching cassette motivated us to generate further pathway variants: deletion of another modifying gene (*mxnH*), which encodes a putative carboxy-methyltransferase. MxnH and its homologue CorH (corallopyronin biosynthetic pathway) are assumed to introduce the O-methyl functionality during eastern chain biosynthesis. Using the established gene-deletion procedure, we constructed two additional mutant strains, *M. fulvus* Mx f50 $\Delta$ pHSU-mxn22 ( $\Delta$ *mxnC-H*), in which *mxnH* and the  $\beta$ -branching cassette (*mxnC-G*) were deleted, and *M. fulvus* Mx f50 $\Delta$ pHSU-mxn23 ( $\Delta$ *mxnH*), in which exclusively *mxnH* was deleted. This modification might lead to the production of myxopyronin derivatives with a free carbamic acid moiety instead of the eastern chain methyl carbamate.

Interestingly, HPLC-MS analysis of culture extracts revealed that myxopyronin production was completely abolished in both mutants (Figure 1). As discussed by Erol and co-workers for corallopyronin biosynthesis, the starter unit carbonic acid functionality might be rather unstable, especially after the first elongation step with glycine.<sup>[10]</sup> It was speculated that CorH might attach the O-methyl group to the starter unit immediately or, alternatively, to the carbamate moiety after the first chain elongation. The missing methylation activity in *mxnH* deletion mutants thus might cause a breakdown in myxopyronin biosynthesis due to the instability of eastern chain intermediates. Additionally (or alternatively), it should be considered that the altered intermediates are not processed because of certain substrate specificities in the eastern chain assembly line or at the final chain condensation step. However, to exclude that the genetic modifications ( $\Delta$ *mxnH* or  $\Delta$ *mxnC-H*) had negative impacts on the functional expression of the remaining *mxn* biosynthetic genes, we performed chemical and genetic complementation studies with the  $\Delta$ *mxnH* mutant strain. After reintegration of *mxnH* by insertional mutagenesis at the 3' end of the gene cluster, myxopyronin production was restored. The production yields were tenfold lower than wild-type, thus indicating that the genetic modifications within the *mxn* biosynthetic operon might (partially) reduce gene expression levels. However, the successful complementation suggests that the *mxn* biosynthetic genes should in principle be functional in the *mxnH* deletion mutants, and thus that formation of a methyl carbamate might be essential for eastern chain biosynthesis. At which stage of the biosynthesis methylation occurs is currently unknown. Because of the instability of the methyl carbamate moiety we assume that methylation occurs, at the latest, after the first elongation step (condensation with glycine). Feeding of triethylmethylammonium methyl carbonate did not restore myxopyronin production, thus

indicating that a methylated starter unit precursor might not be accepted. However, further experiments, for example feeding studies including mimics of putative intermediates bound to the loading module or module 1<sup>E</sup>, have to be performed to shed more light on the methylation scenario.

## 2.4 Conclusion

The  $\alpha$ -pyrone class of antibiotics exhibits promising antibacterial activity, specifically by interaction with the RNA polymerase "switch region". In this study we have identified the gene cluster for myxopyronin biosynthesis and revealed the overall similarity (but also significant differences) to the structurally related compound coralopyronin. Bioinformatic analysis and a set of gene deletions have revealed interesting features of myxopyronin biosynthesis. The O-methylation in eastern chain assembly seems to be a key reaction that eventually affects myxopyronin biosynthesis. Furthermore, an unexpected derivative was obtained from the  $\beta$ -branching cassette deletion. This gene cluster information will be the basis for the generation of novel myxopyronin analogues by genetic engineering.

## 2.5 Experimental Section

### Bacterial strains and culture conditions

Bacterial strains and plasmids used during this study are listed in Table S1. *Myxococcus fulvus* Mx f50 wild type and mutants were grown in Casitone Yeast (CY) medium (0.3 % casitone, 0.1 % yeast extract, 0.1 %  $\text{CaCl}_2 \times 2 \text{H}_2\text{O}$ ) supplemented with  $5 \times 10^{-4} \mu\text{g L}^{-1}$  vitamin B12 after autoclaving. For liquid cultures, the strains were grown at 30 °C and 105 rpm on an orbital shaker and harvested after 3 days. *E. coli* strains were cultured in lysogeny broth (LB) medium (1 % tryptone, 0.5 % yeast extract, 0.5 % NaCl) at 37 °C. Appropriate antibiotic selection at a final concentration of 100  $\mu\text{g ml}^{-1}$  ampicillin, 50  $\mu\text{g ml}^{-1}$  kanamycin, 5  $\mu\text{g ml}^{-1}$  tetracycline or 6.25  $\mu\text{g ml}^{-1}$  oxytetracycline was added whenever necessary.

### DNA preparations and PCR

*M. fulvus* Mx f50 genomic DNA was prepared either via the Phenol Chloroform Isoamyl alcohol extraction method<sup>[27]</sup> or by using the Genra Puregene Genomic DNA Purification Kit (Qiagen) according to the manufacturer's protocol. Plasmid DNA was either purified by standard alkaline lysis<sup>[27]</sup> or by using the GeneJet Plasmid Miniprep Kit (Thermo Fisher Scientific). The PCR reactions were carried out in a peqSTAR 96 Universal Gradient thermocycler (Peqlab): initial

denaturation (3 min, 95 °C); 30 cycles of denaturation (30 s, 95 °C), annealing (30 s, 53 or 57 °C) and elongation (varied based on PCR product length 1 kb/min, 72 °C); and final extension (10 min, 72 °C). DNA fragments were separated by agarose gel electrophoresis and isolated using the peqGold Gel Extraction (Peqlab). The PCR products were cloned into pCRII-TOPO (Invitrogen) or pJET1.2 blunt (Thermo Fisher Scientific) vector and sequenced using the primers M13For/M13Rev or pJET1.2For/pJET1.2Rev, respectively. Primer sequences are listed in Table S2.

### Genome sequence and bioinformatic analysis of sequences

The shotgun genome sequence data were generated on Illumina Hi-Seq2000 instrument (Fasteris SA, Switzerland). The assembly revealed 578 sequence contigs, which could be combined to 235 scaffolds. The myxopyronin gene cluster was identified by homology search against the identified coralopyronin gene cluster. We performed analysis on protein sequence homology searches using BLAST (<http://blast.ncbi.nlm.nih.gov/>) and Pfam (<http://pfam.sanger.ac.uk/search/sequence>) searches. The prediction of PKS/NRPS region was performed with online application NRPS-PKS (<http://nrps.igs.umaryland.edu/nrps/>).<sup>[28]</sup> Analysis and annotation of DNA and protein sequences were performed with Geneious 6.0.3 software packages (Biomatters, New Zealand). Sequencing data are accessible at GenBank under accession number KF356280.

### Construction of in-frame deletion mutants *mxnCDEFG* ( $\Delta$ *mxnC-G*), *mxnCDEFGH* ( $\Delta$ *mxnC-H*), *mxnH*, *mxnL*, *mxnM*

In general, construction of in-frame deletion mutants was carried out by amplifying 1000-1250 bp homology regions on each side of the desired deletion area by PCR (see Supporting Information). Each fragment was subcloned to the pJET1.2 blunt vector and sequenced using the primers pJET1.2For and pJET1.2Rev. After sequence verification the homology regions were cloned into the pSWU41 vector<sup>[23]</sup>, which contains a neomycin phosphotransferase (*nptII*) and levansucrose (*sacB*) gene cassette, by using restriction sites indicated in Table S2. The resulting constructs were subsequently electroporated into *M. fulvus* Mx f50. *M. fulvus* Mx f50 was grown in baffled flask with CY medium until an OD<sub>600</sub> between 0.6-0.9 was reached. Cells were then harvested from 2-4 ml culture (1-2 x 10<sup>9</sup> cells ml<sup>-1</sup>) by centrifugation at 12500 rpm for 1 min at room temperature. After two washing steps with 1 ml H<sub>2</sub>O at room temperature, cells were



resuspended in 65  $\mu\text{l}$   $\text{H}_2\text{O}$ . Plasmid DNA (1-2  $\mu\text{g}$ ) was mixed with the cell suspension, and electroporation was carried out under the following conditions: 25  $\mu\text{F}$ , 400  $\Omega$ , 650 V using 0.1 cm electroporation cuvettes and a GenePulser XCell device (Bio-Rad). 1 ml CY medium was directly added to the cell suspension immediately after electroporation and the cells were transferred into a 2 ml centrifuge tube. After 6-8 h cultivation at 30  $^{\circ}\text{C}$  and 800 rpm on a thermomixer, the cells were mixed with 2 ml CY soft agar (CY medium containing 0.7 % agar) and plated on CY agar plates (CY medium containing 1.7 % agar) supplemented with 50  $\mu\text{g ml}^{-1}$  kanamycin or 6.25  $\mu\text{g ml}^{-1}$  oxytetracycline. The plates were incubated at 30  $^{\circ}\text{C}$  for 7-10 days until colonies became visible.

For the construction of markerless double crossover mutants the following strategy was applied: After verification of the single crossover mutants (kanamycin-resistant mutants) by PCR (integration via two different homology regions was possible), a selected single cross over mutant was grown in CY medium in the absence of antibiotics. After 3-4 days 1 ml of the well-grown culture was transferred into 50 ml fresh medium to start another cultivation cycle at 30  $^{\circ}\text{C}$  for 3-4 days. This procedure was repeated for three times to increase the possibility for a second cross over event, which would result in the loss of the inactivation plasmid. Depending on the homology region used for the second cross over this can yield either the wildtype genotype ('revertants') or the expected mutant strain, in which the targeted region is deleted (double cross over mutant). To select for clones in which a second cross over took place, a counter selection system based on the *sacB* gene was used.<sup>[23]</sup> For this, different dilutions of the cell population were plated on CY agar supplemented with 6 % sucrose for counterselection. After 7-10 days, first colonies became visible, which were then grown in liquid culture (CY medium) to isolate genomic DNA for genotypic verification and to extract the cultures for phenotypic analysis as described below.

### **Construction of the *mxnI* mutant by insertional mutagenesis**

To inactivate *mxnI* by insertional mutagenesis, the knock-out plasmid pHSU-mxn13 was constructed. A 1474 bp fragment for homologous recombination was amplified from *M. fulvus* Mx f50 genomic DNA by PCR using the primers mxn50 and mxn51 containing *Bam*HI and *Eco*RV restriction sites. The resulting fragment was cloned into pCRII-TOPO vector to generate pHSU-mxn13. The plasmid was transformed into *M. fulvus* Mx f50 by electroporation as described above. For genotypic analysis, a set of different PCRs using the primer combinations

mxn58/pTOPO-in and mxn59/pTOPO-out was carried out to verify the correct integration of the inactivation plasmid.

### **Phenotypic analysis of wild-type and mutant strain**

Well-grown pre-cultures ( $OD_{600} = 0.7-1.0$ ) of *M. fulvus* Mx f50 and mutants thereof were used to inoculate production cultures in 300 ml baffled flask containing 40 ml CY medium (1 % inoculum). After cultivation for 3 days at 30 °C and 105 rpm, the cultures were harvested by centrifugation. Myxopyronin A is almost exclusively present in the supernatant, which was extracted twice with an equal volume of ethyl acetate after pH adjustment (pH 6.0-7.0). After evaporation of the organic phase, the residue was dissolved in 1 ml methanol. A 2 µl aliquot of the extract was analyzed by High Performance Liquid Chromatography-Mass Spectrometry (HPLC-MS) (Thermo Ultimate 3000 RSLC, coupled to a Bruker Daltonics Amazon Electrospray Ionization (ESI)-MS ion trap instrument) operating in positive ionization mode. Compounds were separated on a Waters Acquity BEH C18 column (50 x 2.1 mm; 1.7 µm particle diameter) at a flow rate of 600 µl min<sup>-1</sup> and 45 °C by a linear gradient with (A) H<sub>2</sub>O + 0.1 % formic acid (FA) to (B) acetonitrile (ACN) + 0.1 % FA at a flow rate of 600 µl min<sup>-1</sup> and 45 °C. The gradient was initiated by a 0.33 min isocratic step at 5 % B, followed by an increase to 95 % B in 9 min to end up with a 1 min flush step at 95 % B before re-equilibration with initial conditions. Detection was carried out by both diode array (DAD) and ESI-MS. For high resolution mass spectrometry analysis, measurements were performed on a Dionex Ultimate 3000 RSLC system using a Waters BEH C18 column (50 x 2.1 mm, 1.7 µm dp) by injecting 2 µl of the methanolic extract. Separation was achieved by the same gradient as above with 0.33 min isocratic step at 5 % B. UV and MS detection were performed simultaneously. Coupling the HPLC to the MS was supported by an Advion Triversa Nanomate nano-ESI system attached to a Thermo Fisher Orbitrap. Mass spectra were acquired in centroid mode ranging from 200-2000 m/z at a resolution of R = 30000.

### **Isolation of 21-desmethyl-myxopyronin A from the $\Delta$ mxnC-G mutant**

A 10 L cultivation was performed in 5 L Erlenmeyer flasks, each containing 2 L CY medium. The flasks were inoculated with 25 ml preculture and incubated on a rotary shaker (130 rpm) at 30 °C. After 3 days, the culture was centrifuged for 20 min at 8000 rpm and the supernatant was extracted two times with a total volume of 5 L ethyl acetate. After evaporation of the organic

phase, the residue was dissolved in 125 ml of methanol-water (95:5), and partition between methanol-water phase and heptane was performed. The methanol-water phase was then evaporated to dryness to yield 460 mg crude extract, which was subjected to a Waters Autopurifier system (XBridge C18 150 x 19 mm, 5  $\mu$ m dp) with a mobile phase consisting of (A) H<sub>2</sub>O + 0.1 % FA and (B) ACN + 0.1 % FA. A linear gradient of 10 % (B) to 85 % (B) in 21 min at a flow rate of 25 ml min<sup>-1</sup> was applied. The fractions containing the derivative were combined and dried in vacuo to give 1.1 mg that was subsequently purified by semipreparative reverse-phase HPLC (Phenomenex Luna C18, 250 x 4.6 mm, 5  $\mu$ m dp column, DAD at 220 and 310 nm). Separation was achieved by a linear gradient of 10 % to 85 % ACN + 0.1 % FA in 20 min at a flow rate of 2.5 ml min<sup>-1</sup> and 30 °C of column temperature to afford 21-desmethyl-myxopyronin A (0.35 mg,  $t_R$  = 25.3 min). NMR data of pure compound were acquired in CD<sub>3</sub>OD at Bruker Ascend 500 MHz.

## 2.6 Supporting Information

**Inactivation of *mxnCDEFG* by in-frame deletion:** To disrupt *mxnCDEFG* by in-frame deletion, a gene inactivation plasmid harbouring two fragments, which are 1016 bp and 1250 bp in size and homologous to the upstream and downstream area of the chromosomal target region, was constructed. These fragments were amplified from *M. fulvus* Mx f50 genomic DNA by PCR using the primers mxn85/mxn119 and mxn87/mxn88. After hydrolysis of the upstream fragment (mxn85/mxn119 product) with *PvuI* and *NotI*, and the downstream fragment (mxn87/88 product) with *NotI* and *BamHI*, the fragments were ligated into pSWU41 hydrolyzed with *PvuI* and *BamHI* to generate pHSU-mxn21. For genotypic analysis of the single cross-over, a set of different PCRs using the primer combinations mxn102/mxn104 and mxn105/mxn103 was carried out to verify the correct integration of the inactivation plasmid. For genotypic analysis of the putative double cross-over mutants, PCRs using the primers mxn102/mxn104, mxn105/mxn103 and mxn102/mxn150 were carried out.

**Inactivation of *mxnCDEFGH* by in-frame deletion:** To disrupt *mxnCDEFGH* by in-frame deletion, a gene inactivation plasmid harbouring two fragments, which are 1016 bp and 1237 bp in size and homologous to the upstream and downstream area of the chromosomal target region, was constructed. These fragments were amplified from *M. fulvus* Mx f50 genomic DNA by PCR using the primers mxn85/mxn119 and mxn83/mxn84. After hydrolysis of the upstream fragment (mxn85/mxn119 product) with *PvuI* and *NotI*, and the downstream fragment (mxn83/84 product)

with *NotI* and *SpeI*, the fragments were ligated into pSWU41 hydrolyzed with *PvuI* and *SpeI* to generate pHSU-mxn22. For genotypic analysis of the single cross-over, a set of different PCRs using the primer combinations mxn102/mxn104 and mxn106/mxn107 was carried out to verify the correct integration of the inactivation plasmid. For genotypic analysis of the putative double cross-over mutants, PCRs using the primers mxn102/mxn104, mxn106/mxn107 and mxn102/mxn149 were carried out.

**Inactivation of *mxnH* by in-frame deletion:** To disrupt *mxnH* by in-frame deletion, a gene inactivation plasmid harbouring two fragments, which are 1121 bp and 1250 bp in size and homologous to the upstream and downstream area of the chromosomal target region, was constructed. These fragments were amplified from *M. fulvus* Mx f50 genomic DNA by PCR using the primers mxn117/mxn118 and mxn83/mxn84. After hydrolysis of the upstream fragment (mxn117/mxn118 product) with *PvuI* and *NotI*, and the downstream fragment (mxn83/84 product) with *NotI* and *SpeI*, the fragments were ligated into pSWU41 hydrolyzed with *PvuI* and *SpeI* to generate pHSU-mxn23. For genotypic analysis of the single cross-over, a set of different PCRs using the primer combinations mxn110/mxn111 and mxn112/mxn107 was carried out to verify the correct integration of the inactivation plasmid. For genotypic analysis of the putative double cross-over mutants, PCRs using the primers mxn110/mxn111, mxn112/mxn107 and mxn110/mxn149 were carried out.

**Complementation of  $\Delta$ *mxnH* by insertional mutagenesis:** To complement  $\Delta$ *mxnH* by insertional mutagenesis, the knock-out plasmid pHSU-mxn47 was constructed. A 981 bp fragment covering part of *mxnL* and *mxnM* for homologous recombination was amplified from *M. fulvus* Mx f50 genomic DNA by PCR using the primers mxn155 and mxn156. In another PCR, the *mxnH* was amplified from the genomic DNA using the primers mxn157 and mxn158. After gel purification, both PCR products were stitched together by overlapping PCR using the primers mxn155 and mxn158. The resulting product was hydrolysed with *PvuI* and *NotI* and ligated to pSWU41 vector hydrolysed with the same enzymes to generate pHSU-mxn47. The plasmid was transformed into *M. fulvus* Mx f50 $\Delta$ pHSU-mxn23 ( $\Delta$ *mxnH*) by electroporation as described above. For genotypic analysis, a set of different PCRs using the primer combinations mxn162/mxn70 and pSWU41-F/mxn163 was carried out to verify the correct integration of the complementation plasmid.

**Inactivation of *mxnL* by in-frame deletion:** To disrupt *mxnL* by in-frame deletion, a gene inactivation plasmid harbouring two fragments, which are 1232 bp and 1109 bp in size and homologous to the upstream and downstream area of the chromosomal target region, was constructed. These fragments were amplified from *M. fulvus* Mx f50 genomic DNA by PCR using the primers mxn113/mxn114 and mxn115/mxn116. After hydrolysis of the upstream fragment (mxn113/mxn114 product) with *PvuI* and *NotI*, and the downstream fragment (mxn115/116 product) with *NotI* and *BamHI*, the fragments were ligated into pSWU41 hydrolyzed with *PvuI* and *BamHI* to generate pHSU-mxn20. For genotypic analysis of the single cross-over, a set of different PCRs using the primer combinations mxn98/mxn100 and mxn101/mxn99 was carried out to verify the correct integration of the inactivation plasmid. Confirmation of the deletion mutant was obtained by Southern Blot analysis (see Figure S1).

**Inactivation of *mxnM* by in-frame deletion:** To disrupt *mxnM* by in-frame deletion, a gene inactivation plasmid harbouring two fragments, which are 1110 bp and 1199 bp in size and homologous to the upstream and downstream area of the chromosomal target region, was constructed. These fragments were amplified from *M. fulvus* Mx f50 genomic DNA by PCR using the primers mxn132/mxn133 and mxn134/mxn135. After hydrolysis of the upstream fragment (mxn132/mxn133 product) with *PvuI* and *SacI*, and the downstream fragment (mxn134/135 product) with *SacI* and *BamHI*, the fragments were ligated into pSWU41 hydrolyzed with *PvuI* and *BamHI* to generate pHSU-mxn34. For genotypic analysis of the single cross-over, a set of different PCRs using the primer combinations mxn140/mxn141 and mxn142/mxn143 was carried out to verify the correct integration of the inactivation plasmid. For notypic analysis of the putative double cross-over mutants, PCRs using the primers mxn140/mxn141, mxn142/mxn143 and mxn140/mxn143 were carried out.

**Table S1.** List of Strains and Plasmids used in this study

Strain/Plasmid	Characteristics	Reference
<b><i>E. coli</i> strains</b>		
HS996	Host for general cloning	Invitrogen
SCS110	Host for cloning to prepare plasmid DNA, free of Dam or Dcm methylation	Stratagene
<b><i>Myxococcus fulvus</i> strains</b>		
Mx f50	Myxopyronin producing wild-type strain	[1]
Mx f50::pHSU-mxn13	Mx f50 harbouring pHSU-mxn13 integrated via a 1474 bp homologous fragment of <i>mxnI</i> ; no myxopyronin production	this study
Mx f50ΔpHSU-mxn20 ( $\Delta mxnL$ )	<i>mxnL</i> in-frame deletion mutant; myxopyronin production	this study
Mx f50ΔpHSU-mxn21 ( $\Delta mxnC-G$ )	<i>mxnCDEFG</i> in-frame deletion mutant; producing of a myxopyronin derivative (21-desmethyl-myxopyronin A)	this study
Mx f50ΔpHSU-mxn22 ( $\Delta mxnC-H$ )	<i>mxnCDEFGH</i> in-frame deletion mutant; no myxopyronin production	this study
Mx f50ΔpHSU-mxn23 ( $\Delta mxnH$ )	<i>mxnH</i> in-frame deletion mutant; no myxopyronin production	this study
Mx f50ΔpHSU-mxn34 ( $\Delta mxnM$ )	<i>mxnM</i> in-frame deletion mutant; myxopyronin production	this study
Mx f50ΔpHSU-mxn23::pHSU-mxn47 ( $\Delta mxnH$ complementation)	$\Delta mxnH$ complementation mutant; myxopyronin production	this study
<b>Plasmids</b>		
pSWU41	Vector contains a neomycin phosphotransferase ( <i>nptII</i> ) gene for selection and a levansucrose ( <i>sacB</i> ) gene for counter selection	[2]
pHSU-mxn13	<i>mxnI</i> gene disruption construct containing 1474 bp homologous fragment of <i>mxnI</i>	this study
pHSU-mxn20	<i>mxnL</i> gene deletion construct, in which a 1632 bp fragment of <i>mxnL</i> was deleted in-frame	this study
pHSU-mxn21	<i>mxnC-mxnG</i> gene deletion construct, in which a 4219 bp fragment of <i>mxnC-mxnG</i> was deleted in-	this study

---

	frame	
pHSU-mxn22	<i>mxnC</i> - <i>mxnH</i> gene deletion construct, in which a 5097 bp fragment of <i>mxnC</i> - <i>mxnH</i> was deleted in-frame	this study
pHSU-mxn23	<i>mxnH</i> gene deletion construct, in which a 756 bp fragment of <i>mxnH</i> was deleted in-frame	this study
pHSU-mxn34	<i>mxnM</i> gene deletion construct, in which a 786 bp fragment of <i>mxnM</i> was deleted in-frame	this study
pHSU-mxn47	$\Delta$ <i>mxnH</i> complementation construct containing 861 bp fragment of <i>mxnH</i>	this study

Table S2. List of primers used in this study

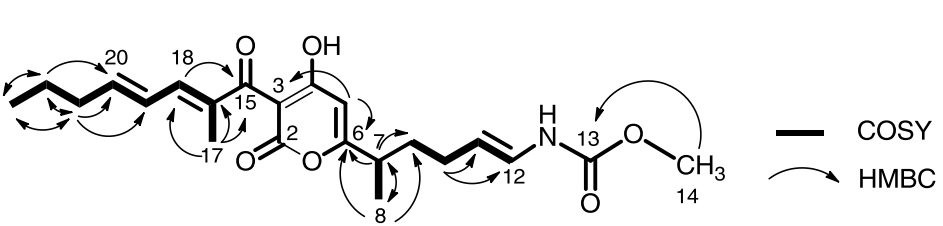
Primer name	Sequence (5'→3')	Restriction sites (in bold)
mxn50	CATGTAGATATCGAACGGCTC CGGTACATC	<i>EcoRV</i>
mxn51	TGTCTAGGATCCACAGCCGCTCCAGGATTC	<i>BamHI</i>
mxn58	GTACGTGCCGTTGGAT	
mxn59	GAGGGGTACTTGAAGAGC	
mxn70	CTTGCGCCCTGAGTGCTT	
mxn79	GGAGGAATACGTCCGAGA	
mxn80	CAATCTGGAGGATCTGCC	
mxn83	GAGCGGCCGCTCGAGATGAAGGTGGAT	<i>NotI</i>
mxn84	ATGACTAGTCTCCTCGCTCTCGAAGTC	<i>SpeI</i>
mxn85	GACACGATCGCAACAGCGGTTCTTTCTCTTTG	<i>PvuI</i>
mxn87	CAAGGCGGCCGCGGGTGATCGCAGGTGAG	<i>NotI</i>
mxn88	TCTGGGATCCTTCGACCTCGGACAGCAG	<i>BamHI</i>
mxn102	CGTCATTCATCCTTGCTCG	
mxn103	TCCAGGCCTCGTAGTTC	
mxn104	TTTCCTCACGTCTCATGG	
mxn105	TGTCGCTGTTGAAGGCAC	
mxn106	TTCTCATCGCGGACTACG	
mxn107	GAGAGAGATTGACGCGAC	
mxn110	GATTCTCTGGGGGCTCCT	
mxn111	CAATCACAACGCAGTCC	
mxn112	TTCTCATCGCGGACTACG	
mxn113	GATACGATCGCCTGGAGGAATACGTCCG	<i>PvuI</i>
mxn114	GTCGCGGCCGCTTTCGTCATGGTGGCTCC	<i>NotI</i>
mxn115	GATACGCGGCCGCTTGAAGGGACTGGGCAAG	<i>NotI</i>
mxn116	TTGCGGATCCACAATCTATCGCGGGTCG	<i>BamHI</i>
mxn117	GACACGATCGGCATGCATGAGGCCTACA	<i>PvuI</i>
mxn118	AATCGCGGCCGCGCATCAGGATCCCCAAGG	<i>NotI</i>
mxn132	GATACACGATCGCGAGCAGGAGGGGTATGT	<i>PvuI</i>
mxn133	TCTATGGAGCTCCATTCCGAAGAACTGGGA	<i>SacI</i>
mxn134	GATACAGAGCTCTTCCTCAATCACCACGGT	<i>SacI</i>
mxn135	TCTATGGGATCCTGACTGACGACGATGAGC	<i>BamHI</i>
mxn140	ACATGTTGGAAGCCGACG	
mxn141	GCTCAGCGTGAAGAGGCT	
mxn142	ACCGTGGAACAGCTCAGG	
mxn143	CGAGATCCAGCACACCAT	
mxn149	GCTTCGCGTGGAGGTCAT	
mxn155	GATACACGATCGGCCGTGCAGGACTACTTG	<i>PvuI</i>
mxn156	ACAATCTATCGCGGGTCG	
mxn157	ATCGACCCGCGATAGATTGTGGAGCTGCAGCG GGTGAT	
mxn158	TCTATGGCGGCCGCTCATGAGTGGCCTCGGCT	<i>NotI</i>
mxn162	GCTTTCCCATCATGACGC	
mxn163	CTCCGCGGTGGTATGTC	



pSWU41-F	GTGCAAAAAAGCGGTTAG	
pTOPO-in	CCTCTAGATGCATGCTCGAG	
pTOPO-out	TTGGTACCGAGCTCGGATCC	
pJET1.2For	CGACTCACTATAGGGAGAGCGGC	
pJET1.2Rev	AAGAACATCGATTTCCATGGCAG	

**Table S3.** Antimicrobial activity of myxopyronin A and its derivative

Test Organism	MIC50 ( $\mu\text{g} / \text{mL}$ )	
	Myxopyronin A	21-Desmethyl-myxopyronin A
<i>Staphylococcus aureus</i> Newman	0.3	11.2
<i>Escherichia coli</i> DH5 $\alpha$	14	>64
<i>Escherichia coli</i> TolC	0.2	0.67
<i>Pseudomonas aeruginosa</i> PA14	>64	>64
<i>Mucor hiemalis</i>	3.5	10.5

**Table S4.** NMR Spectroscopic Data for 21-desmethyl-myxopyronin A (CD<sub>3</sub>OD)


	$\delta_C^a$	$\delta_H^b$ ( <i>J</i> in Hz)	COSY <sup>c</sup>	HMBC <sup>d</sup>
2	no			
3	102.5			
4	no			
5	107.2	5.74 s (7.4)		3, 6
6	168.8			
7	38.6	2.50 m	Me-8	6, Me-8, 9
Me-8	18.4	1.22 d (7.04)	H-7	6, 7, 9
9	35.7	1.53 1.74 m		
10	28.4	2.02 m	H-9, H-11	11, 12
11	110.8	5.06 m	H-10, H-12	
12	125.5	6.4 d (14.1)	H-11	
13	156.5			
OMe-14	52.5	3.66 s		13
15	201.0			
16	136.7			
Me-17	11.8	1.93 s	H-18	15, 16, 18
18	141.5	6.93 d (10.82)	Me-17, H-19	15
19	143.9	6.48 t (14.0)	H-18, H-20	no
20	128.2	6.04m	H-19, H-21	no
21	36.3	2.18 m	H-20, H-22	19, 20, 22, 23
22	23.2	1.46 m	H-21, H-23	20, 21, 23
23	13.9	0.93 t (7.3)	H-22	21, 22

*a* Recorded at 125 MHz; referenced to residual CD<sub>3</sub>OD at  $\delta$  49.15 ppm. *b* Recorded at 500 MHz; referenced to residual CD<sub>3</sub>OD at  $\delta$  3.31 ppm. *c* Proton showing COSY correlation to indicated proton. *d* Proton showing HMBC correlation to indicated carbon No: not observed.

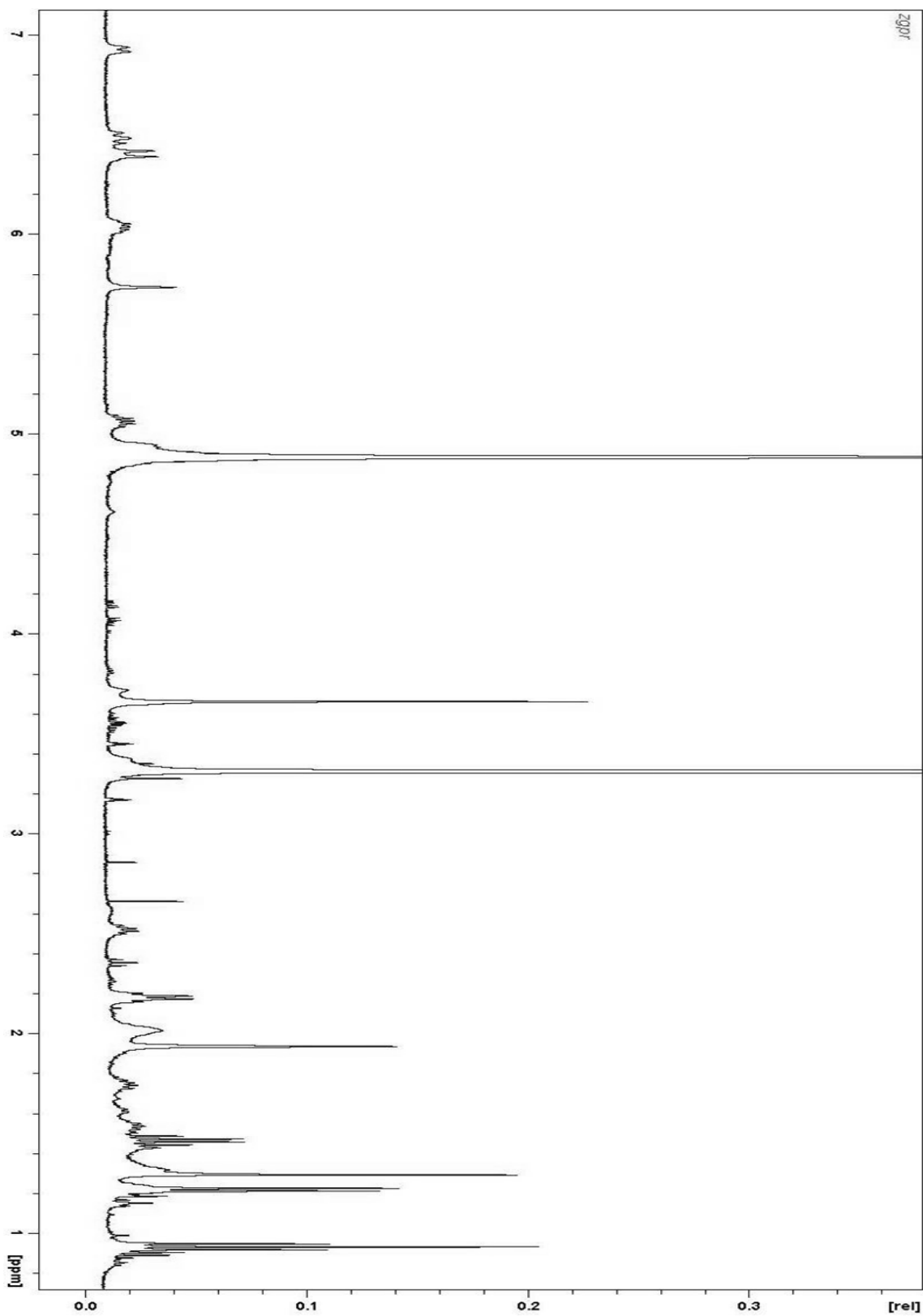


Figure S1.  $^1\text{H}$  NMR spectrum of 21-desmethyl-myxopyronin A in  $\text{CD}_3\text{OD}$

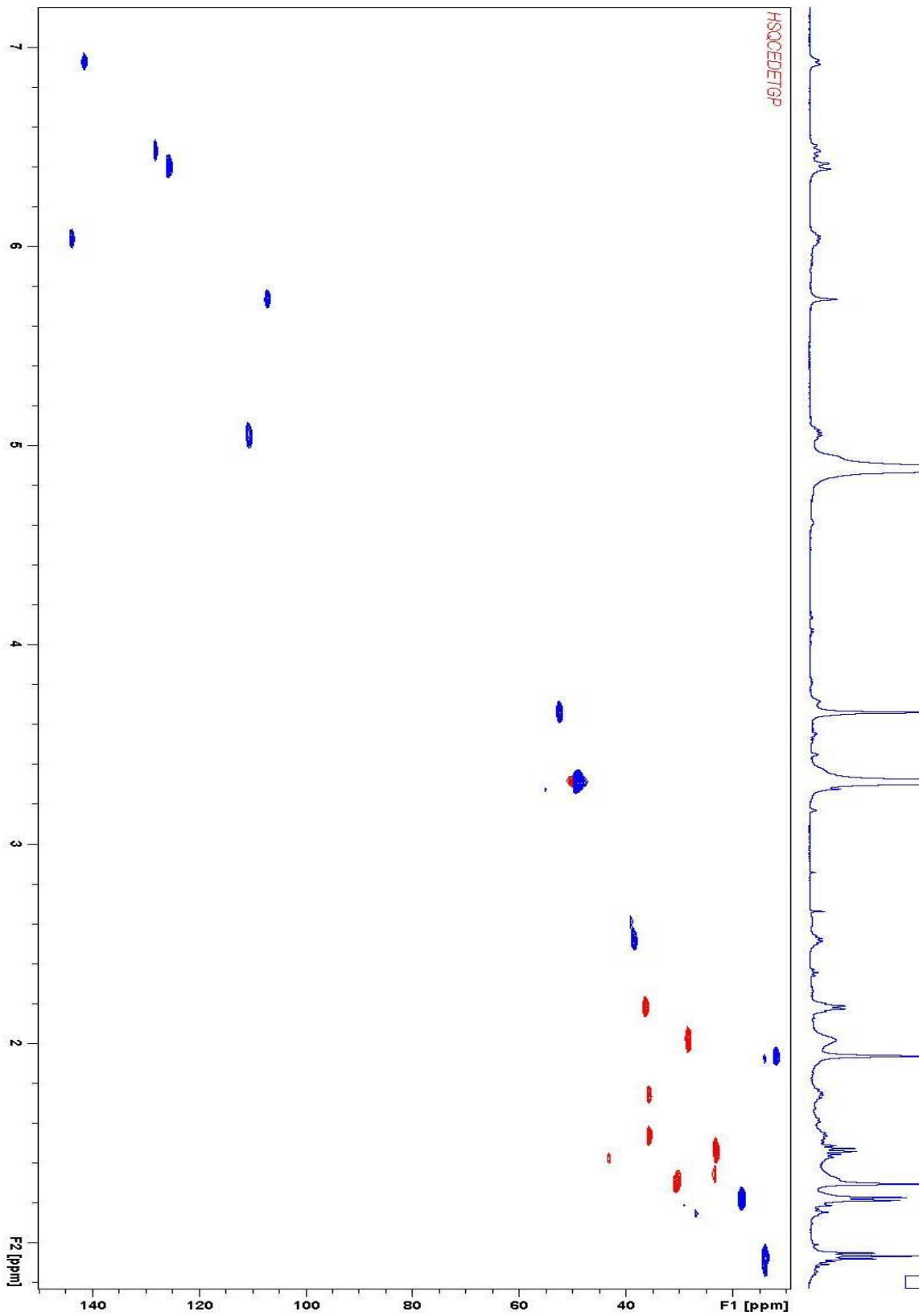
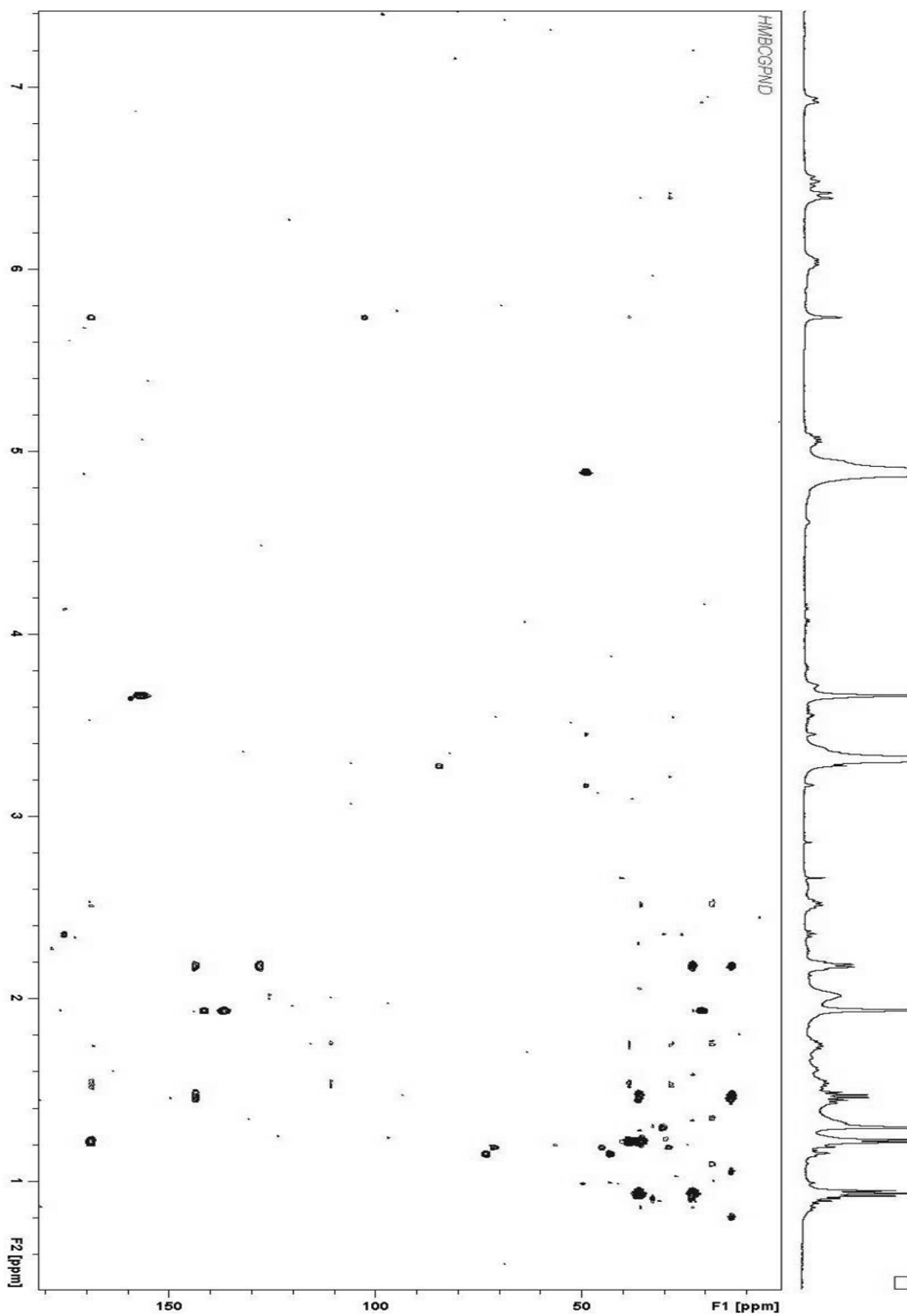


Figure S2. HSQC spectrum of 21-desmethyl-myxopyronin A in CD<sub>3</sub>OD



**Figure S3.** HMBC spectrum of 21-desmethyl-myxopyronin A in CD<sub>3</sub>OD. Signal of the carbonylic C-15 is dropped (21.0 ppm instead of 201.0 ppm) due to a SW of 180.0 ppm.

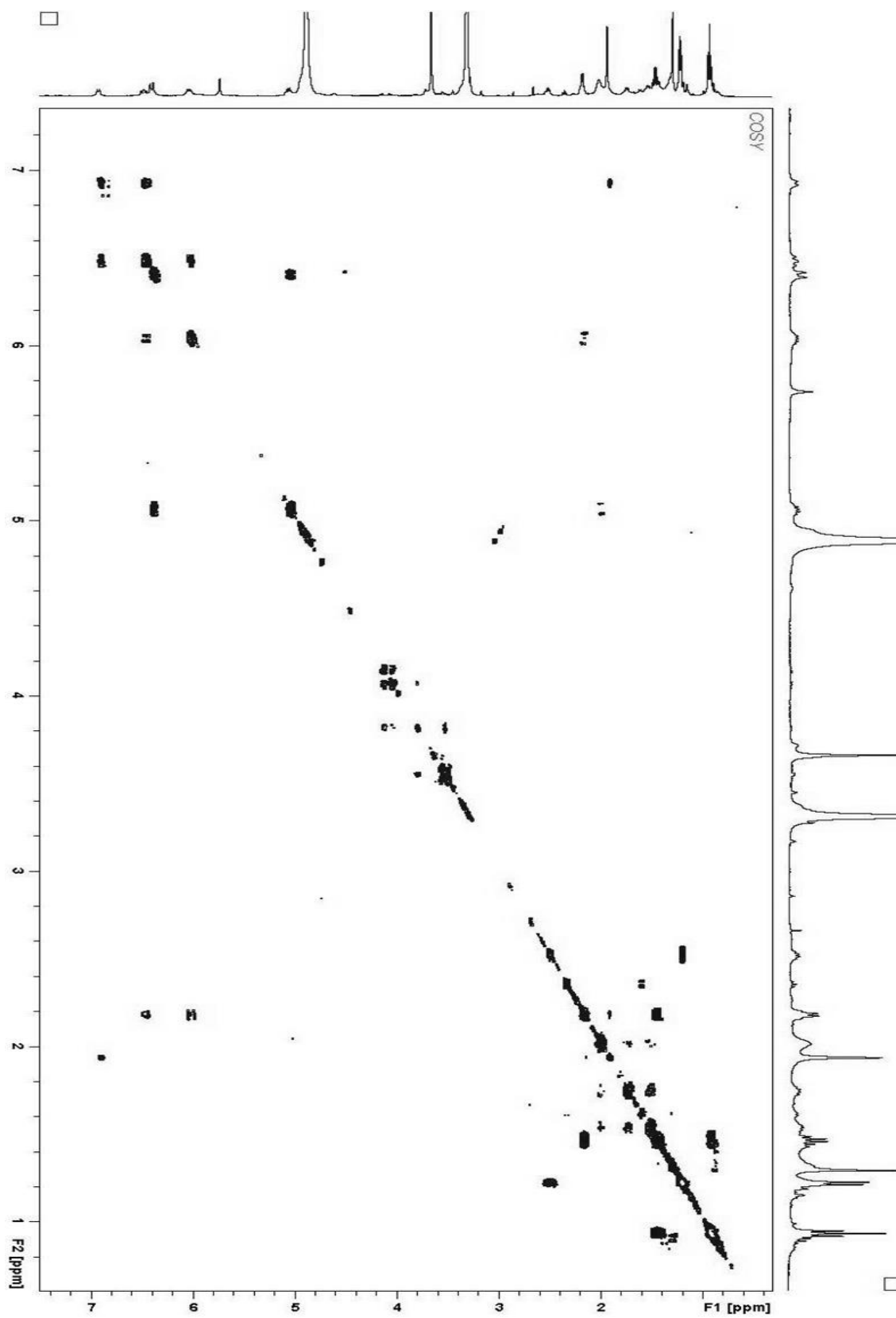
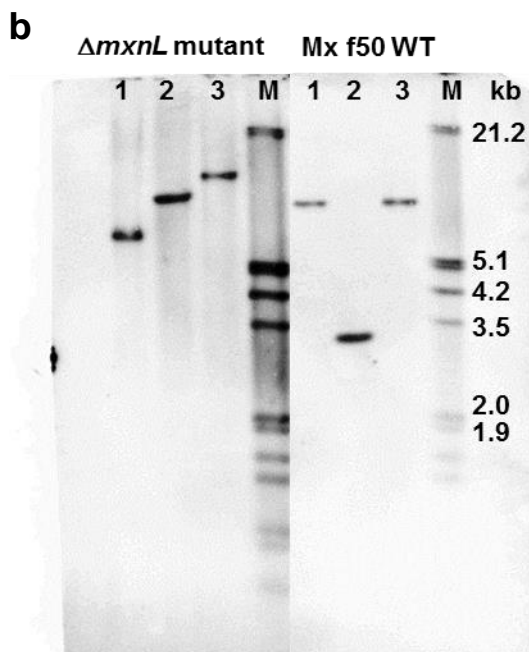
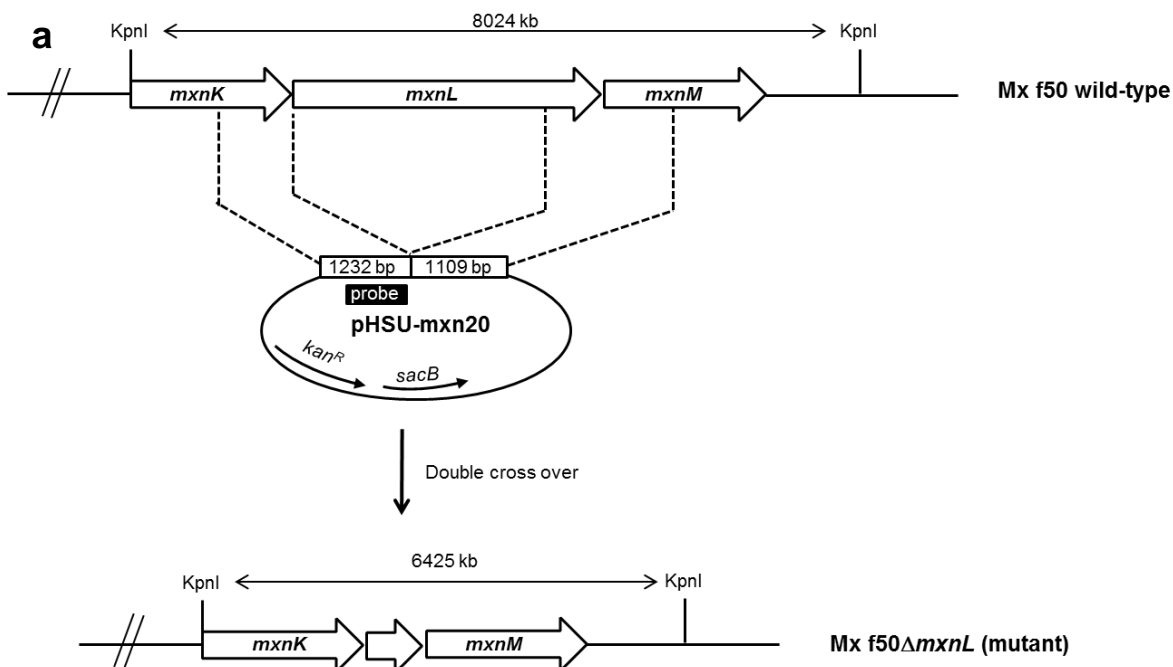


Figure S4. COSY spectrum of 21-desmethyl-myxopyronin A in CD<sub>3</sub>OD



**c**

No.	Restriction enzymes	Mutant (kb)	Wildtype (kb)
1	<i>KpnI</i>	6.4	8.0
2	<i>SphI</i>	>5.7	3.2
3	<i>AgeI</i>	> 10.8	7.9

**Figure S5.** Schematic representation of the in-frame deletion of a 1.6 kb *mxnL* fragment using the construct pHSU-*mxn20* (a), confirmation by Southern blot (b) and the expected fragment size after hydrolysis of wild type and mutant genomic DNA with a set of three restriction enzymes and a DIG-labeled 602 bp probe amplified from Mx f50 genomic DNA using the primers *mxn79* and *mxn80*. M: Marker III (Roche), 1: hydrolysis with *KpnI*, 2: hydrolysis with *SphI*, 3: hydrolysis with *AgeI*.

CP-L	GGAHF <b>D</b> SISL
CP-E1	G---FT <b>S</b> VTL
CP-E2	G---Y <b>D</b> SISF
CP-E3	G---LT <b>S</b> LSL
CP-E4	G---V <b>D</b> SLIG
CP-E5	G---L <b>D</b> SIRV
CP-E6	G---L <b>D</b> SIMT
CP-E6*	G---FD <b>Q</b> LAL
CP-W1	G---L <b>D</b> SLIL
CP-W2	G---F <b>D</b> SITF
CP-W3	G---L <b>D</b> SILA
CP-W4	G---V <b>D</b> SLVN
CP-W5*	G---V <b>D</b> HLDM
CP-W5	G---L <b>D</b> SINV
KS-E1	SEAVDAACASSLVALH-----VEA <b>H</b> GTGT-----IG <b>H</b> AE
KS-E2	SEAVDTACSSSLVAIH-----IET <b>H</b> GTGT-----IG <b>H</b> LE
KS-E3	SEPVDTL <b>C</b> SSSLVAIH-----IEA <b>H</b> GTGT-----V <b>G</b> HLE
KS-E4	SEAITD <b>A</b> CSSSLVAIH-----IEA <b>H</b> GTGT-----IG <b>H</b> LE
KS-E5*	SFAVDS <b>A</b> CASASLTAIH-----VECAAAGS-----V <b>G</b> HLE
KS-E6	SEPVDT <b>A</b> CSSSLIAVQ-----IEA <b>H</b> GTGT-----IG <b>H</b> LE
KS-W1	SFTIDA <b>A</b> CASSLVALH-----VEA <b>H</b> GTGT-----IG <b>H</b> LE
KS-W2*	SLAVDT <b>A</b> CSSSLAAIH-----VECQATGT-----IG <b>H</b> LE
KS-W3	SEPCDT <b>A</b> CSSSLIAIH-----IEA <b>H</b> GSgt-----IG <b>H</b> LE
KS-W4	AMQVDT <b>A</b> CSSSLVAVH-----VEA <b>H</b> GTGT-----IG <b>H</b> TS
KS-W5	SLMVDT <b>A</b> CSSSLTALH-----VEA <b>H</b> GTGT-----IG <b>H</b> LE
MxnB	AITVNAS <b>C</b> LSFFVALE-----EYLPKFTE-----IP <b>H</b> QP
MxnD	GCTVGG <b>A</b> SASGNVALA-----INA <b>H</b> GSAS-----V <b>G</b> HCL
DH-E2	LRD <b>H</b> VIG <b>G</b> KKLL <b>P</b>
DH-E3	LRD <b>H</b> TV <b>F</b> GQRVLL
DH-E4	LRD <b>H</b> VVGSRGV <b>L</b> <b>P</b>
DH-W1	IRD <b>H</b> VV <b>G</b> GNRL <b>I</b> <b>P</b>
DH-W4	VS <b>Q</b> HQ <b>V</b> H <b>G</b> RPV <b>F</b> <b>P</b>
	HXXXGXXXXP
KR-E2	TGGAG <b>A</b> L <b>G</b> -----HAAGQR <b>Q</b> D <b>Q</b> -----F <b>S</b> SLVALTGNVGQTD <b>Y</b> A <b>F</b> A <b>N</b> A
KR-E4	VGGT <b>G</b> G <b>I</b> G-----HSALVL <b>Q</b> D <b>A</b> -----F <b>S</b> SAVGIAGGAGQSN <b>Y</b> A <b>A</b> A <b>S</b> R
KR-W1	VGGGG <b>L</b> G-----HLGGVL <b>S</b> D <b>K</b> -----F <b>S</b> SIVSLLGNVGQAD <b>Y</b> A <b>A</b> G <b>N</b> S
KR-W4	VGGL <b>G</b> G <b>L</b> G-----HSAIVL <b>K</b> D <b>A</b> -----F <b>S</b> SAESFICEAGQSN <b>Y</b> A <b>A</b> A <b>S</b> R

**Figure S6.** Amino acid alignments of conserved regions of the PKS domains by ClustalW. CP: carrier protein;<sup>[3]</sup> KS: ketosynthase;<sup>[4]</sup> DH: dehydratase;<sup>[5]</sup> KR: ketoreductase.<sup>[6]</sup> The active sites or the key conserved amino acid residues are marked in bold. Putative inactive domains are marked with asterisk.



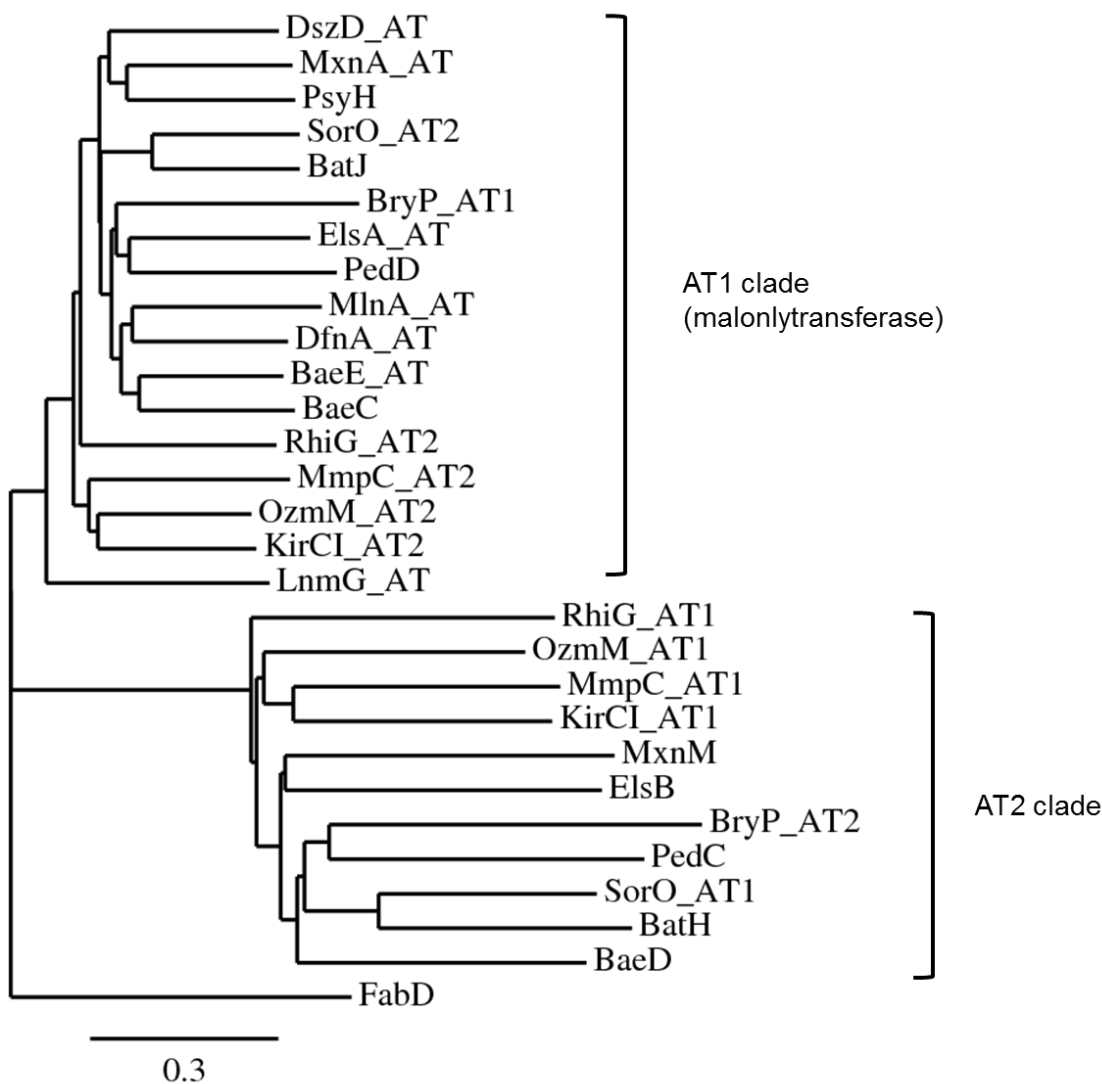


**Figure S7.** Phylogram of AT-like enzymes from various *trans*-AT pathways. Protein sequences were aligned using MUSCLE. Phylogenetic analysis was performed by maximum likelihood interference using PhyML with a Jones-Taylor-Thornton amino acid replacement model.<sup>[7]</sup> Tip labels consist of the protein name with the domain architecture. Sequences from the following pathways were used: BaeC (YP\_001421285), BaeD (YP\_001421286) and BaeE (YP\_001421287) - bacillaene (*Bacillus amyloliquefaciens*); BatH (ADD82949), BatJ (ADD82951) - batumin/kalimantacin (*Pseudomonas fluorescens*); BryP (ABK51299) - bryostatin (*Candidatus Endobugula sertula*); DfnA (ABK51299) - difficidin (*B. amyloliquefaciens*); DszD (AAY32968) - disorazol (*Sorangium cellulosum*); ElsB (YP\_003124936) - elansolid (*Chitinophaga pinensis*); KirCI (CAN89639) - kirromycin (*Streptomyces collinus*); LnmG (AAN85520) - leinamycin (*Streptomyces atroolivaceus*); MlnA (YP-001421027) - macrolactin (*Bacillus amyloliquefaciens*); MmpIII (AAM12912) - mupirocin (*Pseudomonas fluorescens*); OzmM (ADI12766) - oxazolomycin (*Streptomyces bingchengensis*); PedC (AAS47559) and PedD (CAE01104) - pederin (*Paederus fuscipes*); PsyH (ADA82589) - psymberin (uncultured symbiont of sponge *Psammocinia* aff. *bulbosa*); RhiG (YP\_004029399) - rhizoxin (*Burkholderia rhizoxina*); SorO (ADN68489) - soraphen (*Sorangium cellulosum*). Outgroup is the *E. coli* AT from fatty acid biosynthesis, FabD (YP\_489360).

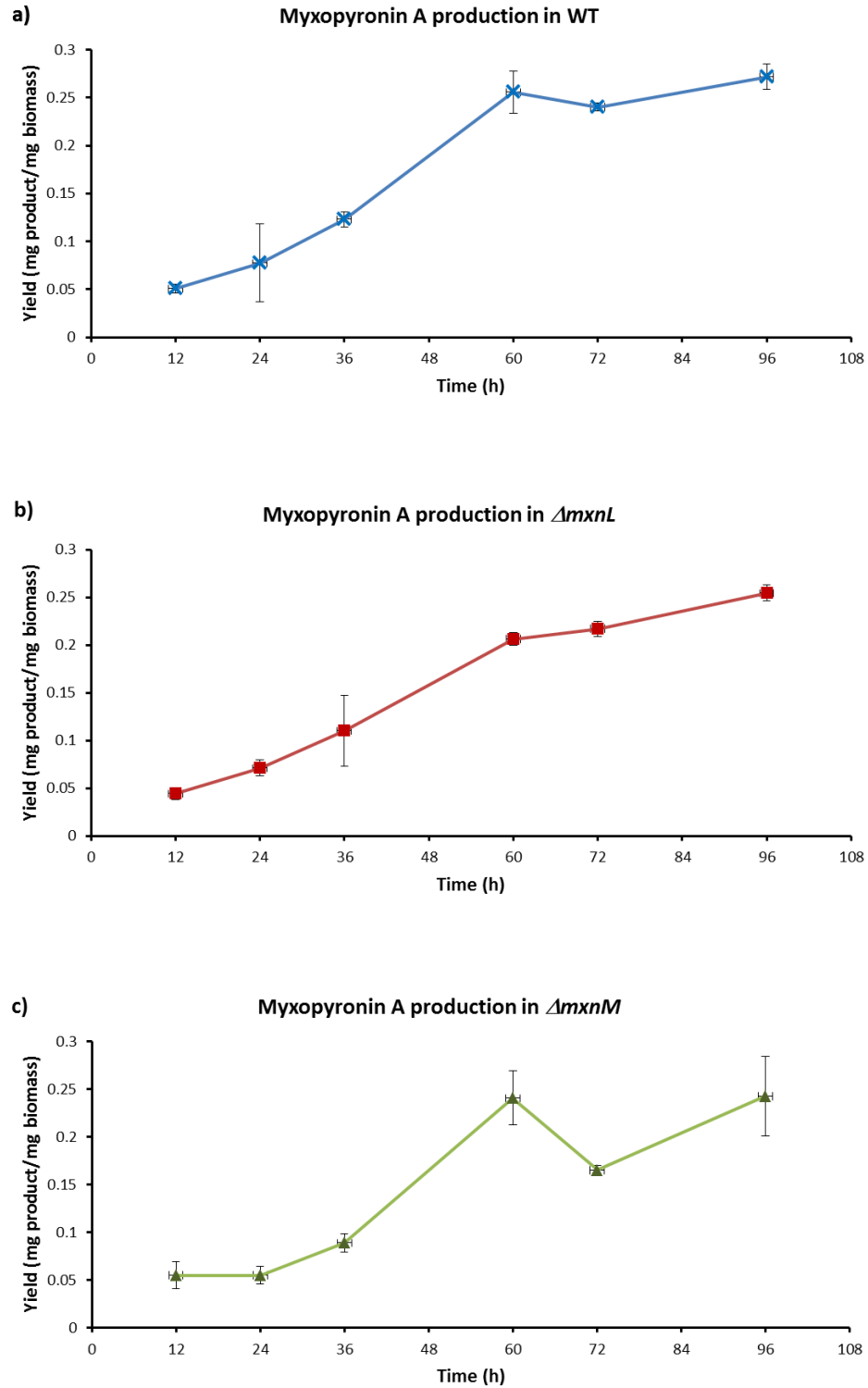
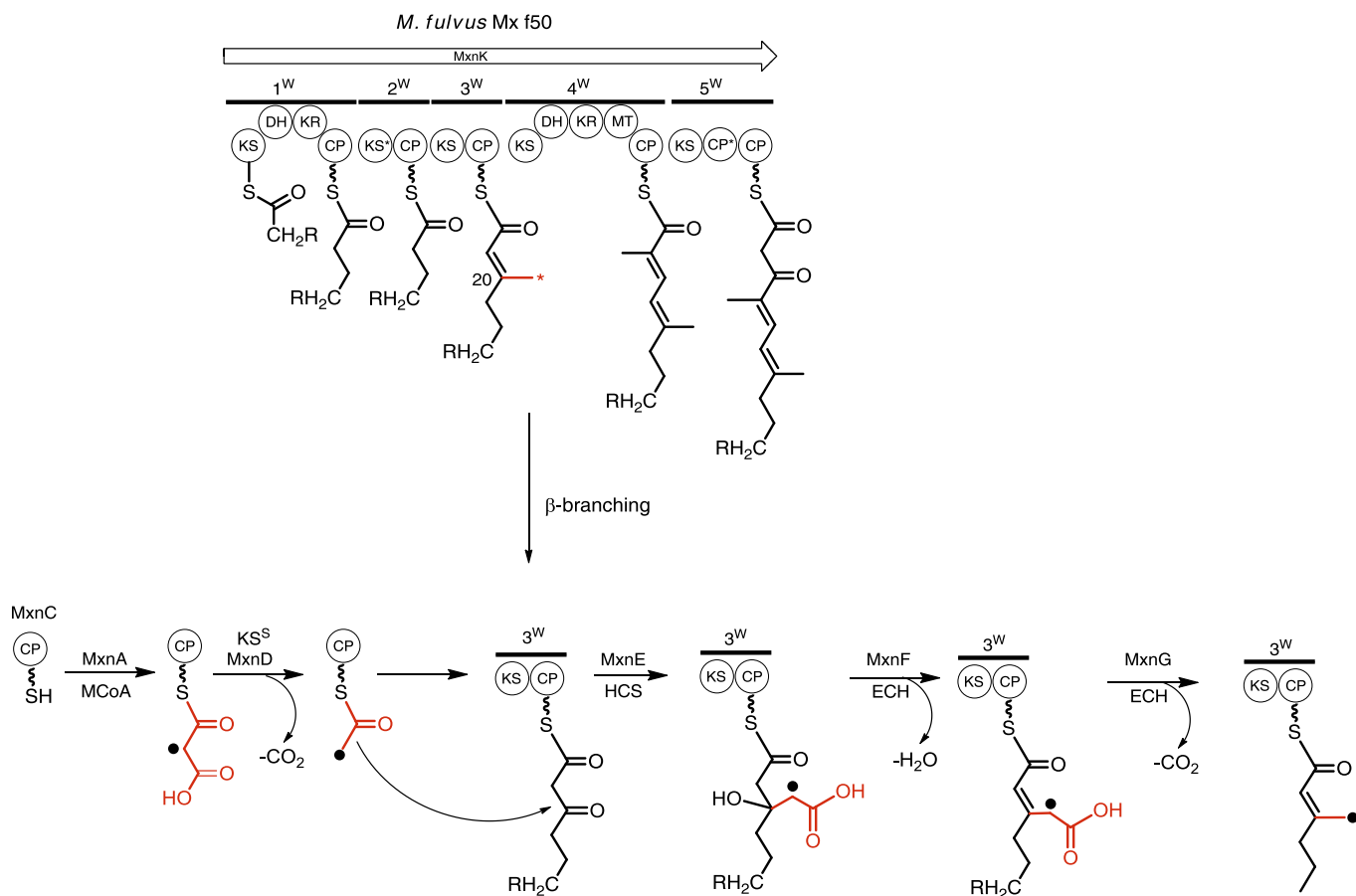


**Figure S8.** Myxopyronin A production profile. Production profile of myxopyronin A by a) *M. fulvus* Mxf50 wild-type (WT), b) *M. fulvus* $\Delta$ pHSU-mxn20 ( $\Delta mxnL$ ), and c) *M. fulvus* $\Delta$ pHSU-mxn34 ( $\Delta mxnM$ ). The data presented in the graph represent the means of three measurements from three independent supernatants



**Scheme S2.** Possible reaction mechanism of MxnC-MxnG in myxopyronin A biosynthesis

## 2.7 References

### 2.7.1 References for Main Text

- [1] M. A. Cooper, D. Shlaes, *Nature* **2011**, 472, 32.
- [2] D. J. Newman, G. M. Cragg, *J. Nat. Prod.* **2012**, 75, 311–335.
- [3] M. S. Butler, A. D. Buss, *Biochem. Pharmacol.* **2006**, 71, 919–929.
- [4] J. Mukhopadhyay, K. Das, S. Ismail, D. Koppstein, M. Jang, B. Hudson, S. Sarafianos, S. Tuske, J. Patel, R. Jansen, H. Irschik, E. Arnold, R. H. Ebright, *Cell* **2008**, 135, 295–307.
- [5] G. A. Belogurov, M. N. Vassilyeva, A. Sevostyanova, J. R. Appleman, A. X. Xiang, R. Lira, S. E. Webber, S. Klyuyev, E. Nudler, I. Artsimovitch, D. G. Vassilyev, *Nature* **2009**, 457, 332–335.
- [6] H. Irschik, K. Gerth, G. Höfle, W. Kohl, H. Reichenbach, *J. Antibiot.* **1983**, 36, 1651–1658.
- [7] H. Irschik, R. Jansen, G. Höfle, K. Gerth, H. Reichenbach, *J. Antibiot.* **1985**, 38, 145–152.
- [8] H. Irschik, H. Augustiniak, K. Gerth, G. Höfle, H. Reichenbach, *J. Antibiot.* **1995**, 48, 787–792.
- [9] S. C. Wenzel, R. Müller, *Mol. BioSyst.* 2009, 5, 567–574.
- [10] Ö. Erol, T. F. Scherberle, A. Schmitz, S. Rachid, C. Gurgui, M. El Omari, F. Lohr, S. Kehraus, J. Piel, R. Müller, G. M. Kçnig, *ChemBioChem* **2010**, 11, 1253–1265.
- [11] C. Hertweck, *Angew. Chem.* 2009, 121, 4782–4811; *Angew. Chem. Int. Ed.* **2009**, 48, 4688–4716.
- [12] W. Kohl, H. Irschik, H. Reichenbach, G. Höfle, *Liebigs Ann. Chem.* **1984**, 1088–1093.
- [13] L. Shimkets, M. Dworkin, H. Reichenbach in *The Prokaryotes*, Vol. 7: Proteobacteria: Delta and Epsilon Subclasses. *Deeply Rooting Bacteria* (Eds.: M. Dworkin, S. Falkow), Springer, Berlin, **2006**, pp. 31–115.
- [14] Y.-Q. Cheng, J. M. Coughlin, S.-K. Lim, B. Shen, *Methods Enzymol.* **2009**, 459, 165–186.
- [15] J. Piel, *Nat. Prod. Rep.* 2010, 27, 996–1047.
- [16] T. Nguyen, K. Ishida, H. Jenke-Kodama, E. Dittmann, C. Gurgui, T. Hochmuth, S. Taudien, M. Platzer, C. Hertweck, J. Piel, *Nat. Biotechnol.* **2008**, 26, 225–233.
- [17] E. M. Musiol, T. Weber, *MedChemComm* 2012, 3, 871–886.
- [18] B. Kusebauch, B. Busch, K. Scherlach, M. Roth, C. Hertweck, *Angew. Chem.* **2010**, 122, 1502–1506; *Angew. Chem. Int. Ed.* **2010**, 49, 1460–1464.
- [19] C. T. Calderone, *Nat. Prod. Rep.* **2008**, 25, 845–853.
- [20] L. Gu, J. Jia, H. Liu, K. Håkansson, W. H. Gerwick, D. H. Sherman, *J. Am. Chem. Soc.* **2006**, 128, 9014–9015.
- [21] Y. Sun, F. Hahn, Y. Demydchuk, J. Chettle, M. Tosin, H. Osada, P. F. Leadlay, *Nat. Chem. Biol.* **2010**, 6, 99–101.
- [22] M. Kopp, H. Irschik, F. Gross, O. Perlova, A. Sandmann, K. Gerth, R. Müller, *J. Biotechnol.* **2004**, 107, 29–40.
- [23] S. S. Wu, D. Kaiser, *J. Bacteriol.* **1996**, 178, 5817–5821.
- [24] K. Jensen, H. Niederkrüger, K. Zimmermann, A. L. Vagstadt, J. Moldenhauer, N. Brendel, S. Frank, P. Pçplau, C. Kohlhaas, C. A. Townsend, M. Oldiges, C. Hertweck, J. Piel, *Chem. Biol.* **2012**, 19, 329–339.
- [25] N. B. Lopanik, J. A. Shields, T. J. Buchholz, C. M. Rath, J. Hothersall, M. G. Haygood, K. Håkansson, C. M. Thomas, D. H. Sherman, *Chem. Biol.* **2008**, 15, 1175–1186.
- [26] A. K. El-Sayed, J. Hothersall, S. M. Cooper, E. Stephens, T. J. Simpson, C. M. Thomas, *Chem. Biol.* **2003**, 10, 419–430.

- [27] J. Sambrook, D. W. Russell, *Molecular Cloning: A Laboratory Manual*, Cold Spring Harbor Laboratory Press, Cold Spring Harbor, NY, **2001**.
- [28] B. O. Bachmann, J. Ravel, *Methods Enzymol.* **2009**, 458, 181–217.

### 2.7.2 References for Supporting Information

- [1] H. Irschik, K. Gerth, G. Höfle, W. Kohl, H. Reichenbach, *J. Antibiot.* **1983**, 36, 1651-1658.
- [2] S. S. Wu, D. Kaiser, *J. Bacteriol.* **1996**, 178, 5817-5821.
- [3] S. C. Findlow, C. Winsor, T. J. Simpson, J. Crosby, M. P. Crump, *Biochem.* **2003**, 42, 8423-8433.
- [4] A. Witkowski, A. K. Joshi, Y. Lindqvist, S. Smith, *Biochem.* **1999**, 38, 11643-11650.
- [5] D. L. Akey, J. R. Razelun, J. Tehranisa, D. H. Sherman, W. H. Gerwick, J. L. Smith, *Structure* **2010**, 18, 94-105.
- [6] P. Caffrey, *ChemBioChem* **2003**, 4, 654-657.
- [7] S. Guindon, O. Gascuel, *Syst. Biol.* **2003**, 52, 696–704.



---

## Chapter 3

# ***In Vitro* Reconstitution of $\alpha$ -Pyrone Ring Formation in Myxopyronin Biosynthesis**

*Hilda Sucipto,<sup>†</sup> Jan Henning Sahner,<sup>†</sup> Evgeny Prusov, Silke C. Wenzel,  
Rolf W. Hartmann, Jesko Koehnke, and Rolf Müller*

*<sup>†</sup> These authors contributed equally to this work*

*Chemical Science*, **2015**, 6, 5076–5085

DOI: 10.1039/C5SC01013F

Published online: 18.05.2015

Reproduced by permission of The Royal Society of Chemistry

### 3 *In Vitro* Reconstitution of $\alpha$ -Pyrone Ring Formation in Myxopyronin Biosynthesis

#### 3.1 Abstract

Myxopyronins are  $\alpha$ -pyrone antibiotics produced by the terrestrial bacterium *Mycrococcus fulvus* Mx f50 and possess antibacterial activity against Gram-positive and Gram-negative pathogens. They target the bacterial RNA polymerase (RNAP) “switch region” as non-competitive inhibitors and display no cross-resistance to the established RNAP inhibitor rifampicin. Recent analysis of the myxopyronin biosynthetic pathway led to the hypothesis that this secondary metabolite is produced from two separate polyketide parts, which are condensed by the stand-alone ketosynthase MxnB. Using *in vitro* assays we show that MxnB catalyzes a unique condensation reaction forming the  $\alpha$ -pyrone ring of myxopyronins from two activated acyl chains in form of their  $\beta$ -keto intermediates. MxnB is able to accept thioester substrates coupled to either N-acetylcysteamine (NAC) or a specific carrier protein (CP). The turnover rate of MxnB for substrates bound to CP was 12-fold higher than for NAC substrates, demonstrating the importance of protein-protein interactions in multimodular polyketide synthases (PKSs). The crystal structure of MxnB reveals the enzyme to be an unusual member of the ketosynthase group capable of binding and condensing two long alkyl chains bound to carrier proteins. The geometry of the two binding tunnels supports the biochemical data and allows us to propose an order of reaction, which is supported by the identification of novel myxopyronin congeners in the extract of the producer strain. Insights into the mechanism of this unique condensation reaction do not only expand our knowledge regarding the thiolase enzyme family but also opens up opportunities for PKS bioengineering to achieve directed structural modifications.

#### 3.2 Introduction

Pathogens are becoming resistant to clinical antibiotics at an accelerating rate. Hence there is an urgent need for new antibacterials, which either act upon new antibiotic targets or exploit novel binding sites in established ones.<sup>1</sup> Myxobacteria are a rich source of bioactive compounds, most of which are derived from polyketide synthase (PKS) and non-ribosomal peptide synthetase (NRPS) pathways.<sup>2</sup> The underlying biosynthetic principles provide a fascinating modular platform to accomplish difficult chemical reactions and became a major source for current clinical drugs. PKS systems are classified into various subtypes according to their functions and

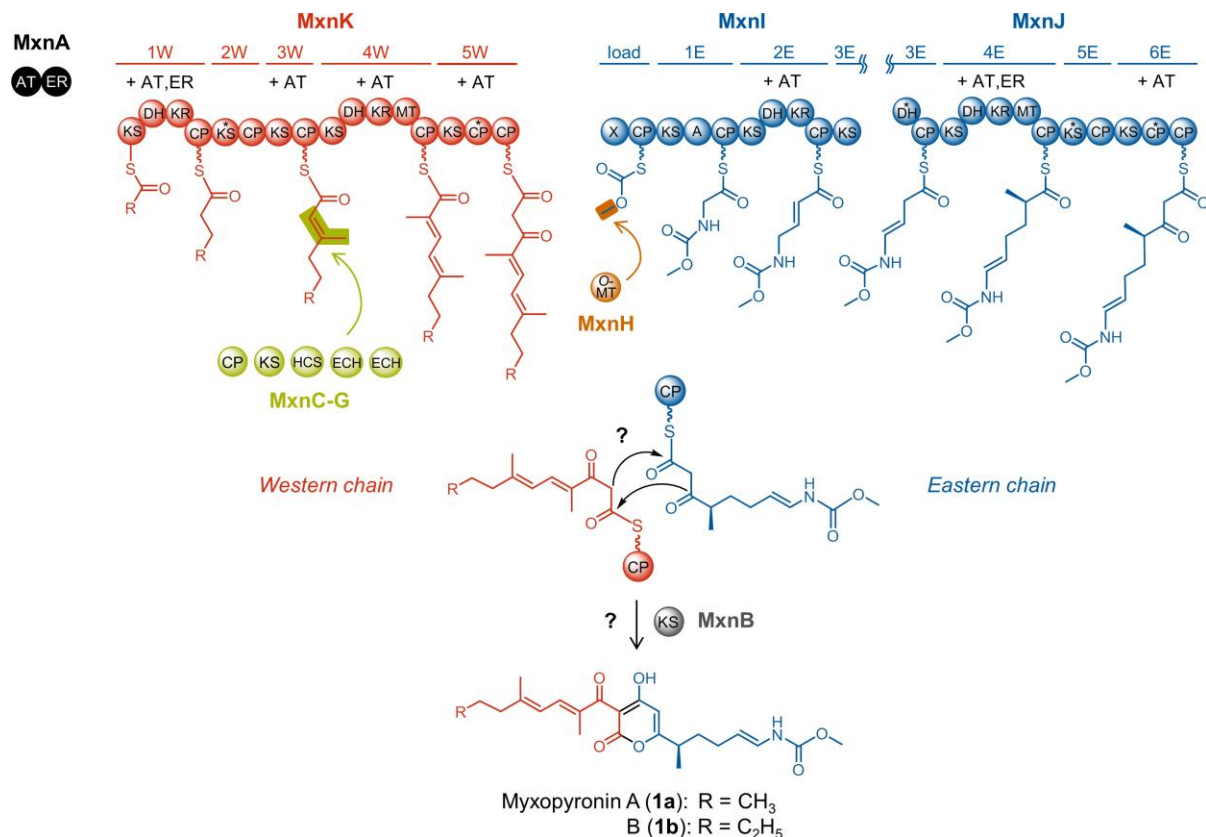


architecture.<sup>3</sup> To date, three types of bacterial PKSs are known; Type I PKSs are composed of multifunctional enzymes organized in modules responsible for non-iterative catalytic steps of one cycle of polyketide chain elongation.<sup>4</sup> Type II PKSs are multi-enzyme complexes that carry a single set of iteratively acting activities.<sup>5</sup> Type III PKSs, or chalcone synthase-like PKSs, also act iteratively as condensing enzymes.<sup>6</sup> One hallmark activity of all PKS pathways are ketosynthases (KSs), usually catalyzing the Claisen condensation of an acyl thioester and a malonyl thioester.

Myxopyronins (1) belong to the  $\alpha$ -pyrone compound class and have been isolated from the Gram-negative soil bacterium *Myxococcus fulvus* Mx f50.<sup>7</sup> Myxopyronins (together with coralopyronin (2) and ripostatin) bind to the “switch region” of bacterial RNA polymerase (RNAP), which represents a novel binding site for RNAP-binding antibiotics. They also display a different mode of inhibition compared to existing RNAP-targeting drugs. Since RNAP is a highly conserved protein, myxopyronins represent a very promising compound class for the development of broad spectrum antibacterial therapeutic agents.<sup>8,9</sup> Feeding studies and the analysis of the biosynthetic gene cluster revealed that myxopyronins as well as coralopyronins are most likely derived from two linear polyketide chains, the eastern and western parts of the molecule. These chains were proposed to be produced by two distinct multimodular PKS/NRPS megasynthetases (Scheme 1).<sup>10-12</sup> It has been postulated that in the last step of myxopyronin and coralopyronin biosynthesis the fully matured  $\beta$ -keto intermediates of the eastern and western chains undergo condensation catalyzed by the stand-alone ketosynthase (KS) enzyme MxnB and CorB, respectively, to form the characteristic  $\alpha$ -pyrone ring.<sup>11,12</sup> The  $\alpha$ -pyrone ring structure proved to significantly contribute to the bioactivity of myxopyronin since the replacement of the pyrone ring with the more stable N-methyl pyridone or phenol led to the loss of its antibacterial activity.<sup>13</sup> Furthermore, the crystal structure of RNAP with myxopyronin showed interactions of the oxygens of the  $\alpha$ -pyrone ring with RNAP residues indicating the importance of this moiety towards its bioactivity.<sup>8</sup>

In fact, there are a number of natural products containing pyrone rings derived from type II and type III PKS systems such as wailupemycin<sup>14</sup> and csypyronin,<sup>15</sup> respectively (Fig. 1). Recently, CsyB has been biochemically characterized as a type III PKS that couples two  $\beta$ -ketoacyl-CoAs, forming the  $\alpha$ -pyrone ring in csypyronin.<sup>16</sup> Only one example of 5-membered ring formation by a type I PKS has been reported so far; a stand-alone KS (RkD, 22 % sequence identity to MxnB) condenses the carrier protein (CP)-bound substrate, forming the tetronate ring during the biosynthesis of the phosphatase inhibitor RK-682.<sup>17</sup> To the best of our knowledge, to

date 6-membered pyrone ring formation by a stand-alone KS has not been reported for a type I PKS pathway.



**Scheme 1.** Model for myxopyronin biosynthesis based on analyses of the native producer strain *Myxococcus fulvus* Mxf50.<sup>12</sup> Western and eastern chain biosynthesis are catalyzed by two separate assembly lines, MxnK shown in red and MxnI/J shown in blue. Abbreviations for assembly line domains: A: adenylation domain, CP: carrier protein domain, DH: dehydratase domain, KR: ketoreductase domain, KS: ketosynthase domain, MT: methyltransferase domain, X: putative inactive KR or truncated phosphoglucomutase/phosphomannomutase domain. Domains marked with an asterisk are assumed to be inactive; assembly line modules 2W, 3E and 5E do presumably not participate in chain elongation. Required acyltransferase (AT) and enoylreductase (ER) activities are indicated for each module and supplied in trans by MxnA. The module 3W intermediate is modified by a  $\beta$ -branching cassette shown in yellow-green consisting of a CP (MxnC), a KS (MxnD), a hydroxymethylglutaryl (HMG)-CoA synthase (HCS; MxnE) and two enoyl-CoA hydratases/isomerases (ECH; MxnF and MxnG). As highlighted in orange, the eastern chain starter unit is modified by an O-methyltransferase (O-MT; MxnH). After chain assembly, the ketosynthase (KS) MxnB is proposed to catalyze pyrone ring formation, which is investigated in the present study.

Here we demonstrate that MxnB is responsible for the condensation of the eastern and the western chains giving rise to myxopyronin. We show that MxnB exhibits substrate flexibility for  $\beta$ -ketoacyl intermediates linked through a thioester bond to either NAC or CP. In addition, the

crystal structure of MxnB reveals an overall typical thiolase fold, which is altered to accommodate the binding and condensation of two long alkyl chains. Structural analysis supports the biochemical findings and allows us to propose an order of reaction for  $\alpha$ -pyrone ring formation in myxopyronin biosynthesis.

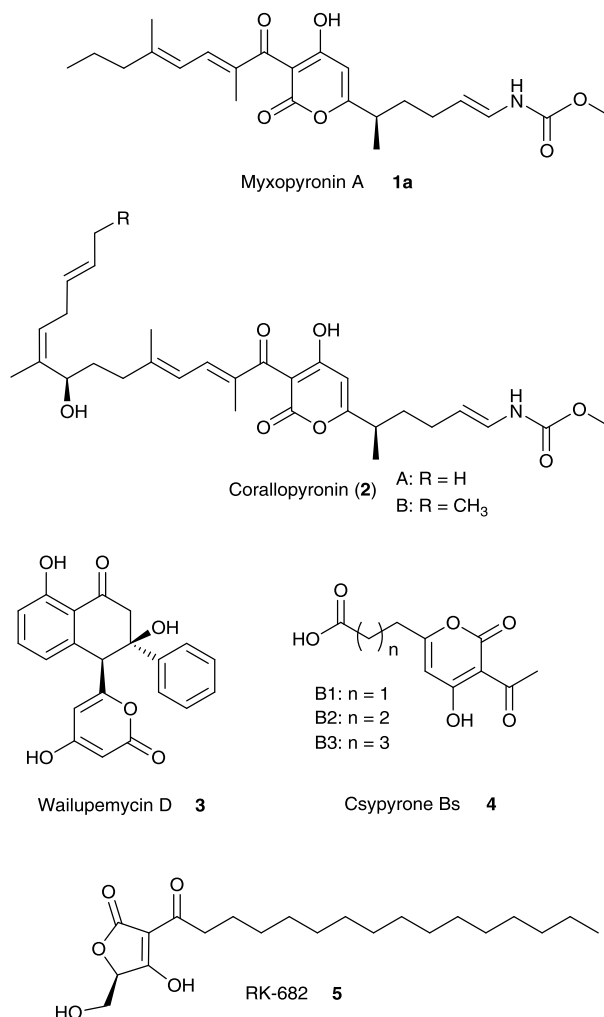


**Figure 1.** Structures of natural products, which are biosynthesized by type I, II, and III PKSs and contain  $\alpha$ -pyrone rings (**1a** and **2**, **3**, and **4** respectively). Compound **5** is generated by a type I PKS and contains a tetronate ring.

### 3.3 Results and Discussion

#### 3.3.1 MxnB is Responsible for $\alpha$ -Pyrone Ring Formation in Myxopyronins

MxnB belongs to the thiolase superfamily of proteins that catalyzes the formation of carbon-carbon bonds via Claisen condensation. BLAST search results identified MxnB as a homolog of

FabH, a  $\beta$ -ketoacyl-[acyl carrier protein (ACP)] synthase III (KAS III), highlighted by the presence of the archetypical cysteine-histidine-asparagine (CHN) catalytic triad.<sup>18,19</sup> The catalytic cysteine (C112 in FabH from *E. coli*) is responsible for the transacylation process, while the histidine and asparagine residues are required for the Claisen-like condensation reaction, interacting with the incoming malonylated CP to enable enolization of the substrate.<sup>19</sup>

We could not identify any protein exhibiting more than 40% sequence identity to MxnB which has been previously biochemically characterized (Table S2). Based on the CHN catalytic triad, KAS III belongs to the same subgroup as chalcone synthase (CHS) enzymes in the thiolase superfamily.<sup>4</sup> CHSs act as homodimeric iterative PKSs catalyzing a series of decarboxylation, condensation, and cyclization reactions.<sup>14;15</sup> Phylogenetic analysis places MxnB between FabH-like and CHS-type enzymes (Fig. S1). Therefore, characterization of MxnB can be seen as a valuable addition to widen the scope of biochemical mechanisms catalyzed within the KAS III family.

In order to provide first experimental evidence that MxnB is responsible for  $\alpha$ -pyrone ring formation we aimed to establish the cyclization reaction *in vitro*. Soluble recombinant MxnB protein with an N-terminal His<sub>6</sub>-tag was overproduced in *E. coli* BL21 (DE3) and purified using one-step Ni-NTA affinity chromatography, to yield 0.3 mg of MxnB from 100 mL of liquid culture. The purified His-tagged MxnB protein had the expected molecular weight of approximately 38.7 kDa (Fig. 2B). The enzyme was incubated with NAC thioesters of the western (**6**) and eastern chains (**7**), serving as mimics of the CP's phosphopantetheine arm bound substrates (Fig. 2A). During biosynthesis the western and eastern chains are assumed to be bound to CP-W5 and CP-E6, respectively (Scheme 1). Analysis of the reaction products using LC-MS showed the formation of **1a** exhibiting an MS<sup>2</sup> fragmentation pattern that was identical to authentic myxopyronin A (Fig. S2).

The limited quantity of available native eastern NAC thioester forced us to use an analogous eastern chain lacking a methyl group and a double bond (**8**) for detailed *in vitro* studies (Fig. 2A). This eastern chain mimic (**8**) was found to be loaded onto MxnB equally well as the native eastern chain (**7**) (Fig. S2). When the experiment was repeated using this modified eastern chain a new product corresponding to the expected myxopyronin derivative **9** (Fig. 2C, assay 3) was detected in the LC-MS analysis. High-resolution mass spectrometry (HRMS) of the compound displayed an ion with  $m/z$  406.2221 (calc. for C<sub>22</sub>H<sub>32</sub>NO<sub>6</sub>, 406.2224), which was assigned as [M+H]<sup>+</sup> of **9**. Its fragmentation was slightly different to standard myxopyronin A,

which is due to the variance in the eastern part of the molecule (Fig. S3). In order to confirm the structure of this novel derivative, it was isolated from an *in vitro* assay and subjected to NMR analysis (Table S3, Fig. S4). To rule out a non-enzymatic condensation, the assay was repeated in the absence of MxnB (assay 1) and in the presence of heat-inactivated MxnB (assay 2). In both cases the reaction did not occur (Fig. 2C). These data provided clear evidence that MxnB is the enzyme responsible for pyrone ring formation.

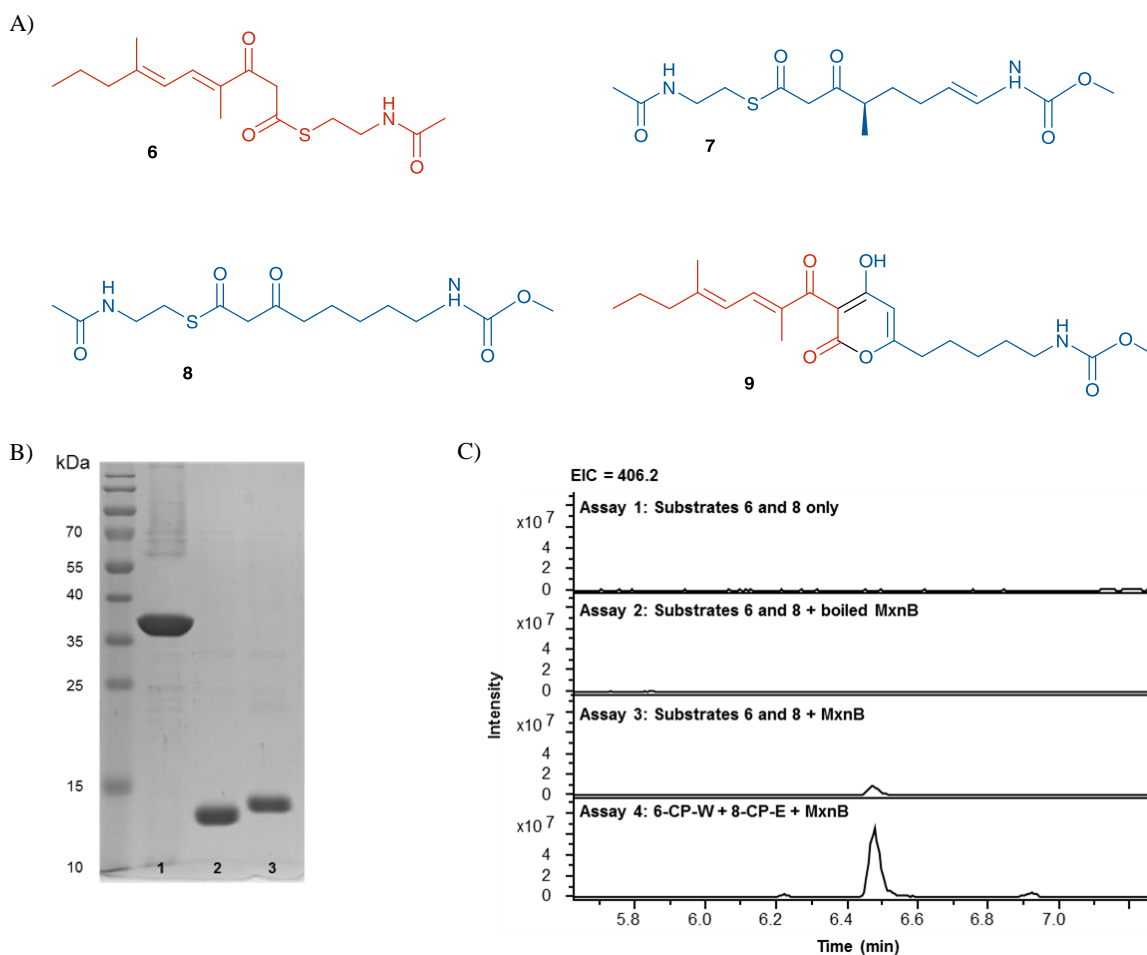


**Figure 2.** Substrates and myxopyronin analogue, SDS Page and LC-MS Analysis of *in vitro* assays. A) SNAC substrates as native western mimic (**6**), native eastern mimic (**7**), analogue mimic of native eastern (**8**), and myxopyronin derivative (**9**). B) Lane 1: His-MxnB (38.7 kDa), lane 2: His-CP-E co-expressed with MtaA (14.7 kDa), and lane 3: His-CP-W co-expressed with MtaA (14.6 kDa) on a 15% SDS gel; C) LC-MS analysis of *in vitro* assays showing extracted ion chromatograms (EIC)  $[M+H]^+ = 406.2$ : assay 1 (**6** and **8** only); assay 2 (**6**, **8**, and boiled MxnB); assay 3 (**6**, **8**, and MxnB); assay 4 (**6-CP-W**, **8-CP-E**, and MxnB).

The small amount of product formed when using NAC substrates suggested that the interaction between cognate CPs and MxnB might be an important factor for efficient

condensation. It has been shown that CP-bound substrates were processed much faster than the corresponding NAC thioesters in a study of 6-deoxyerythronolide B synthase.<sup>20</sup> To optimize the *in vitro* assay we attempted to mimic the *in vivo* conditions by overexpressing CPs from the last module of the western (CP-W5) and eastern (CP-E6) chain assembly lines (hereafter referred to as CP-W and CP-E, respectively). Soluble recombinant CP-W and CP-E proteins with N-terminal His<sub>6</sub>-tags were overproduced in *E. coli* BL21 (DE3) cells and purified by one-step Ni-NTA affinity chromatography, to yield 2.5 mg of each, CP-W or CP-E, from 100 mL of liquid culture. The purified His-tagged CP-W and CP-E proteins had molecular weights of 14.3 kDa and 14.4 kDa, respectively. To simplify the phosphopantetheinylation of the CPs, CP-W and CP-E were phosphopantetheinylated *in vivo* by co-expressing *mtaA*, a gene encoding a broad spectrum 4'-phosphopantetheinyl transferase from *Stigmatella aurantiaca*.<sup>21</sup> We thereby obtained *holo*-CP-W and *holo*-CP-E exhibiting masses of 14.6 kDa and 14.7 kDa, respectively (Fig. 2B, Fig. S5-S6).

It is known that CPs are able to perform self-acylation using CoA or SNAC esters.<sup>22</sup> Thus, we analyzed the ability of *holo*-CP-W and *holo*-CP-E to conduct self-acylation with substrates **6** and **8**, respectively. LC-MS analysis of the product showed a mass shift of 192 Da for *holo*-CP-W indicating the formation of **6**-S-CP-W and a mass shift of 213 Da for *holo*-CP-E in agreement with the generation of **8**-S-CP-E (hereafter referred to as **6**-CP-W and **8**-CP-E, respectively) (Fig. S5-S6).

Incubation of MxnB, **6**-CP-W, **8**-CP-E resulted in a 12-fold increase of product formation compared to the reactions with NAC substrates (Fig. 2C, assay 4). This revealed the importance of CP-MxnB interactions for pyrone ring formation. It also highlights the effect of protein-protein interactions compared to substrate-protein interactions in PKS and especially carrier protein dependent biosynthetic systems.<sup>23</sup>

### 3.3.2 Overall Structure of MxnB

Since the condensation of western and eastern chain requires MxnB to bind two long acyl chain substrates we intended to investigate if there is a structural rationale for this ability. Full-length MxnB (335 residues) with an N-terminal His<sub>6</sub>-tag was expressed and purified as described in the materials and methods section. MxnB crystals belonged to space group P1 and diffracted to 1.67 Å. The structure of MxnB (PDB ID 4V2P) was determined by molecular replacement using the *E. coli* FabH structure (PDB ID 1EBL) as a search model. The crystals contained one biological dimer in the asymmetric unit and the refined

model includes residues 8 - 335 in chain A and 7 - 335 in chain B (Fig. 3A). The missing residues are presumed to be disordered. The MxnB monomer displays the overall typical ketosynthase fold consisting of a five-layered core structure,  $\alpha$ - $\beta$ - $\alpha$ - $\beta$ - $\alpha$ , similar to that of thiolase I.<sup>24</sup> Although the sequence identity of MxnB to *E. coli* FabH is low (29 %), pairwise alignment of the structures gives a C $\alpha$  rmsd of just 1.5 Å over 254 (monomer) and 2.1 Å over 508 (dimer) residues, respectively. The active site of MxnB contains the catalytic CHN triad (C121, H264 and N292, Fig. 3B). The active site C121 is oxidized to cysteine sulfinic acid, but this modification appears to be either transient or a result of crystallization / data collection, since LC-MS analysis of the intact protein showed the expected mass for MxnB with unmodified cysteines.

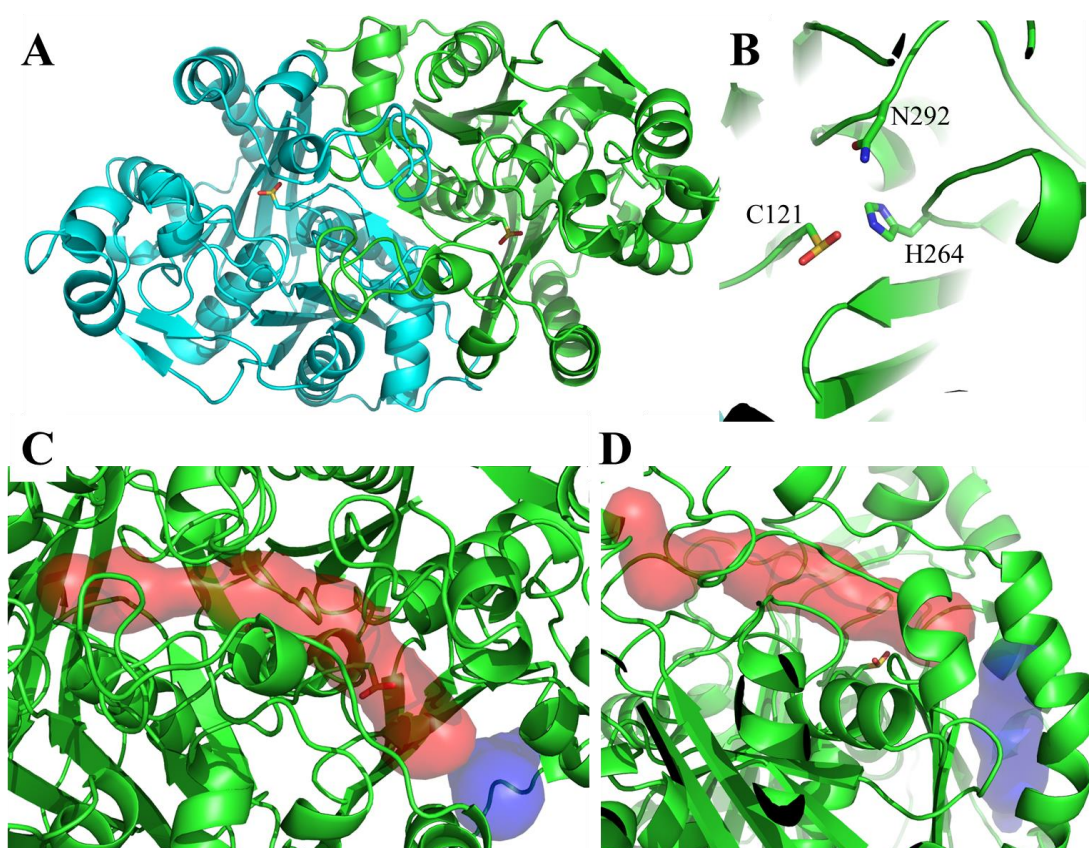


**Figure 3.** A. cartoon representation of the MxnB dimer structure, with monomers colored in cyan and green. The active-site cysteines (C121) are shown as sticks. B. Cartoon representation of the MxnB active site. The residues comprising the catalytic triad are shown as sticks. C. Top view and D. Side view of the two proposed substrate-binding tunnels in MxnB. Canonical tunnel (red) and additional tunnel (blue). Tunnels were predicted using Mole 2.0.<sup>27</sup>

Unlike other ketosynthases such as FabH, MxnB is required to bind and condense two long alkyl chains bound to carrier proteins. The only ketosynthase catalyzing a similar reaction characterized structurally to date (although from a completely unrelated pathway) is OleA.<sup>25</sup> This enzyme aids in synthesizing long chain olefins in *Xanthomonas campestris* and was proposed to possess a second substrate-binding tunnel. Although sequence conservation is low (25 % over 301 residues) the structures are reasonably well conserved (C $\alpha$  rmsd of 2.5 Å over 231 residues, PDB ID 3S23). It was argued that the two helices forming the new hydrophobic binding tunnel were spread apart further in OleA than in other FabH-like structures, where binding of a second long alkyl chain is not required (Fig. S7).<sup>25</sup>

The enzyme CsyB was very recently reported to carry out a similar  $\alpha$ -pyrone ring formation reaction.<sup>26</sup> The sequence identity between MxnB and CsyB (PDB ID 3WXY) is 17 % and pairwise alignment of the structures gives a C $\alpha$  rmsd of 3.7 Å over 262 residues (monomer). The core of both proteins is quite similar on the level of secondary structure and the main structural differences can be found in the periphery, removed from the active site. The relative position of the catalytic triad forming residues (CHN) is conserved in both proteins. CsyB has an additional histidine (H377), which was described as essential for enzymatic activity. In MxnB, this position (CsyB H377) is occupied by a serine (S324). Compared to the structures of MxnB and OleA, the proposed second substrate-binding tunnel is blocked in CsyB.

In MxnB the catalytic C121 is located at a crossroads between two substrate-binding tunnels (Fig. 3C, D). The first, canonical, tunnel (red) and the second (blue) tunnel, positioned as proposed for OleA, have amphipathic character (based on electrostatic surface potential maps generated in ccp4mg<sup>28</sup>). The position of the catalytic C121 in relation to both tunnel entrances strongly suggests that binding of substrate in the blue tunnel and its subsequent transacylation from the CP to MxnB C121 results in the obstruction of the red tunnel entrance. Therefore, we propose that binding of substrate in the red tunnel would have to precede binding in the blue tunnel. Since only one major product is formed by MxnB, it is likely that each tunnel has a chain preference (“eastern chain tunnel” and “western chain tunnel”). Based on the above-mentioned geometry considerations, the substrate accepted by the tunnel marked in red is transferred first during the transacylation process.



### 3.3.3 Initial Biochemical Characterization of MxnB

**Catalytic site of MxnB.** In general, condensation reactions catalyzed by KSs start by loading of the enzyme with the acyl chain. The chain is transferred from the CP and covalently attached to the active site cysteine residue via a thioester bond prior to condensation. We investigated the covalent attachment of **6** or **8** to MxnB and LC-MS analyses confirmed transfer of both substrates to the enzyme (Fig. S8). We then expressed and purified the putative active site mutant C121A (MxnB<sup>#</sup>) to investigate if substrates could still be transferred. We did not observe any mass shift after incubation of MxnB<sup>#</sup> with **6** or **8** and no myxopyronin derivative was formed employing this mutant (loss of catalytic function). These results confirmed that C121 is the catalytic cysteine playing a major role in the transacylation process.

**Substrate Preference for MxnB Priming.** To obtain deeper insights into the reaction mechanism we first addressed the question whether the eastern or western chain substrate is preferentially loaded onto MxnB prior to condensation with the second chain. We performed transacylation experiments with MxnB and primed CPs (**6**-CP-W and **8**-CP-E). Free substrate was completely removed before incubation with MxnB to avoid any interference in the assays. As complete CP priming could not be achieved via self-acylation, the percentages of substrate-loaded CPs were normalized using the deconvoluted mass peak heights in order to establish comparable assay conditions.<sup>29</sup> After incubation of MxnB with a slight excess of either **6**-CP-W (assay 5) or **8**-CP-E (assay 6) the substrate transfer was analyzed at specific time-points using LC-MS. As shown in Figure 4A, the percentage of **6**-CP-W (in relation to unprimed CP-W) decreased much faster than the amount of **8**-CP-E (in relation to CP-E). At the same time, the amount of primed MxnB increased faster in the western chain assay than in the eastern chain assay (**6**-MxnB vs. **8**-MxnB). These results suggest that during myxopyronin biosynthesis MxnB is first loaded with the western chain and then condensed with the eastern chain to form the  $\alpha$ -pyrone ring structure.

**Substrate Preference for the Condensation Reaction.** To further investigate this finding we set up a series of *in vitro* condensation assays including experiments where MxnB was already preloaded with either **6** or **8** to give **6**-MxnB and **8**-MxnB, respectively. The percentages of substrate-loaded MxnB were calculated using the same method as applied to the CPs. The experiments were set up as follows: assay 7 (**6**-MxnB and **8**-CP-E), assay 8 (MxnB, **6**-CP-W and **8**-CP-E), assay 9 (**8**-MxnB and **6**-CP-W), and assay 10 (MxnB, **6**, and **8**). Formation of the myxopyronin derivative (**9**) was analyzed at specific time points as summarized in Fig. 4B. Most

efficient production of **9** was observed in assay 7 containing **6**-MxnB and **8**-CP-E. Production yields in assay 9 (the reverse experiment) were significantly reduced and even lower than in assay 8 with non-primed MxnB. These results indicate that priming of MxnB with the western chain (**6**), which was the preferred scenario in the transacylation experiment (assay 5 vs. assay 6), is important for efficient product formation.

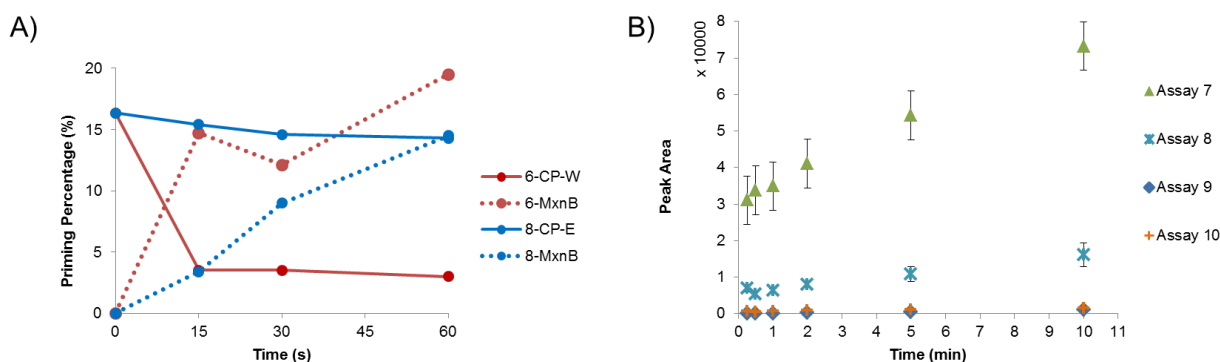


**Figure 4.** LC-MS analysis of substrate transfer and competition assays. A) Percentage of primed MxnB and the remaining loaded-CP B) Time-course for the production of **9** from 15 s to 10 min. Peak area of extracted ion chromatograms for **8** were used for quantification. Assay 7-10: assay 7 (**6**-MxnB and **8**-CP-E), assay 8 (MxnB, **6**-CP-W and **8**-CP-E), assay 9 (**8**-MxnB and **6**-CP-W), and assay 10 (MxnB, **6**, and **8**). Values for assay 9 and 10 data points overlay. Error bars represent the standard error of the mean from three repeats.

### Formation of Myxopyronin Side-products by MxnB

Surprisingly, in addition to the major product **9** we also observed trace amounts of MxnEW (**13**) (reverse orientation), MxnEE (**14**) and MxnWW (**12**) (homo-condensation) in the *in vitro* assays (Fig. 5, Fig. S3). To date, myxopyronin A (**1a**) and myxopyronin B (**1b**) have been the only  $\alpha$ -pyrone compounds reported from the native producer *M. fulvus* Mx f50.<sup>7</sup> To investigate whether these side-products were an artifact of the *in vitro* assays or also produced *in vivo* we performed detailed LC-MS analysis of the *M. fulvus* Mx f50 culture extract. We detected a compound that eluted 0.8 min earlier than **1a** (MxnWE) with an  $m/z$  of 418.22 Da, suggesting the formation of **10** (MxnEW). Comparative MS<sup>2</sup> fragmentation of **1a** and **10** showed three identical fragments:  $[M+H-H_2O]^+$ ,  $[M+H-CH_3OH]^+$ ,  $[M+H-H_2N-CO_2CH_3]^+$  while no further related fragments were observed in **10** due to structural differences (Fig. 5, Fig. S9). HRMS of two additional peaks showed an  $[M+H]^+$  signal at  $m/z$  451.2077 (calc. for C<sub>22</sub>H<sub>30</sub>N<sub>2</sub>O<sub>8</sub>, 451.2074) indicating the presence of MxnEE (**11**) and an  $[M+H]^+$  signal at  $m/z$  385.2374 (calc. for C<sub>24</sub>H<sub>33</sub>O<sub>4</sub>, 385.2373), matching MxnWW (**12**) (Fig. 5, Fig. S9). The pathway is therefore permissive to the formation of

MxnEW, -WW and -EE, even though MxnWE is the main product. Due to the small amounts of these derivatives full structure elucidation by NMR could not be performed.

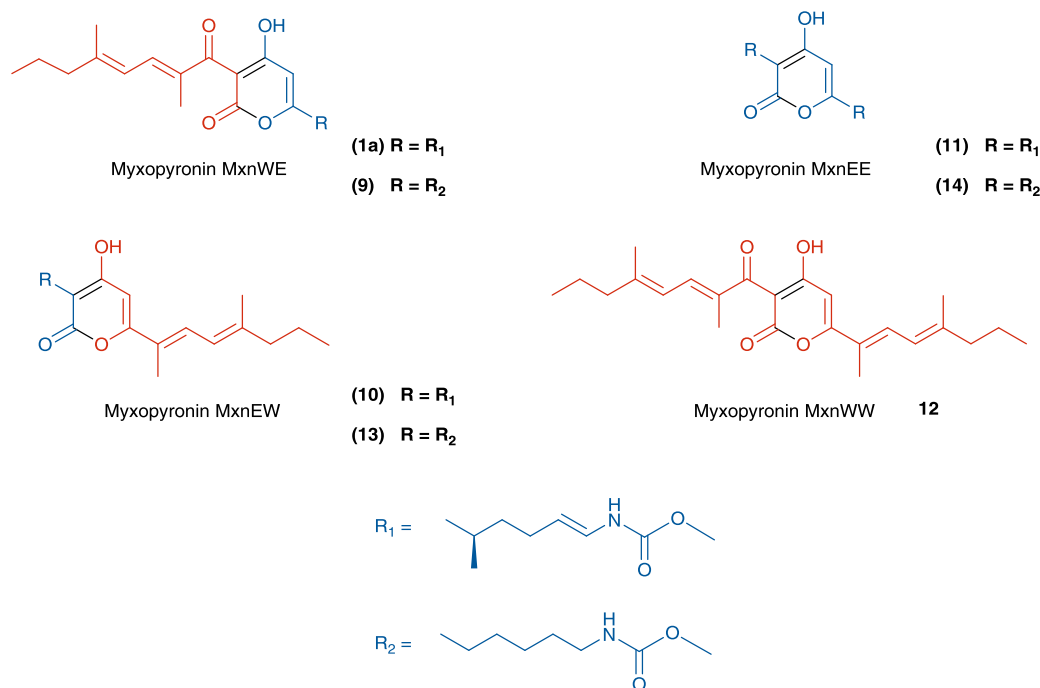


**Figure 5.** Compounds produced by the myxopyronin wild type producer and in the scope of *in vitro* assays. Red represents the western chain, blue represents the eastern chain and black represents the C-C bond formed during the condensation reaction.

The observed production of additional myxopyronin derivatives indicates that in general the biochemistry of  $\alpha$ -pyrone ring formation tolerates a ‘switch’ of one (MxnWW, MxnEE) or even both chains (MxnEW). However, as MxnWE is clearly the dominant product the question arose whether the CPs, the substrates, or a combination of both confers specificity during the transacylation and condensation reaction.

### 3.3.4 Biochemical Insights into $\alpha$ -Pyrone Ring Formation

To investigate possible routes to side-product formation we performed *in vitro* competition assays consisting of MxnB and equal amounts of CP-W and CP-E primed with either substrate **6** or **8** (Fig. S5-S6). Both CPs could be loaded with either substrate and displayed no obvious preference for their native cargo.<sup>30</sup> As expected, rapid product formation (MxnWE) was observed in the presence of **6**-CP-W and **8**-CP-E (assay 11) (Fig. 6). We also detected a small amount of **6**-MxnB, which we assume to be the reaction intermediate. After substrate swapping to **8**-CP-W

and **6-CP-E** (assay 12), MxnWE production decreased significantly (~90-fold after 10 min) indicating that one or both CPs have an impact on the reaction sequence (Fig. 6, Fig. S10). In contrast to assay 11, we observed an additional, large peak corresponding to **8-MxnB**. This might be due to the formation of a ‘catalytically incompetent’ species (**8-MxnB**) as a result of fast eastern chain transfer by CP-W. A similar observation was made in assay 13 where both chains were loaded on CP-W (Fig. 6). Transacylation occurs, but only a very small amount of product is formed (~20-fold decrease after 10min). When both substrates are loaded onto CP-E (assay 14) we observed MxnWE production comparable to assay 11 (Fig. S10).

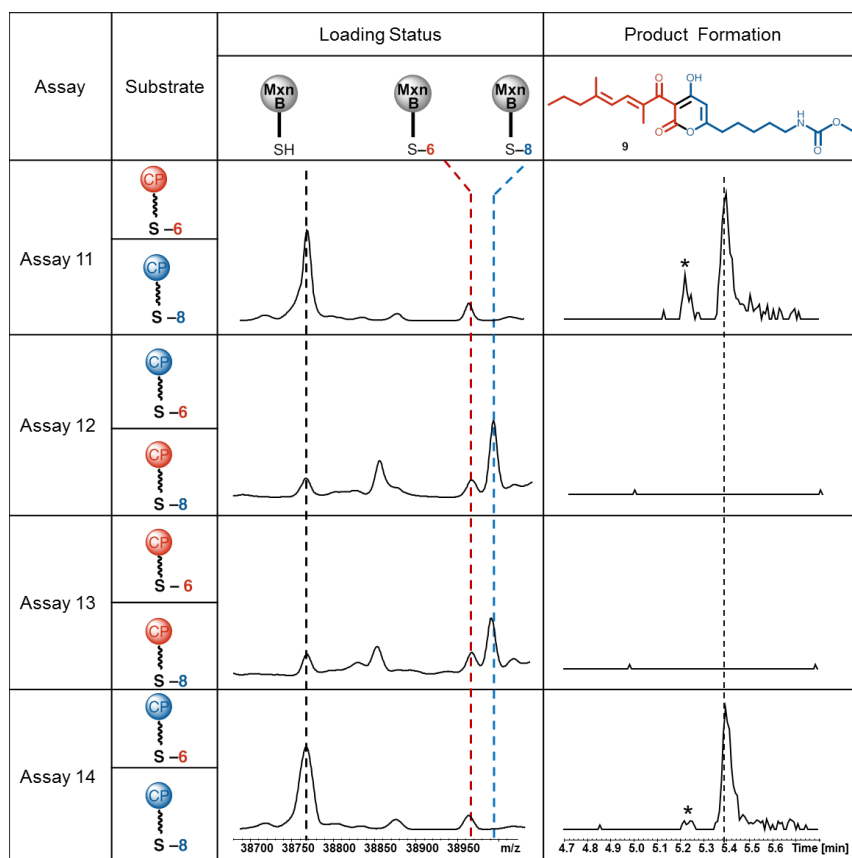


**Figure 6.** LC-MS analysis of competition assays at 1 min. Competition assay 11 (MxnB, **6-CP-W**, **8-CP-E**), assay 12 (MxnB, **8-CP-W** and **6-CP-E**), assay 13 (MxnB, **6-CP-W**, **8-CP-W**) and assay 14 (MxnB, **6-CP-E** and **8-CP-E**). Competition assays were performed in a time course of 15 s to 10 min observing transfer of substrate to MxnB (loading status). EIC of **9** at  $[M+H]^+ = 406.22$  for product formation are shown. Peak with asterisk (\*) is the isomer of **9**.

Detection of side-product formation in the above assays proved difficult. Since we observed a much higher production rate of MxnWE in our preloading experiments (assay 7), we repeated them with two additional combinations. **6-MxnB** incubated with **8-CP-E** (assay 15, a

repeat of assay 7) showed very fast formation of MxnWE (**9**) again. **6**-MxnB incubated with **6**-CP-W (assay 16) results in only trace amounts of MxnWW (**11**) after prolonged incubation. When **8**-MxnB is incubated with **6**-CP-W (assay 17, a repeat of assay 9), we could not observe product formation of the expected MxnEW (**13**). Finally, we tested **8**-MxnB with **8**-CP-E (assay 18) and observed rapid formation of MxnEE (**14**) (Fig. S11).

Overall, these data indicate that substrate transfer (transacylation) by CP-W is rapid and highly specific. In contrast, the results demonstrate that CP-E is able to efficiently mediate both the transacylation as well as the condensation reaction, which may be the result of a less specific substrate transfer. On the substrate side the western chain appears to be more readily transferred to MxnB but we cannot exclude that use of the native eastern chain could alter this observation. We believe that a combination of both CP and substrate confers specificity for  $\alpha$ -pyrone ring formation.

The complexity of the MxnB catalyzed condensation reaction involving CPs and small molecule specificities render a general analysis of substrate specificity *in vitro* difficult. However, we recently indirectly addressed this question *in vivo* in a mutasynthesis study employing a *M. fulvus* mutant unable to biosynthesize the western chain. This study revealed that MxnB is capable of condensing a wide variety of activated synthetic western chains with the CP bound native eastern chain.<sup>31</sup> We used a set of substrate combinations from the mutasynthesis experiments *in vitro*, including those that did not give product *in vivo*. These additional *in vitro* assays (Fig. S12) show a high tolerance of MxnB for non-native SNAC substrates. Even substrates lacking the  $\alpha$ -methyl group and the  $\alpha,\beta$ -double bond of the western chain, which did not give product *in vivo*, were condensed *in vitro* to produce the expected analogues. It is not clear whether the differences between *in vivo* and *in vitro* experiments are due to difficulties in incorporating the non-native analogs into the biosynthetic pathway, or a result of relaxed enzyme specificity in the *in vitro* system. Due to the limited availability of substrates as well as the overall complexity of the reaction we did not attempt further analyses.

### 3.3.5 Mechanism Proposal

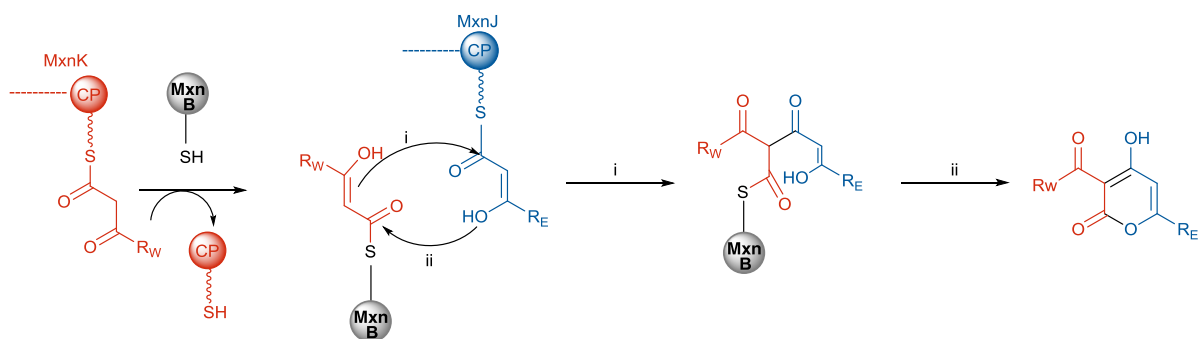
The MxnB structural data suggested that binding of substrate in the red tunnel precedes binding in the blue tunnel. In agreement with the biochemical data, we propose that the western chain is preferentially delivered to and/or bound in the red tunnel, while the eastern chain is preferentially supplied via the blue tunnel. We sought to investigate the existence of the blue tunnel by blocking it via mutagenesis. However, the half of the blue tunnel proximal to the catalytic

cysteine is not trivial to block by mutagenesis. It consists of two helices engaged in complex hydrophobic interactions with each other and a central  $\beta$ -sheet. Only one residue (T322) offers a side-chain orientation suitable for a straightforward mutation (i.e. not contacting other residues). Unfortunately, the candidate residue T322 is close to the junction connecting both tunnels. Therefore mutations are likely to affect binding of chains in both tunnels. In line with this hypothesis mutation of T322 to Leu negatively affected loading of the eastern chain almost twice as much as that of the western chain, but also led to a 7-fold reduction in enzyme activity (Fig. S13, Table S7).

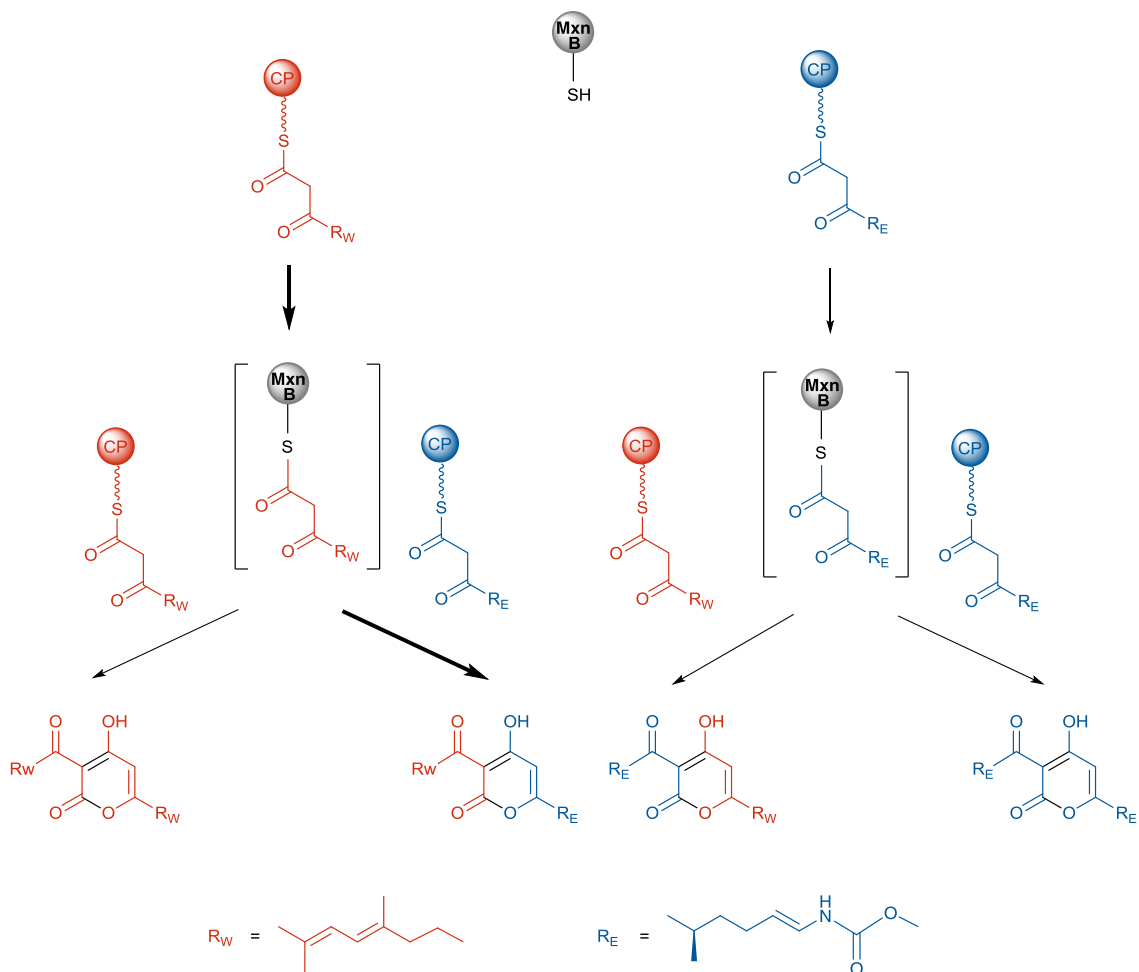
Based on the series of assays described above, we propose the mechanism of pyrone ring formation in myxopyronin as follows: first, CP-W interacts with MxnB and transfers its bound polyketide chain to the MxnB active-site cysteine (C121) (Scheme 2A). CP-E delivers/provides the condensation partner (eastern chain) to the western-chain primed MxnB. Pyrone ring formation results from nucleophilic attack of the  $\alpha,\beta$ -enol-thioester of the KS-bound western chain on the thioester carbonyl of CP-E bound eastern chain to form a diketothioester via a C-C bond formation (i). Subsequently lactonization *via* an enolate intermediate of the eastern chain (ii) occurs to form a C-O bond (Scheme 2A). Although we have no experimental evidence for the timing of the two condensation reactions (i and ii) we consider it more likely that C-C bond formation happens first. Following the same proposed mechanism, all four products, MxnWE and MxnEW, as well as MxnWW and MxnEE could be formed (Scheme 2B). Due to the complexity of the reaction cascade kinetic parameters could not be determined in this study.

An intriguing mechanism proposal was very recently reported for CsyB.<sup>26</sup> This enzyme is a fungal type III PKS involved in acylalkylpyrone (AcAP) formation. In the CsyB catalyzed reaction, acetoacetyl-CoA is loaded onto the active site cysteine C155 and the thioester subsequently undergoes hydrolysis by a water molecule activated through hydrogen bonding to C155 and H377, generating the  $\beta$ -keto acid intermediate. This intermediate was proposed to move to a position of CsyB corresponding to the entrance of the blue tunnel in MxnB. Once the  $\beta$ -keto acid intermediate is relocated, a second reaction cycle occurs: the enzyme is loaded with a fatty acid, which is elongated with one molecule of malonyl-CoA. This  $\beta$ -ketoacyl unit then reacts with the  $\beta$ -keto acid giving rise to AcAP (Fig. S14). A series of *in vitro* assays using  $\text{H}_2^{18}\text{O}$  supported thioester bond cleavage, as this mechanism explains the enzymatic incorporation of one  $^{18}\text{O}$  atom into the product. A similarly positioned water molecule hydrogen bonded to C121 and S324 is observed in the MxnB structure.

A)



B)



**Scheme 2.** A) Proposed mechanism for  $\alpha$ -pyrone ring formation in myxopyronin biosynthesis; B) A flow chart illustrating the reactions that occur during myxopyronin production *in vitro* and *in vivo*. Bold arrow represents the preferred product formation

To investigate whether a similar mechanism exists in the MxnB catalyzed reaction, we performed *in vitro* assays in a similar manner to the work of Mori and coworkers.<sup>26</sup> After quenching of the reaction with iodoacetamide, we could not observe significant incorporation of <sup>18</sup>O into **9** (Table S9). Thus, in myxopyronin biosynthesis two  $\beta$ -ketoacyl chains are condensed to form the  $\alpha$ -pyrone ring without generating a  $\beta$ -ketoacid intermediate through hydrolysis. We therefore hypothesize that the MxnB catalyzed reaction proceeds via a different mechanism than described for CsyB.

### 3.4 Conclusion

The insights gained from this study enable us to propose a biochemical mechanism for  $\alpha$ -pyrone ring formation in myxopyronin biosynthesis. It should be noted that other biochemically characterized ketosynthases related to ring formation and condensation of two substrates such as RkD and CsyB significantly differ from MxnB. RkD is a type I PKS ketosynthase that condenses CP-bound substrates forming the tetronate ring in RK-682 biosynthesis.<sup>17</sup> Furthermore, CsyB represents a type III PKS from *Aspergillus oryzae* that condenses two  $\beta$ -ketoacyl-CoAs to form an  $\alpha$ -pyrone ring.<sup>16</sup> Through biochemical and crystallographic studies, we here elucidated the reaction mechanism of MxnB as catalyzing  $\alpha$ -pyrone formation and thus establish MxnB as a novel member of the ketosynthase family. The unique biochemical features of MxnB might also be used as a starting point to expand the variety of  $\alpha$ -pyrone compounds formed by *in vitro* and *in vivo* reactions.

### 3.5 Experimental Section

**Materials.** The PCR reactions were carried out using Phusion or Taq DNA polymerase (Fermentas) in a peqSTAR 96 Universal Gradient thermocycler (Peqlab): Initial denaturation (3 min, 95 °C); 30 cycles of denaturation (30 s, 95 °C), annealing (30 s, 53 or 57 °C) and elongation (varied based on PCR product length 1 kb/min, 72 °C); and final extension (10 min, 72 °C). DNA fragments were separated by agarose gel electrophoresis and isolated using the peqGold Gel Extraction (Peqlab). The PCR products were cloned into the pJET1.2 blunt (Thermo Fisher Scientific) vector and sequenced using the primers pJET1.2For/pJET1.2Rev.

**Cloning of MxnB.** *mxnB* was amplified from *M. fulvus* Mx f50 genomic DNA by PCR using primers mxn9: 5'-GTC AGA CAT ATG AAC AAC AGC GGT-3' (*Nde*I site is underlined) and mxn10: 5'-CGT CGT AAG CTT TCA GTA GGT GAA AAC CA-3' (*Hind*III site is underlined).



The PCR products were subcloned into the pJET1.2 blunt vector resulting in pJET-HSU-mxn5 and sequenced. pJET-HSU-mxn5 was digested with *NdeI* and *HindIII* and the DNA fragment harboring the MxnB encoding region was cloned into the *NdeI* and *HindIII* site of pColdI resulting in pColdI-HSU-mxn5 encoding MxnB with an N-terminal hexahistidine tag. All strains and plasmids used in this study are listed in Table S1.

**Mutagenesis of MxnB.** MxnB mutants was generated by adapting the method from the QuikChange II XL Site-Directed Mutagenesis (Stratagene) and pColdI-HSU-mxn5 as the template. For the C121A mutation, primers mxn236: 5'-CCATCACCGTCAACGCCTCCGCCCTGAGTTTCTTCGTCGC-3' and mxn237: 5'-GCGACGAAGAACTCAGGGCGGAGGCGTTGACGGTGATGG-3' (mutated nucleotides are underlined) were used. For the T322L mutation, primers mxn296: 5'-GCCGTGCTGACCGGCTGGCTCCGGAGTCTCCTTCGTGG-3' and mxn297: 5'-CCACGAAGGAGACTCCGGAGCCCAGGCCGGTCAGCACGGC-3'. The primers were used to amplify the template to obtain pColdI-MxnB-C121A, pColdI-mxnB-T322L. The clones were verified by sequencing.

**Cloning of CP-E6 and co-expression with MtaA.** *CP-E6* was amplified from *M. fulvus* Mx f50 genomic DNA by PCR using the primers mxn214: 5'-GAT ACG CAT ATG GTC CCC TTC GAG TCG AGC-3' (*NdeI* site is underlined) and mxn215: 5'-TCT ATG AAG CTT TCA TGG CTT CGC TCC CGC-3' (*HindIII* site is underlined). The PCR products were subcloned into the pJET1.2 blunt vector resulting in pJET-HSU-mxn59 and sequenced. pJET-HSU-mxn59 was digested with *NdeI* and *HindIII* and the DNA fragment harboring the CP-E6 encoding region was cloned into the *NdeI* and *HindIII* site of pColdI resulting in pColdI-HSU-mxn59 (CP-E6) encoding CP-E6 with an N-terminal hexahistidine tag. Consequently, pColdI-HSU-mxn59 and pSUMtaA were co-transformed. Subsequent co-expression enabled phosphopantetheinylation of apo-CP-E6 *in vivo* forming holo-CP-E6.

**Cloning of CP-W5 and co-expression with MtaA.** *CP-W5* was amplified from *M. fulvus* Mx f50 genomic DNA by PCR using the primers mxn230: 5'-CTG AGG CAT ATG CGT GCG TTC GAG TCG-3' (*NdeI* site is underlined) and mxn231: 5'- TCT ATG AAG CTT TCA GGC ACA CCA CTC ATT-3' (*HindIII* site is underlined). The PCR products were cloned into the pJET1.2 blunt vector resulting in pJET-HSU-mxn63 and sequenced. pJET-HSU-mxn63 was digested with

*NdeI* and *HindIII* and the DNA fragment harboring the CP-W5 encoding region was cloned into the *NdeI* and *HindIII* site of pColdI resulting in pColdI-HSU-mxn63 (CP-W5) encoding CP-W5 with an N-terminal hexahistidine tag. Furthermore, pColdI-HSU-mxn63 was co-transformed with pSUMtaA to obtain a strain co-expressing pColdI-HSU-mxn63 and pSUMtaA. This co-expression enabled phosphopantetheinylation of apo-CP-W5 *in vivo* forming holo-CP-W5.

**Expression and purification of proteins.** For expression and purification of MxnB, MxnB<sup>#</sup> (C121A), Mxn104 (T322L), holo-CP-E6 and holo-CP-W5, the expression plasmids pHSU-mxn5, pHSU-mxnB<sup>#</sup>, pHSU-mxn104, respectively, were introduced into *Escherichia coli* BL21(DE3). For co-expression of pColdI-HSU-mxn59 and pSUMtaA as well as coexpression of pColdI-HSU-mxn63 and pSUMtaA the respective plasmids were introduced into *Escherichia coli* BL21(DE3). The *E. coli* BL21(DE3) strains carrying the expression plasmids were cultured in LB medium containing 100 µg/mL of ampicillin or with additional 25 µg/mL chloroamphenicol for co-expression with MtaA at 37°C until they reached an OD<sub>600</sub> = 0.5 – 0.6. Expression was induced by addition of isopropyl-β-D-thiogalactopyranoside (IPTG, 0.15 mM) and cultivation was continued at 16°C for 20 h. The cells were harvested by centrifugation (8,000 rpm; 20 min) and resuspended in lysis buffer (40 mM Tris-HCl buffer pH 7.5 containing glycerol 10%, 300 mM NaCl and 10 mM imidazole). Cells were lysed by sonication and a cell-free extract was prepared by removing cell debris by centrifugation at 8,000 rpm for 10 min at 4°C. The cell-free extract was purified by using Ni-NTA Superflow resin (Qiagen), washed sequentially with buffer containing imidazole (10 mM and 20 mM), and eluted with high imidazole (100 mM for CPs and 200 mM for MxnB; MxnB<sup>#</sup>) in the same buffer. The elution buffer was exchanged with buffer (40 mM Tris-HCl buffer pH 7.5 containing glycerol 10%, 300 mM NaCl) using Amicon Ultra 10-k or 30-k (Milipore) to remove imidazole and also to concentrate the proteins. Protein concentrations were estimated based on Bradford assays (Bio-Rad) employing bovine serum albumin as a standard.<sup>1</sup> The purified proteins were flash frozen in liquid nitrogen and stored at -80°C until further use. The recombinant protein masses are listed in Table S4.

**Expression and purification for crystallography.** Full-length *mxnB* with an N-terminal His<sub>6</sub>-tag was cloned into the pCold1 plasmid. The protein was expressed in *Escherichia coli* BL21 (DE3) grown on Lysogeny broth. Cells were grown at 37 °C to an OD<sub>600</sub> = 0.6, cultures subjected to a cold-shock for 30 min and expression induced by addition of 0.1 mM IPTG. Cells were harvested after 16 h growth at 16 °C by centrifugation at 4,000 x g, 4 °C for 15 min and re-

suspended in lysis buffer (200 mM NaCl, 20 mM Tris pH 8.5, 20 mM imidazole, 10 % glycerol and 3 mM  $\beta$ -mercaptoethanol (BME)) with the addition of complete EDTA-free protease inhibitor tablets (Roche) and 0.4 mg DNase  $g^{-1}$  wet cells (Sigma). Cells were lysed by passage through a cell disruptor at 30 kPSI (Constant Systems Ltd) and the lysate was cleared by centrifugation at 40,000  $\times g$ , 4 °C for 20 min. The cleared lysate was applied to a Nickel Sepharose 6 Fast Flow (GE Healthcare) column pre-washed with lysis buffer and protein eluted with 250 mM imidazole in the same buffer. The protein was then subjected to size-exclusion chromatography (Superdex™ 200, GE Healthcare) in 200 mM NaCl, 10 mM Tris pH 8.5, 1 mM TCEP, 10 % glycerol and concentrated to 4.5 mg mL<sup>-1</sup>.

**Crystallization, data collection, and crystallographic analysis.** Crystallization trials of MxnB were set up at 4.5 mg ml<sup>-1</sup>. MxnB crystals were obtained in 0.2 M Ammonium phosphate, 0.1 M Tris pH 8.5 and 50 % MPD. The crystals did not need additional cryoprotection and were flash-cooled in liquid nitrogen. The crystals belonged to space group P1 with cell dimensions  $a = 50.19$  Å  $b = 58.79$  Å,  $c = 62.82$  Å,  $\alpha = 104.75$ ,  $\beta = 105.48$  and  $\gamma = 93.90$ . Diffraction data was collected at ESRF beamline ID29 at 100 K and processed with xia2. The structure of MxnB was determined by molecular replacement using Phaser<sup>2,3</sup> with the Crystal structure of 3-oxoacyl-[acyl-carrier-protein] synthase III from Aquifex aeolicus VF5 as a search model (PDB: 2EBD). Complete manual rebuilding was performed with COOT<sup>4</sup> and refinement was performed using CCP4 REFMAC5<sup>5</sup> and Phenix Refine.<sup>6</sup> The statistics of data collection and refinement are summarized in Table S4. All molecular graphics figures were generated with the program Pymol.<sup>7</sup>

**In vitro reconstitution of myxopyronin (or derivatives) formation.** The one pot reaction mixture in 40 mM Tris-HCl buffer pH 7.5, glycerol 10%, 300 mM NaCl (100  $\mu$ L) containing 100  $\mu$ M CP-W5, 100  $\mu$ M CP-E6, 30  $\mu$ M MxnB and 1 mM substrates (**6** with **7** or **6** with **8** or **S1-S4** with **8**) was incubated at 37 °C for 2 h. Reaction mixtures were extracted with ethyl acetate and the organic layer was evaporated. The residue was dissolved in 100  $\mu$ l methanol and a 5  $\mu$ l aliquot of the extract was analyzed by HPLC-MS.

**Isolation of in vitro product.** Large scale of *in vitro* assay containing 100  $\mu$ M CP-W5, 100  $\mu$ M CP-E6, 30  $\mu$ M MxnB and 0.5 mM **6** and **8** was incubated in 40 mM Tris-HCl buffer pH 7.5, glycerol 10%, 300 mM NaCl (total 9 mL) for 9 h at 37 °C. Reaction mixtures were extracted with

ethyl acetate and the organic layer was concentrated *in vacuo*. The crude extract was subsequently purified by semi preparative reverse-phase HPLC (Phenomenex Jupiter® 4  $\mu\text{m}$  Proteo 90 Å, C12, 250 x 10 mm, DAD at 220 and 310 nm). Separation was achieved by a linear gradient of 10% ACN + 0.1 % FA for 6 min, 10 % to 85 % ACN + 0.1 % FA in 4 min, 85% to 100% ACN + 0.1 % FA in 20 min at a flow rate of 2.5 ml min<sup>-1</sup> and 30 °C of column temperature to afford semipure **9** (0.3 mg,  $t_{\text{R}}$  = 17.5 min). A full set of NMR spectra was recorded with the semipure fraction (due to low quantity) before final purification was achieved. NMR data of semipure and pure compound (0.1 mg) were acquired in CD<sub>3</sub>OD on a 700 MHz *Avance III* (Ascend) spectrometer by *Bruker BioSpin GmbH*, equipped with a 5mm TXI cryoprobe, at 298 K.

***In vitro* self-acylation of the CPs and MxnB.** A reaction mixture containing 100  $\mu\text{M}$  of CP-W5 or 100  $\mu\text{M}$  of CP-E6 or 30  $\mu\text{M}$  of MxnB with 1 mM of **6** (JHS486) or **8** (JHS274) was incubated at 37°C for 2 h in 40 mM Tris-HCl buffer pH 7.5, glycerol 10%, 300 mM NaCl to obtain **6-CP-W**, **8-CP-W**, **6-CP-E**, **8-CP-E**, **6-MxnB**, and **8-MxnB**. For the purpose of competition assays, the leftover substrates were removed by gel filtration using a PD-10 column and further concentrated with Amicon Ultra 10-K or 30-K concentrators as described above. Substrate transfer to CPs was confirmed by LC-ESI-MS and the percentage of loaded-substrate CPs were calculated using the deconvoluted mass peak heights.

**Assays 5-6 and Assays 15-18.** The reaction master mixture in the same buffer as above (225  $\mu\text{L}$ ) containing 3.76  $\mu\text{M}$  of loaded CPs final concentration as produced in the assay above was aliquoted to 10 eppendorf tubes which were kept on ice. In these assays, we keep the ratio between the non-acylated and acylated CPs constant. When the experiment was started, the eppendorf tube was incubated at 30 °C for 1 min before addition of MxnB (2.3  $\mu\text{M}$  a final concentration). The reaction was stopped by putting the tubes into liquid N<sub>2</sub> at time points: 15 s, 30 s, 1 min, 2 min, 5 min, 10 min. Liquid N<sub>2</sub> was chosen as a way to avoid MxnB precipitation. One part of the sample was used for protein analysis and another part of the sample was quenched by the addition of ice-cold 40% MeOH for product analysis. All sample preparations were performed in the cold room and the autosampler of the HPLC was kept at 5 °C to avoid occurrence of any further reactions.

**Competition Assays 7-10 and Assays 11-14.** The reaction master mixture in the same buffer as above (200  $\mu$ L) containing 4  $\mu$ M of loaded CPs and 4  $\mu$ M of loaded MxnB was incubated at 30 °C, and samples of 20  $\mu$ L were taken at time points: 15 s, 30 s, 1 min, 2 min, 5 min, 10 min. In these assays, we keep the ratio between the non-acylated and acylated CPs constant. For assay 10, 14.81  $\mu$ M of MxnB was and 0.5 mM of **6** or **8** was used. The reaction was quenched by the addition of 30  $\mu$ L ice-cold 40% MeOH. The samples were then measured by HPLC-MS for product detection.

**H<sub>2</sub><sup>18</sup>O water experiments.** A 50  $\mu$ L reaction mixture in 40 mM Tris-HCl buffer pH 7.5 containing 2  $\mu$ M of loaded CPs and 7.5  $\mu$ M of MxnB in 75% H<sub>2</sub><sup>18</sup>O was incubated at 37 °C for 2 h. The mixture was then quenched with iodoacetamide (final 1 mM). After centrifugation at 15,000 rpm for 2 min, the supernatant was divided into two aliquots. One volume of MeOH was added to the first aliquot for LCMS measurement. The second aliquot was dried using a Genevac evaporator and dissolved in H<sub>2</sub><sup>16</sup>O for 5 h further incubation. One volume of MeOH was added to the aliquot for LCMS measurement.

**LC-ESI-MS measurements for protein analysis.** All ESI-MS-measurements for intact proteins were performed on a Dionex Ultimate 3000 RSLC system using an Aeris Widepore XB-C8, 150 x 2.1 mm, 3.6  $\mu$ m dp column (Phenomenex, USA). Separation of 1  $\mu$ L sample was achieved using a linear gradient from (A) H<sub>2</sub>O + 0.05 % FA to (B) ACN + 0.05 % FA at a flow rate of 300  $\mu$ L min<sup>-1</sup> and 45 °C. The gradient was initiated by a 1.0 min isocratic step at 2 % B, followed by an increase to 60 % B at 8 min to end up with a 3 min step at 60 % B before reequilibration in initial conditions. UV spectra were recorded with a DAD in the range from 200 to 600 nm. The LC flow was split to 75  $\mu$ L/min before entering the maXis 4G hr-ToF mass spectrometer (Bruker Daltonics, Bremen, Germany) using the standard Bruker ESI source. In the source region, the temperature was set to 180 °C, the capillary voltage was 4000 V, the dry-gas flow was 6.0 l/min and the nebulizer was set to 1.1 bar. Mass spectra were acquired in positive ionization mode ranging from 600 – 1800 m/z at 2.5 Hz scan rate. Protein masses were deconvoluted by using the Maximum Entropy algorithm (Copyright 1991-2004 Spectrum Square Associates, Inc.).

**HPLC-MS measurements to analyze the products of *in vitro* assays.** High Performance Liquid Chromatography-Mass Spectrometry (HPLC-MS) (Thermo Ultimate 3000 RSLC, coupled to a Bruker Daltonics amaZon Electrospray Ionization (ESI)-MS ion trap instrument)

was operated in positive ionization mode. Compounds were separated on a Waters Acquity BEH C18 column (50 x 2.1 mm; 1.7  $\mu\text{m}$  particle diameter) at a flow rate of 600  $\mu\text{l min}^{-1}$  and 45  $^{\circ}\text{C}$  by a linear gradient with (A)  $\text{H}_2\text{O} + 0.1\%$  formic acid (FA) to (B) acetonitrile (ACN) + 0.1 % FA at a flow rate of 600  $\mu\text{l min}^{-1}$  and 45  $^{\circ}\text{C}$ . The gradient was initiated by a 0.33 min isocratic step at 5 % B, followed by an increase to 95 % B in 9 min to end up with a 1 min flush step at 95 % B before re-equilibration with initial conditions. Detection was carried out by both diode array (DAD) and ESI-MS. For high-resolution mass spectrometry analysis, measurements were performed on a Dionex Ultimate 3000 RSLC system using a Waters BEH C18 column (50 x 2.1 mm, 1.7  $\mu\text{m}$  dp) by injecting 5  $\mu\text{l}$  of the methanolic extract. Separation was achieved using the same gradient as above with a 0.33 min isocratic step at 5 % B. UV and MS detection were performed simultaneously. Coupling the HPLC to the MS was supported by an Advion Triversa Nanomate nano-ESI system attached to a Thermo Fisher Orbitrap. Mass spectra were acquired in centroid mode ranging from 200-2000  $\text{m/z}$  at a resolution of  $R = 30000$ .

**HPLC-MS measurements to analyze the products of *in vitro* competition assays.** All measurements were performed on a Dionex Ultimate 3000 RSLC system using a Waters BEH C18, 50 x 2.1 mm, 1.7  $\mu\text{m}$  dp column. Separation of 10-15  $\mu\text{l}$  sample was achieved by a linear gradient with (A)  $\text{H}_2\text{O} + 0.1\%$  FA to (B) ACN + 0.1 % FA at a flow rate of 600  $\mu\text{l/min}$  and 45  $^{\circ}\text{C}$ . The gradient was initiated by a 1 min isocratic step at 5 % B, followed by an increase to 95 % B in 6 min to end up with a 1.5 min step at 95 % B before reequilibration with initial conditions. UV spectra were recorded by a DAD in the range from 200 to 600 nm. The LC flow was split to 75  $\mu\text{l/min}$  before entering the maXis 4G hr-ToF mass spectrometer (Bruker Daltonics, Bremen, Germany) using the standard ESI source. Mass spectra were acquired in centroid mode ranging from 50 – 1000  $\text{m/z}$  at 2 Hz scan speed.

### 3.6 Supporting Information

Full supporting information is available online:

<http://www.rsc.org/suppdata/c5/sc/c5sc01013f/c5sc01013f1.pdf>

**Table S1.** List of strains and plasmids used in this study

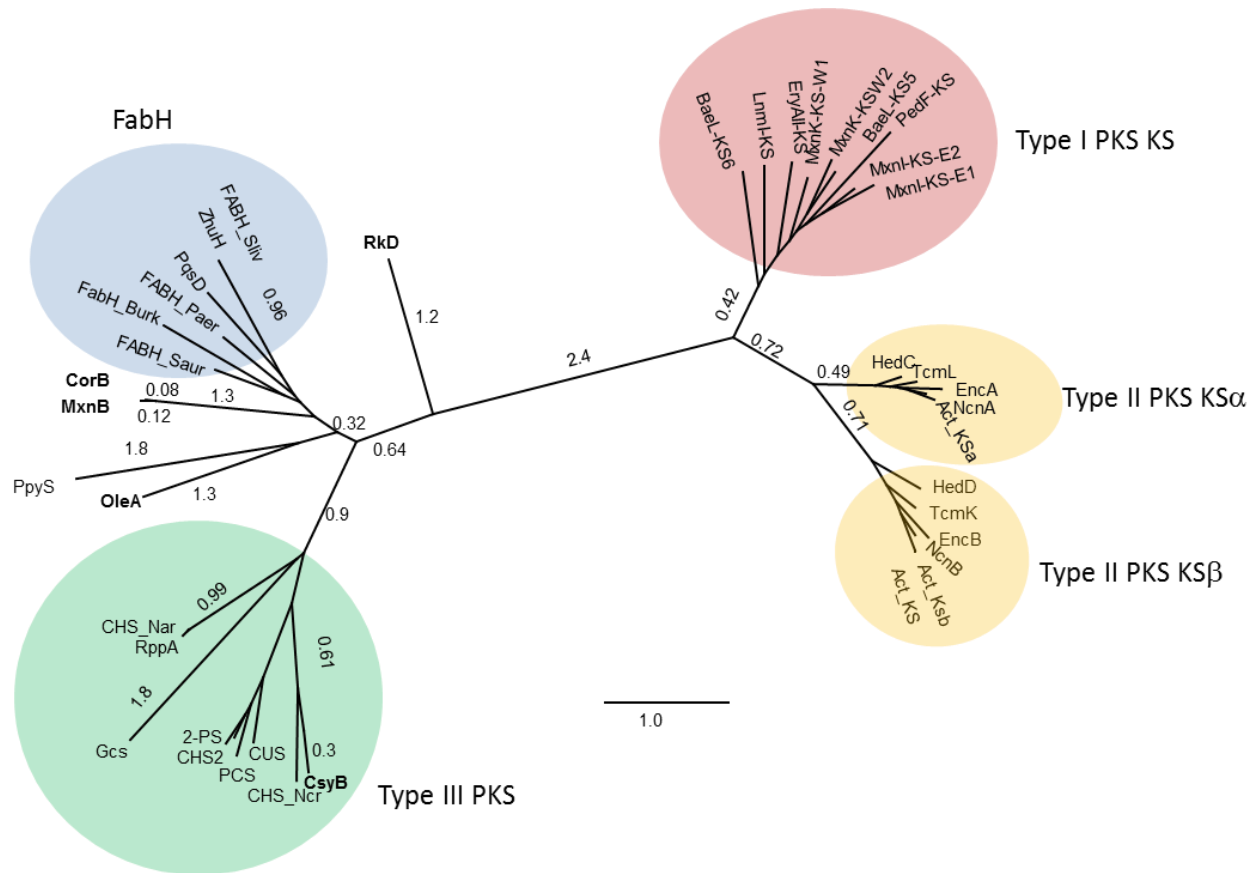
Strain/Plasmid	Characteristics	Reference
<b><i>E. coli</i> strains</b>		
HS996	Host for general cloning	Invitrogen
BL21 (DE3)	Host for protein expression	Invitrogen
<b><i>Myxococcus fulvus</i> strains</b>		
Mx f50	Myxopyronin producing wild-type strain	7
<b>Plasmids</b>		
pColdI	<i>E. coli</i> protein expression vector	Takara
pSUMtaA	containing a 4'-phosphopantetheinyl transferase <i>sfp</i> gene	8
pHSU-mxn5 (pColdI-MxnB)	MxnB protein expression construct with N-terminal His-tag based on pColdI	this study
pHSU-mxn5 <sup>#</sup> (pColdI-MxnB <sup>#</sup> )	MxnB mutant (C121A) protein expression construct with N-terminal His-tag based on pColdI	this study
pHSU-mxn104 (pColdI-MxnB-T322L)	MxnB mutant (T322L) protein expression construct with N-terminal His-tag based on pColdI	this study
pHSU-mxn68 (pColdI-CP-W5-MtaA)	CP-E6 protein expression construct with N-terminal His-tag based on pColdI co-expressed with pSUMtaA	this study
pHSU-mxn69 (pColdI-CP-E6-MtaA)	CP-W5 protein expression construct with N-terminal His-tag based on pColdI co-expressed with pSUMtaA	this study

### 3.7 Supplementary Results

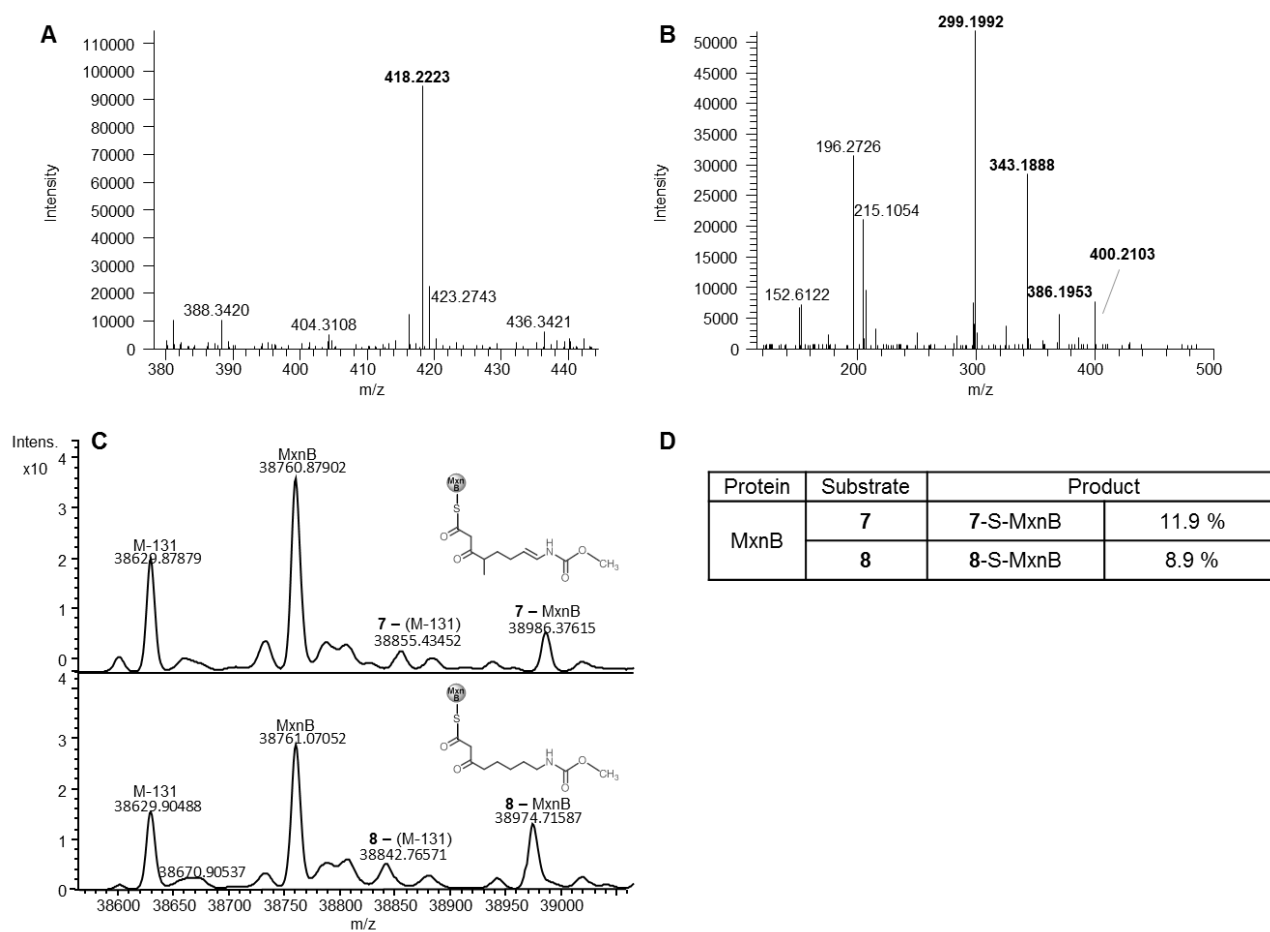
**Table S2.** Blast search of MxnB. First 20 hits of the BLAST search of MxnB from the NCBI database (non-redundant) sorted by their E-values (as per 09 March 2015).

Accession Number	Description	E Value
AGS77282.1	ketosynthase [ <i>Myxococcus fulvus</i> ]	0.0
ADI59524.1	CorB [ <i>Corallocooccus coralloides</i> ]	0.0
WP_012507654.1	3-oxoacyl-ACP synthase [ <i>Pelodictyon phaeoclathratiforme</i> ]	8e-97
WP_006366404.1	3-oxoacyl-ACP synthase [ <i>Chlorobium ferrooxidans</i> ]	2e-91
WP_036102127.1	3-oxoacyl-ACP synthase [ <i>Lysobacter capsici</i> ]	1e-90
WP_025696271.1	3-oxoacyl-ACP synthase [ <i>Paenibacillus forsythiae</i> ]	2e-85
WP_026559228.1	3-oxoacyl-ACP synthase [ <i>Bacillus</i> sp. J37]	5e-84
WP_000833196.1	3-oxoacyl-ACP synthase [ <i>Bacillus cereus</i> ]	7e-83
WP_000833203.1	3-oxoacyl-ACP synthase [ <i>Bacillus cereus</i> ]	3e-82
WP_020062449.1	3-oxoacyl-ACP synthase [ <i>Bacillus</i> sp. 123MFChir2]	3e-82
WP_001989055.1	3-oxoacyl-ACP synthase [ <i>Bacillus cereus</i> ]	4e-82
WP_000833206.1	3-oxoacyl-ACP synthase [ <i>Bacillus cereus</i> ]	4e-82
NP_845551.1	putative 3-oxoacyl-ACP synthase III [ <i>Bacillus anthracis</i> str. Ames]	4e-82
WP_000833198.1	MULTISPECIES: 3-oxoacyl-ACP synthase [ <i>Bacillus cereus</i> group]	6e-82
WP_029438921.1	3-oxoacyl-ACP synthase [ <i>Bacillus thuringiensis</i> ]	7e-82
YP_037326.1	3-oxoacyl-ACP synthase [ <i>Bacillus thuringiensis</i> serovar konkukian str.97-27]	7e-82
WP_016083203.1	3-oxoacyl-[acyl-carrier-protein] synthase 3 [ <i>Bacillus cereus</i> ]	1e-81
WP_000833202.1	3-oxoacyl-ACP synthase [ <i>Bacillus thuringiensis</i> ]	2e-81
KGZ76433.1	3-oxoacyl-ACP synthase [ <i>Bacillus anthracis</i> ]	2e-81
WP_000833204.1	3-oxoacyl-[acyl-carrier-protein] synthase 3 [ <i>Bacillus cereus</i> ]	2e-81

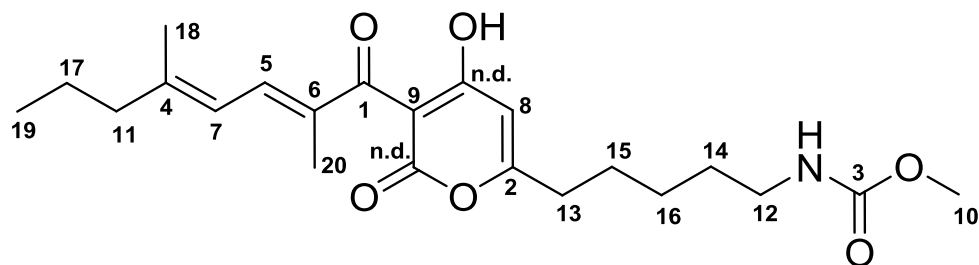




**Figure S1.** Phylogram of ketosynthases from various pathways. Protein sequences were aligned using ClustalW. Phylogenetic analysis was performed with a maximum-likelihood estimation approach (Whelan-and-Goldman 2001) in Geneious 8.1.4. Tip labels reflect the protein names. The proteins explained in the main text are marked bold. The scale bar indicates the degree of divergence as substitutions per sequence position. The following list comprises the locus name, the organism, and the access number of all given proteins: 2-PS (*Gerbera hybrida*, CAA86219), Act\_KS (*Streptomyces lividans*, WP\_003973890), Act\_KSa (*S. coelicolor* A3(2),CAC44200), Act\_KSb (*S. coelicolor* A3(2),CAC44201), BaeL-KS5 (*Bacillus amyloliquefaciens* subsp. plantarum AS43.3, WP\_040238120.1), BaeL-KS6 (*Bacillus amyloliquefaciens* subsp. plantarum AS43.3, WP\_040238120.1), CHS2 (*Medicago sativa*, P30074), CHS\_Nar (*S. fulvissimus* DSM 40593, AGK75504), CHS\_Ncr (*Neurospora crassa* OR74A, XP\_960427), CorB (*Corallococcus coralloides*, ADI59524), CsyB (*Aspergillus oryzae*, BAD97391), CUS (*O. sativa* Japonica, Q8LIL0), EncA (*S. maritimus*, AAF81728), EncA (*S. maritimus*, AAF81729), EryAII-KS (*Saccharopolyspora erythraea* NRRL 2338, CAA44448.1), FabH\_Burk (*Burkholderia xenovorans*, WP\_011490245), FabH\_Paer (*Pseudomonas aeruginosa* PAO1, Q9HYR2), FabH\_Saur (*Staphylococcus aureus*, Q8NXE2), FABH\_Sliv (*S. lividans*, Q9F6D4), Gcs (*S. coelicolor*, WP\_011031521), HedC (*S. griseoruber*, AAP85362), HedD (*S. griseoruber*, AAP85361), LnmI-KS (*S. atroolivaceus*, AAN85522.1), MxnB (*Myxococcus fulvus* Mx f50, AGS77282.1), MxnI-KS-E1 (*M. fulvus* Mx f50, AGS77289.1), MxnI-KS-E2 (*M. fulvus* Mx f50, AGS77289.1), MxnK-KS-W1 (*M. fulvus* Mx f50, AGS77291.1), MxnK-KS-W2 (*M. fulvus* Mx f50, AGS77291.1), NcnA (*S. arenae*, AAD20267), NcnB (*S. arenae*, AAD20268), OleA (*Xanthomonas campestris*, WP\_011035468), PCS (*Aloe arborescens*, Q58VP7), PedF-KS (symbiont bacterium of *Paederus fuscipes*, AAS47564.1), PpyS (*Photorhabdus luminescens*, AGO97060), PqsD (*P. aeruginosa*, P20582), RkD (*Streptomyces* sp. 88-682, ACZ65477), RppA (*S. griseus*, BAA33495), TcmK (*S. davawensis*, WP\_015657287), TcmL (*S. davawensis*, WP\_015657288), ZhuH (*Streptomyces* sp. R1128, AAG30195).



**Figure S2.** ESI-MS analysis of myxopyronin A produced *in vitro* using substrates **6** and **7** and LC-MS analysis for the *in vitro* formation of MxnB with **7** or **8**. (A) MS spectrum in positive mode of myxopyronin A (**1a**). (B) Fragment spectrum of the parent ion  $[M+H]^+$   $m/z = 418.2224$  corresponds to **1a** (calc. for  $C_{23}H_{31}NO_6$ , 418.2224). The related  $MS^2$  fragments are marked in bold. (C) LC-MS of the reaction mixtures containing MxnB and **7** forming **7-S-MxnB** (38,986 Da, top) and MxnB and **8** forming **8-S-MxnB** (38,974 Da, bottom). (D) MS analysis of the loading of **7** or **8** (0.025 mM) onto MxnB (7.5  $\mu$ M). Percentages were calculated using the deconvoluted mass peak heights and they are relative to the total amount of protein species present.

**Table S3.** NMR Spectroscopic Data for Myxopyronin Derivative (9)Chemical shifts measured in CD<sub>3</sub>OD:

No	$\delta_C^a$	$\delta_H(J \text{ in Hz})^b$	COSY <sup>c</sup>	HMBC <sup>d</sup>
1	199.4	-	-	-
2	164.2	-	-	-
3	158	-	-	-
4	147.9	-	-	-
5	136.5	7.32	7	-
6	134.5	-	-	-
7	121.2	6.26	5	-
8	106	5.75	-	2
9	101	-	-	-
10	50.7	3.61 (s)	-	3
11	42.1	2.17 (t, $J=7.4$ )	17	4,7,17
12	40.1	3.09	14	3,14,15
13	32.8	2.42 (t, $J=7.3$ )	15	2,15
14	29.5	1.51 (m)	12,16	12
15	25.9	1.68 (sxt, $J=7.3$ )	13,16	13,14
16	22.5	1.38 (m)	14,15	-
17	20.4	1.53 (m)	11,19	4,11,19
18	15.5	1.79 (s)	-	4,7,11
19	12.2	0.92 ( $J=7.3$ )	17	11,17
20	9.9	1.92 (s)	-	1,5,6

<sup>a</sup>Recorded at 176 MHz; referenced to residual CD<sub>3</sub>OD at  $\delta=49.1$ . <sup>b</sup>Recorded at 700 MHz; referenced to residual CD<sub>3</sub>OD at  $\delta$  3.30. <sup>c</sup>Proton showing COSY correlation to indicated proton. <sup>d</sup>Proton showing HMBC key correlations to the indicated carbon. Signals corresponding to quaternary carbon atoms C-1, C-2 and C-9 were assigned from HMBC spectra of an impure fraction (see Experimental Procedures: Isolation of *In Vitro* Product).

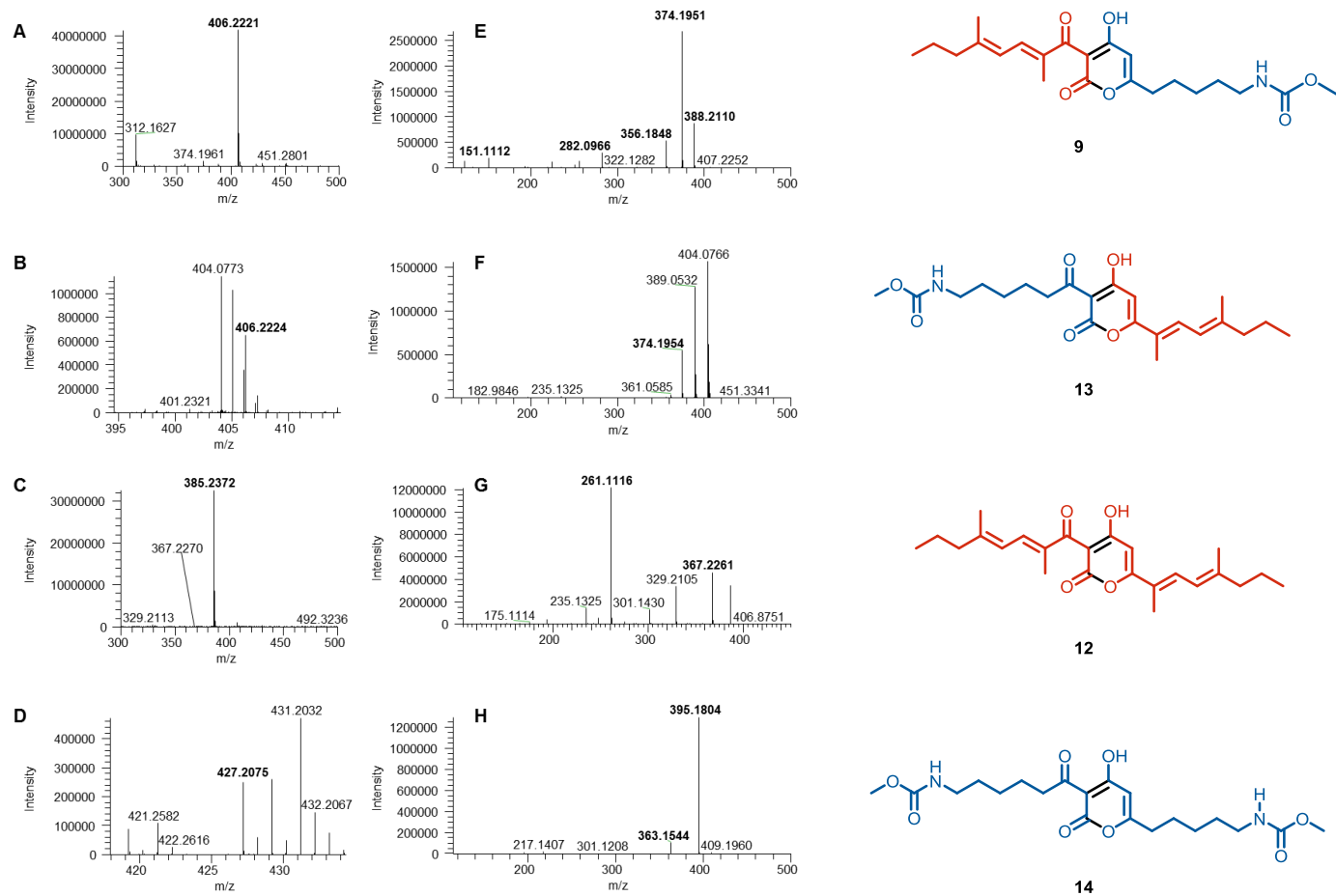


**Figure S3.** ESI-MS analysis of myxopyronin derivative produced *in vitro* by using substrate **6** and **8**. (A-D) MS spectrum of myxopyronin derivatives (**9**, **13**, **12**, **14**) was recorded in positive mode. (E-H) Fragment spectrum of its corresponding parent ion, respectively. The related MS<sup>2</sup> fragments are marked with bold. The mass at [M+H]<sup>+</sup> *m/z* = 406.2221 or 406.2224 corresponds to **9** and the mass at [M+H]<sup>+</sup> *m/z* = 406.2224 (calc. for C<sub>22</sub>H<sub>32</sub>NO<sub>6</sub>, 406.2224) to **13**. The mass at [M+H]<sup>+</sup> *m/z* = 385.2372 Da corresponds to **12** (calc. for C<sub>24</sub>H<sub>33</sub>O<sub>4</sub>, 385.2373) and the mass at [M+H]<sup>+</sup> *m/z* = 427.2075 to **14** (calc. for C<sub>20</sub>H<sub>30</sub>N<sub>2</sub>O<sub>8</sub>, 427.2074). (F-H) MS<sup>2</sup> analyses for MxnWE (**9**), MxnEW (**13**), MxnWW (**12**), and MxnEE (**14**) (also see Table S6).

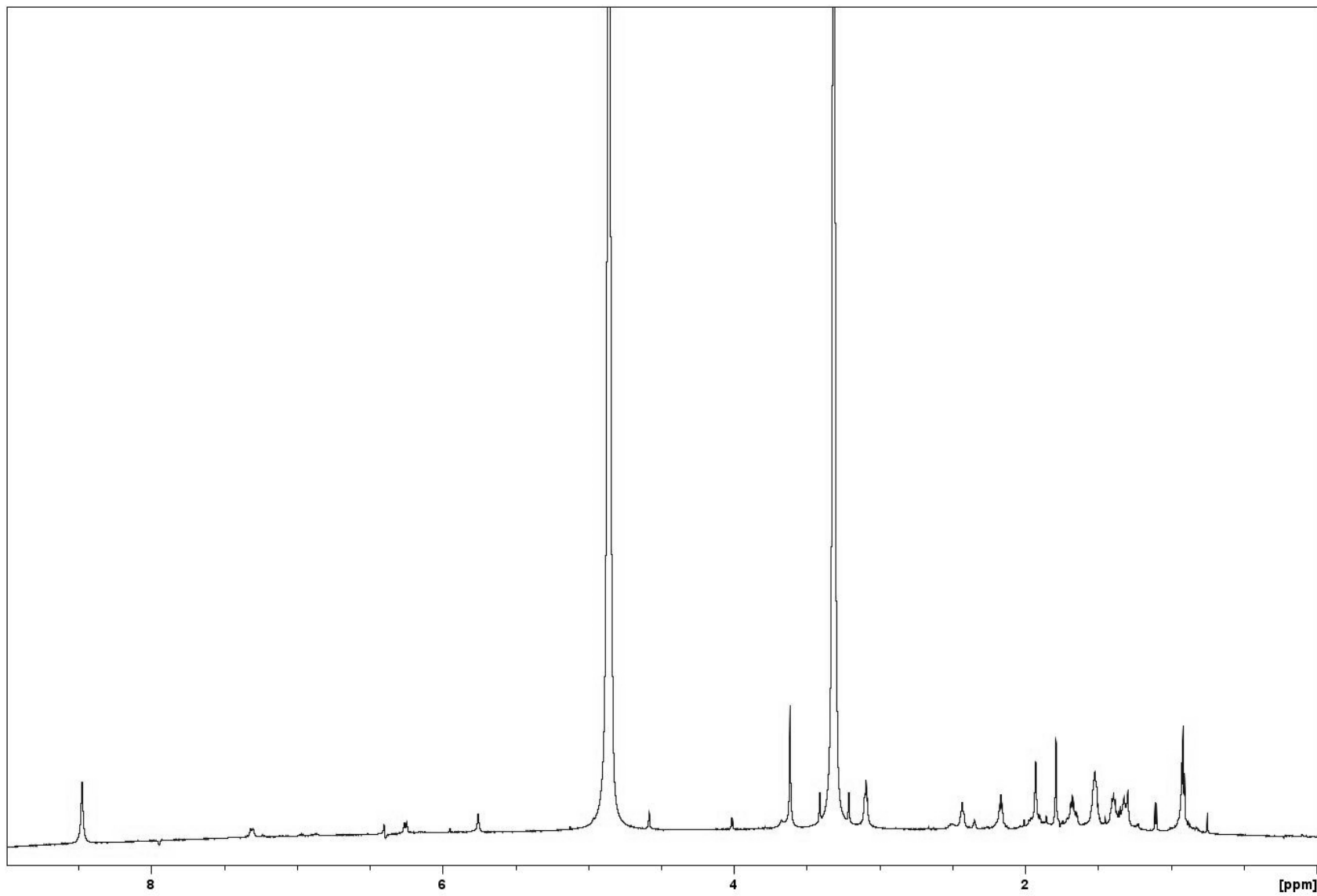


**Figure S4a.** <sup>1</sup>H NMR Spectrum of **9** in CD<sub>3</sub>OD at 700 MHz

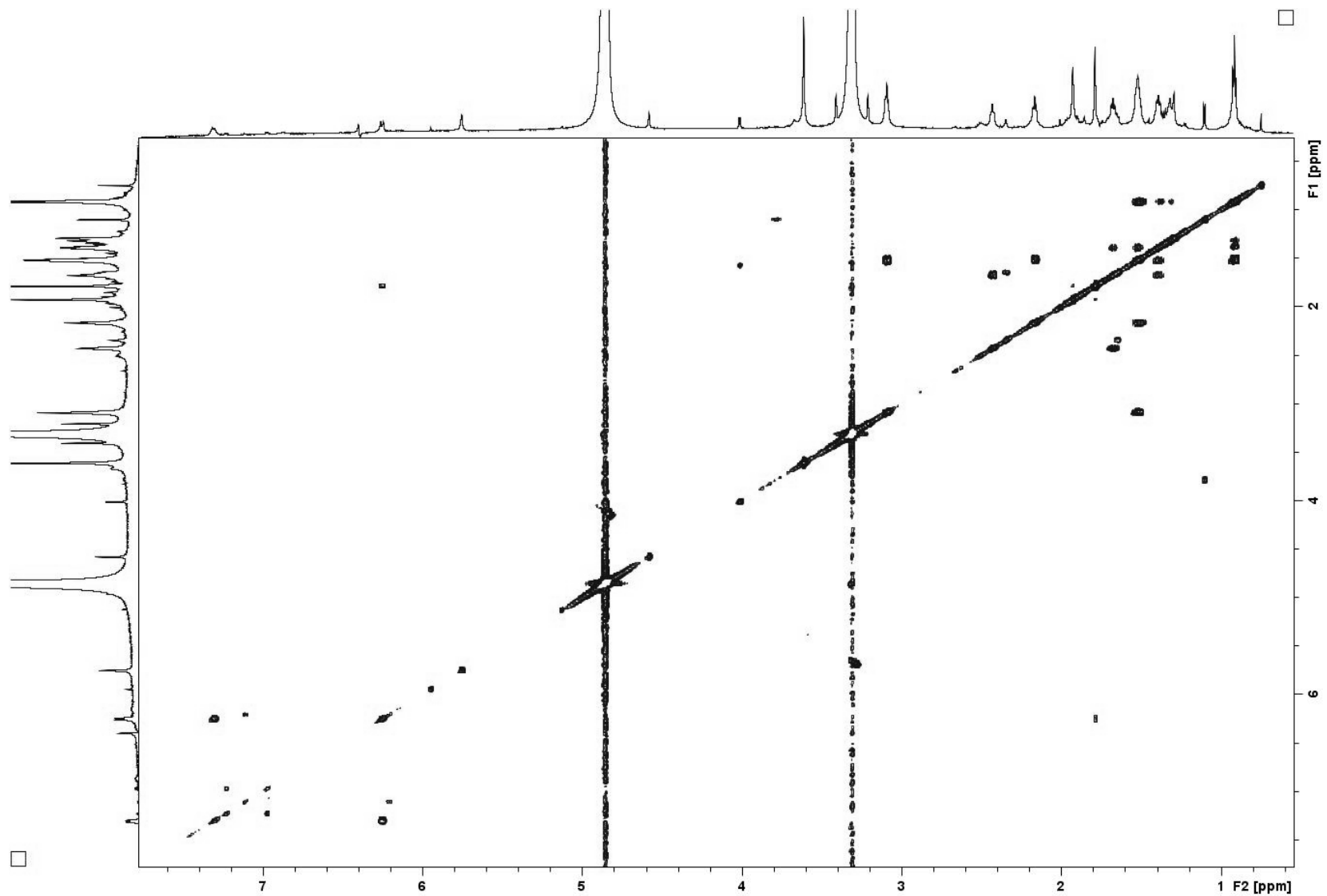
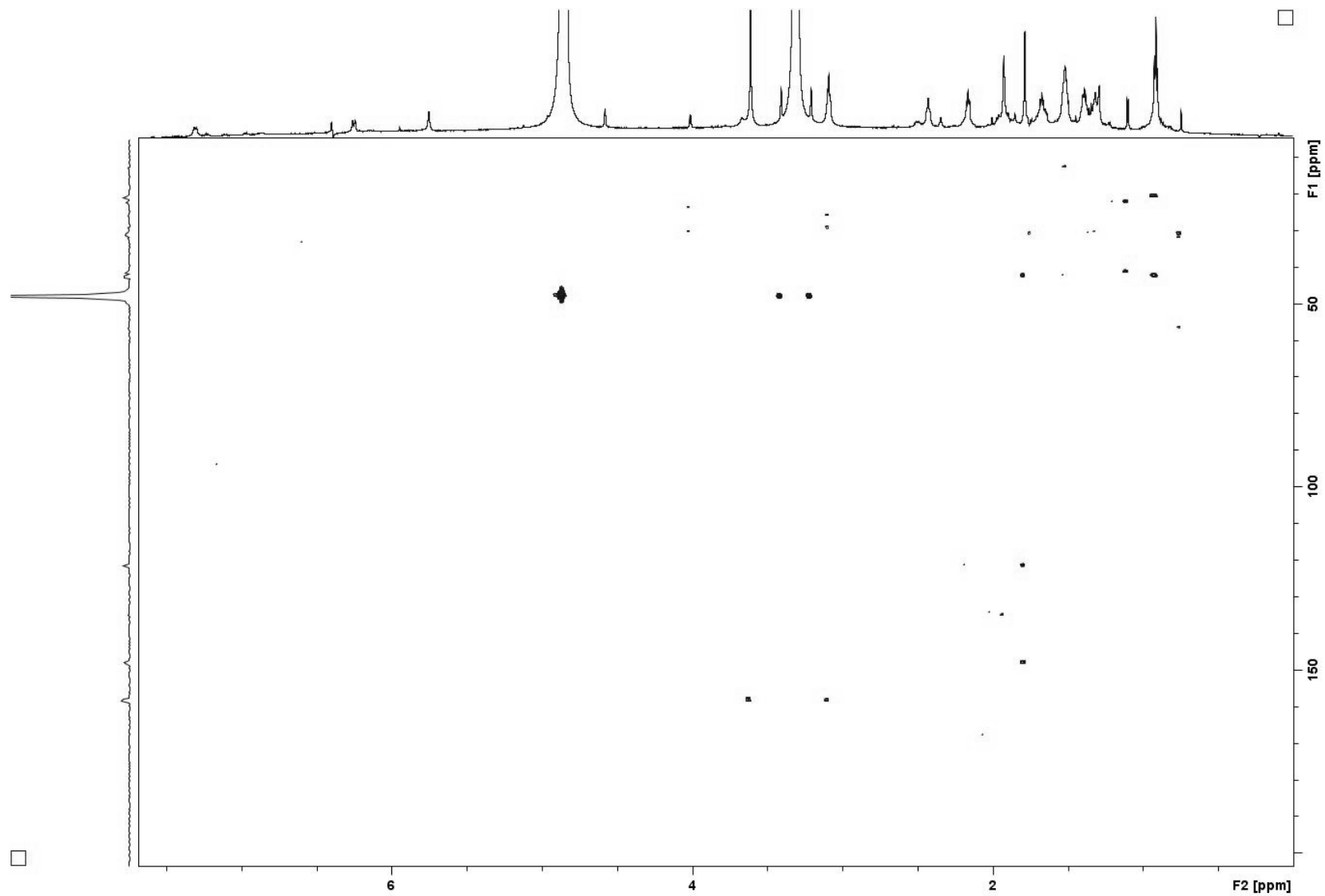


Figure S4b. COSY NMR Spectrum of **9** in CD<sub>3</sub>OD at 700 MHz



**Figure S4c.** HMBC NMR Spectrum of **9** in CD<sub>3</sub>OD at 700 MHz

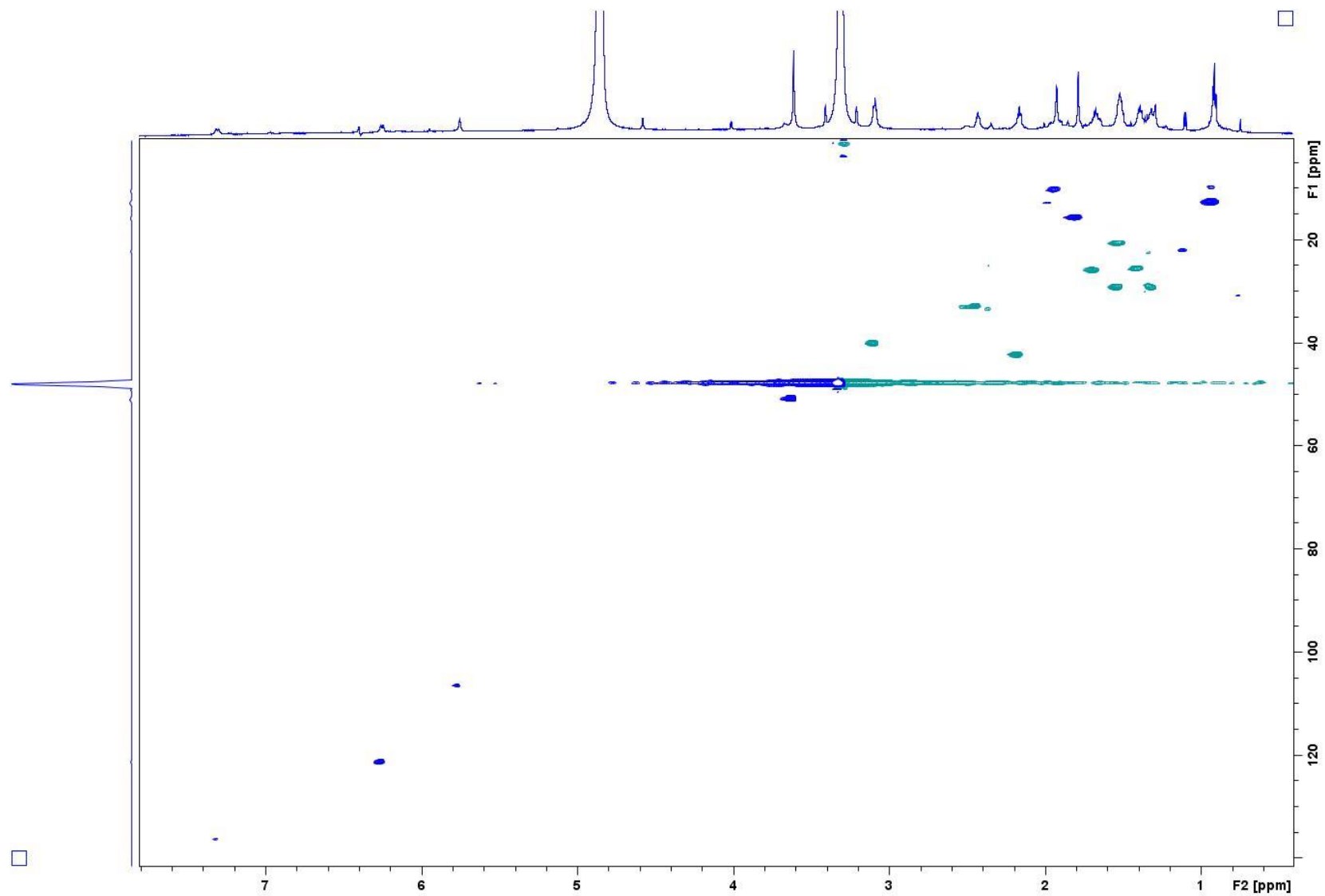


Figure S4d. HSQC NMR Spectrum of **9** in CD<sub>3</sub>OD at 700 MHz



**Table S4.** ESI-MS Analysis of the Recombinant Proteins

Protein	Calculated average mass (Da)		Observed mass (Da)
	Intact protein	Protein – Methionine	
MxnB	38761	38630	38761 and 38629
MxnB <sup>#</sup> (C121A)	38729	38598	38729 and 35898
MxnB* (H264A)	38695	38564	38695 and 38564
MxnB (T322L)	38773	38642	38772.7 and 38642
MtaA/ACP-W5	14628	14497	14627.7 and 14496.7
MtaA/ACP-E6	14771	14640	14771 and 14640

All proteins were expressed with an N-terminal His<sub>6</sub>-tag

**Table S5.** MS analysis of the loading of **6** or **8** onto MxnB, CP-E and CP-W, which were used in the competition assays.

Protein	Substrate	Product	
		Product	Percentage
MxnB	6	6-S-MxnB	46.45%
	8	8-S-MxnB	27%
CP-E	6	6-S-CP-E	50.05%
	8	8-S-CP-E	16.35%
CP-W	6	6-S-CP-W	37.57%
	8	8-S-CP-W	19.94%

Percentages are calculated using the deconvoluted mass peak heights and they are relative to the total amount of protein species present.

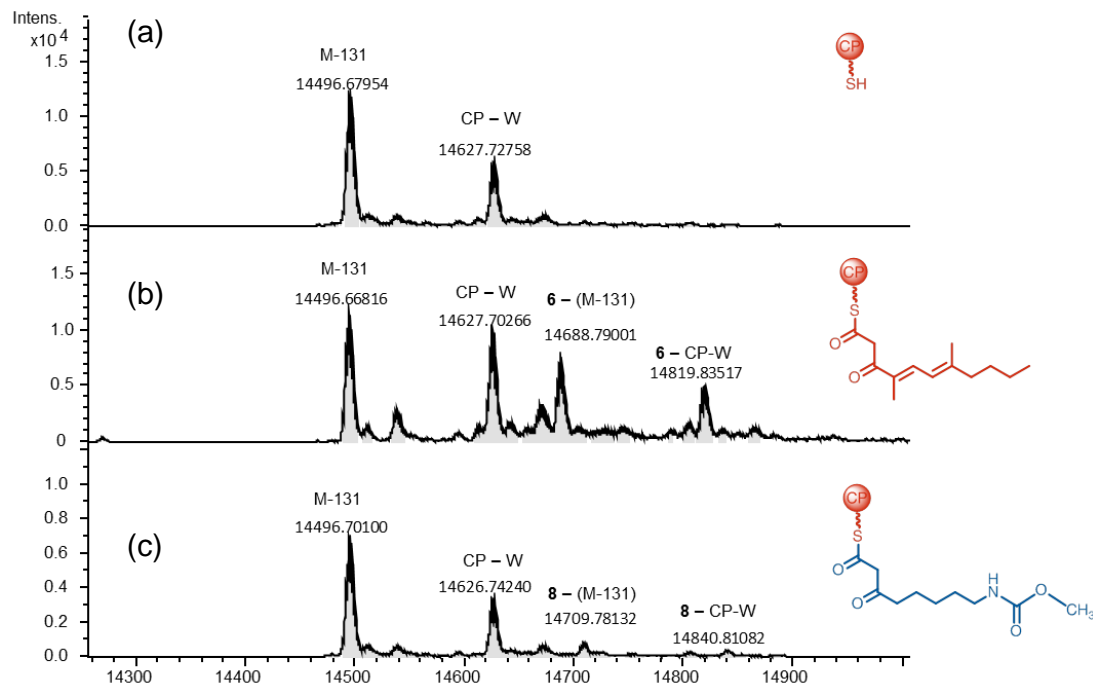


**Figure S5.** LC-MS analysis of the formation of **6-S-CP-W** and **8-S-CP-W**. The deconvoluted spectra correspond to (a) holo-CP-W (CP-W), (b) the reaction mixture containing CP-W and **6** forming **6-S-CP-W** (14820 Da) and (c) the reaction mixture containing CP-W and **8** forming **8-S-CP-W** (14841 Da). The additional peak at M-131 represents the loss of the N-terminal methionine during expression of the recombinant protein in *E. coli*.

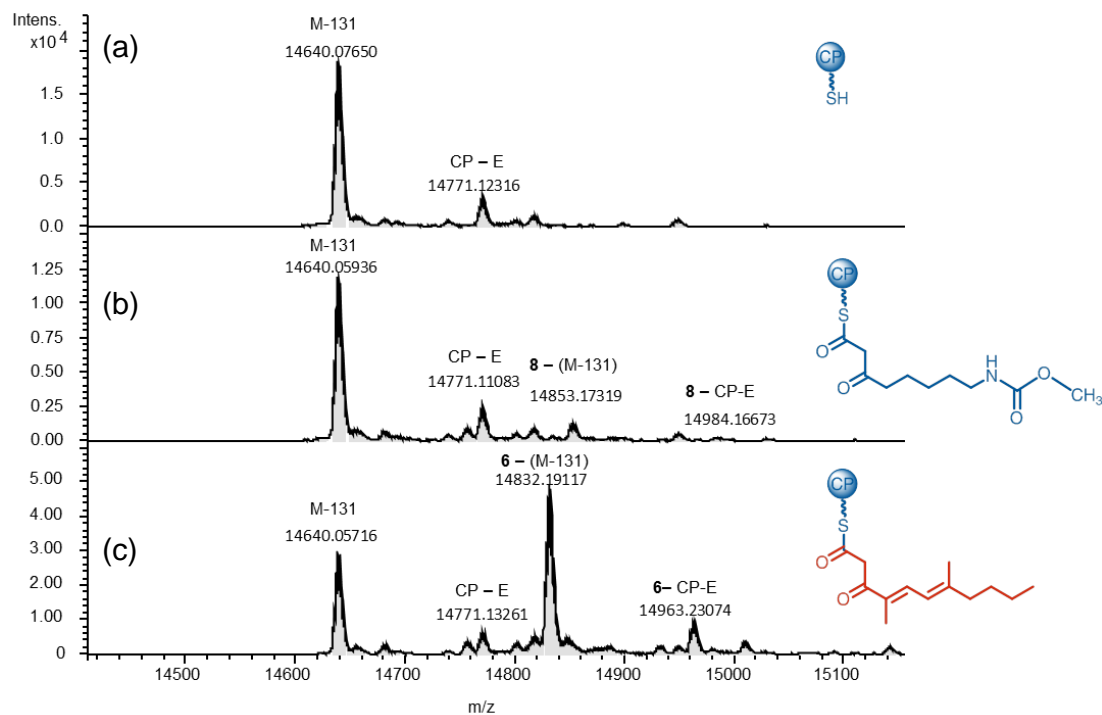


**Figure S6.** LC-MS analysis for formation of **8-S-CP-E** and **6-S-CP-E**. The deconvoluted spectra correspond to (a) holo-CP-E (CP-E), (b) the reaction mixture containing CP-E and **8** forming **8-S-CP-E** (14984 Da) and (c) the reaction mixture containing CP-E and **6** forming **6-S-CP-E** (14963 Da). The additional peak at M-131 represents the loss of the N-terminal methionine during expression of the recombinant protein in *E. coli*.

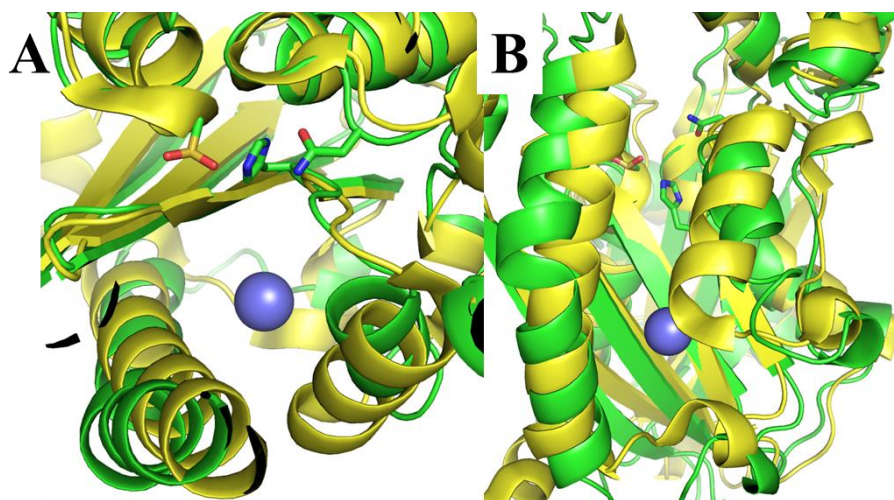


**Figure S7.** A and B: Superposition of MxnB (green) (PDB ID 4V2P) and OleA (yellow) (PDB ID 3S23). Active site residues of MxnB are shown as sticks. The Xe atom used to identify the second long-chain fatty acid binding channel in OleA is shown as a purple sphere.

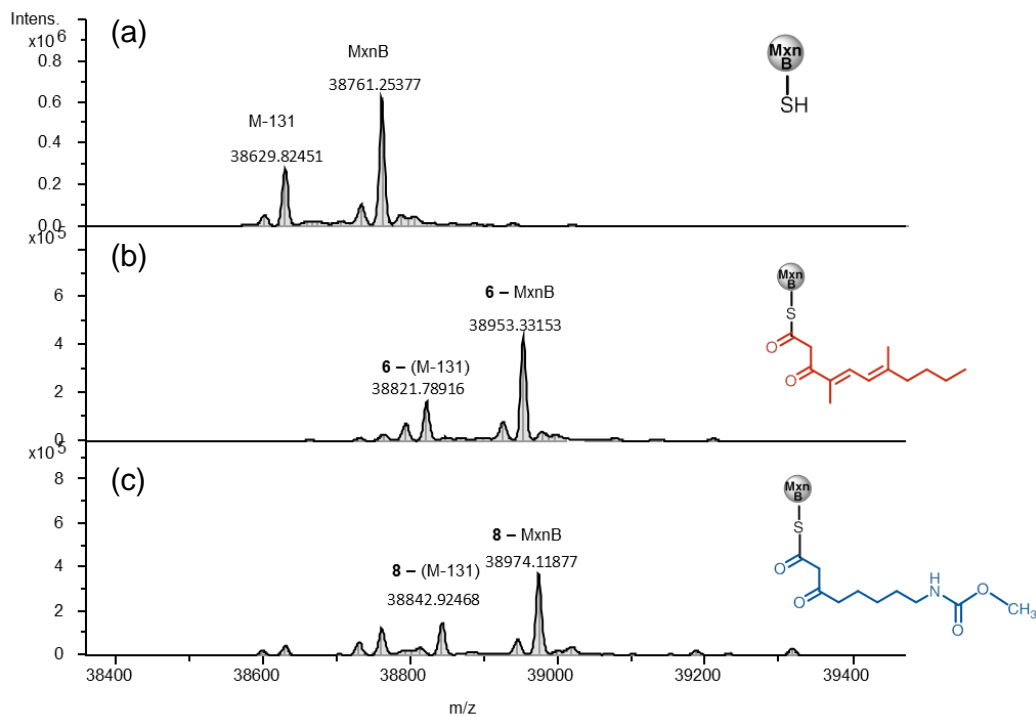


**Figure S8.** LC-MS analysis for the *in vitro* formation of MxnB. LC-MS analysis for the formation of 6-S-MxnB and 8-S-MxnB. The deconvoluted spectra correspond to (a) MxnB, (b) the reaction mixture containing MxnB and **6** forming 6-S-MxnB (38953 Da) and (c) the reaction mixture containing MxnB and **8** forming 8-S-MxnB (38974 Da). The additional peak at M-131 represents the loss of the N-terminal methionine during expression of the recombinant protein in *E. coli*.

**Table S6.** Characterization of Myxopyronin A and Its Analogues with Representative Fragmentation Patterns Observed

	Chemical Formula	Calculated mass $m/z$ [M+H] <sup>+</sup>	Observed $m/z$ [M+H] <sup>+</sup>	Fragmentation due to losses of				
				H <sub>2</sub> O ( $m/z = 18$ )	CH <sub>3</sub> OH ( $m/z = 32$ )	H <sub>2</sub> N-CO <sub>2</sub> CH <sub>3</sub> ( $m/z = 75$ )	H <sub>2</sub> N-CO <sub>2</sub> CH <sub>3</sub> , CO <sub>2</sub> ( $m/z = 119$ )	Other fragment
MxnA ( <b>1a</b> )	C <sub>23</sub> H <sub>32</sub> NO <sub>6</sub>	418.2224	418.2224	400.2114	386.1958	343.1899	299.2002	
MxnA ( <b>1a</b> ) from <i>in vitro</i>	C <sub>23</sub> H <sub>32</sub> NO <sub>6</sub>	418.2224	418.2223	400.2103	386.1953	343.1888	299.1992	
<b>10</b>	C <sub>23</sub> H <sub>32</sub> NO <sub>6</sub>	418.2224	418.2224	400.2118	386.1950	343.1895	n.o.	
<b>11</b>	C <sub>22</sub> H <sub>30</sub> N <sub>2</sub> O <sub>8</sub>	451.2074	451.2076	n.o.	n.o.	n.o.	n.o.	
<b>12</b>	C <sub>24</sub> H <sub>33</sub> O <sub>4</sub>	385.2373	385.2375	367.2255	N/A	N/A	N/A	C <sub>9</sub> H <sub>16</sub> ( $m/z = 124$ ) 261.1155
	Chemical Formula	Calculated mass $m/z$ [M+H] <sup>+</sup>	Observed $m/z$ [M+H] <sup>+</sup>	Fragmentation due to losses of				
				H <sub>2</sub> O ( $m/z = 18$ )	CH <sub>3</sub> OH ( $m/z = 32$ )	C <sub>9</sub> H <sub>16</sub> ( $m/z = 124$ )	C <sub>12</sub> H <sub>16</sub> NO <sub>5</sub> ( $m/z = 255$ )	Other fragment 2CH <sub>3</sub> OH ( $m/z = 64$ )
<b>9</b>	C <sub>22</sub> H <sub>31</sub> NO <sub>6</sub>	406.2224	406.2219	388.2110	374.1957	282.0966	151.1112	N/A
<b>13</b>	C <sub>22</sub> H <sub>31</sub> NO <sub>6</sub>	406.2224	406.2224	n.o.	374.1954	n.o.	n.o.	N/A
<b>14</b>	C <sub>20</sub> H <sub>30</sub> N <sub>2</sub> O <sub>8</sub>	427.2074	427.2075	n.o.	395.1804	n.o.	n.o.	363.1544
<b>15</b>	C <sub>21</sub> H <sub>29</sub> NO <sub>6</sub>	392.2067	392.2065	374.1953	360.1797	282.0962	137.0952	N/A
<b>16</b>	C <sub>20</sub> H <sub>27</sub> NO <sub>6</sub>	378.1911	378.1910	360.1794	346.1637	282.0961	123.0796	N/A
<b>17</b>	C <sub>21</sub> H <sub>31</sub> NO <sub>6</sub>	394.2224	394.2222	376.2099	362.1949	n.o.	139.1107	N/A
<b>18</b>	C <sub>21</sub> H <sub>33</sub> NO <sub>6</sub>	396.2380	396.2377	378.2262	264.2104	n.o.	n.o.	N/A

n.o. = not observed, N/A = not applicable

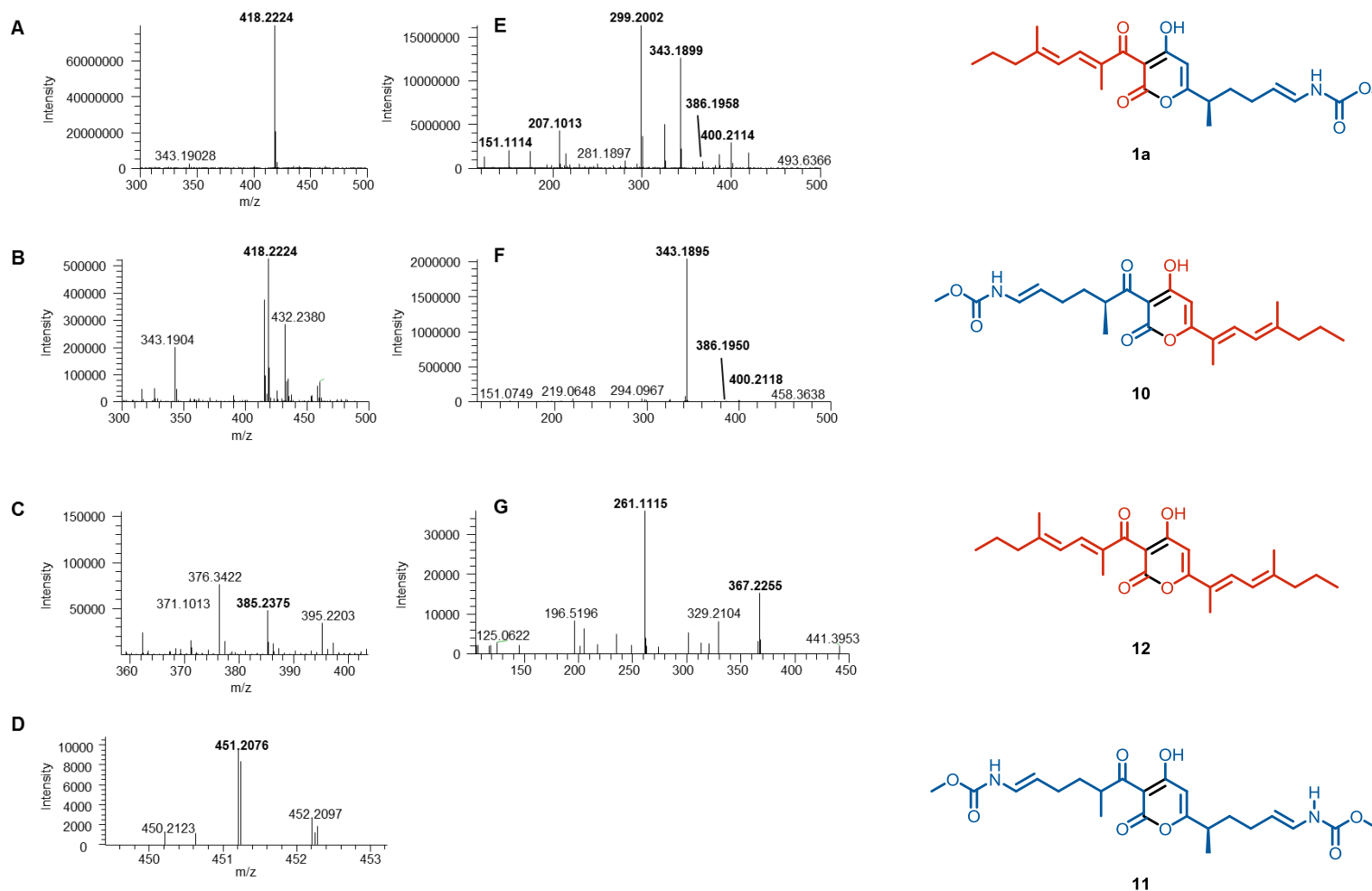


**Figure S9.** ESI-MS Analysis of myxopyronin and its derivatives produced *in vivo*. (A-D) ESI-MS spectra of myxopyronin A (**1a**) and its derivatives **10**, **12** and **11** in positive mode. (E-G) Fragment spectra of the corresponding parent ion, respectively. The related MS<sup>2</sup> fragments are labelled in bold. The mass at [M+H]<sup>+</sup> *m/z* = 418.2224 correspond to **1a** and **10** (calc. for C<sub>23</sub>H<sub>31</sub>NO<sub>6</sub>, 418.2224). The mass at [M+H]<sup>+</sup> *m/z* = 385.2375 Da correspond to **12** (calc. for C<sub>24</sub>H<sub>33</sub>O<sub>4</sub>, 385.2373) and the mass at [M+H]<sup>+</sup> *m/z* = 451.2076 correspond to **11** (calc. for C<sub>22</sub>H<sub>30</sub>N<sub>2</sub>O<sub>8</sub>, 451.2074). (E-G) MS<sup>2</sup> analyses for MxnWE (**1a**), MxnEW (**10**), and MxnWW (**12**) (also see Table S6), while only high-resolution mass spectrometry (HRMS) could be obtained for MxnEE (**11**).

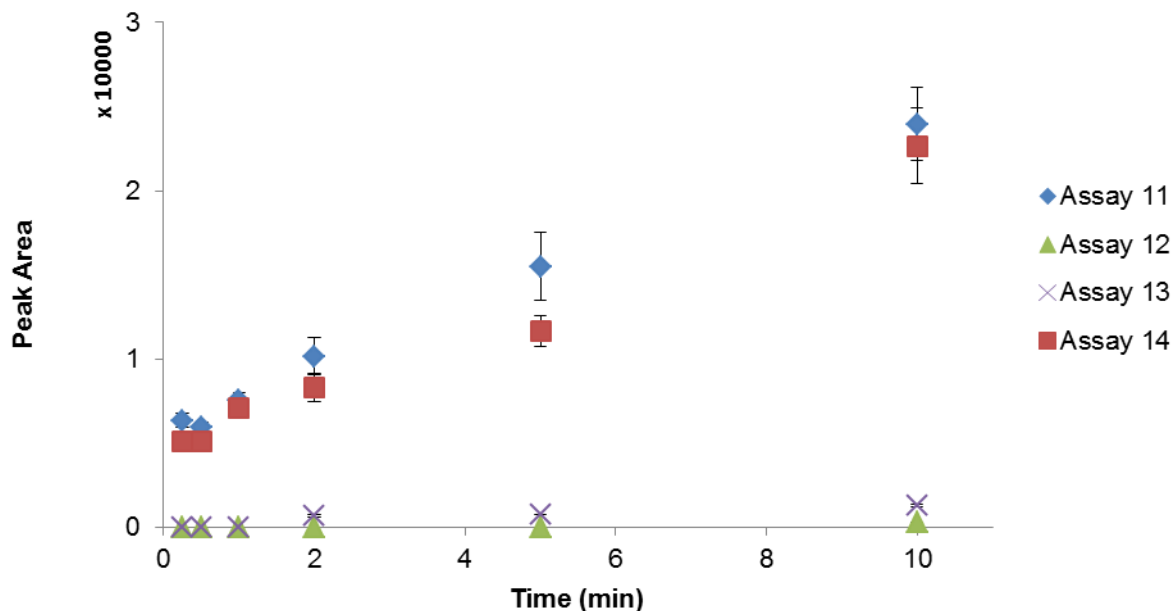


**Figure S10.** LC-MS analysis of Assays 11-14. Time-course of the production of **9** from 15 s to 10 min. The peak area of extracted ion chromatograms (EIC) for **9** was used for quantification. Assay 11-14: Assay 11 (MxnB, **6**-CP-W and **8**-CP-E), Assay 12 (MxnB, **8**-CP-W, and **6**-CP-E), Assay 13 (MxnB, **6**-CP-W and **8**-CP-W), and Assay 14 (MxnB, **6**-CP-E and **8**-CP-E).

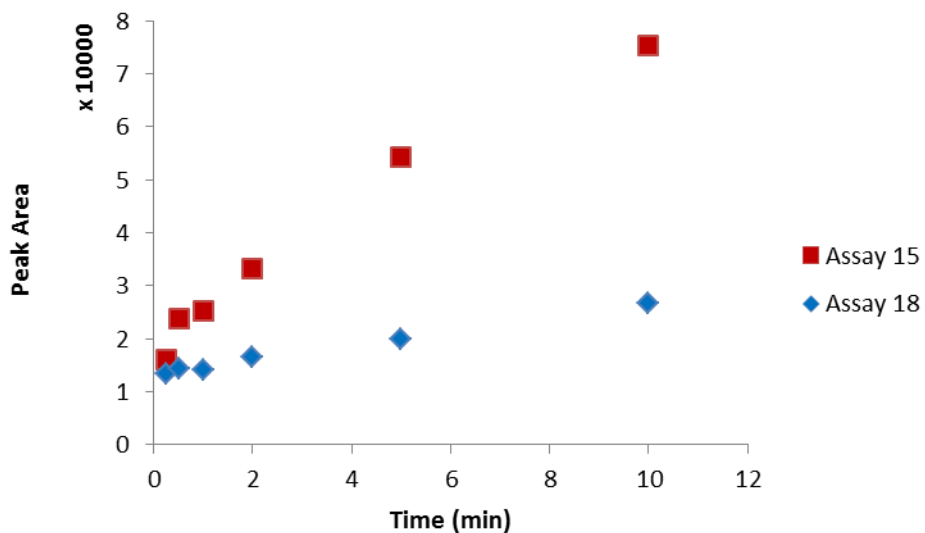


**Figure S11.** LC-MS analysis of Assays 15-18. The peak area of the EIC for **9** at  $[M+H]^+ = 406.22$  was used for Assay 15 (**6**-MxnB and **8**-CP-E) and the EIC for **14** at  $[M+H]^+ = 427.20$  was used for Assay 18 (**8**-MxnB with **8**-CP-E). Assay 16 (**6**-MxnB incubated with **6**-CP-W) and Assay 17 (**8**-MxnB is incubated with **6**-CP-W) are not shown due to the very low amount observed. Assays were performed as a time course between 15 s to 10 min.

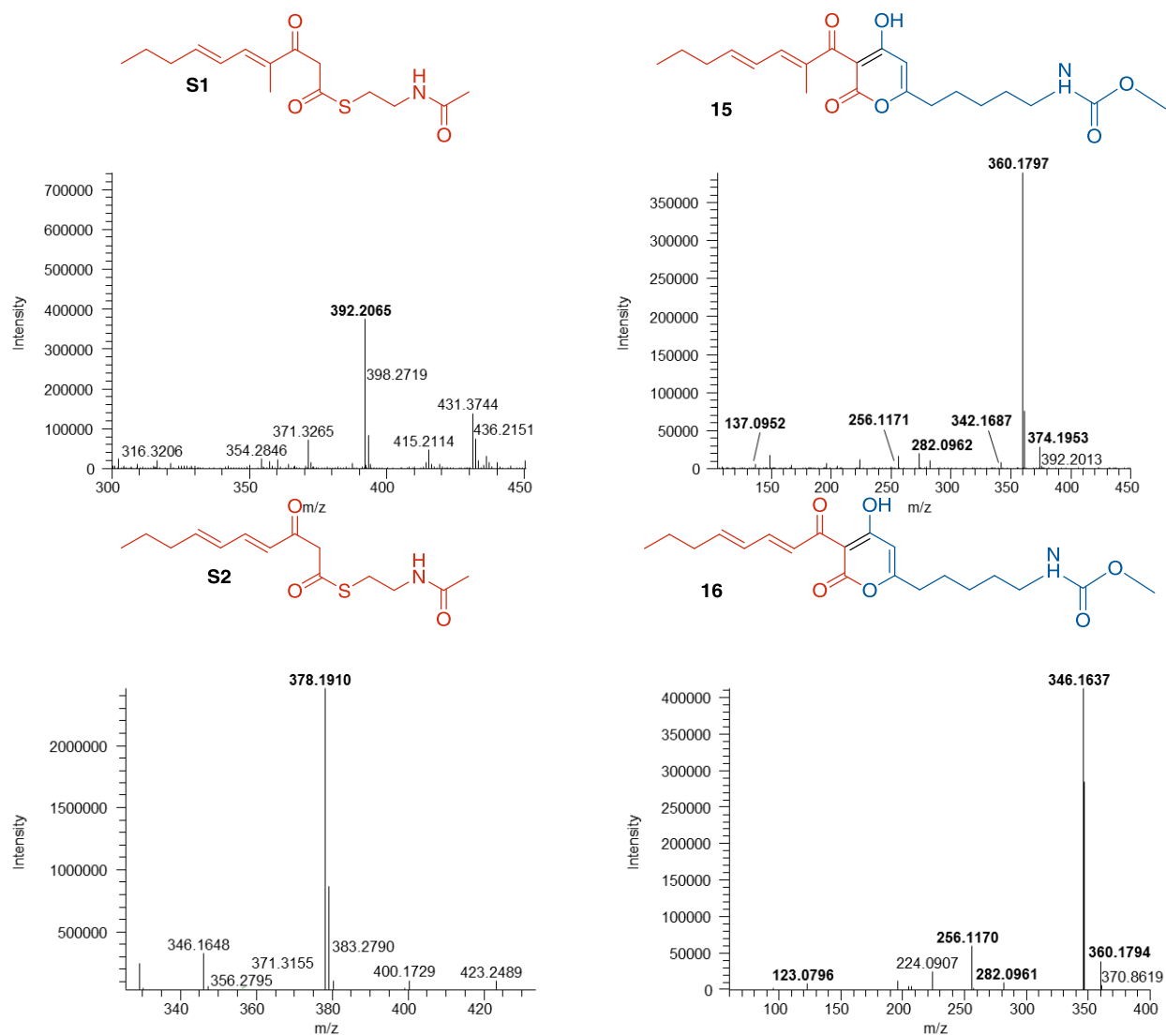


**Figure S12.** ESI-MS analysis of other myxopyronin derivatives produced *in vitro* in positive mode. The *in vitro* assays were performed using MxnB, CP-W, CP-E and western SNAC (S1-S4) independently with **8**, resulting in **15-18**, respectively. Left panel: MS spectra; right panel: Fragment spectra of the parent ion of **15**  $[M+H]^+$   $m/z = 392.2065$ , **16**  $[M+H]^+$   $m/z = 378.1910$ , **17**  $[M+H]^+$   $m/z = 394.2377$ , **18**  $[M+H]^+$   $m/z = 396.2377$  (see also Table S6)

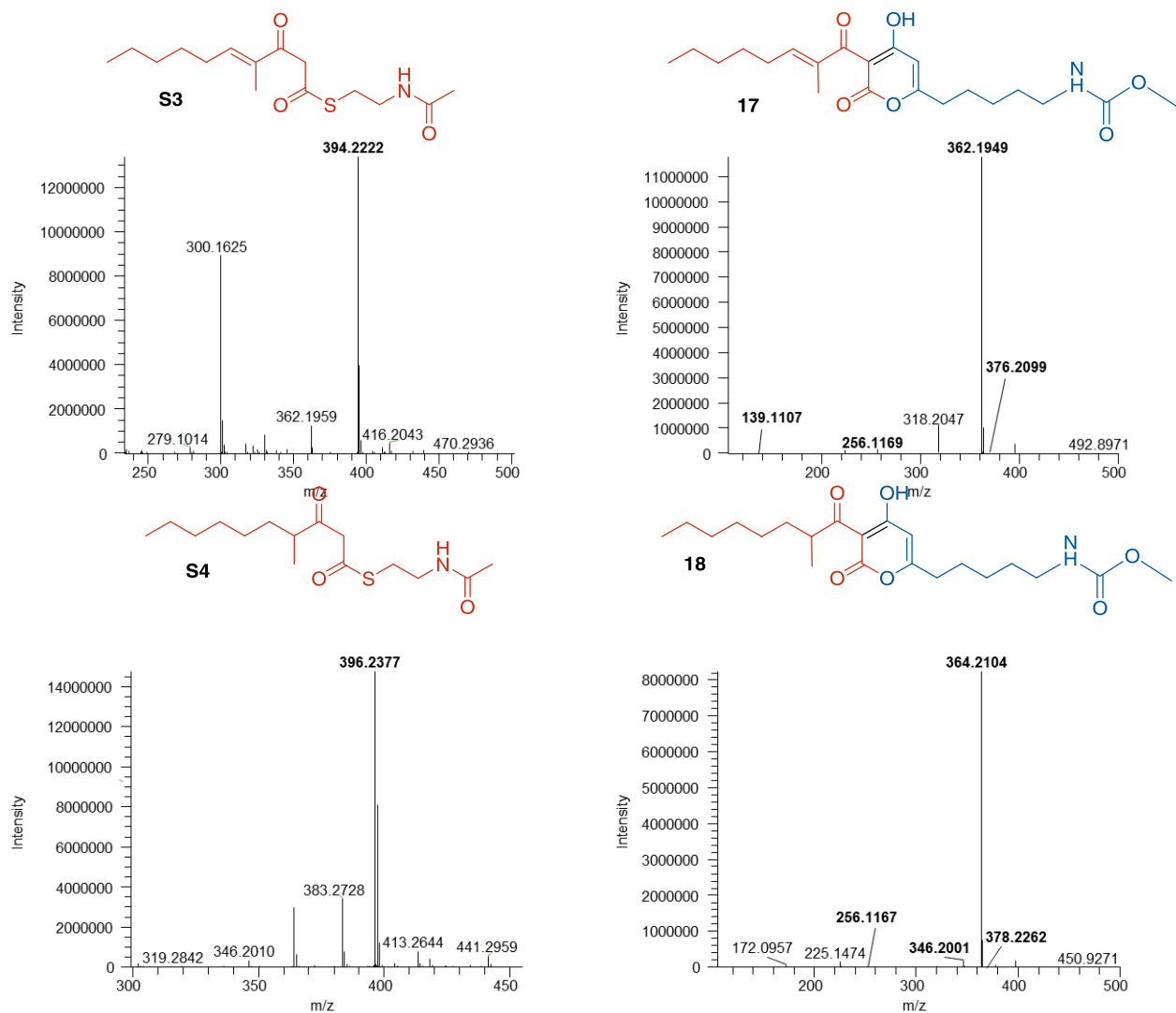


**Figure S12 continued.** ESI-MS analysis of other myxopyronin derivatives produced *in vitro* in positive mode. The *in vitro* assays were performed using MxnB, CP-W, CP-E, western SNAC (S1-S4) independently with **8**, resulting in **15-18**, respectively. Left panel: MS spectrum; right panel: Fragment spectrum of the parent ion of **15**  $[M+H]^+$   $m/z = 392.2065$ , **16**  $[M+H]^+$   $m/z = 378.1910$ , **17**  $[M+H]^+$   $m/z = 394.2377$ , **18**  $[M+H]^+$   $m/z = 396.2377$  (see also Table S6)



## 3.8 References

### 3.8.1 References for Main Text

- 1 (a) A. R. Coates, G. Halls and Y. Hu, *Br. J. Pharmacol.*, 2011, **163**, 184–194; (b) L. Freire-Moran, B. Aronsson, C. Manz, I. C. Gyssens, A. D. So, D. L. Monnet and O. Cars, in *Drug Resistance Updates*, 2011, **14**, 118–124;
- 2 (a) S. C. Wenzel and R. Müller, *Nat. Prod. Rep.*, 2007, **24**, 1211–1224; (b) K. J. Weissman and R. Müller, *Bioorganic Med. Chem.*, 2009, **17**, 2121–2136.
- 3 C. Hertweck, *Angew. Chem. Int. Ed. Engl.*, 2009, **48**, 4688–4716.
- 4 M. A. Fischbach and C. T. Walsh, *Chem. Rev.*, 2006, **106**, 3468–3496.
- 5 B. Shen, *Top. Curr. Chem.*, 2000, **209**, 1–51.
- 6 M. B. Austin and J. P. Noel, *Nat. Prod. Rep.*, 2003, **20**, 79–110.
- 7 H. Irschik, K. Gerth, G. Höfle, W. Kohl and H. Reichenbach, *J. Antibiot.*, 1983, **36**, 1651–1658.
- 8 J. Mukhopadhyay, K. Das, S. Ismail, D. Koppstein, M. Jang, B. Hudson, S. Sarafianos, S. Tuske, J. Patel, R. Jansen, H. Irschik, E. Arnold and R. H. Ebright, *Cell*, 2008, **135**, 295–307
- 9 G. A. Belogurov, M. N. Vassilyeva, A. Sevostyanova, J. R. Appleman, A. X. Xiang, R. Lira, S. E. Webber, S. Klyuyev, E. Nudler, I. Artsimovitch and D. G. Vassilyev, *Nature*, 2009, **457**, 332–335.
- 10 W. Kohl, H. Irschik, H. Reichenbach and G. Höfle, *Liebigs Ann. Chem.*, 1984, 1088–1093.
- 11 Ö. Erol, T. F. Schäberle, A. Schmitz, S. Rachid, C. Gurgui, M. El Omari, F. Lohr, S. Kehraus, J. Piel, R. Müller and G. M. König, *ChemBioChem*, 2010, **11**, 1235–1265.
- 12 H. Sucipto, S. C. Wenzel and R. Müller, *ChemBioChem*, 2013, **14**, 1581–1589.
- 13 R. Lira, A. X. Xiang, T. Doundoulakis, W. T. Biller, K. A. Agrios, K. B. Simonsen, S. E. Webber, W. Sisson, R. M. Aust, A. M. Shah, R. E. Showalter, V. N. Banh, K. R. Steffy and J. R. Appleman, *Bioorganic Med. Chem. Lett.*, 2007, **17**, 6797–6800.
- 14 J. A. Kalaitzis, Q. Cheng, P. M. Thomas, N. L. Kelleher and B. S. Moore, *J. Nat. Prod.*, 2009, **72**, 469–472.
- 15 Y. Seshime, P. R. Juvvadi, I. Fujii and K. Kitamoto, *Biochem. Biophys. Res. Commun.*, 2005, **331**, 253–260.
- 16 M. Hashimoto, T. Koen, H. Takahashi, C. Suda, K. Kitamoto and I. Fujii, *J. Biol. Chem.*, 2014, **289**, 19976–19984.
- 17 Y. Sun, F. Hahn, Y. Demydchuk, J. Chettle, M. Tosin, H. Osada and P. F. Leadlay, *Nat. Chem. Biol.*, 2010, **6**, 99–101.
- 18 X. Qiu, C. A. Janson, A. K. Konstantinidis, S. Nwagwu, C. Silverman, W. W. Smith, S. Khandekar, J. Lonsdale and S. S. Abdel-Meguid, *J. Biol. Chem.*, 1999, **274**, 36465–36471.
- 19 C. Davies, R. J. Heath, S. W. White and C. O. Rock, *Structure*, 2000, **8**, 185–195
- 20 N. Wu, D. E. Cane and C. Khosla, *Biochemistry*, 2002, **41**, 5056–5066.
- 21 N. Gaitatzis, B. Kunze and R. Müller, *Proc. Natl. Acad. Sci. U. S. A.*, 2001, **98**, 11136–11141.
- 22 (a) C. J. Arthur, A. Szafranska, S. E. Evans, S. C. Findlow, S. G. Burston, P. Owen, I. Clark-Lewis, T. J. Simpson, J. Crosby and M. P. Crump, *Biochemistry*, 2005, **44**, 15414–15421; (b) T. S. Hitchman, J. Crosby, K. J. Byrom, R. J. Cox and T. J. Simpson, *Chem. Biol.*, 1998, **5**, 35–47;
- 23 J. L. Meier and M. D. Burkart, *Chem. Soc. Rev.*, 2009, **38**, 2012–2045.
- 24 R. J. Heath and C. O. Rock, *Nat. Prod. Rep.*, 2002, **19**, 581–596.
- 25 B. R. Goblirsch, J. A. Frias, L. P. Wackett and C. M. Wilmot, *Biochemistry*, 2012, **51**, 4138–4146.
- 26 T. Mori, D. Yang, T. Matsui, M. Hashimoto, H. Morita, I. Fujii and I. Abe, *J. Biol. Chem.*, 2015, **290**, 5214–5225.
- 27 S. McNicholas, E. Potterton, K. S. Wilson and M. E. M. Noble, *Acta Crystallogr. Sect. D Biol. Crystallogr.*, 2011, **67**, 386–394.

- 28 D. Sehnal, R. Svobodová Vařeková, K. Berka, L. Pravda, V. Navrátilová, P. Banáš, C.-M. Ionescu, M. Otyepka and J. Koča, *J. Cheminform.*, 2013, **5**, 39.
- 29 L. M. Miller, M. T. Mazur, S. M. McLoughlin and N. L. Kelleher, *Protein Sci.*, 2005, **14**, 2702–2712.
- 30 J. Crosby and M. P. Crump, *Nat. Prod. Rep.*, 2012, **29**, 1111–1137.
- 31 J. H. Sahner, H. Sucipto, S. C. Wenzel, M. Groh, R. W. Hartmann and R. Müller, *ChemBioChem*, 2015, **16**, 946–953.

### 3.8.2 References for Supporting Information

- 1 M. M. Bradford, *Anal. Biochem.*, 1976, **72**, 248–254.
- 2 A. J. McCoy, R. W. Grosse-Kunstleve, L. C. Storoni and R. J. Read, *Acta Crystallogr. D Biol. Crystallogr.*, 2005, **61**, 458–464.
- 3 L. C. Storoni, A. J. McCoy and R. J. Read, *Acta Crystallogr. D Biol. Crystallogr.*, 2004, **60**, 432–438.
- 4 P. Emsley and K. Cowtan, *Acta Crystallogr. D Biol. Crystallogr.*, 2004, **60**, 2126–2132.
- 5 G. N. Murshudov, P. Skubák, A. A. Lebedev, N. S. Pannu, R. A. Steiner, R. A. Nicholls, M. D. Winn, F. Long and A. A. Vagin, *Acta Crystallogr. D Biol. Crystallogr.*, 2011, **67**, 355–367.
- 6 P. D. Adams, K. Gopal, R. W. Grosse-Kunstleve, L.-W. Hung, T. R. Ioerger, A. J. McCoy, N. W. Moriarty, R. K. Pai, R. J. Read, T. D. Romo, J. C. Sacchettini, N. K. Sauter, L. C. Storoni and T. C. Terwilliger, *J. Synchrotron Radiat.*, 2004, **11**, 53–55.
- 7 H. Irschik, K. Gerth, G. Höfle, W. Kohl and H. Reichenbach, *J. Antibiot.*, 1983, **36**, 1651–1658.
- 8 N. Gaitatzis, B. Kunze and R. Müller, *Proc. Natl. Acad. Sci. U. S. A.*, 2001, **98**, 11136–11141.





---

## Chapter 4

# Advanced Mutasynthesis Studies on the Natural $\alpha$ -Pyrone Antibiotic Myxopyronin from *Myxococcus fulvus*

*J. Henning Sahner,<sup>†</sup> Hilda Sucipto,<sup>†</sup> Silke C. Wenzel, Matthias Groh,  
Rolf W. Hartmann and Rolf Müller*

<sup>†</sup>These authors contributed equally to this work

ChemBioChem, **2015**, 16, 946–953

DOI: 10.1002/cbic.201402666

Published online: 10.03.2015

## 4 Mutasynthesis Studies on Myxopyronin

### 4.1 Abstract

Myxopyronin is a natural  $\alpha$ -pyrone antibiotic from the soil bacterium *Myxococcus fulvus* Mx f50. Myxopyronin inhibits the bacterial RNA polymerase (RNAP) by binding to a part of the enzyme not targeted by the clinically used rifamycins. This mode of action makes myxopyronins promising molecules for the development of novel broad-spectrum antibacterials. We describe the derivatization of myxopyronins by an advanced mutasynthesis approach as a first step towards this goal. Site-directed mutagenesis of the biosynthetic machinery was used to block myxopyronin biosynthesis at different stages. The resulting mutants were fed with diverse precursors that mimic the biosynthetic intermediates to restore production. Mutasynthon incorporation and production of novel myxopyronin derivatives was analyzed by HPLC-MS/MS. This work sets the stage for accessing numerous myxopyronin derivatives, thus significantly expanding the chemical space of the class of  $\alpha$ -pyrone antibiotics.

### 4.2 Introduction

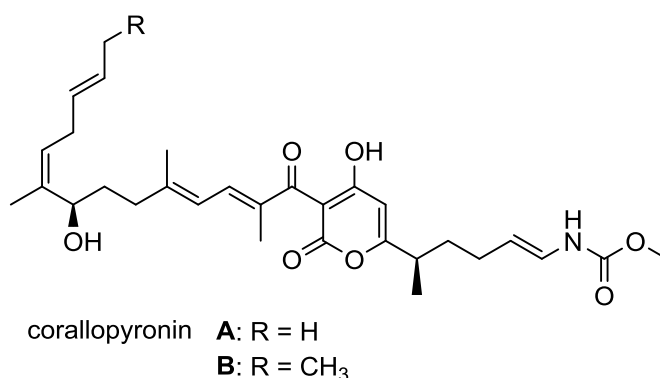
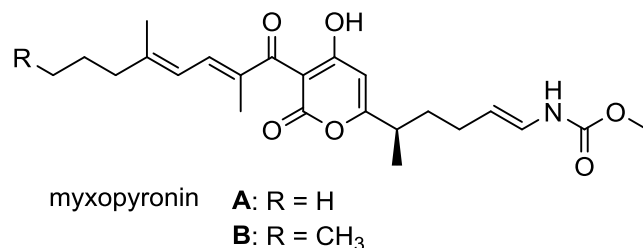
The current evolving of bacterial resistances against clinic antibiotics is alarming. Resistant *Mycobacterium tuberculosis* (MTB) strains, for example, represent a major health threat; approximately 1.5 million patients die from tuberculosis infections each year.<sup>[1]</sup> The evolved multidrug-resistant tuberculosis (MDR-TB) strains in recent decades are resistant to the first-line TB drugs rifampicin and isoniazid.<sup>[2]</sup> These strains gave rise to the increasingly prevalent extensively drug-resistant tuberculosis strains (XDR-TB). These strains are also resistant to at least one of the second-line TB drugs.<sup>[3, 4]</sup> Rifampicin is the most prominent anti-TB drug; it binds at the active site of the bacterial RNA polymerase (RNAP), thus inhibiting the initiation of RNA synthesis and hence transcription.<sup>[5, 6]</sup> Widespread rifampicin resistance dramatically hampers tuberculosis therapy,<sup>[7]</sup> thus highlighting the importance of developing new antibiotics to overcome existing resistance.

Substances addressing known and exploited targets involve the risk of cross-resistance. It is more promising to identify inhibitors of novel targets and binding sites to avoid such effects.<sup>[8-10]</sup> Recently the switch region of bacterial RNAP was discovered as a new binding site. It is targeted by the natural  $\alpha$ -pyrone antibiotic myxopyronin,<sup>[11]</sup> which was isolated from the terrestrial myxobacterium *Myxococcus fulvus* Mx f50.<sup>[12, 13]</sup> It was shown that rifampicin-resistant mutants exhibit no cross-resistance to myxopyronin, thus making myxopyronins a promising starting point for drug development.<sup>[14]</sup> Coralloyronins, which

are structurally closely related to myxopyronins, are further members of the  $\alpha$ -pyrone class of antibiotics.

Despite the close structural similarity between myxopyronins and corallopyronins, there are remarkable differences in their pharmacodynamic profiles. Whereas corallopyronin completely blocks RNA synthesis *in vitro*, myxopyronin only achieves inhibition to a certain extent, even at high concentrations.<sup>[15]</sup> Nevertheless, myxopyronin shows a lower minimal inhibitory concentration (MIC,  $1.6 \mu\text{g mL}^{-1}$ ) against several pathogens (including *M. tuberculosis* H37Rv) than does corallopyronin (MIC  $3.1 \mu\text{g mL}^{-1}$ ).<sup>[16]</sup>

The total synthesis of myxopyronin, corallopyronin, and several derivatives has been reported.<sup>[17–19]</sup> Because of the complexity of the compounds the described procedures are laborious, comprise many steps with relatively low final yields, and are not economically viable.



Mutasythesis represents an attractive approach for the generation of derivatives of complex natural products, without the necessity of multi-step organic synthesis.<sup>[20–23]</sup> In this method, small and chemically relatively simple precursors (mutasynthons, mimicking biosynthetic intermediates) are added to the culture of a mutagenized microbe in which natural product biosynthesis has been blocked at a particular stage. The mutasynthons enter the cells and are incorporated into the modified biosynthetic pathway thereby resulting in structurally diverse compounds. Currently, most successful examples have targeted biosynthesis precursors, such as the 3-amino-5-hydroxybenzoic acid (AHBA) moiety of

ansamitocins.<sup>[24, 25]</sup> The technology has rarely been used to incorporate more-advanced biosynthetic intermediates or even complex parts of the final molecule.

Recently, the biosynthetic pathways of myxopyronin (Figure 1A) and corallopyronin were elucidated, thus establishing the basis for mutasynthesis approaches.<sup>[26, 27]</sup> The natural products are composed of a central pyrone core decorated with two side chains (“western” (green) and “eastern” (blue), Figure 1A). The western and eastern moieties are synthesized by two enzymatic machineries that independently catalyze the assembly of each chain (here described for myxopyronins). The western chain is generated by the polyketide synthase (PKS) MxnK, and the carbamate-containing eastern chain is produced by the hybrid PKS/non-ribosomal peptide synthetase (NRPS) system MxnI/MxnJ. Such multimodular megasynthetases catalyze the stepwise assembly of simple precursors into complex molecules by using a distinct set of catalytic domains ordered in modules. Each module incorporates one specific unit into the growing biosynthetic intermediate. After chain assembly, the halves are condensed by the ketosynthase MxnB to result in the characteristic  $\alpha$ -pyrone core structure.

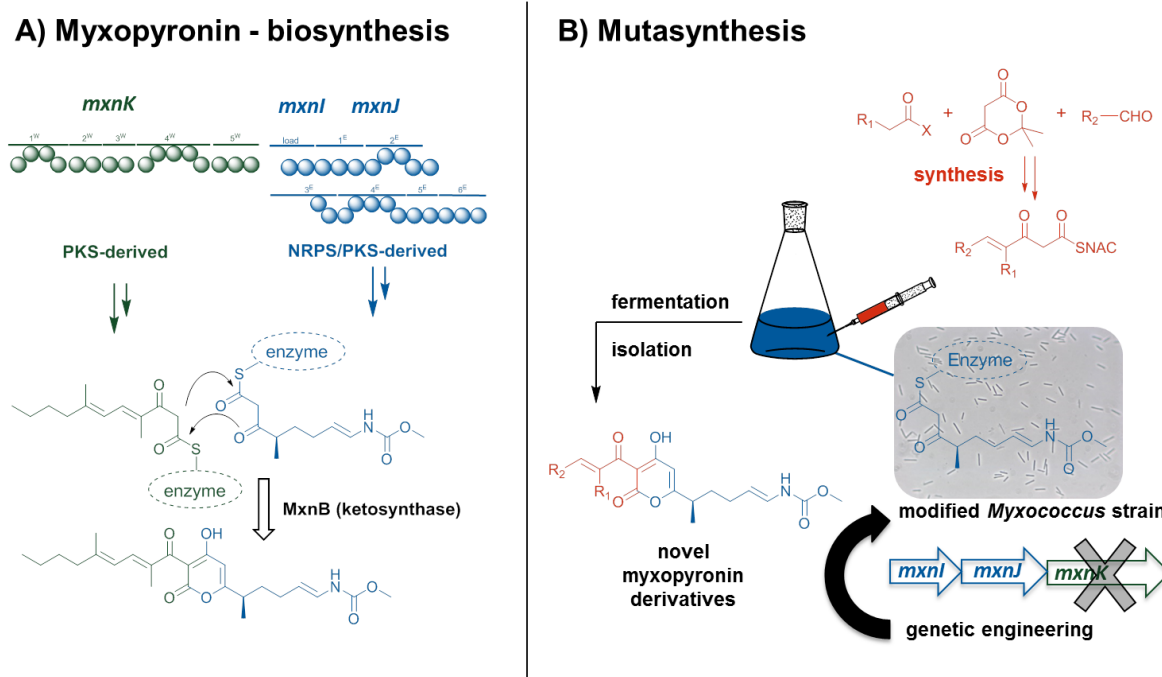


**Figure 1.** A) Biosynthetic pathway of myxopyronin.<sup>[26]</sup> The western chain (green) is produced by the PKS system MxnK. The eastern chain (blue) is derived from the PKS/NRPS hybrid system MxnI/MxnJ. The two chains are connected by the ketosynthase MxnB. B) Mutasynthesis approach. Synthetic western chains (red) are fed to a *M. fulvus*  $\Delta$ mxnK mutant (incapable of producing the native western chain). During fermentation, the synthetic precursors are combined with the native eastern chain to yield novel myxopyronin derivatives.

The physicochemical properties of myxopyronin are more complex than those of common clinical antibiotics.<sup>[7, 28]</sup> Its high lipophilicity results in decreasing MIC in the presence of serum albumin. The compound also features a conjugated doublebond system,



which makes it unstable and sensitive to UV light.<sup>[7, 29]</sup> Moreover, its high flexibility incurs a significant entropic penalty when binding to its target site, thus probably reducing its potency.

This work sets the stage for the advanced mutasythesis based development of new myxopyronin derivatives (Figure 1B), which could potentially overcome these problems and would ideally display higher inhibitory potency. So far the coralopyronin producer *Coralloccocus coralloides* Cc c127 was not amenable to the genetic modifications required for mutasythesis, and we therefore focused on myxopyronin. The major aim of this study was to elucidate the structural requirements for mutasythons to be taken up by the producing strain and to be accepted by the myxopyronin biosynthetic machinery. Because of the high structural similarity between myxopyronin and coralopyronin it is expected that our results will be transferable to the coralopyronin system.

### 4.3 Results and Discussion

Myxopyronin adopts a U-shaped conformation inside the switch region of the bacterial RNAP (Figure 2). The eastern chain extends into a narrow channel delimited by V1037, W1038, and E1041 of the RNAP  $\beta$ -subunit and by K1097, V1099, D1100, H805, K1463, V1466, and I1467 of the  $\beta'$ -subunit. Its polar carbamate function forms several crucial water-mediated hydrogen bonds with D1100, K1463 ( $\beta'$ ), and W1038 ( $\beta$ ). Initial structure–activity relationship (SAR) studies showed that slight variations in the eastern part of the molecule result in a dramatic loss of inhibitory activity, with one exception: the derivative lacking the R methyl group, adjacent to the  $\alpha$ -pyrone core (desmethyl myxopyronin), possesses the highest activity so far, approximately three times that of the natural product.<sup>[19]</sup>

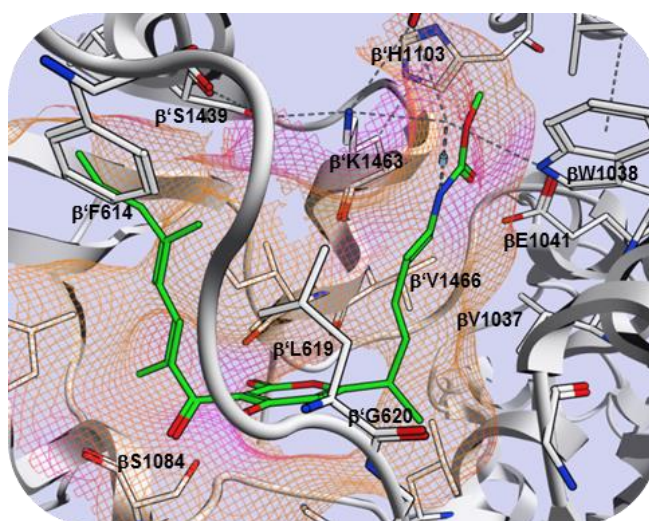
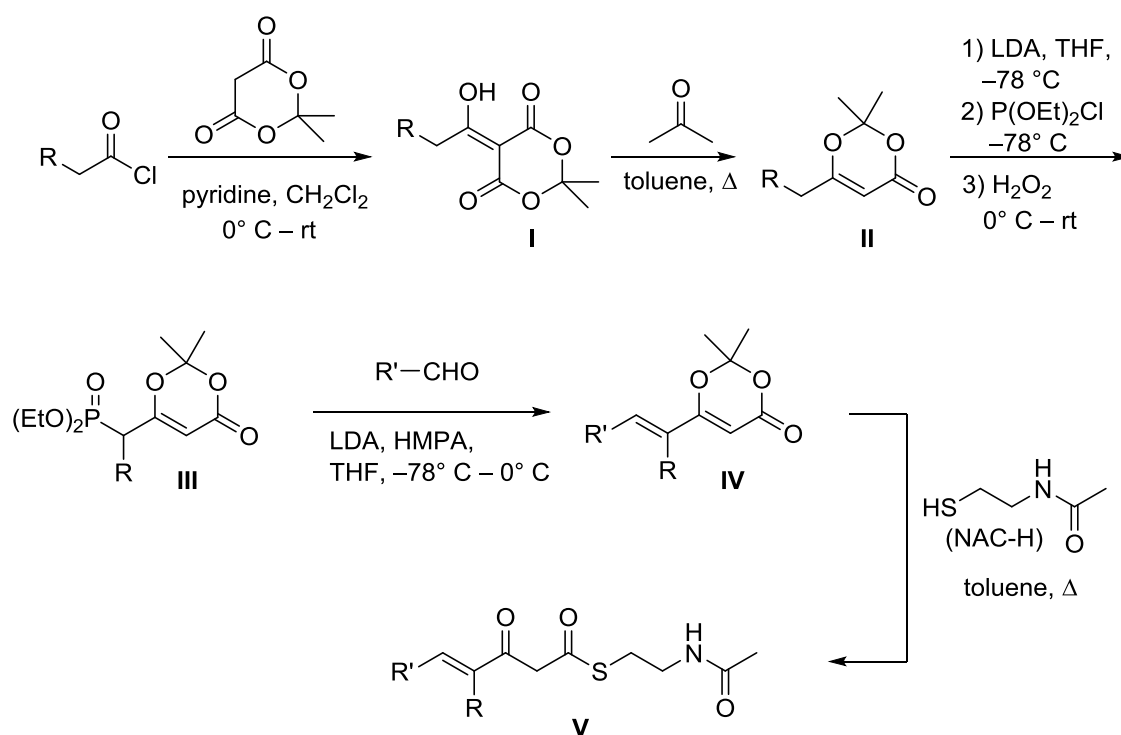


**Figure 2.** Crystal structure of myxopyronin inside the switch region of *Thermus thermophilus* RNAP (PDB-ID: 3DXJ).<sup>[11]</sup>

The western chain of myxopyronins provides wider scope for structural variation. It is composed of only hydrophobic functionalities, which do not significantly contribute to interactions with the RNAP switch region. Potentially, however, interactions with several polar amino acids and protein backbones are possible in this region. Establishment of a single specific hydrogen bond could therefore result in improved RNAP inhibition. Moreover, the larger RNAP binding pocket in this area provides the option to introduce bulkier groups, thereby resembling corallopyronins, which are significantly larger in the western chain. Thus, we focused on the production of myxopyronin derivatives with modified western chains. *N*-acetyl cysteamine (NAC) thioesters were chosen as substrates for feeding experiments, as they mimic carrier protein (CP)-bound biosynthetic intermediates of the assembly line. The application of NAC thioesters for mutasynthesis approaches with PKS/NRPS assembly lines is well established. They are known to enter cells and to be accepted as substrates by biosynthetic enzymes.<sup>[20]</sup>

In a first attempt we aimed to synthesize mimics of the fully matured western chain intermediate, which should directly enter the chain-condensation reaction catalyzed by MxnB. Synthesis of the required  $\beta$ -keto NAC-thioesters from the corresponding  $\beta$ -ketoacids is intractable because of instability of the free acids or undesired side products under coupling conditions.<sup>[30]</sup> Therefore, we developed a synthetic route that involves dioxinones as protected  $\beta$ -ketoacid equivalents. Most of the desired  $\beta$ -keto NAC thioesters were obtained according to the synthesis route shown in Scheme 1. The first step involves acylation of Meldrum's acid (**I**)<sup>[31]</sup> followed by a rearrangement to yield dioxinone **II**.<sup>[32]</sup> After conversion to the dioxinone phosphonate **III**,<sup>[33]</sup> the resulting compound was coupled with the appropriate aldehyde in a Horner–Wadsworth–Emmons reaction to yield the unsaturated dioxinone **IV**.<sup>[34]</sup> Final conversion with NAC gave the desired  $\beta$ -keto-NAC-thioester **V**.<sup>[30]</sup>

The generated mutasynthons **1–12** (details of the synthesis can be found in the Supporting Information) are mimics of fully matured western chain intermediates bound to the terminal CP domain of MxnK (Table 1). In order to block native western chain biosynthesis (to avoid competition with the mutasynthons), MxnK was inactivated by deletion of a 5.6 kb internal fragment of the 18 kb *mxnK* gene. This chromosomal modification was performed according to a previously established procedure for markerless site-directed mutagenesis in *M. fulvus* Mx f50.<sup>[26]</sup> LC-MS analysis revealed that, as expected, myxopyronin production was completely abolished in the mutant strain  $\Delta$ *mxnK* (Mx f50 $\Delta$ pHSU-*mxn18*, Table S1).

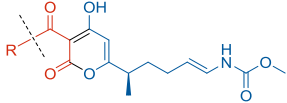
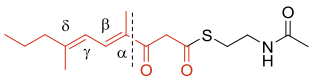
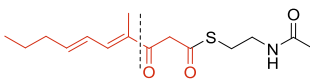
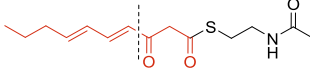
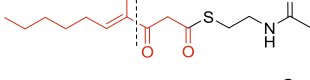
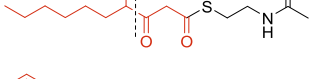
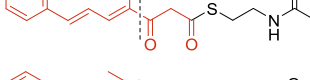
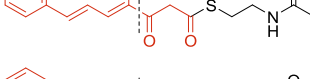
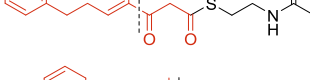
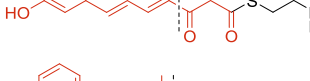
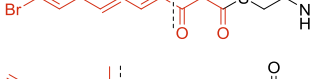
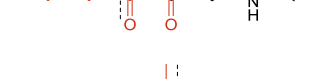
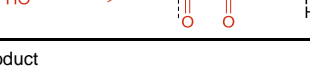


**Scheme 1.** Synthesis of the  $\beta$ -keto intermediates. a) pyridine,  $\text{CH}_2\text{Cl}_2$ ,  $0^\circ\text{C}$ –RT; b) toluene,  $\Delta$ ; c) LDA, THF,  $-78^\circ\text{C}$ ; d)  $\text{P(OEt)}_2\text{Cl}$ ,  $-78^\circ\text{C}$ ; e)  $\text{H}_2\text{O}_2$ ,  $0^\circ\text{C}$ –RT; f)  $\text{R}'\text{-CHO}$ , LDA, HMPA, THF,  $-78$ – $0^\circ\text{C}$ .

Subsequently, mutasynthesis experiments were carried out by feeding the precursors to small-scale  $\Delta\text{mxnK}$  cultures. Analysis of the culture extracts by HPLC-MS/MS revealed the successful incorporation of most of the mutasynthons (see below). Production of the expected myxopyronin derivatives was verified by high-resolution MS and fragmentation pattern analysis (Table 2 and Figures S3–S18 in the Supporting Information).

As a proof of concept, **1** (the  $\beta$ -keto NAC thioester; representing the exact mimic of the native biosynthetic intermediate) was investigated. Myxopyronin production was restored when **1** was fed to  $\Delta\text{mxnK}$ . The successful incorporation and restoration of myxopyronin production demonstrated that the mutasynthesis system is fully functional. Functional groups of the “natural” precursor were then systematically removed to analyze whether they are mandatory for the chain condensation catalyzed by MxnB. Although removal of the methyl group in the  $\delta$ -position (**2**) was tolerated and resulted in the production of the novel derivative W2, additional elimination of the methyl at the  $\alpha$ -position (**3**) did not yield the expected product. Compound **4** (lacking the  $\delta$ -methyl and the  $\gamma$ -double bond) was accepted, whereas the completely saturated precursor **5** was not incorporated.

**Table 1.** Synthetic western side-chain mimics. If accepted, the red part is incorporated into the resulting myxopyronin derivative.

		
	Formula	Myx derivative
1		W1
2		W2
3		n.p. <sup>[a]</sup>
4		W4
5		n.p. <sup>[a]</sup>
6		W6
7		W7
8		W8
9		W9
10		W10
11		W11
12		W12

[a] n.p. no product

**Table 2.** Characterization of novel myxopyronin A analogues with representative fragmentation patterns observed

	Chemical formula	$m/z$ [M+H] <sup>+</sup>		Fragmentation due to losses of			
		Calcd	Obs.	H <sub>2</sub> O ( $m/z$ = 18)	CH <sub>3</sub> OH ( $m/z$ = 32)	H <sub>2</sub> N-CO <sub>2</sub> CH <sub>3</sub> ( $m/z$ = 75)	H <sub>2</sub> N-CO <sub>2</sub> CH <sub>3</sub> , CO <sub>2</sub> ( $m/z$ = 119)
Myx A	C <sub>23</sub> H <sub>32</sub> NO <sub>6</sub>	418.22241	418.22217	400.21129	386.19576	343.18988	299.20017
W1	C <sub>23</sub> H <sub>32</sub> NO <sub>6</sub>	418.22241	418.22227	400.21112	386.19567	343.18981	299.20007
W2	C <sub>22</sub> H <sub>30</sub> NO <sub>6</sub>	404.20676	404.20666	386.19588	372.18020	329.17446	285.18464
W4	C <sub>22</sub> H <sub>32</sub> NO <sub>6</sub>	406.22241	406.22250	388.21078	374.19559	331.18951	287.19987
W6	C <sub>25</sub> H <sub>28</sub> NO <sub>6</sub>	438.19111	438.19103	420.17930	406.16392	363.15828	319.16866
W7	C <sub>26</sub> H <sub>30</sub> NO <sub>6</sub>	452.20676	452.20686	434.19544	420.18146	377.17400	333.18430
W8	C <sub>25</sub> H <sub>30</sub> NO <sub>6</sub>	440.20676	440.20659	422.19529	408.17954	365.17410	321.18438
W9	C <sub>25</sub> H <sub>28</sub> NO <sub>7</sub>	454.18602	454.18643	436.17468	n.o. <sup>[a]</sup>	379.15314	335.16345
W10	C <sub>25</sub> H <sub>26</sub> NO <sub>6</sub> Br	516.10163	516.10175	498.09073	484.07530	441.06942	397.07952
W11	C <sub>21</sub> H <sub>26</sub> NO <sub>6</sub>	388.17546	388.17557	n.o. <sup>[a]</sup>	n.o. <sup>[a]</sup>	313.14233	269.15311
W12	C <sub>22</sub> H <sub>30</sub> NO <sub>7</sub>	420.20167	420.20148	402.19059	n.o. <sup>[a]</sup>	345.16920	301.17982
W13	C <sub>23</sub> H <sub>32</sub> NO <sub>6</sub>	418.22241	418.22232	400.21163	386.19590	343.18984	299.19999
W14	C <sub>26</sub> H <sub>30</sub> NO <sub>6</sub>	452.20676	452.20670	434.19736	420.18027	377.17516	333.18508
W16	C <sub>23</sub> H <sub>32</sub> NO <sub>6</sub>	418.22241	418.22235	400.21137	386.19598	343.18972	299.20000
W17	C <sub>22</sub> H <sub>30</sub> NO <sub>6</sub>	404.20676	404.20675	386.19635	372.18204	329.17496	285.18512
W18	C <sub>25</sub> H <sub>28</sub> NO <sub>6</sub>	438.19111	438.19118	420.18041	406.16491	363.15886	319.16910

[a] n.o. : not observed

We concluded that both the  $\alpha$ -methyl group and the  $\alpha$ -double bond are essential for substrate acceptance and pyrone ring formation by MxnB. Hence, these structural features were included in all further synthesized mutasythons, in order to maximize the probability of incorporation. Next we tested whether mutasythons with terminal phenyl substituents are incorporated. Such aromatic systems allow easy introduction of a variety of functional groups; when attached at the appropriate positions of the ring, these groups can be used to engineer new and specific interactions with bacterial RNAP. A closer look at the crystal structure of bacterial RNAP complexed with myxopyronin (PDB ID: 3DXJ) revealed that the pocket accepting the western part should be wide enough to accommodate this dramatic structural change. Compound **6** was initially tested, and it resulted in production of the desired derivative **W6** (Figure 3). Replacement of the  $\alpha$ -methyl group by an ethyl function (**7**) or omitting the  $\gamma$ -double bond (**8**) also allowed incorporation.

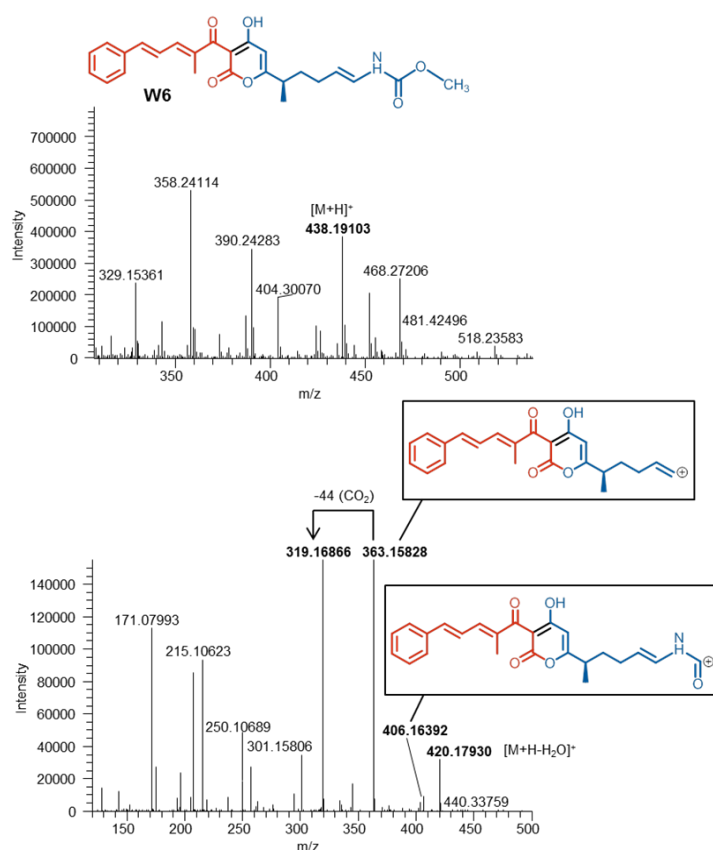


**Figure 3.** **W6** detected in an extract from a culture of Mx f50  $\Delta$ *mxnK* after feeding with **6**. Top: MS spectrum; bottom: fragment spectrum of the parent ion  $m/z$  438.19  $[M+H]^+$  (Table 2).

Molecular modeling studies with **W6** suggested that a hydroxy function in the meta position of the phenyl ring might lead to a water-mediated H-bond with W1434 ( $\beta'$ -subunit). Moreover, the additional hydrophilic function could lead to improved physicochemical properties. Thus, **9** was synthesized and successful incorporation yielded derivative **W9**. Encouraged by these results, a precursor with a bromo substituent (**10**) instead the hydroxy function was synthesized and fed; this enabled the production of the expected myxopyronin analogue (**W10**). Such a brominated derivative provides possibilities for further derivatization (e.g., under Suzuki <sup>[35]</sup> or Buchwald Hartwig <sup>[36]</sup> conditions) to attain a broader chemical space.

We next attempted to introduce a terminal alkyne functionality, in order to allow subsequent synthetic modifications of the expected mutasynthesis product. The resulting myxopyronin analogue could, for example, react with different azides under mild conditions (click chemistry) <sup>[37]</sup> to generate triazole containing myxopyronin derivatives with various substitution patterns. A corresponding mutasynthon (**11**) was synthesized and successfully incorporated, thereby resulting in the production of derivative **W11**. Inspired by

corallopyronin, we finally synthesized a mutasython bearing a terminal hydroxy group (**12**) at the same position as in the corallopyronin western chain. There is no X-ray structure of a corallopyronin–RNAP complex, but because of the close similarity to myxopyronin (as well as several mutagenesis studies),<sup>[38]</sup> its binding mode can be assumed to be analogous to that of myxopyronin. The additional alkyl chain of corallopyronin likely extends into an adjacent lipophilic pocket to interact with  $\beta$ -L1326 (Figure 4).<sup>[11, 16]</sup> The hydroxy function presumably contributes to its activity by forming a hydrogen bond with the protein. A corresponding myxopyronin derivative (**W12**) might therefore benefit from an additional interaction (similar to corallopyronin) and was obtained after feeding **12** to  $\Delta$ *mxnK*.

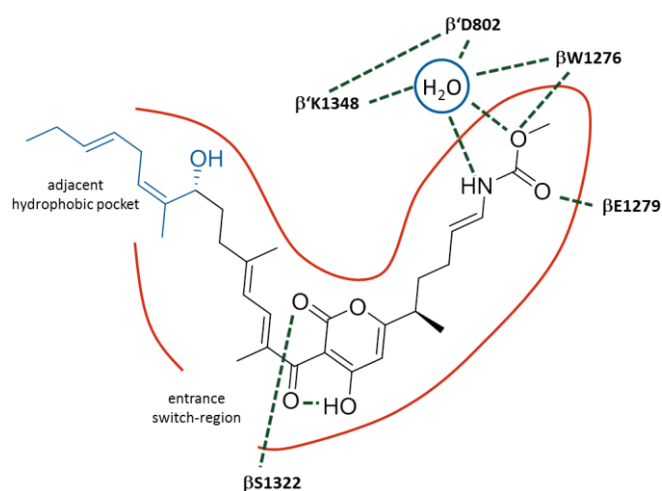


**Figure 4.** Myxopyronin (black) and corallopyronin (black+blue) inside the switch region. Adapted from Mukhopadhyay et al.<sup>[11]</sup>

The first attempts to isolate sufficient quantities of the new myxopyronin derivatives generated by mutasythesis failed (low production yields). Possible bottlenecks might be limited uptake of the  $\beta$ -keto NAC thioesters, their fast degradation after feeding to the culture, or inefficient incorporation by the biosynthetic process. Closer analysis of the fermentation culture extracts revealed that trace amounts of the mutasythons were left, thus indicating that precursor degradation/instability might be a limiting factor. Therefore we decided to increase the chemical stability of the mutasythons and to re-design the myxopyronin mutasythesis approach. In the experiments described above, western chain biosynthesis was completely blocked, and complementation was achieved by feeding mimics of fully matured western-chain intermediates. Thus,  $\beta$ -keto thioesters are required as mutasythons to enable the final pyrone ring formation by Claisen condensation. In order to circumvent the use of the rather unstable  $\beta$ -keto thioesters (which precludes long-term

storage), we aimed to block and complement western chain biosynthesis at earlier stages. This would enable feeding experiments with simplified and more stable mutasynthons (Figure S2A and B). Two additional mutants were generated by site-directed mutagenesis to inactivate the carrier protein (CP) domains from modules 1 and 4 (CP-1<sup>W</sup> or CP-4<sup>W</sup>). In both cases, the CP active-site serine required for post-translational modification<sup>[39]</sup> was mutated to alanine (strains  $\Delta$ CP-1<sup>W</sup> and  $\Delta$ CP-4<sup>W</sup>, respectively). Interestingly, western chain biosynthesis was not completely abolished, as trace amounts of myxopyronin A could still be detected in culture extracts of both mutants. We reasoned that in the case of  $\Delta$ CP-1<sup>W</sup>, butyryl-CoA might act as starter unit, which would be directly elongated and incorporated into the assembly process at module 3. However, the production of myxopyronin A by  $\Delta$ CP-4<sup>W</sup> is difficult to explain with standard PKS biochemistry. One possible scenario involves an additional (iterative) elongation round without keto reduction by module 1W and subsequent modification of the  $\beta$ -keto moiety, possibly on CP-2W (or CP-1<sup>W</sup>) to introduce the methyl branch.

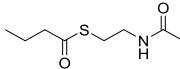
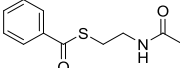
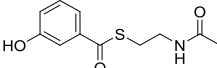
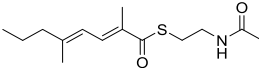
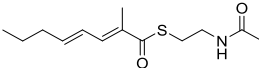
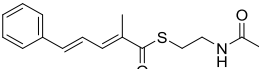
Although myxopyronin biosynthesis was not completely inhibited, feeding experiments with simplified and more-stable mutasynthons were performed. Cultures of  $\Delta$ CP-1<sup>W</sup> were supplemented with precursors **13–15**, and myxopyronin production was analyzed by HPLC-MS/MS (Table 3). As expected, myxopyroninA was produced after feeding **13** in larger quantities than in the control (without feeding). Precursor **14** was also accepted, as myxopyronin derivative **W14** was detected. Interestingly, **15** (hydroxy group in the meta position) did not result in the production of a hydroxylated myxopyronin derivative, as was observed when the  $\beta$ -keto thioester (**9**) was fed. It is possible that selectivity issues of downstream catalytic domains in the PKS are responsible, as these are circumvented in feeding experiments with fully matured western-chain mimics like **9**.

Mutant  $\Delta$ CP-4W was analyzed by using extended NAC-thioesters **16–18** to mimic module 4<sup>W</sup> intermediates. All substrates were accepted, and the respective myxopyronin derivatives were detected by HPLC-MS/MS analysis (increased levels of myxopyronin A in the  $\Delta$ CP-4<sup>W</sup> culture fed with 16 compared to the control). Although the NAC-thioesters without a  $\beta$ -keto function were more stable, the yields of the final products were still too low for product isolation (1–10  $\mu\text{g mL}^{-1}$ ) for bioactivity testing. The detection of large amounts of substrates in the culture supernatants suggested that insufficient uptake into cells was a limiting factor. To address this, modified feeding procedures were evaluated: addition of detergents like poly(ethylene glycol) (PEG), Tween, or DMSO to increase cell permeability, as well as increasing the number of feeding events. However, improved myxopyronin production yields could not be obtained. Further experiments to improve yield will be carried



out to fully exploit the established mutasythesis systems and to access compounds from the culture extracts after biotechnological process optimization. With regard to this bottleneck, engineering the efflux pumps of the producer strain might hold promise to improve precursor uptake. Furthermore, we shall focus on establishing a heterologous production system to improve yields.

**Table 3.** Synthetic western side-chain mimics.

	Formula	Myx derivative
13		W13 (=W1)
14		W14
15		n.p. <sup>[a]</sup>
16		W16 (=W1)
17		W17
18		W18

[a] n.p. : no product

## 4.4 Conclusion

Mutasythesis represents a powerful approach to produce libraries of natural product derivatives that are difficult to access by purely synthetic routes. Here we established such an approach for the bacterial RNAP inhibitor myxopyronin. Mutants of the native myxopyronin producer *M. fulvus* Mx f50 were generated to block (or, at least, significantly reduce) native western-chain assembly. Intriguingly, most of the synthesized mutasythons were successfully incorporated by the mutasythesis systems. This indicates that the participating enzymes display relatively high tolerance to variation in substrate structure. The substrate specificity of MxnB, which is responsible for the last step of myxopyronin biosynthesis, could be evaluated. The mutant with a nonfunctional MxnK required feeding of  $\beta$ -keto NAC thioesters (1–12) to generate products. On the one hand, these substrates allow the highest flexibility in variation of the resulting myxopyronin derivatives, because of the late stage of incorporation. On the other hand, their synthesis is more laborious, and the compounds are

relatively unstable. Mutants expressing a partly functional western-chain assembly line enabled feeding experiments with shorter precursors without a  $\beta$ -keto function. These mutasynthons are more stable and easier to synthesize in large quantities. However, the variability in terms of tolerated structural variations is more restricted compared to the  $\beta$ -keto mutasynthons. Although productivity is currently too low to allow full characterization of the products (and thus clearly has to be improved), the established mutasynthesis systems provide a comprehensive basis for planned studies to generate new myxopyronin derivatives. This will allow us to further exploit this promising class of  $\alpha$ -pyrone antibiotics. The broad western-chain substrate tolerance in the final condensation reaction even allows exploration of the coralopyronin chemical space by this mutasynthesis system. The resulting compounds could be streamlined to improve their physicochemical properties and potentially overcome the problems of current antibiotic resistance.

## 4.5 Experimental Section

### Bacterial strains and culturing conditions

Bacterial strains and plasmids used in this study are listed in Table S1. Wild-type *M. fulvus* Mx f50 and mutants were grown in Casitone Yeast (CY) medium (casitone (0.3 %), yeast extract (0.1 %),  $\text{CaCl}_2 \cdot 2\text{H}_2\text{O}$  (0.1 %)) supplemented with vitamin B12 (500 mg/mL) after autoclaving. For liquid cultures, the strains were grown at 30 °C in an orbital shaker (105 rpm) and harvested after 3 days. *Escherichia coli* strains were cultured in lysogeny broth (LB: tryptone (1 %), yeast extract (0.5 %), NaCl (0.5 %)) at 37 °C, with ampicillin (100  $\mu\text{g mL}^{-1}$ ) or kanamycin (50  $\mu\text{g mL}^{-1}$ ) where necessary.

### DNA preparations and PCR

*M. fulvus* Mx f50 genomic DNA was prepared either by the phenol/chloroform/isoamyl alcohol extraction method<sup>[40]</sup> or by using the Gentra Puregene Genomic DNA Purification Kit (Qiagen) according to the manufacturer's protocol. Plasmid DNA was either purified by standard alkaline lysis<sup>[40]</sup> or by using a GeneJET Plasmid Miniprep Kit (Thermo Fisher Scientific). PCR reactions were carried out in a peqSTAR 96 Universal Gradient thermocycler (Peqlab, Erlangen, Germany): initial denaturation (3 min, 95 °C); 30 cycles of denaturation (30 s, 95 °C), annealing (30 s, 53 or 57 °C), and elongation (duration depends on PCR product length, 1 kb  $\text{min}^{-1}$ , 72 °C); final extension (10 min, 72 °C). DNA fragments were separated by agarose gel electrophoresis and isolated with a peqGold Gel Extraction kit (Peqlab). The PCR products were cloned into pJET1.2 blunt (Thermo Scientific) vector and sequenced with primers pJET1.2For/pJET1.2Rev (all primer sequences used in this study are

given in Table S2). General procedure for site-directed mutagenesis of *mxnK* by in-frame deletion and point mutation: In general, construction of in-frame deletion mutants was carried out by amplifying 1000–1250 bp homology regions on each side of the desired deletion area by PCR. Each fragment was subcloned to pJET1.2 and sequenced. After sequence verification the homology regions were cloned into the pSWU41 vector, <sup>[41]</sup> kindly provided by Dale Kaiser, by using the restriction sites indicated in Table S2. The vector contains a neomycin phosphotransferase (*nptII*) and levansucrose (*sacB*) gene cassette and derives from pSWU35 <sup>[41]</sup> by deletion of the 1045 bp PvuI fragment (Samuel Wu, personal communication). The resulting constructs were electroporated into *M. fulvus* Mx f50. The culture was grown in CY medium in a baffled flask. At OD<sub>600</sub>=0.6–0.9, the cells were harvested from the culture (2–4 mL; 1–2x10<sup>9</sup> cells mL<sup>-1</sup>) by centrifugation (14900 g 1 min, RT). After washing with H<sub>2</sub>O (2x1 mL) at room temperature, cells were resuspended in H<sub>2</sub>O (65 µL). Plasmid DNA (1–2 mg) was mixed with the cell suspension, and electroporation was carried out in 0.1 cm electroporation cuvettes in a GenePulser XCell device (Bio-Rad; 25 mF, 400 W, 650 V). CY medium (1 mL) was added to the cell suspension immediately after electroporation, and the cells were transferred into a 2 mL centrifuge tube. After 6–8 h culturing on a thermomixer (30 °C, 800 rpm), the cells were mixed with CY soft agar (2 mL, CY medium containing agar (0.7 %)) and plated on CY agar plates (CY medium containing agar (1.7 %)) supplemented with kanamycin (50 µg mL<sup>-1</sup>). The plates were incubated at 30 °C until colonies became visible (7–10 days). Construction of markerless double-crossover mutants: After verification of the single crossover mutant (kanamycin resistant) by PCR (integration at two different homology regions is possible), a selected single-crossover mutant was grown in CY medium in the absence of antibiotics. After 3–4 days the culture (1 mL) was transferred into fresh medium (50 mL) for further culturing at 30 °C for 3–4 days. This procedure was repeated three times to increase the possibility of a second crossover event, which would result in loss of the inactivation plasmid. Depending on the homology region used for the second crossover, this can yield either the wild-type genotype (“revertant”) or the expected double-crossover mutant strain, in which the targeted region is deleted. To select clones in which a second crossover had taken place, a counter selection system based on the *sacB* gene was used. <sup>[41]</sup> For this, different dilutions of the cell population were plated on CY agar supplemented with sucrose (6 %). After 7–10 days, the first colonies appeared; these were grown in CY medium to isolate genomic DNA for genotypic verification and to extract the cultures for phenotypic analysis.

### **Inactivation of *mxnK* by in-frame deletion**

To disrupt *mxnK* by in-frame deletion, a gene-inactivation plasmid harboring two fragments (1001 and 1262 bp, homologous to upstream and downstream regions around the chromosomal target) was constructed. These fragments were amplified from *M. fulvus* Mx f50 genomic DNA by PCR with primers mxn54/mxn55 and mxn56/mxn57 (Table S2). After digestion of the upstream fragment (mxn54/mxn55 product) with *Bam*HI and *Not*I, and the downstream fragment (mxn56/57 product) with *Not*I and *Sac*I, the fragments were ligated into pSWU41 digested with *Bam*HI and *Sac*I to generate pHSU-mxn18. All subcloning steps were performed in *E. coli* HS996 (Invitrogen). For genotypic analysis of the single crossover, PCRs with primers mxn68/mxn69, mxn70/mxn72, and mxn73/mxn71 were carried out to verify correct integration of the inactivation plasmid. For genotypic analysis of putative double-crossover mutants, PCR was performed with primers mxn68/mxn71. Confirmation of the deletion mutant was obtained by Southern blot analysis (Figure S1).

### **Inactivation of *mxnK* by point mutation at CP-1<sup>W</sup>**

A gene inactivation plasmid harboring a 2445 bp fragment was constructed. The fragment was amplified from *M. fulvus* Mx f50 genomic DNA by overlap PCR with primer pairs mxn169/mxn170 and mxn171/mxn172. After digestion of the fragment and vector with *Pvu*II and *Not*I, ligation into pSWU41 generated pHSU-mxn48. For genotypic analysis of the single crossover, PCR with mxn185/mxn70 and pSWU41-F/mxn187 was carried out to verify correct integration of the inactivation plasmid. For genotypic analysis of the double crossover, PCR with mxn189/mxn205 was performed, and the amplified product was sequenced.

### **Inactivation of *mxnK* by point mutation at CP-4<sup>W</sup>**

A gene inactivation plasmid harboring a 2486 bp fragment was constructed. The fragment was amplified from *M. fulvus* Mx f50 genomic DNA by overlap PCR with primers mxn174/mxn175 and mxn176/mxn177. After digestion of the fragment and vector with *Pvu*II and *Not*I, ligation into pSWU41 generated pHSU-mxn49. Correct integration of the inactivation plasmid was verified by PCR with mxn191/mxn70, pSWU41-F/mxn193, and mxn195/mxn70. For genotypic analysis of the double crossover, PCR with mxn195/mxn206 was performed, and the amplified product was sequenced. Feeding for mutasynthesis experiments: A preculture of *M. fulvus* Mx f50 ( $\Delta$ *mxnK*), *M. fulvus* Mx f50 $\Delta$ CP-1<sup>W</sup>, or *M. fulvus* Mx f50 $\Delta$ CP-4<sup>W</sup> was grown in CY medium at 30 °C until OD<sub>600</sub>=0.3–0.6. The preculture inoculated into CY medium (20 mL; 7.2x10<sup>6</sup> cells mL<sup>-1</sup>). Culturing was carried out

for a further 12–24 h before feeding with substrate mimics. *N*-acetyl-cysteamine (SNAC)-esters (20–100  $\mu$ M) mimicking western chain 1–12 were fed to *M. fulvus* Mx f50 $\Delta$ *mxnK* cultures, **13–15** were fed to *M. fulvus* Mx f50 $\Delta$ CP-1<sup>W</sup>, and **16–18** were fed to *M. fulvus* Mx f50 $\Delta$ CP-4<sup>W</sup>. Cultures were grown for a further 48 h, and the cells were harvested. The supernatant was extracted twice with an equal volume of ethyl acetate. After evaporation of the organic phase, the residue was dissolved in methanol (100 mL). Analysis by LC-MS of the crude extract from the cultures showed formation of the novel myxopyronin analogues. High-resolution MS confirmed incorporation of the precursors (showing the same fragmentation pattern).

### HPLC-MS/MS analysis

All measurements were performed on a Dionex Ultimate 3000 RSLC system (Thermo Scientific) with a BEH C18 column (50 x 2.1 mm, 1.7  $\mu$ m; Waters) by injection of methanolic samples (5 mL). Separation was achieved by a linear gradient of A (FA (0.1%) in H<sub>2</sub>O) to B (FA (0.1%) in CAN) at 45 °C with a flow rate of 600  $\mu$ L min<sup>-1</sup>: 0.33 min isocratic step at 5% B; increase to 95% B (9 min); flush step at 95% B (1 min); re-equilibration with initial conditions. UV and MS detections were performed simultaneously. Coupling HPLC to MS was achieved with a TriVersa Nano-Mate nano-ESI system (Advion, Ithaca, NY) attached to an Orbitrap LC-MS (Thermo Scientific). Mass spectra were acquired in centroid mode (200–2000 *m/z*, resolution *R* = 30000).

## 4.6 Supporting Information

Full supporting information is available online:

[http://onlinelibrary.wiley.com/store/10.1002/cbic.201402666/asset/supinfo/cbic\\_201402666\\_sm\\_miscellaneous\\_information.pdf](http://onlinelibrary.wiley.com/store/10.1002/cbic.201402666/asset/supinfo/cbic_201402666_sm_miscellaneous_information.pdf)

**Table S1.** List of strains and plasmids used in this study

Strain/Plasmid	Description	Reference
<b><i>E. coli</i> strains</b>		
HS996	Host for general cloning experiments	Invitrogen
SCS110	Host for cloning experiments to prepare plasmid DNA free of Dam or Dcm methylation	Stratagene
<b><i>Myxococcus fulvus</i> strains</b>		
Mx f50	Myxopyronin producing wild-type strain	Irschik et al. <sup>[1]</sup>
Mx f50ΔpHSU-mxn18 (Δ <i>mxnK</i> )	<i>mxnK</i> in-frame deletion mutant; no myxopyronin production	this study
Mx f50ΔpHSU-mxn48 (ΔCP-1 <sup>W</sup> , point mutation at CP-1 <sup>W</sup> , S1686A)	CP-1 <sup>W</sup> point mutation; myxopyronin production (trace amount)	this study
Mx f50ΔpHSU-mxn49 (ΔCP-4 <sup>W</sup> , point mutation at CP-4 <sup>W</sup> , S5168A)	CP-3 <sup>W</sup> point mutation; myxopyronin production (trace amount)	this study
<b>Plasmids</b>		
pSWU41	Vector contains a neomycin phosphotransferase ( <i>nptII</i> ) gene for selection and a levansucrose ( <i>sacB</i> ) gene for counter selection	Wu et al. <sup>[2]</sup>
pHSU-mxn18	<i>mxnK</i> gene deletion construct, in which a 5624 bp fragment of <i>mxnC-mxnH</i> was deleted in-frame	
pHSU-mxn48	CP-1 <sup>W</sup> point mutation construct in which the active site serine residue is exchanged with alanine residue (S1668A)	this study
pHSU-mxn49	CP-3 <sup>W</sup> point mutation construct in which the active site serine residue is exchanged with alanine residue (S5168A)	this study

**Table S2.** List of primers used in this study

Primer name	Sequence (5'→3')	Restriction sites (in bold)
mxn54	GCGTTGAT <b>GGATCC</b> ACAGCA	<i>Bam</i> HI
mxn55	TGTATC <b>GCGGCCG</b> CTCAGTGCCGCTGAACCCGAAC	<i>Not</i> I
mxn56	GATACAG <b>GCGGCCG</b> CCTTTCCGAGTCCAGCAGC	<i>Not</i> I
mxn57	GTATC <b>GAGCTC</b> ATCTGCTGTCTCTGCCT	<i>Sac</i> I
mxn70	CTTGCGCCCTGAGTGCTT	
mxn71	AACACCTCACGGTCCGAC	
mxn72	CCCATCGTCCACAGCTTC	
mxn73	GCACTACAAGCGGCTCTG	
mxn169	GATACAC <b>GATCG</b> CACGAGTTCCGAGTCCTC	<i>Pvu</i> I
mxn170	CTGCAGGATGAGGGCGTC	
mxn171	TCGACGCCCTCATCCTGCAGGAGTTGATGGCGGAGCTG	
mxn172	TCTAT <b>GCGGCCG</b> CGAGCGCGACCTTGATGAC	<i>Not</i> I
mxn174	GATACAC <b>GATCG</b> GACACACACCGGAAGCTG	<i>Pvu</i> I
mxn175	ATCACCAGCGCGTCCGAC	
mxn176	CGGCGTCGACGCGCTGGTGAATCTGAGAATCGTCC	
mxn177	TCTAT <b>GAGCTC</b> TTGAGCTGCAGGATGACC	<i>Not</i> I
mxn185	TCGCTCATCCTGCAGGA	
mxn187	CGAGTCGAGTCCCATGG	
mxn189	CAACAGCTTCCTCGACG	
mxn191	TCCCTGGTGAATCTGAGA	
mxn193	GGAGTCGACGCCGAAC	
mxn195	TCGGACTGATGAAGGGGT	
mxn205	CCTTCGGGGAGATGTTGA	
mxn206	GAAGGCCTCCACGTTCTC	
pJET1.2For	CGACTCACTATAGGGAGAGCGGC	
pJET1.2Rev	AAGAACATCGATTTTCCATGGCAG	
pSWU41-F	GTGCAAAAAGCGGTTAG	

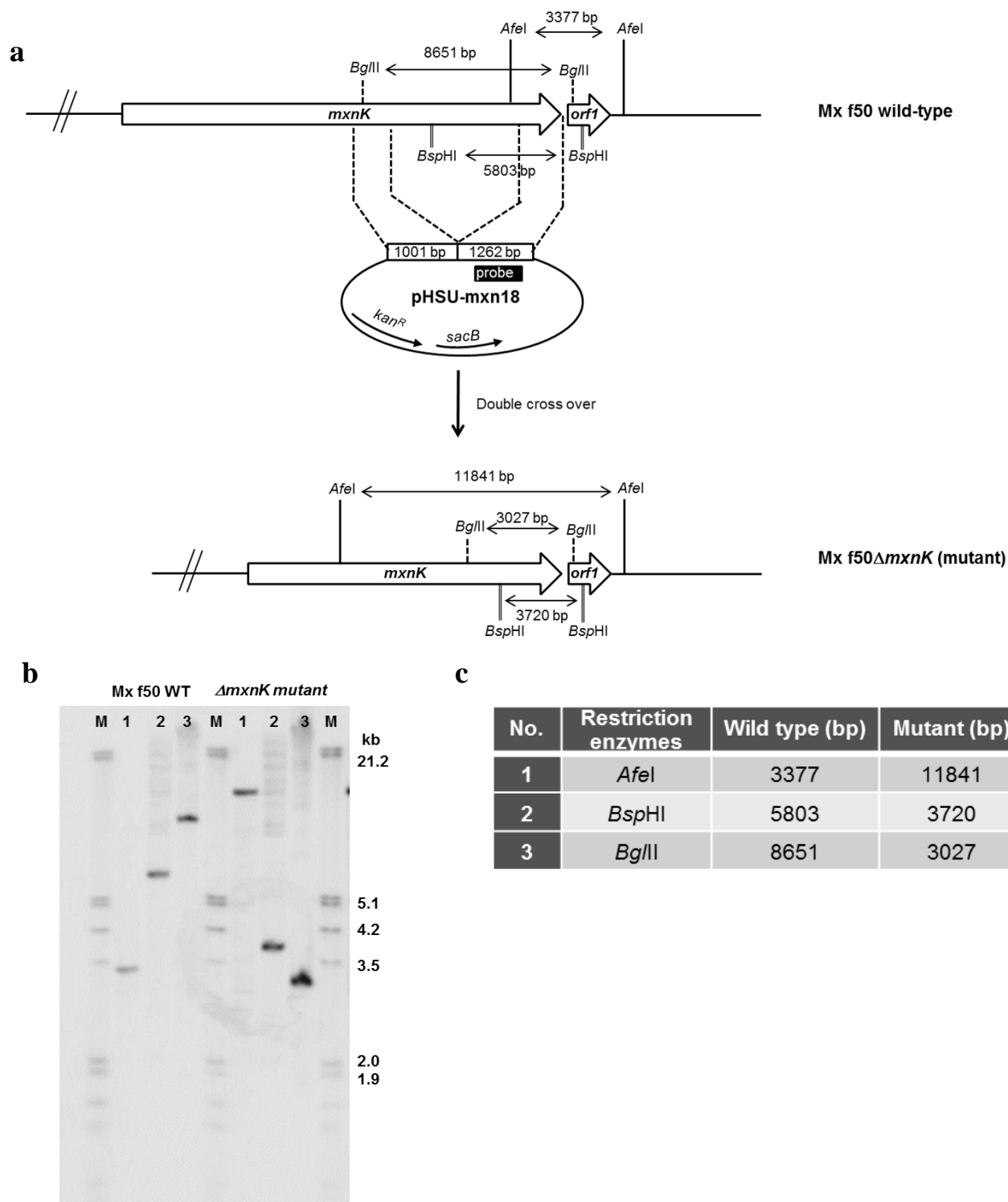


**Figure S1.** Schematic representation of in-frame deletion of 5.6 kb *mxnK* by construct pHSU-*mxn18*. (a), confirmation by Southern blot (b) and the expected fragment size after hydrolysis of wild type and mutant genomic DNA with a set of three restriction enzymes and a DIG-labelled 602 bp probe amplified from Mx f50 genomic DNA using the primers *mxn79* and *mxn80*. M: Marker III (Roche), 1: hydrolysis with *AfeI*, 2: hydrolysis with *BspHI*, 3: hydrolysis with *BglII*.



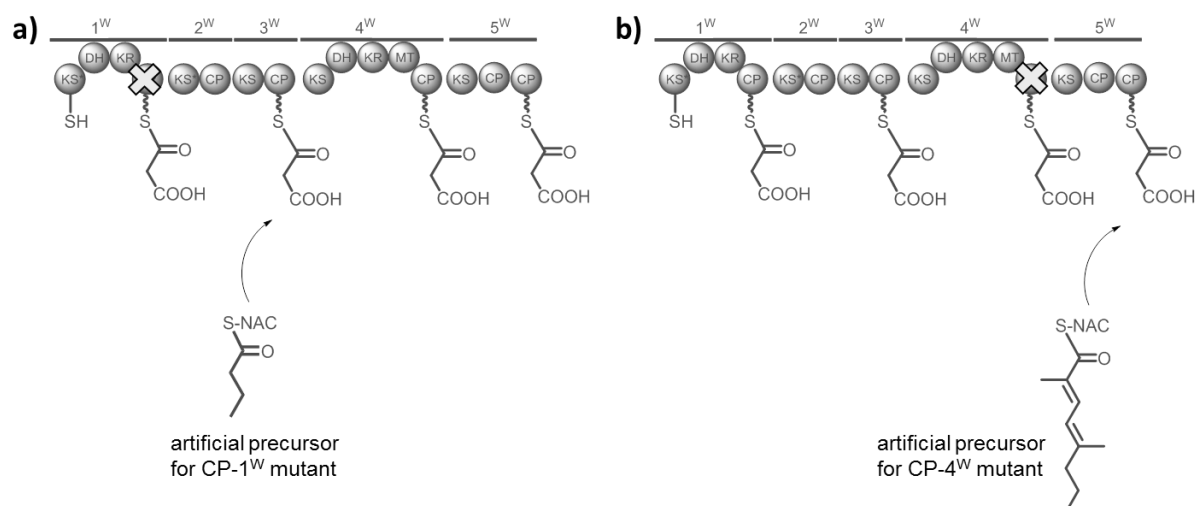


**Figure S2.** Schematic illustration of mutasythesis using *M. fulvus* Mx X50 mutants with partially functional western chain assembly line. a) A culture of a CP-1<sup>W</sup> mutant was supplemented with the appropriate precursor which is incorporated in the subsequent biosynthesis pathway. b) A culture of a CP-4<sup>W</sup> mutant was supplemented with the appropriate precursor which is incorporated in the subsequent biosynthesis pathway.

---

## 4.7 References

### 4.7.1 References for Main Text

- [1] World Health Organization, *Global Tuberculosis Report 2014*, WHO, Geneva, **2014**, [http://www.who.int/tb/publications/global\\_report/en/](http://www.who.int/tb/publications/global_report/en/).
- [2] T. Dalton, P. Cegielski, S. Akkslip, L. Asencios, J. C. Caoili, S.-N. Cho, V. V. Erokhin, J. Ershova, M. T. Gler, B. Y. Kazenyy, H. J. Kim, K. Kliiman, E. Kurbatova, C. Kvanovsky, V. Leimane, M. van der Walt, L. E. Via, G. V. Volchenkov, M. A. Yagui, H. Kang, Global PETTS investigators, *Lancet* **2012**, *380*, 1406-1417.
- [3] World Health Organization, *Guidelines for the Programmatic Management of Drug-Resistant Tuberculosis: Emergency Update*. **2008**, [http://whqlibdoc.who.int/publications/2008/9789241547581\\_eng.pdf](http://whqlibdoc.who.int/publications/2008/9789241547581_eng.pdf).
- [4] M. Zignol, W. van Gemert, D. Falzon, C. Sismanidis, P. Glaziou, K. Floyd, M. Raviglione, *Bull. W.H.O.* **2012**, *90*, 111-119.
- [5] E. A. Campbell, N. Korzheva, A. Mustaev, K. Murakami, S. Nair, A. Goldfarb, S. A. Darst, *Cell* **2001**, *104(6)*, 901-912.
- [6] I. Chopra, *Curr. Opin. Investig. Drugs*. **2007**, *8(6)*, 600-607.
- [7] D. Haebich, F. von Nussbaum, *Angew. Chem. Int. Ed.* **2009**, *48(19)*, 3397-3400; *Angew. Chem.* **2009**, *121*, 3447-3451
- [8] C. T. Barrett, J. F. Barrett, *Curr. Opin. Biotechnol.* **2003**, *14*, 621-626.
- [9] J. Wang, A. Galgoci, S. Kodali, K. B. Herath, H. Jayasuriya, K. Dorso, F. Vicente, A. González, D. Cully, D. Bramhill, S. Singh, *J. Biol. Chem.* **2003**, *278*, 44424-44428.
- [10] A.R.M. Coates, G. Halls, Y. Hu, *Br. J. Pharmacol.* **2011**, *163*, 184-194.
- [11] J. Mukhopadhyay, K. Das, S. Ismail, D. Koppstein, M. Jang, B. Hudson, S. Sarafianos, S. Tuske, J. Patel, R. Jansen, H. Irschik, E. Arnold, R. H. Ebright, *Cell* **2008**, *135*, 295-307.
- [12] H. Irschik, K. Gerth, G. Höfle, W. Kohl, H. Reichenbach, *J. Antibiot.* **1983**, *36*, 1651-1658.
- [13] W. Kohl, H. Irschik, H. Reichenbach, G. Höfle, *Liebigs Ann. Chem.* **1983**, 1656-1667.
- [14] A. O'Neill, B. Oliva, C. Storey, A. Hoyle, C. Dishwick, I. Chopra, *Antimicrob. Agents Chemother.* **2000**, *44*, 3163-3166.
- [15] H. Irschik, R. Jansen, G. Höfle, K. Gerth, H. Reichenbach, *J. Antibiot.* **1985**, *38*, 145-152.
- [16] A. Srivastasa, M. Talaue, S. Liu, D. Degen, R. Y. Ebright, E. Sineva, A. Chakraborty, S. Y. Druzhinin, S. Chatterjee, J. Mukhopadhyay, Y. W. Ebright, A. Zozula, J. Shen, S. Sengupta, R. R. Niedfeldt, C. Xin, T. Kaneko, H. Irschik, R. Jansen, S. Donadio, N. Conell, R. H. Ebright, *Curr. Opin. Microbiol.* **2011**, *14*, 532-543.
- [17] A. Rentsch, M. Kalesse, *Angew. Chem. Int. Ed.* **2012**, *51(45)*, 11381-11384; *Angew. Chem.* **2012**, *124*, 11543-11547.
- [18] R. Lira, A. X. Xiang, T. Doundoulakis, W. T. Biller, K. A. Agrios, K. B. Simonsen, S. E. Webber, W. Sisson, R. M. Aust, A. M. Shah, R. E. Showalter, V. N. Banh, K. R. Steffy, J. R. Appleman, *Bioorg. Med. Chem. Lett.* **2007**, *17*, 6797-6800.
- [19] T. Doundoulakis, A. X. Xiang, R. Lira, K. A. Agrios, S. E. Webber, W. Sisson, R. M. Aust, A. M. Shah, R. E. Showalter, J. R. Appleman, K. B. Simonsen, *Bioorg. Med. Chem. Lett.* **2004**, *14(22)*, 5667-5672.
- [20] A. Kirschning, F. Taft, T. Knobloch, *Org. Biomol. Chem.* **2007**, *5*, 3245-3259.

- [21] C. J. Dutton, S. P. Gibson, A. C. Goudie, K. S. Holdom, M. S. Pacey, J. C. Ruddock, *J. Antibiot.* **1991**, *44*, 357-365.
- [22] S. J. Daum, J. R. Lemke, *Ann. Rev. Microbiol.* **1979**, *33*, 241-265.
- [23] W. T. Shier, K. L. Rinehart Jr., D. Gottlieb, *Proc. Natl. Acad. Sci. USA.* **1969**, *63*, 198-204.
- [24] T. Knobloch, G. Dräger, W. Collisi, F. Sasse, A. Kirschning, *J. Org. Chem.* **2012**, *8*, 861-869.
- [25] K. Harmrolfs, L. Mancuso, B. Drung, F. Sasse, A. Kirschning, *J. Org. Chem.* **2014**, *10*, 535-543.
- [26] H. Sucipto, S. C. Wenzel, R. Müller, *ChemBioChem* **2013**, *14*, 1581-1589.
- [27] Ö. Erol, T. F. Schäberle, A. Schmitz, S. Rachid, C. Gurgui, M. El Omari, F. Lohr, S. Kehraus, J. Piel, R. Müller, G. M. König, *ChemBioChem* **2010**, *11*, 1253-1265.
- [28] R. O'Shea, H. E. Moser, *J. Med. Chem.* **2008**, *51*, 2871-2878.
- [29] T. I. Moy, A. Daniel, C. Hardy, A. Jackson, O. Rehrauer, Y. S. Hwang, D. Zou, K. Nguyen, J. A. Silverman, Q. Li, C. Murphy, *FEMS Microbiol. Lett.* **2011**, *319*(2), 176-179.
- [30] I. H. Gilbert, M. Ginty, J. A. O'Neill, T. J. Simpson, J. Staunton, C. L. Willis, *Bioorg. Med. Chem. Lett.* **1995**, *5*(15), 1587-1590.
- [31] Y. Oikawa, K. Sugano, O. Yonemitsu, *J. Org. Chem.* **1978**, *43*, 2087-2088.
- [32] B. M. Trost, J. P. N. Papillon, T. Nussbaumer, *J. Am. Chem. Soc.* **2005**, *127*, 17921-17937.
- [33] R. K. Boeckman Jr., T. M. Kamenecka, S. G. Nelson, J. R. Pruitt, T. E. Barta, *Tetrahedron Lett.* **1991**, *32*(23), 2581-2584.
- [34] T. Yoshinari, K. Ohmori, M. G. Schrems, A. Pfaltz, K. Suzuki, *Angew. Chem. Int Ed.* **2010**, *49*(5), 881-885.
- [35] a) N. Miyaura, K. Yamada, A. Suzuki, *Tetrahedron Lett.* **1979**, *20*, 3437-3440. b) N. Miyaura, A. Suzuki, *J. Chem. Commun.* **1979**, 866-867.
- [36] a) J. Louie, J. F. Hartwig, *Tetrahedron Lett.* **1995**, *36*, 3609-3612. b) A. S. Guram, R. A. Rennels, S. L. Buchwald, *Angew. Chem. Int Ed.* **1995**, *34*, 1348-1350.
- [37] a) V. V. Rostovtsev, L. G. Green, V. V. Fokin, K. B. Sharpless, *Angew. Chem. Int Ed.* **2002**, *41*, 2596-2599. b) C. W. Tornøe, C. Christensen, M. Meldal, *J. Org. Chem.* **2002**, *67*, 3057-3064.
- [38] K. Mariner, M. McPhillie, R. Trowbridge, C. Smith, A. J. O'Neill, C. W. G. Fishwick, I. Chopra, *Antimicrob. Agents Ch.* **2011**, *55*, 2413-2416.
- [39] R. H. Lambalot, A. M. Gehring, R. S. Flugel, P. Zuber, M. LaCelle, M. A. Marahiel, R. Reid, C. Khosla, C. T. Walsh, *Chem. Biol.* **1996**, *3*, 923-936.
- [40] J. Sambrook and D. W. Russell in *Molecular cloning: A laboratory manual*, Cold Spring Harbor Laboratory Press, Cold Spring Harbor, New York, **2001**.
- [41] S. S. Wu, D. Kaiser, *J. Bacteriol.* **1996**, *178*, 5817-5821.

#### 4.7.2 References for Supporting Information

- [1] H. Irschik, K. Gerth, G. Höfle, W. Kohl, H. Reichenbach, *J. Antibiot.* **1983**, *36*, 1651-1684.
- [2] S. S. Wu, D. Kaiser, *J. Bacteriol.* **1996**, *178*, 5817-5821.



---

## **Chapter 5**

# **Genetic Engineering and Heterologous Expression of the Myxopyronin Biosynthetic Gene Cluster**

*Hilda Sucipto, Silke C. Wenzel, and Rolf Müller*  
(Unpublished Results)

## 5 Heterologous Production of Myxopyronin

### 5.1 Introduction

Myxobacteria continue to be a prolific source of anti-infectives with novel scaffolds possessing novel modes of action or binding sites.<sup>1-3</sup> Myxopyronins, antibiotics belonging to the  $\alpha$ -pyrone class of compounds, are produced by *Myxococcus fulvus* Mx f50.<sup>4</sup> They are active against several Gram-negative and Gram-positive bacteria as RNA polymerase (RNAP) inhibitors. In recent structural studies, myxopyronin was shown to interact with the RNAP switch region - the hinge that mediates opening and closing of the RNAP active center cleft - to prevent interaction of RNAP with promoter DNA.<sup>5,6</sup> Other myxobacterial compounds, the structurally related  $\alpha$ -pyrone coralopyronin and the macrolactone ripostatin, are also functioning analogously to myxopyronin.<sup>5</sup> Importantly, the target site at the RNAP switch region has a significant distance to the rifampicin binding site. Rifampicin has been used as a first-line anti-tuberculosis (anti-TB) drug for a few decades and the resistance to it has caused the rapid emergence of multiple drug resistant (MDR) and extensive drug resistant (XDR) *Mycobacterium tuberculosis*. Antibiotics like myxopyronin which target a different site on RNAP will be an alternative to combat rifampicin resistant bacteria and it will open up opportunities to develop broad spectrum antibiotics. However, myxopyronin cannot be used directly as clinical drugs for various reasons such as inadequate physicochemical profile. Thus, it is desirable to bioengineer myxopyronin biosynthetic gene cluster to achieve structural modifications with an eye towards better bioactivity and properties.

The myxopyronin gene cluster has been identified and revealed that the biosynthesis of myxopyronin is catalyzed by a hybrid of multimodular polyketide synthase (PKS) and nonribosomal peptide synthetase (NRPS). The coding region responsible for the biosynthesis of myxopyronin spans approximately 53 kb.<sup>7</sup> In agreement with the previously performed myxopyronin feeding studies,<sup>8</sup> the characterization of the key enzyme MxnB proved that myxopyronin is formed from two polyketide chains (named western and eastern chain).<sup>9</sup> The role of the biosynthetic genes involved in myxopyronin formation was also investigated by directed mutagenesis after establishing suitable mutagenesis procedures for the native producer strain including a markerless in-frame deletion method based on *sacB* counterselection.<sup>7</sup> However, the established mutagenesis procedure is a rather time-consuming process because it usually takes around 6–8 weeks to generate and verify the double crossover mutants.

The increasing number of genome sequences has improved the efficiency of finding the responsible gene cluster for a compound of interest. However, further targeted modifications of the natural product or attempts to increase the production are not always feasible in the native producer. In order to engineer natural product biosynthesis more efficiently, heterologous expression of the corresponding biosynthetic gene cluster has been widely applied, especially for genetically limited, difficult to handle, or slow growing microorganisms such as myxobacteria, cyanobacteria or marine microorganisms.<sup>10-12</sup> Various strategies have been used for heterologous expression, which aim to improve the yield and the structure of the natural products.<sup>13-15</sup> Some examples from myxobacterial gene clusters are epothilone,<sup>16-20</sup> soraphen,<sup>21</sup> myxochromide S,<sup>22,23</sup> myxothiazol,<sup>24</sup> and tubulysin,<sup>25</sup> where the biosynthetic pathways have been successfully subcloned with innovative cloning strategies, reconstituted, engineered and expressed in heterologous hosts with different effect on the production yields compared to the natural producer.

In the present study, we aimed to establish a heterologous production and engineering platform for  $\alpha$ -pyrone antibiotics. By using a combination of directed mutagenesis, Red/ET recombineering, and conventional cloning strategies we managed to reconstitute the entire 53 kb myxopyronin biosynthetic gene cluster on one expression construct. The reconstituted gene cluster was then introduced into the chromosome of the related myxobacterial strain *M. xanthus* DK1622 to achieve a production level comparable to that of the natural producer. After achieving reconstitution of the complete set of the gene cluster as one construct; any further modification could be efficiently performed in *E. coli* by Red/ET and transformed into the heterologous host strain in one step. The whole process would require a shorter time than performing the markerless mutagenesis strategy in the native host. The obtained myxopyronin heterologous expression plasmid was also exploited for mutasynthesis experiments to generate myxopyronin analogues.

## 5.2 Result and Discussion

### 5.2.1 Reconstitution of the complete myxopyronin gene cluster

Heterologous expression of complete secondary metabolite pathways in amenable host strains has become an important tool in natural product research and drug discovery.<sup>14</sup> When the products are from relatively small biosynthetic gene clusters (<30 kb), it was often possible to retrieve the entire gene set from a single cosmid within a genomic library of the natural product

strain.<sup>13</sup> On the other hand, many natural product biosynthetic gene clusters are larger than the regular insert size of common cosmid vectors. One of the strategies to overcome this size limitation is to use bacterial artificial chromosome (BAC) shuttle vectors for library construction which can accommodate inserts in excess of 100 kb. This approach has been successfully applied in the expression of 128 kb daptomycin biosynthetic gene cluster from *Streptomyces roseosporus* in a related streptomyces strain.<sup>26</sup> Another strategy is termed multi plasmid approach where a subset of the biosynthetic gene cluster is cloned into compatible expression plasmids followed by their stepwise introduction and coexpression in suitable host strains.<sup>18,27</sup> However, these approaches usually rely on several rounds of cloning and heterologous host modification, which is tedious and time-consuming.

In the last decade, an alternative to these classical, time-consuming cloning and mutagenesis approaches is the reassembly of large natural product pathways on a single transferable vector system, by using Red/ET technology. In principle, Red/ET is an *in vivo* homologous recombination-based genetic engineering method utilized mainly in *E. coli* by using short homology arms, catalyzed by two equivalent phage protein pairs, Red $\alpha$ /Red $\beta$  from  $\lambda$  phage and RecE/RecT from  $\lambda$  phage, which are integrated in the *E. coli* K12 chromosome.<sup>28–30</sup> Red/ET recombination technology has greatly facilitated genetic manipulation of complex biosynthetic pathways by skipping many steps needed in the standard restriction/ligation genetic modification.<sup>29,31,32</sup>

In most of the cases, complete biosynthetic pathways from myxobacteria or other microorganisms have been reconstructed and engineered by construction and screening of BAC or cosmid libraries, followed by Red/ET recombination for stitching and modification for the purpose of heterologous expression.<sup>24,25,33–35</sup> Here we applied another strategy to reconstitute the complete set of *mxn* gene cluster without cosmid or BAC library generation. We aimed to subclone the entire pathway from chromosomal DNA of the producer strain *via* plasmid recovery by introducing two unique restriction sites (*PacI*) upstream and downstream of the gene cluster by two consecutive directed mutagenesis steps using previously established procedures.<sup>7</sup> For this purpose, two suicide vectors pHSU-mxn16 for integration at the beginning of the cluster and pHSU-mxn19 for integration at the end of the cluster were constructed (Fig. 1).

Suicide vector pHSU-mxn16 containing a ~1.2 kb homologous fragment, p15A replication origin (*p15A ori*), *PacI* restriction site, and a tetracycline resistance gene (*tet<sup>R</sup>*), was introduced to the upstream of the *mxn* gene cluster using the established directed mutagenesis<sup>7</sup>



procedure to obtain *M. fulvus* Mx f50::pHSU-mxn16 (Fig. 1A). The tetracycline resistance gene was introduced as the homologous fragment to transfer the expression construct into *M. xanthus* later on. The *p15A ori* was used in order to generate the complete biosynthetic gene cluster propagated at a lower copy number and to allow greater stability of DNA sequences.

Another round of directed mutagenesis was performed to introduce the *PacI* restriction site by integrating suicide vector pHSU-mxn19 into *M. fulvus* Mx f50::pHSU-mxn16 through homologous fragment downstream of the *mxn* gene cluster to obtain *M. fulvus* Mx f50::pHSU-mxn16::pHSU-mxn19 (Fig. 1B). The initial strategy was to digest the genomic DNA of this resulting mutant through *PacI* restriction digest and subsequently re-ligate it to achieve cloning of the complete *mxn* gene cluster in one step. Despite several attempts, this one-step subcloning approach was not successful, presumably due to the large size of the gene cluster.

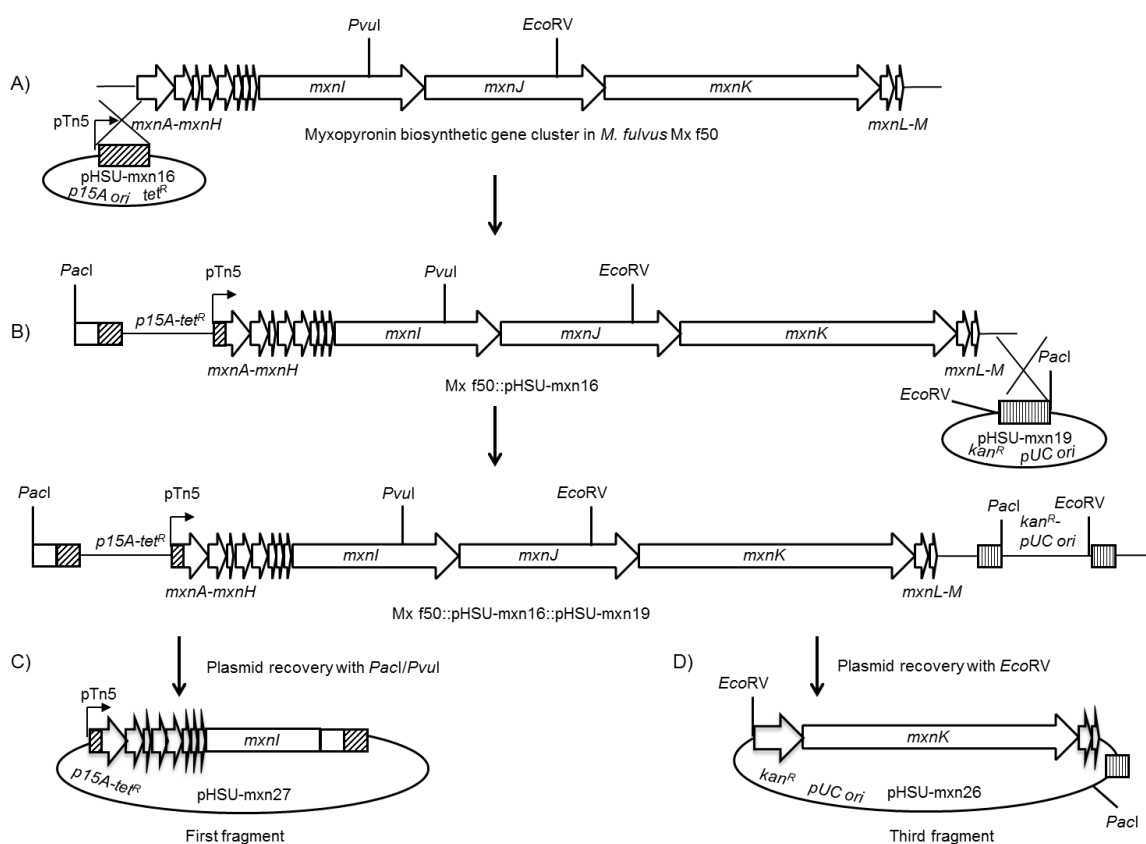


**Figure 1.** Strategy for subcloning myxopyronin biosynthetic pathway fragments. A) and B) Successive single cross over to introduce pHSU-mxn16 and pHSU-mxn19, respectively, resulting in Mx f50::pHSU-mxn16::pHSU-mxn19. The order of step A) and B) is not restricted; it can also be performed vice versa. Subsequent plasmid recovery to obtain C) pHSU-mxn27 containing the first fragment and D) pHSU-mxn26 containing the third fragment.

An alternative strategy was then applied to overcome the gene cluster size problem. The *mxn* gene cluster was isolated in three fragments. The first fragment, covering *mxnA* and downstream genes until half of *mxnI*, was achieved by restriction digest with *PacI/PvuI* (compatible cohesive ends) of chromosomal DNA from the mutant *M. fulvus* Mx f50::pHSU-mxn16::pHSU-mxn19 and subsequent re-ligation to obtain pHSU-mxn27 (17.1 kb) (Fig. 1C). The second fragment covering the 3'-end of *mxnI* until and including a part of *mxnJ* was isolated using the following steps. A directed mutagenesis was performed using pHSU-mxn32 to introduce several restriction sites and a zeocin resistance gene (*zeo<sup>R</sup>*) yielding *M. fulvus* Mx f50::pHSU-mxn32 (Fig. 2). A plasmid recovery from the resulting mutant genomic DNA using *PvuI* yielded pHSU-mxn35. The *zeo<sup>R</sup>* was exchanged with *amp<sup>R</sup>* to form pHSU-mxn40 (21 kb).

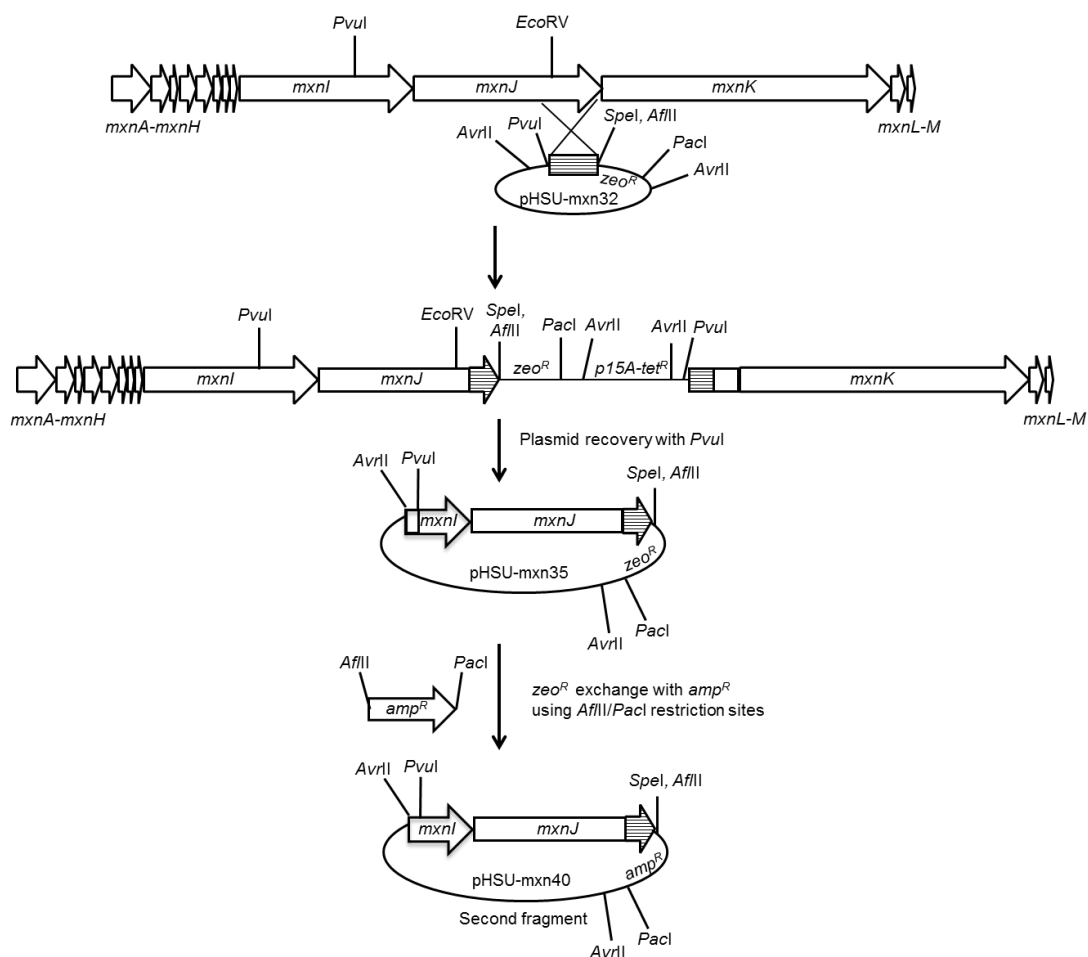


**Figure 2.** Subcloning strategy for the second fragment of the myxopyronin biosynthetic pathway to generate pHSU-mxn40.

Subsequently, the first fragment (in pHSU-mxn27) and the second fragment (in pHSU-mxn40) were combined by Red/ET recombination (Fig. 3). pHSU-mxn40 was linearized via *AvrII* restriction digest, and the generated linear fragment was used in Red/ET recombination with pHSU-mxn27 to achieve pHSU-mxn41 covering *mxnA-mxnJ* (35.6 kb) (Fig. 3).

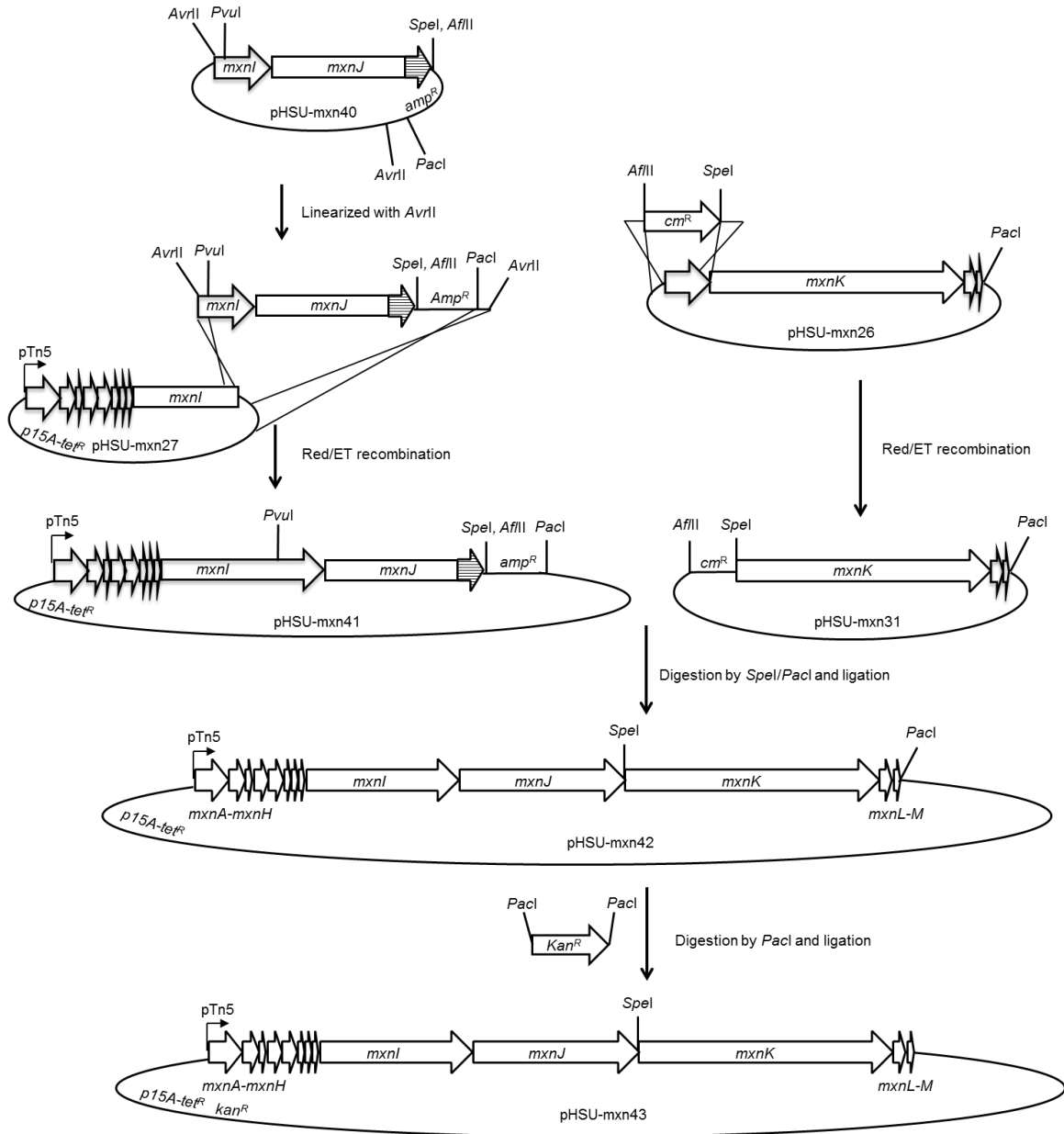


**Figure 3.** Cloning strategy to reconstitute the complete myxopyronin biosynthetic pathway on one expression construct.

To complete the *mxn* gene cluster reconstitution, the third fragment, covering a part of *mxnJ* and downstream genes until *mxnM* was isolated from the mutant *M. fulvus* Mx f50::pHSU-

mxn16::pHSU-mxn19 DNA through *EcoRV* restriction digest and re-ligation to obtain pHSU-mxn26 (31.6 kb) (Fig. 1D). In order to enable complete cluster stitching *via* conventional cloning strategy, a unique restriction site *SpeI* was introduced at the 5'-end of *mxnK* (pHSU-mxn26) by Red/ET recombination to form pHSU-mxn31 (26.3 kb) (Fig. 3).

Finally, the complete *mxn* gene cluster was stitched together by digesting pHSU-mxn41 (*mxnA-mxnJ*) and pHSU-mxn31 (*mxnK-mxnM*) with *SpeI/PacI* restriction enzymes and ligating the linear fragments to achieve pHSU-mxn42. The resulting construct, pHSU-mxn42, contains the complete *mxn* biosynthetic pathway on a plasmid backbone harboring a p15A *ori* and *tet<sup>R</sup>* resistance gene. In order to enable selection in a modified *M. xanthus* DK1622 host strain that already contains a *tet<sup>R</sup>* marker, *kan<sup>R</sup>* was lastly introduced to pHSU-mxn42 to form pHSU-mxn43 (Fig. 3). To confirm the individual cloning steps, each of the constructs that were obtained by recombination experiments including conventional cloning experiments were digested with a set of restriction enzymes or confirmed by sequencing, e.g. to exclude mutations within the homologous gene cluster fragments used for recombination.

### 5.2.2 Heterologous Expression of the Myxopyronin Gene Cluster in *M. xanthus*

In the last 15 years, several myxobacterial gene clusters have been heterologously expressed in different host strains, such as myxochromide, myxothiazol, and tubulysin in *Pseudomonas putida* and myxobacterium *M. xanthus*,<sup>22,25,36</sup> epothilones in *Streptomyces coelicolor*, *M. xanthus*, and *E. coli*,<sup>16,18,19,34</sup> and soraphen in *Streptomyces lividans* (*S. lividans*).<sup>21</sup> Generally, the heterologous host is selected based on its characteristic compatibility in producing the compound of interest.<sup>13</sup> In particular, PKS and NRPS must be post-translationally modified for their activity,<sup>37</sup> therefore the heterologous host must carry a phosphopantetheinyl transferase needed for the modification of carrier proteins. In addition the heterologous host must provide activated short-chain carboxylic acids and/or amino acids for secondary metabolite production and must be essentially resistant/not sensitive to the produced compound. Streptomycetes and related actinomycetes are so far the most extensively used systems for heterologous expression in general<sup>38</sup> because they provide necessary machinery for polyketide synthesis.

*E. coli* is another host strain option because it is easy to handle and genetically accessible. The disadvantages of *E. coli* are the need of strain engineering before being utilized in the polyketide biosynthesis (lacking postranslational activation of the carrier protein) and the different GC content compared with that of most biosynthetic gene clusters. In addition to GC

content factor, codon usage of the genes of interest, precursor production, functionality of native promoter in the heterologous host strain, and the size of the introduced gene clusters are crucial for successful production of secondary metabolites in the heterologous host.<sup>13,39</sup>

In addition to streptomycetes and *E. coli*, pseudomonads have also been used as heterologous hosts. Pseudomonads possess the combination of favorable properties from streptomycetes and *E. coli*. However, pseudomonads similarly to *E. coli* are unable to produce methylmalonyl-CoA which is often used as extender unit in polyketides.<sup>40,41</sup> While pseudomonads require additional metabolic engineering of the host strain,<sup>36</sup> the myxobacterium *M. xanthus* has been successfully utilized for heterologous expression of several myxobacterial compounds such as epothilone,<sup>16</sup> myxothiazol,<sup>24</sup> and tubulysin<sup>25</sup> without additional modification. Since *M. xanthus* contains the necessary properties for polyketide synthesis and is phylogenetically close to the native producer of myxopyronin *M. fulvus*, it was chosen as a model for a myxopyronin heterologous expression system. In particular, a mutant of *M. xanthus* DK1622 in which the myxochromide A gene cluster has been deleted (*M. xanthus* DK1622  $\Delta$ mchA::tet, Wenzel, unpublished result) was employed. Myxochromide A is one of the major compounds produced by *M. xanthus* DK1622, and its gene cluster deletion was expected to provide a greater precursor pool for production of other secondary metabolites. In brief, the myxochromide A gene cluster was completely deleted from *M. xanthus* DK1622 and replaced by a tetracycline resistance gene which will serve as the target site for the chromosomal integration for the myxopyronin gene cluster.

The generated expression construct (pHSU-mxn43, approximately 57 kb), containing the complete *mxn* gene cluster, was transferred to *M. xanthus* DK1622  $\Delta$ mchA::tet by electroporation (Fig. 4A). After 6 days, the colonies obtained on soft agar plates containing the kanamycin resistance gene were transferred into liquid medium to isolate the genomic DNA. The correct integration of the cluster was then verified by PCR using a set of primers (Fig. 4B). As expected, the amplification products could be detected only in the mutant clones containing the *mxn* biosynthetic genes when compared to the control reaction (*M. xanthus* DK1622 $\Delta$ mchA::tet). The correct clone was grown in culture medium and the culture extract was analyzed by LC-MS. Myxopyronin A and B heterologous production was confirmed in comparison to the production of myxopyronins in the native producer *M. fulvus* (Fig. 4C). Under the applied culture conditions at 30°C, myxopyronin production reached around 5 mg/L in 3 days which is in the comparable range of the native producer, at 5-10 mg/L in the same cultivation time.<sup>4</sup>

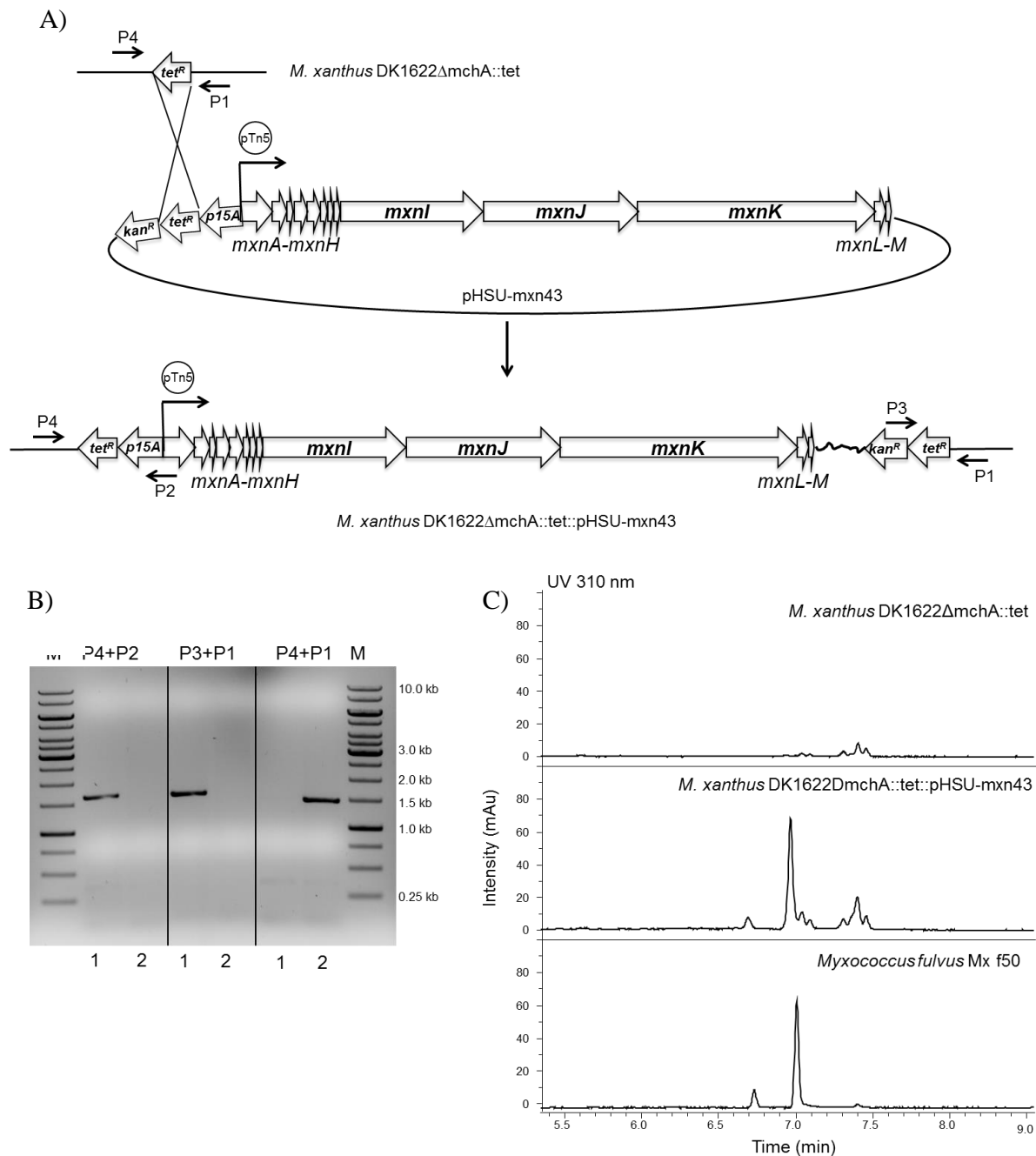


**Figure 4.** Transformation of the myxopyronin biosynthesis gene cluster into *M. xanthus*, PCR analysis and HPLC analysis. A) Illustration of the transfer of pHSU-mxn43 into *M. xanthus* DK1622ΔmchA::tet; B) PCR analysis using primer sets P4/P2, P3/P1, and P4/P1. Number 1 is the resulting mutant *M. xanthus* DK1622ΔmchA::tet::pHSU-mxn43 and number 2 is the control *M. xanthus* DK1622ΔmchA::tet; C) HPLC analysis at UV=310 nm for the control *M. xanthus* DK1622ΔmchA::tet, the resulting mutant and the native producer *M. fulvus* Mx f50. The peaks at 6.7 min and 7 min, are myxopyronin A and its isomer, respectively. The peaks between 7.3-7.4 min are keto-enol tautomers of myxopyronin A, myxopyronin B, and myxovirescin (from *M. xanthus* DK1622).

Other myxobacterial biosynthetic pathways that have been expressed in *M. xanthus* show different effects on the production yields: epothilone ( $\approx 1$  fold, 23 mg/L),<sup>16,42</sup> myxochromide S

(↑ 125 fold, 1 g/L),<sup>34</sup> myxothiazol (↑ 6 fold, 60 mg/L),<sup>24</sup> and pretubulysin (↓ 5-8 fold, 0.19 mg/L).<sup>25</sup> The tubulysin heterologous expression system showed ~20-fold decrease in production yields which might be caused by the interruption of coupled translation within the gene cluster.<sup>25</sup> The other myxobacterial biosynthetic gene clusters responsible for production of epothilone, myxochromide S, and myxothiazol showed comparable or significant increase in production yields when heterologously expressed in *M. xanthus*. The successful myxopyronin heterologous expression in *M. xanthus* further demonstrates the suitability of this host for the production of myxobacterial secondary metabolites.

### 5.2.3 Genetic Modification of the Myxopyronin Heterologous Expression System

In order to generate myxopyronin analogues, we recently established a mutasynthesis system in the native producer *M. fulvus*. In this system, the production of myxopyronin's western part of the molecule was blocked by in-frame deletion of 5.6 kb *mxnK* gene and subsequently various mutasynthons were fed to the mutant cultures (see details in Chapter 3). However, fast degradation of the  $\beta$ -keto *N*-acetylcysteamine (NAC) in the culture and possible difficulties regarding cell penetration of the substrates have made the attempts to isolate analogues unsuccessful so far.

The heterologous expression system described here provides the basis for engineering the *mxn* biosynthetic pathway to generate novel analogues. Based on the Red/ET recombineering technology,<sup>29</sup> in-frame deletions at any desired position within the expression construct are feasible. As a proof of concept, we aimed to perform mutasynthesis in the heterologous system by deleting an identical *mxnK* fragment as deleted in the native producer. For this, an ampicillin resistance gene (*amp<sup>R</sup>*) with 42 bp homology arms to enable homologous recombination was amplified by PCR. After replacement of the target fragment at *mxnK* against the selection marker *amp<sup>R</sup>* in pHSU-mxn43 by Red/ET recombination, the *amp<sup>R</sup>* gene was removed by *AflIII* restriction digest and re-ligated to generate pHSU-mxn46 (Fig. 5).

The resulting construct was subsequently transformed into *M. xanthus* DK1622 $\Delta$ mchA::tet, and deletion of the fragment was confirmed by PCR analysis. As expected, *M. xanthus* DK1622 $\Delta$ mchA::tet::pHSU-mxn46 was not able to produce myxopyronin. This mutant was then used for mutasynthesis experiments revealing similar results compared to the mutasynthesis studies in the native producer strain. Although in principle the mutasynthesis system also works in the heterologous host, further work to improve the yield and to enable isolation of analogues remains to be performed.

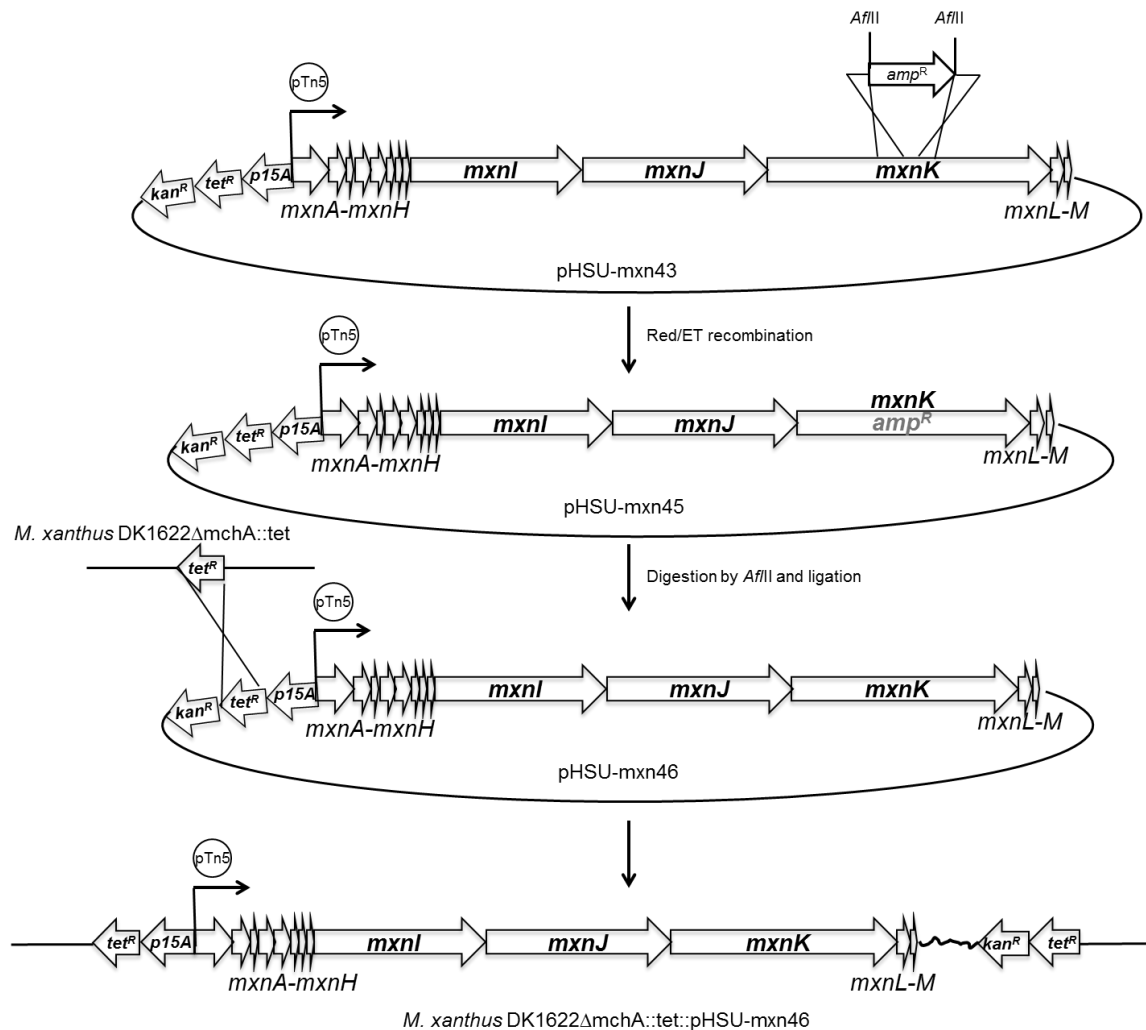


**Figure 5.** Cloning strategy to modify the myxopyronin heterologous expression system

### 5.3 Conclusions and Perspectives

Myxobacterial  $\alpha$ -pyrone antibiotics were recently characterized as RNAP inhibitors with a new target site, representing promising candidates for the development of broad-spectrum antibiotics. In order to further exploit these natural products, sufficient compound material and novel structural derivatives have to be generated. Here we aimed to establish an efficient and flexible biotechnological production platform for  $\alpha$ -pyrone antibiotics by combining directed mutagenesis, Red/ET and conventional cloning techniques to reconstitute the complete myxopyronin gene cluster without cosmid or BAC library generation. The assembled gene cluster was then transferred to *M. xanthus*, resulting in the heterologous production of



myxopyronins. As a further proof of principle, the heterologous expression system was then engineered to perform the mutasynthesis studies as already conducted in the native producer.

The current results presented in this chapter have set up the basis for pathway engineering to generate not only myxopyronin derivatives but also other  $\alpha$ -pyrones such as corallopyronin derivatives. To date, the corallopyronin producer is not yet amenable for genetic manipulation. Therefore, utilizing the presented heterologous expression platform, corallopyronin can be produced in a heterologous host by constructing a “hybrid” of myxopyronin (*mxnA-mxnI*) and corallopyronin (*corJ-corO*) genes (Fig. 6). Altogether, this study has opened up opportunities to facilitate  $\alpha$ -pyrone analogue generation in order to improve the pharmacokinetic properties and to gain more information about the structure-activity relationship (SAR) with RNAP for developing broad spectrum therapeutic agents.

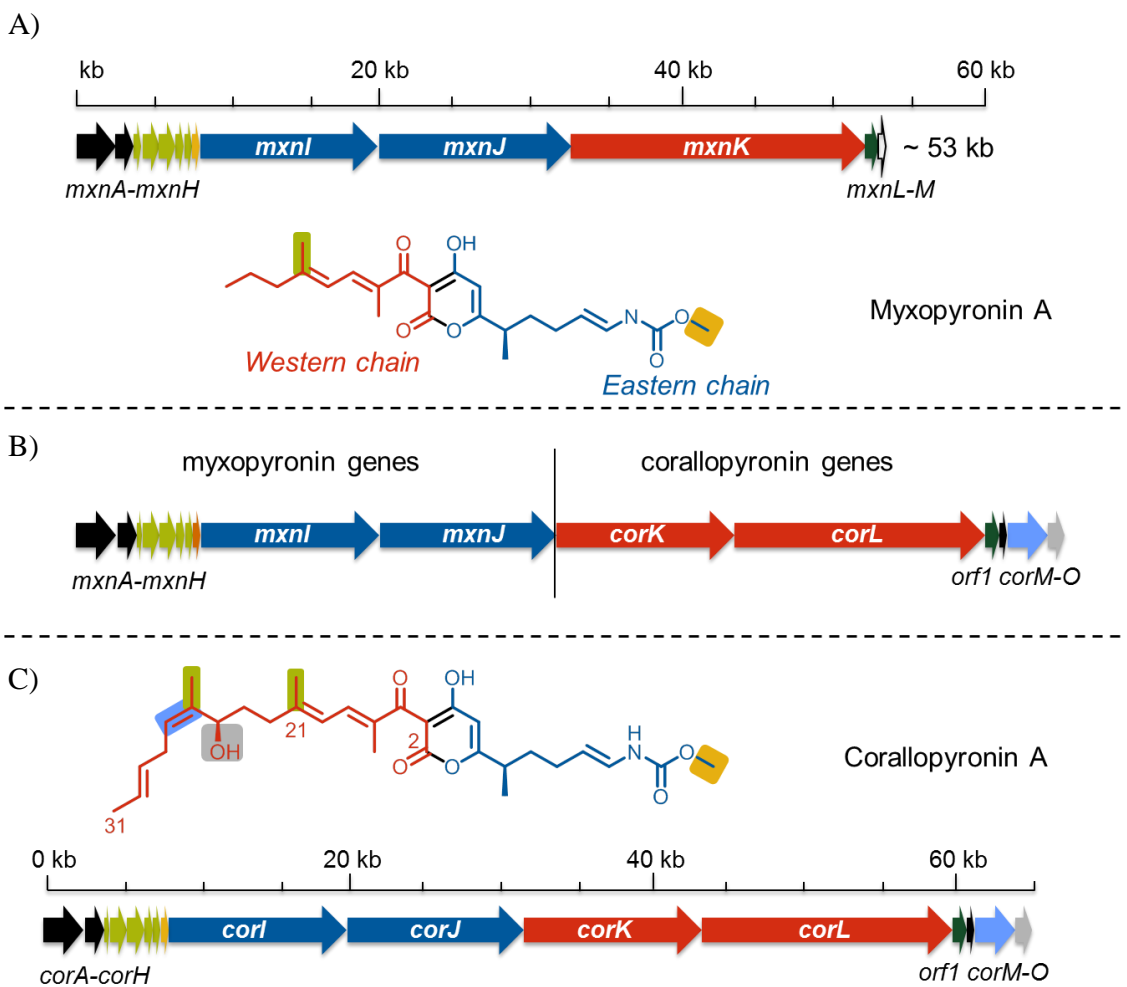


**Figure 6.** A) Myxopyronin gene cluster, B) Illustration of the “hybrid” cluster of myxopyronin and corallopyronin which is expected to result in corallopyronin A production in heterologous host, and C) Corallopyronin gene cluster

## 5.4 Experimental Section

### Bacterial strains and culture conditions

Bacterial strains and plasmids used during this study are listed in Table S1. *Myxococcus fulvus* Mx f50 wild type and mutants were grown in Casitone Yeast (CY) medium (0.3 % casitone, 0.1 % yeast extract, 0.1 %  $\text{CaCl}_2 \times 2 \text{H}_2\text{O}$ ) supplemented with  $5 \times 10^{-4} \mu\text{g L}^{-1}$  vitamin B12 after autoclaving. For liquid cultures, the strains were grown at 30 °C and 105 rpm on an orbital shaker and harvested after 3 days. *E. coli* strains were cultured in lysogeny broth (LB) medium (1 % tryptone, 0.5 % yeast extract, 0.5 % NaCl) at 37 °C. Appropriate antibiotic at a final concentration of 100  $\mu\text{g ml}^{-1}$  ampicillin, 50  $\mu\text{g ml}^{-1}$  kanamycin, 5  $\mu\text{g ml}^{-1}$  tetracycline or 6.25  $\mu\text{g ml}^{-1}$  oxytetracycline was added whenever necessary.

### DNA Isolation and PCR

*M. fulvus* Mx f50 genomic DNA was prepared either via the Phenol Chloroform Isoamyl alcohol extraction method<sup>43</sup> or by using the Genra Puregene Genomic DNA Purification Kit (Qiagen) according to the manufacturer's protocol. Plasmid DNA was either purified by standard alkaline lysis<sup>43</sup> or by using the GeneJet Plasmid Miniprep Kit (Thermo Fisher Scientific). The PCR reactions were carried out in a peqSTAR 96 Universal Gradient thermocycler (Peqlab) or Mastercycler® pro (Eppendorf) using Phusion polymerase or Taq DNA polymerase (Thermo Fisher Scientific): initial denaturation (3 min, 95 °C); 30 cycles of denaturation (30 s, 95 °C), annealing (30 s, 53 or 57 °C) and elongation (varied based on PCR product length 1 kb/min, 72 °C); and final extension (10 min, 72 °C). DNA fragments were separated by agarose gel electrophoresis and isolated using the peqGold Gel Extraction (Peqlab). The PCR products were cloned into pJET1.2 blunt vector (Thermo Fisher Scientific) or pCRII-TOPO vector (Invitrogen) and sequenced using the primers pJET1.2For/pJET1.2Rev or M13For/M13Rev, respectively. Generated primer sequences are listed in Table S2.

### Reconstitution of the Myxopyronin Biosynthetic Gene Cluster

To establish a heterologous expression system for the myxopyronin biosynthetic pathway (1) the pathway genes were first subcloned in fragments and (2) then the expression construct was generated, which was later transferred into suitable host strain.

### (1) Subcloning of pathway fragments

Three different suicide plasmids were constructed for integration at different sites of the myxopyronin pathway region: (1) Tn5 promoter was amplified by PCR using primers mxn33/mxn41 with pCRII-TOPO vector as a template to obtain fragment 1. A 1191 bp fragment of *mxnA* was amplified from *M. fulvus* Mxf50 genomic DNA by PCR using primers mxn42/mxn30 to obtain fragment 2. Fragment 1 and fragment 2 were linked together using overlap PCR with primers mxn33/mxn30. The joined fragments were then subcloned into pJET1.2 vector to obtain plasmid pTn5-*mxnA*/pJET. In parallel, a minimal linear cloning vector p15A-Tet was obtained by PCR using primers mxn52/mxn53 with pACYC184 as a template. pTn5-*mxnA*/pJET plasmid was hydrolyzed with *PacI/EcoRV* and ligated to the *PacI/PvuII* hydrolyzed cloning vector p15A-Tet to generate pHSU-*mxn16*; (2) A 1491 bp fragment right after the 3'-end of myxopyronin A gene cluster was amplified from *M. fulvus* Mxf50 genomic DNA using primers mxn64/mxn65. The amplified fragment was cloned into pCRII-TOPO vector to create pHSU-*mxn19*; (3) A 1380 bp fragment of *mxnJ* was amplified from *M. fulvus* Mxf50 genomic DNA using primers mxn124 and mxn125. A zeocin resistance cassette was amplified using primers mxn128/mxn129 with pCDNA-Zeo as a template and it was subcloned into a minimal linear cloning vector p15A-Tet obtained by PCR using primers mxn126/mxn127 with pACYC184 as a template to construct p15A-Tet-Zeo plasmid. The 1380 bp fragment of *mxnJ* was then hydrolyzed with *PvuI* and subsequently cloned into p15A-Tet-Zeo hydrolyzed with the same restriction enzyme to create pHSU-*mxn32*.

First, pHSU-*mxn16* was transformed into *M. fulvus* Mx f50 to obtain mutant Mx f50::pHSU-*mxn16*. For genotypic analysis of the single cross-over, a set of different PCRs using the primer combinations mxn60/p15A-Tet1 and mxn61/p15A-Tet2 was carried out to verify the correct integration of the inactivation plasmid resulting at the expected PCR product size 1342 bp and 1473 bp, respectively. Subsequently, the next single crossover was performed by transforming pHSU-*mxn19* into Mx f50::pHSU-*mxn16* to obtain Mx f50::pHSU-*mxn16*::pHSU-*mxn19*. The mutant was confirmed by PCR using the primer combinations mxn94/pTOPO-out and mxn95/pTOPO-in resulting at the expected PCR product size 1720 bp and 1594 bp, respectively. Further confirmation of this mutant was also performed by Southern Blot analysis (Fig. S1). Second, pHSU-*mxn32* was transformed into *M. fulvus* Mxf50 to obtain mutant Mx f50::pHSU-*mxn32*. For genotypic analysis of the single crossover, a set of different PCRs using the primer combinations mxn136/p15A-Tet1 and

p15A-Tet2/mxn137 was carried out to verify the correct integration of the inactivation plasmid resulting at the expected PCR product size 1992 bp and 1527 bp, respectively.

The recovery of pathway fragments was performed as followed: genomic DNA of mutant Mx f50::pHSU-mxn16::pHSU-mxn19 was hydrolyzed with *EcoRV* and subsequently re-ligated to generate pHSU-mxn26. Independently, it was also hydrolyzed with *PacI/PvuI* and subsequently re-ligated to generate pHSU-mxn27. The genomic DNA of mutant Mx f50::pHSU-mxn32 was hydrolyzed with *PvuI* and then re-ligated to generate pHSU-mxn35. An ampicillin cassette was amplified by PCR using primers mxn147/mxn148 with pJET1.2 vector as a template. pHSU-mxn35 was hydrolyzed with *AflIII/PacI* to replace the zeocin cassette with the amplified ampicillin cassette hydrolyzed with the same set of restriction enzymes to generate pHSU-mxn40.

## (2) Generation of an expression construct harbouring the complete *mxn* pathway

The cloning strategy for the generation of an expression construct harbouring the complete pathway is shown in Figure 3. First, the western chain biosynthesis pathway was completed by integration of the 18.5 kb *AvrII* fragment from pHSU-mxn40 into pHSU-mxn27 via Red/ET recombination. The plasmid pHSU-mxn27 was first transformed to *E. coli* GB05-Red and subsequently the cells were electroporated with pHSU-mxn40 linearized fragment. The colonies were selected on ampicillin and tetracycline. The expected Red/ET recombination product (pHSU-mxn 41) was verified by restriction analysis with a set of enzymes.

Another round of Red/ET recombineering was performed to exchange the 6.2 kb 3'-end of *mxnI* in pHSU-mxn26 with a chloramphenicol resistance (*cm<sup>R</sup>*) cassette to generate pHSU-mxn31. The ~1 kb chloroamphenicol resistance cassette flanked by homologous fragments was amplified with primers mxn122/mxn123. The plasmid pHSU-mxn26 was first transformed to *E. coli* HS996-Tet and subsequently the cells were electroporated with linear fragment (mxn122/mxn123 PCR product). The colonies were selected on kanamycin and chloroamphenicol. The expected Red/ET recombination product (pHSU-mxn 31) was verified by restriction analysis with a set of enzymes.

Both, pHSU-mxn31 and pHSU-mxn41, were then hydrolyzed with *SpeI/PacI* to ligate the *mxnK-M* fragment into pHSU-mxn41 to generate pHSU-mxn42. A kanamycin resistance cassette was amplified from pCRII-TOPO vector as a template using primers mxn144/mxn145. The ~1 kb amplified cassette was then subcloned into pJET1.2 vector to

obtain pHSU-mxn37. Both, pHSU-mxn37 and pHSU-mxn42 were hydrolyzed with *PacI* to ligate the kanamycin resistance cassette into pHSU-mxn42 to generate pHSU-mxn43.

### (3) Transformation of the Expression Construct into *Myxococcus xanthus*

The expression construct pHSU-mxn43 described in the section above and shown in Figure 4a was transformed into the expression host *M. xanthus* DK1622 $\Delta$ mchA-tet by electroporation. *M. xanthus* DK1622 $\Delta$ mchA-tet was grown in a flask with CTT medium (1 % casitone, 10 mM Tris buffer pH 7.6, 1 mM KH<sub>2</sub>PO<sub>4</sub> pH 7.6, 8 mM MgSO<sub>4</sub> with final pH 7.6) at 30 °C until an OD<sub>600</sub> between 0.6–0.9 was reached. Cells were then harvested from 2-4 ml culture by centrifugation at 12,500 rpm for 1 min at room temperature. After two washing steps with 1 ml of H<sub>2</sub>O at room temperature, cells were resuspended in 65  $\mu$ l of H<sub>2</sub>O. Plasmid DNA (1-2  $\mu$ g) was mixed with the cell suspension, and electroporation was carried out under the following conditions: 25  $\mu$ F, 400  $\Omega$ , 650 V using 0.1 cm electroporation cuvettes and a GenePulser XCell device (Bio-Rad). 1 ml of CTT medium was directly added to the cell suspension immediately after electroporation and the cells were transferred into a 2 ml centrifuge tube. After 5-6 h cultivation at 30 °C and 800 rpm on a thermomixer, the cells were mixed with 2 ml of CTT soft agar (CTT medium with 0.7 % agar) and plated on CTT agar plates (CTT medium with 1.7 % agar) supplemented with 50  $\mu$ g ml<sup>-1</sup> kanamycin. The plates were incubated at 30 °C for 5-10 days until colonies became visible. Obtained clones were cultured in 1 mL of CTT containing 50  $\mu$ g ml<sup>-1</sup> kanamycin for 2–3 days. The genomic DNA was prepared in the same manner as *M. fulvus* Mx50 genomic DNA preparation. The genomic DNA was then used for PCR verification using primers with the expected size in the brackets: InMchP4/P2 (1635 bp), P3/InMchP1 (1609 bp), and InMchP4/InMchP1(1461 bp) (Fig. 4B).

### Genetic Modification of the *mxn* Gene Cluster in *E. coli* for Mutasynthesis Purpose in *M. xanthus*

The reconstituted *mxn* gene cluster pHSU-mxn43 was initially transformed into *E. coli* GB05-Red. A linear fragment (1171 bp) containing ampicillin resistance cassette (*amp*<sup>R</sup>) and homologous fragment was amplified from pJET1.2 vector with primers mxn153/mxn154. Red/ET recombineering was performed to exchange the 5.6 kb of *mxnK* in pHSU-mxn43 with an *amp*<sup>R</sup> cassette to generate pHSU-mxn45. pHSU-mxn45 was then hydrolyzed with *AflIII* to remove *amp*<sup>R</sup> cassette and was subsequently re-ligated to generate pHSU-mxn46. pHSU-mxn46 was

transformed into *M. xanthus* DK1622 $\Delta$ mchA-tet as described above to achieve *M. xanthus* DK1622 $\Delta$ mchA-tet::pHSU-mxn46. The mutant was verified with PCR using primers mxn68/mxn72 and mxn68/mxn71 with the expected size of 1478 bp and 2326 bp, respectively.

### **Phenotypic analysis of the mutant strains**

Well-grown pre-cultures of *M. fulvus* Mx f50 and the generated expression strain *M. xanthus* DK1622 $\Delta$ mchA-tet::pHSU-mxn43 were used to inoculate 50 ml of CY and CTT production medium (1 % inoculum), respectively, in 300 ml baffled flasks. After cultivation for 2 days at 30 °C and 105 rpm, the cultures were harvested by centrifugation. Myxopyronin A is almost exclusively present in the supernatant, which was extracted twice with an equal volume of ethyl acetate. After evaporation of the organic phase, the residue was dissolved in 1 ml of methanol. A 5  $\mu$ l aliquot of the extract was analyzed by HPLC-MS (Thermo Ultimate 3000 RSLC, coupled to a Bruker Daltonics Amazon ESI-MS ion trap instrument) operating in positive ionization mode. Compounds were separated on Waters Acquity BEH C18 (50 x 2.1 mm; 1.7  $\mu$ m particle diameter; flow rate 600  $\mu$ l/min and 45 °C) with a mobile phase of water/acetonitrile each containing 0.1 % formic acid, using a gradient from 5 % - 95 % acetonitrile over 9 min. Detection was performed by both diode array and ESI-MS. For high resolution mass spectrometry analysis, measurements were performed on a Dionex Ultimate 3000 RSLC system using a Waters BEH C18 column (50 x 2.1 mm, 1.7  $\mu$ m dp) by injecting 5  $\mu$ l of the methanolic extract. Separation was achieved by the same gradient as above with 0.33 min isocratic step at 5 % B. UV and MS detection were performed simultaneously. Coupling the HPLC to the MS was supported by an Advion Triversa Nanomate nano-ESI system attached to a Thermo Fisher Orbitrap. Mass spectra were acquired in centroid mode ranging from 200-2000 m/z at a resolution of R = 30000.

## 5.5 Supporting Information

**Table S1.** List of strains and plasmids used in this study

Strain/Plasmid	Characteristics	Reference
<b><i>E. coli</i> strains</b>		
HS996	Host for general cloning	Invitrogen
SCS110	Host for cloning to prepare plasmid DNA, free of Dam or Dcm methylation	Stratagene
GB05Red	Host for Red/ET cloning	<sup>44</sup>
<b><i>Myxococcus</i> strains</b>		
<i>M. fulvus</i> Mx f50	Myxopyronin producing wild-type strain	<sup>4</sup>
<i>M. fulvus</i> Mxf50::pHSU-mxn16:: pHSU-mxn19	Mxf50 with integrated constructs containing 1191 bp <i>mxnA</i> under the control of Tn5 promoter upstream of <i>mxn</i> gene cluster and 1591 bp homologous fragment downstream of the <i>mxn</i> gene cluster. Both constructs contain several restriction sites for the purpose of recovering the <i>mxn</i> gene cluster	this study
<i>M. fulvus</i> Mxf50::pHSU-mxn32	Mxf50 with integrated construct containing 1378 bp homologous fragment of <i>mxnJ</i> with <i>zeo<sup>R</sup></i> and p15A origin for the purpose of recovering part of <i>mxn</i> gene cluster	this study
<i>M. xanthus</i> DK1622Δ <i>mchA</i> ::tet	<i>M. xanthus</i> DK1622 with deleted myxochromide A ( <i>mchA</i> ) gene cluster and integrated tetracycline resistance gene	Wenzel (unpublished result)
<b>Plasmids</b>		
pSWU41	Vector contains a neomycin phosphotransferase ( <i>nptII</i> ) gene for selection and a levansucrose ( <i>sacB</i> ) gene for counter selection	<sup>45</sup>
pKC1132	Vector contains an apramycin gene for selection	<sup>46</sup>
pACYC184	Vector contains p15A origin of replication, tetracycline gene, and chloroamphenicol for selection	<sup>47</sup>
pCRII-TOPO	Vector contains pUC origin of replication, kanamycin and ampicillin genes for selection	Invitrogen
pHSU-mxn16	Vector for the introduction of restriction sites into the 5' region of <i>mxn</i> gene cluster containing 1214 bp fragment of <i>mxnA</i> under p15A ori and <i>tet<sup>R</sup></i>	this study
pHSU-mxn19	pCRII-TOPO vector containing external ~1.5 kb downstream <i>mxn</i> gene cluster to	this study

	introduce restriction sites <i>NheI</i> , <i>NdeI</i> , <i>SspI</i> , and <i>PacI</i> into the 3' region of <i>mxn</i> gene cluster	
pHSU-mxn26	Vector with the 27.6 kb fragment (third fragment) recovered from the chromosomal DNA of the mutant <i>M. fulvus</i> Mxf50::pHSU-mxn16:: pHSU-mxn19 digested by <i>EcoRV</i> in pCRII-TOPO	this study
pHSU-mxn27	Vector with the 17.1 kb fragment (first fragment) recovered from the chromosomal DNA of the mutant <i>M. fulvus</i> Mxf50::pHSU-mxn16:: pHSU-mxn19 gene cluster digested by <i>PacI</i> and <i>PvuI</i> in p15A-Tet <sup>R</sup>	this study
pHSU-mxn31	A construct containing <i>mxnK-mxnM</i> with <i>cm<sup>R</sup></i> in pCRII-TOPO (26.3 kb)	this study
pHSU-mxn32	A construct containing 1378 bp homologous fragment of <i>mxnJ</i> with <i>zeo<sup>R</sup></i> and p15A origin	this study
pHSU-mxn35	A construct obtained by plasmid recovery from <i>M. fulvus</i> Mxf50::pHSU-mxn32 by <i>PvuI</i> digestion consisting of fragment of <i>mxnI</i> and complete <i>mxnJ</i> (19.9 kb)	this study
pHSU-mxn37	A construct containing <i>kan<sup>R</sup></i> with flanking <i>PacI</i> restriction sites at 5' and 3' ends to be inserted to the 3' end of <i>mxn</i> gene cluster through <i>PacI</i> restriction site (pHSU-mxn42).	this study
pHSU-mxn40	A construct containing fragment of <i>mxnI</i> and complete <i>mxnJ</i> from pHSU-mxn35 where the <i>zeo<sup>R</sup></i> exchanged with <i>amp<sup>R</sup></i> . This is the second fragment in the <i>mxn</i> gene cluster reconstitution.	this study
pHSU-mxn41	A construct containing <i>mxnA-mxnJ</i> with <i>tet<sup>R</sup></i> , <i>amp<sup>R</sup></i> under Tn5 promoter and p15A ori (35.6 kb)	this study
pHSU-mxn42	A construct containing <i>mxnA-mxnM</i> with <i>tet<sup>R</sup></i> under Tn5 promoter and p15A ori (56 kb)	this study
pHSU-mxn43	A construct containing <i>mxnA-mxnM</i> with <i>tet<sup>R</sup></i> , <i>kan<sup>R</sup></i> , under Tn5 promoter and p15A ori (56.9 kb)	this study
pHSU-mxn45	A construct containing <i>mxnA-mxnM</i> ( $\Delta$ 5.6 kb of <i>mxnK</i> ) with <i>tet<sup>R</sup></i> , <i>kan<sup>R</sup></i> , <i>amp<sup>R</sup></i> under Tn5 promoter and p15A ori (52.3 kb)	this study
pHSU-mxn46	A construct containing <i>mxnA-mxnM</i> ( $\Delta$ 5.6	this study



	kb of <i>mxnK</i> ) with <i>tet<sup>R</sup></i> , <i>kan<sup>R</sup></i> under Tn5 promoter and p15A ori (51.3 kb)	
--	--	--

**Table S2.** List of primers used in this study

Primer name	Sequence (5'→3')	Restriction sites (in bold)
mxn9	GTCAGACATATGAACAACAGCGGT	
mxn10	CGTCGTAAGCTTTCAGTAGGTGAAAACCA	
mxn30	<b>TGCTTAATTAATATT CATATG</b> <b>GCTAGCGAGCTCCTGGATGGCCTT</b>	<i>PacI</i> fused with <i>SspI</i> , <i>EcoRV</i> , <i>NheI</i>
mxn33	CAGGTAGATATCTGGACAGCAAGCGAACC	<i>EcoRV</i>
mxn41	AATCTGTACCTCCTTATCCTGTCTCTTGATCAGAT	
mxn42	CAAGATCTGATCAAGAGACAGGATAAGGAGGT ACAGATTATGACTTTCACCGTCGTT	
mxn52	GATACACAGCTGTCCCTCCTGTTTCAGCTAC	<i>PvuII</i>
mxn53	ATCTTAATTAAGGACGCGATGGATATGTT	<i>PacI</i>
mxn60	TGCCATGAGCAGACAGTTA	
mxn61	CGGGTGGTTGATATCGTG	
mxn64	GCTGAGACGGTCTTCCTC	
mxn65	<b>TGCTTAATTAATATT CATATG</b> <b>GCTAGCACGCGATTCACTGTCTCA</b>	<i>PacI</i> fused with <i>SspI</i> , <i>EcoRV</i> , <i>NheI</i>
mxn68	CAACATCTCGCCGAGTGA	
mxn71	AACACCTCACGGTCCGAC	
mxn72	CCCATCGTCCACAGCTTC	
mxn94	TCACGGCGAAGCACATCC	
mxn95	AGGAGGCAGGGTCCGAAT	
mxn122	CCTCTAGATGCATGCTCGAGCGGCCGCCAGTGT GATGGATCTTAAGTACCTGTGACGGAAGATCA C	<i>AflIII</i>
mxn123	AAGCCACCGCCTCCCCTGAGGACCCAGGCTTC TCGTGGGCACTAGTGGGCACCAATAACTGCCT T	<i>SpeI</i>
mxn124	CAATACGATCGCTGGACTGGTGAAG	
mxn125	TGCTACTTAAG TTATCA <b>ACTAGTCATGGCTTCGCTCCCGCC</b>	<i>AflIII</i> , STOP codon, <i>SpeI</i>
mxn126	GATACACCTAGGTCCCTCCTGTTTCAGCTAC	<i>AvrII</i>
mxn127	TCAGGTCCTAGGGGACGCGATGGATATGTT	<i>AvrII</i>
mxn128	ACATCGCCTAGGCGCGCCCTGAGCGCCCTGCG GAACAAGGAGTGTGATGCGGCGATCGGACAT <b>ACTTAAGGGATCTGATCAGCACGTG</b>	<i>AvrII</i> , <i>PvuI</i> , <i>AflIII</i>
mxn129	TCTATGCCTAGGTGCGCAAACCAACCCTTGGC	<i>AvrII</i>

	AGAACATATCCATCGCGTCCTTAATTAATCAGT CCTGCTCCTCGGC	
mxn136	AACATCGGCCACCTGGAG	
mxn137	AGGACCCAGGCTTCTCGT	
mxn147	TATGTCCTTAAGATAATTCGGCTGCAGGGG	<i>Afl</i> III
mxn148	TATCTTAATTAATTACCAATGCTTAATCAGTG	<i>Pac</i> I
mxn153	CGAGGCGGGCGGCGATCAGCTCGTTCGGGTTC AGCGGCACCTGACTTAAGATAATTCGGCTGCA GGGG	<i>Afl</i> III
mxn154	CGGGAGCACCCACGGCGCGAGCCGCTGCTGGA CTCGGAAAGGCTTAAGTTACCAATGCTTAATC AGTG	<i>Afl</i> III
InMchP1	CGAGCAATCCGCTATTGGC	
InMchP4	CTGTGTCCTTCTGCGACGC	
M13For	GTAAAACGACGGCCAG	
M13Rev	CAGGAAACAGCTATGAC	
P2 (p15A- rev-mxnA)	TCGGTTCAAAGAGTTGGTAGC	
P3 (KanInt5)	GAGAACCTGCGTGCAATC	
p15A-Tet1	GGAGAACTGTGAATGCGC	
p15A-Tet2	ACTCCGCTAGCGCTGATG	
pJET1.2For	CGACTCACTATAGGGAGAGCGGC	
pJET1.2Rev	AAGAACATCGATTTTCCATGGCAG	
pTOPO-in	CCTCTAGATGCATGCTCGAG	
pTOPO-out	TTGGTACCGAGCTCGGATCC	

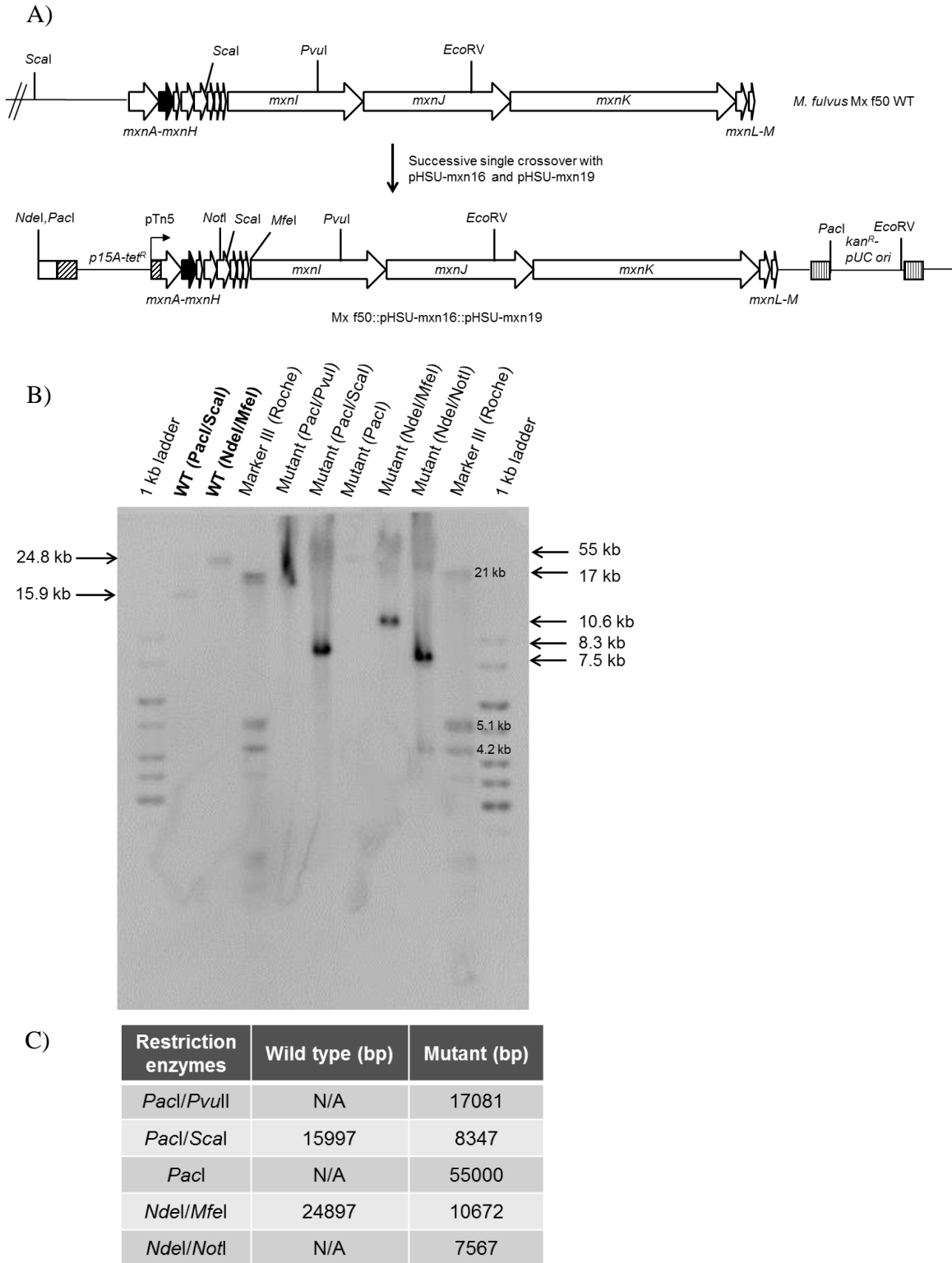


**Figure S1.** A) Schematic representation of successive single crossover integration of constructs pHSU-mxn16 and pHSU-mxn19 into *M. fulvus* Mx f50; B) confirmation of constructs integration by Southern blot; C) the expected fragment size after hydrolysis of wild type and mutant genomic DNA with a set of restriction enzymes and hybridization with a DIG-labelled 1017 bp probe (*mxnB* marked in black, in panel A) amplified from Mx f50 genomic DNA using the primers mxn9 and mxn10. M: Marker III (Roche).

## 5.6 References

1. Weissman, K. J. & Müller, R. Myxobacterial secondary metabolites: bioactivities and modes-of-action, *Nat. Prod. Rep.* **27**, 1276–1295 (2010).
2. Plaza, A. & Müller, R. in *Natural Products*, edited by A. Osbourn, R. J. Goss & G. T. Carter (John Wiley & Sons, Inc, Hoboken, NJ, USA, 2014), pp. 103–124.
3. Schaberle, T. F., Lohr, F., Schmitz, A. & König, G. M. Antibiotics from myxobacteria. *Nat. Prod. Rep.* **31**, 953–972 (2014).
4. Irschik, H. Gerth, K. Höfle, G. Kohl, W. & Reichenbach, H. The myxopyronins, new inhibitors of bacterial RNA synthesis from *Myxococcus fulvus* (Myxobacterales), *J. Antibiot.* **36**, 1651–1658 (1983).
5. Mukhopadhyay, J. *et al.* The RNA polymerase "switch region" is a target of inhibitors, *Cell* **135**, 295–307 (2008).
6. Belogurov, G. A. *et al.* Transcription inactivation through local refolding of the RNA polymerase structure, *Nature* (2008).
7. Sucipto, H. Wenzel, S. C. & Müller, R. Exploring chemical diversity of  $\alpha$ -pyrone antibiotics: molecular basis of myxopyronin biosynthesis, *ChemBioChem* **14**, 1581–1589 (2013).
8. Kohl, W. Irschik, H. Reichenbach, H. & Höfle, G. Antibiotics from gliding bacteria. XXII. The biosynthesis of myxopyronin A, an antibiotic from *Myxococcus fulvus* strain Mx f50, *Liebigs Ann. Chem.* 1088–1093 (1984).
9. Sucipto, H. *et al.* *In Vitro* reconstitution of  $\alpha$ -Pyrone ring formation in myxopyronin biosynthesis, *Chem. Sci.* **6**, 5076–5085 (2015).
10. Reichenbach, H. Myxobacteria, producers of novel bioactive substances, *J. Ind. Microbiol. Biotechnol.* **27**, 149–156 (2001).
11. Harada, K. Production of secondary metabolites by freshwater cyanobacteria, *Chem. Pharm. Bull.* **52**, 889–899 (2004).
12. Fortman, J. L. & Sherman, D. H. Utilizing the power of microbial genetics to bridge the gap between the promise and the application of marine natural products, *ChemBioChem* **6**, 960–978 (2005).
13. Wenzel, S. C. & Müller, R. Recent developments towards the heterologous expression of complex bacterial natural product biosynthetic pathways, *Curr. Opin. Biotechnol.* **16**, 594–606 (2005).
14. Ongley, S. Bian, X. Neilan, B. A. & Müller, R. Recent advances in the heterologous expression of microbial natural product biosynthetic pathways, *Nat. Prod. Rep.* **30**, 1121–1138 (2013).
15. Fujii, I. Heterologous expression systems for polyketide synthases, *Nat. Prod. Rep.* **26**, 155–169 (2009).
16. Julien, B. & Shah, S. Heterologous Expression of Epothilone Biosynthetic Genes in *Myxococcus xanthus*. *Antimicrob. Agents Chemother.* **46**, 2772–2778 (2002).
17. Arslanian, R. L. *et al.* A New Cytotoxic Epothilone from Modified Polyketide Synthases Heterologously Expressed in *Myxococcus xanthus*. *J. Nat. Prod.* **65**, 1061–1064 (2002).
18. Tang, L. *et al.* Cloning and heterologous expression of the epothilone gene cluster, *Science* **287**, 640–642 (2000).
19. Mutka, S. C. Carney, J. R. Liu, Y. & Kennedy, J. Heterologous production of epothilone C and D in *Escherichia coli*, *Biochemistry* **45**, 1321–1330 (2006).
20. Park, S. R. *et al.* Heterologous production of epothilones B and D in *Streptomyces venezuelae*, *Appl. Microbiol. Biotechnol.* **81**, 109–117 (2008).
21. Zirkle, R. Ligon, J. M. & Molnar, I. Heterologous production of the antifungal polyketide antibiotic soraphen A of *Sorangium cellulosum* So ce26 in *Streptomyces lividans*, *Microbiology* **150**, 2761–2774 (2004).

22. Wenzel, S. C. *et al.* Heterologous expression of a myxobacterial natural products assembly line in pseudomonads via red/ET recombineering, *Chem. Biol.* **12**, 349–356 (2005).
23. Perlova, O. Gerth, K. Kuhlmann, S. Zhang, Y. & Müller, R. Novel expression hosts for complex secondary metabolite megasynthetases: Production of myxochromide in the thermophilic isolate *Corallococcus macrosporus* GT-2, *Microbial Cell Factories* **8** (2009).
24. Perlova, O. *et al.* Reconstitution of the myxothiazol biosynthetic gene cluster by Red/ET recombination and heterologous expression in *Myxococcus xanthus*. *Appl. Environ. Microbiol.* **72**, 7485–94 (2006).
25. Chai, Y. *et al.* Heterologous expression and genetic engineering of the tubulysin biosynthetic gene cluster using Red/ET recombineering and inactivation mutagenesis, *Chem. Biol.* **19**, 361–371 (2012).
26. Miao, V. *et al.* Daptomycin biosynthesis in *Streptomyces roseosporus*: Cloning and analysis of the gene cluster and revision of peptide stereochemistry, *Microbiology* **151**, 1507–1523 (2005).
27. Xue, Q., Ashley, G., Hutchinson, C. R. & Santi, D. V. A multiplasmid approach to preparing large libraries of polyketides. *Proc. Natl. Acad. Sci.* **96**, 11740–11745 (1999).
28. Yu, D. *et al.* An efficient recombination system for chromosome engineering in *Escherichia coli*. *Proc. Natl. Acad. Sci.* **97**, 5978–5983 (2000).
29. Zhang, Y., Buchholz, F., Muyrers, J. P. P. & Stewart, A. F. A new logic for DNA engineering using recombination in *Escherichia coli*. *Nat Genet* **20**, 123–128 (1998).
30. Muyrers, J. P. P. Zhang, Y. Testa, G. & Stewart, A. F. Rapid modification of bacterial artificial chromosomes by ET-recombination, *Nucleic Acids Res.* **27**, 1555–1557 (1999).
31. Zhang, Y., Muyrers, J. P. P., Testa, G. & Stewart, A. F. DNA cloning by homologous recombination in *Escherichia coli*. *Nat Biotech* **18**, 1314–1317 (2000).
32. Muyrers, J. P. P., Zhang, Y. & Stewart, A. F. Techniques: Recombinogenic engineering - New options for cloning and manipulating DNA. *Trends in Biochemical Sciences* **26**, 325–331 (2001).
33. Binz, T. M. Wenzel, S. C. Schnell, H. J. Bechthold, A. & Müller, R. Heterologous expression and genetic engineering of the phenalinolactone biosynthetic gene cluster by using Red/ET recombineering, *ChemBioChem* **9**, 447–454 (2008).
34. Fu, J. *et al.* Efficient transfer of two large secondary metabolite pathway gene clusters into heterologous hosts by transposition, *Nucleic Acids Res.* **36**, e113 (2008).
35. Bian, X. *et al.* Direct cloning, genetic engineering, and heterologous expression of the syringolin biosynthetic gene cluster in *E. coli* through Red/ET recombineering, *ChemBioChem* **13**, 1946–1952 (2012).
36. Gross, F. *et al.* Metabolic engineering of *Pseudomonas putida* for methylmalonyl-CoA biosynthesis to enable complex heterologous secondary metabolite formation, *Chem. Biol.* **13**, 1253–1264 (2006).
37. Lambalot, R. H. *et al.* A new enzyme superfamily - the phosphopantetheinyl transferases, *Chem. Biol.* **3**, 923–936 (1996).
38. Peric-Concha, N. & Long, P. F. Mining the microbial metabolome: A new frontier for natural product lead discovery, *Drug Discov. Today* **8**, 1078–1084 (2003).
39. Galm, U. & Shen, B. Expression of biosynthetic gene clusters in heterologous hosts for natural product production and combinatorial biosynthesis, *Expert Opinion on Drug Discovery* **1**, 409–437 (2006).
40. Bannerjee, D. Sanders, L. E. & Sokatch, J. R. Properties of purified methylmalonate semialdehyde dehydrogenase of *Pseudomonas aeruginosa*, *J. Biol. Chem.* **245**, 1828–1835 (1970).
41. Haller, T. Buckel, T. Retey, J. & Gerlt, J. A. Discovering new enzymes and metabolic pathways: Conversion of succinate to propionate by *Escherichia coli*, *Biochemistry* **39**, 4622–4629 (2000).
42. Lau, J. *et al.* Optimizing the heterologous production of epothilone D in *Myxococcus xanthus*, *Biotechnol Bioeng* **78**, 280–288 (2002).

43. Sambrook, J. & Russell, D. W. *Molecular cloning: A laboratory manual* (Cold Spring Harbor Laboratory Press, Cold Spring Harbor, NY, 2001).
44. Fu, J., Teucher, M., Anastassiadis, K., Skarnes, W. & Stewart, A. F. in *Guide to Techniques in Mouse Development, Part B: Mouse Molecular Genetics, 2nd Edition* (ed. Enzymology, P. M. W. and P. M. S. B. T.-M. in) Volume 477, 125–144 (Academic Press, 2010).
45. Wu, S. S. & Kaiser, D. Markerless deletions of pil genes in *Myxococcus xanthus* generated by counterselection with the *Bacillus subtilis* sacB gene, *J. Bacteriol.* **178**, 5817–5821 (1996).
46. Bierman, M. *et al.* Plasmid cloning vectors for the conjugal transfer of DNA from *Escherichia coli* to *Streptomyces* spp. *Gene* **116**, 43–49 (1992).
47. Chang, A. C. & Cohen, S. N. Construction and characterization of amplifiable multicopy DNA cloning vehicles derived from the P15A cryptic miniplasmid, *J. Bacteriol.* **134**, 1141–1156 (1978).







## 6 Discussion and Perspectives

### 6.1 General Scope of the Present Work

Natural products, especially microorganism-derived compounds, have been invaluable resources in the discovery and development of bioactive anti-infectives. The present thesis deals with the identification, elucidation, and engineering of the biosynthetic pathway leading to the natural product family of myxopyronins from *Myxococcus fulvus* Mx f50. Detailed biochemical and structural characterizations were carried out for the key enzyme responsible for the formation of the  $\alpha$ -pyrone ring in myxopyronins. Moreover, synthetic biotechnology tools were applied to improve the production of myxopyronin and to generate novel myxopyronin analogues.

### 6.2 Myxopyronin biosynthesis in *Myxococcus fulvus* Mx f50

The biosynthetic machineries for secondary metabolites are usually encoded by a set of genes organized in so-called ‘biosynthetic gene clusters’ within the bacterial chromosomes. This arrangement of the genes facilitates the identification of complete natural product pathways, as well as the cloning and analysis of both the pathways and their products.<sup>1</sup> The rapid advancement in sequencing technologies such as high-throughput next generation sequencing have made the identification and analysis of natural product encoding gene clusters in sequenced genomes readily accessible.<sup>2,3</sup> Nevertheless, myxobacterial genome sequencing is still quite challenging due to its large genome size (approximately 9 Mbp or more), GC rich sequence and high amount of repetitive sequences.

Many microbial natural products are biosynthesized by polyketide synthases (PKS) and/or nonribosomal peptide synthetase (NRPS) pathways. In recent years, many bioinformatics mining tools have been developed to detect putative genetic blueprints for secondary metabolite biosynthesis based on microbial genome sequences. For example, antiSMASH,<sup>4</sup> ClustScan,<sup>5</sup> CLUSEAN,<sup>6</sup> SBSPKS,<sup>7</sup> and SMURF<sup>8</sup> are tools for the identification and/or analysis of the enzymatic domains in multi-modular PKS and/or NRPS. Myxobacteria have giant chromosomes as exemplified by *Myxococcus xanthus* (9.1 Mbp),<sup>9</sup> *Stigmatella aurantiaca* (10.3 Mbp),<sup>10</sup> *Sorangium cellulosum* (13.0 Mbp),<sup>11</sup> and *Haliangium ochraceum* (9.4 Mbp).<sup>12</sup> More than 8.5% of the *M. xanthus* genome is dedicated to secondary metabolism, a higher percentage than observed in actinomycetal secondary metabolite producers such as *Streptomyces coelicolor* (4.5%) or *Streptomyces avermitilis* (6.6%).<sup>13</sup> For instance, *M. xanthus* chromosome contains 18 secondary metabolite biosynthetic gene clusters encoding PKS and/or NRPS megasynthetases. Through studies such as mutagenesis

experiments, compound isolation, and proteome studies, 11 out of 18 PKS/NRPS gene clusters could be linked to the corresponding gene clusters (e.g. myxovirescin, myxalamid, myxochelin, myxochromide, DKxanthenes).<sup>13-17</sup> The additional seven pathways might be silent clusters or their products might not yet have been detected under laboratory conditions. For *S. cellulosum* So ce56, *in silico* analysis showed 13 regions of the chromosome encoding for proteins containing PKS and/or NRPS domains. However, only four secondary metabolites readily identified (etnangien, flaviolin, myxochelin, and chivosazol) in the culture extract while the products of the other biosynthetic pathways yet to be determined.<sup>11</sup> These two examples reveal that the metabolic potential of *M. xanthus* and *S. cellulosum* is much richer than was observed from traditional fermentation studies. Taken together, the established high throughput sequencing technologies and bioinformatics tools have built an important basis for genome mining approaches. This platform will facilitate exploitation of the biosynthetic capacity of natural product producers not only in identifying new natural products but also deciphering the biosynthesis of already known compounds.

In this study, Illumina HiSeq sequencing system was used to generate the genome sequence of *M. fulvus* Mx f50. To identify the myxopyronin (*mxn*) gene cluster, the genome sequence was screened for gene loci encoding putative polyketide synthase (PKS)/nonribosomal peptide synthetase (NRPS) pathways with high similarity to the coralopyronin (*cor*) biosynthetic pathway.<sup>18</sup> Myxopyronin is synthesized from two separate chains (western and eastern chains), which are derived from a PKS/NRPS system. The eastern chains of myxopyronin and coralopyronin are identical, thus the sequence similarity of *mxnI/mxnJ* and *corI/corJ*, which are responsible for the biosynthesis of eastern chains is very high. The myxopyronin western chain is considerably shorter than that of the coralopyronin structure. A detailed comparison of both pathways was performed *in silico* and the structural differences between the two compounds families could be explained (Fig.1).<sup>18,19</sup> Although the primary sequence information is often available, *in silico* analysis alone is not sufficient to elucidate the role of certain genes in the biosynthetic pathway of natural products. Therefore, extensive *in vivo* and *in vitro* experiments are often necessary to clarify the function of genes in the biosynthetic pathway under study. However, the genetic tools for myxobacteria are quite limited and genetic modification methods usually need to be developed individually for each strain. Here, *M. fulvus* Mx f50 becomes one of the few myxobacteria for which a markerless in-frame deletion (mutagenesis) procedure could be established. The mutagenesis procedure was applied to perform several sets of gene deletions in order to clarify the respective gene functions and to generate analogues. Further detailed discussion on the *mxn* gene cluster elucidation is described in **Chapter 2**.

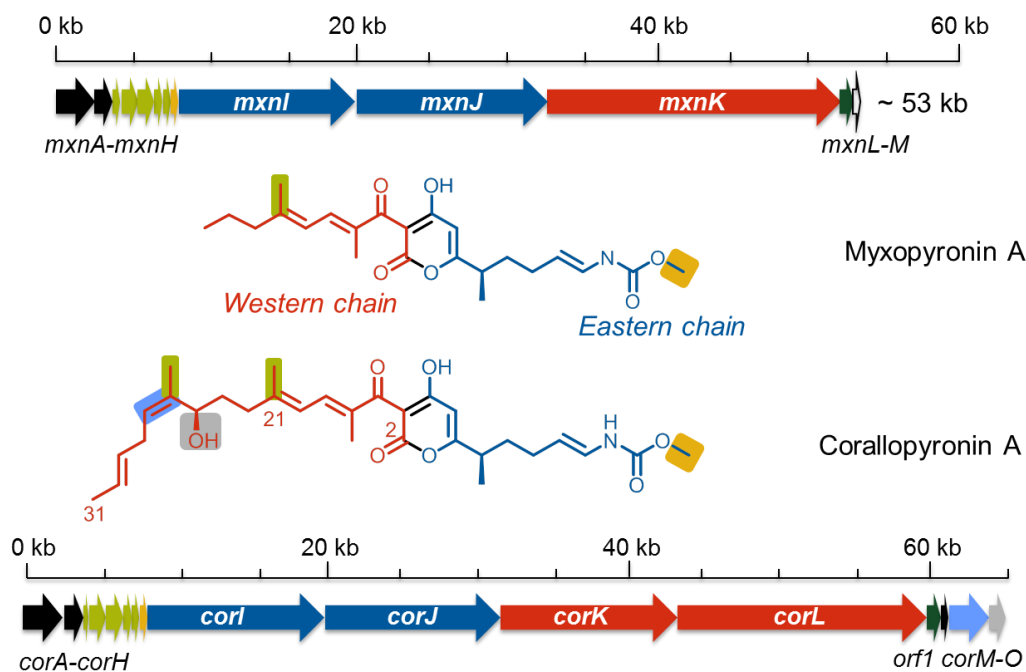


**Figure 1.** Myxopyronin (~53 kb) and coralloypyronin (~65 kb) gene cluster with the corresponding product myxopyronin A and coralloypyronin A, respectively. In general, red represents the western and blue the eastern chain. The coloured boxes in the structures represent the resulting moiety catalyzed by the corresponding genes with the same color arrows in the gene clusters.

### 6.2.1 An unexpected myxopyronin A derivative from $\beta$ -branching cassette deletion

The myxopyronin biosynthetic pathway belongs to the growing number of *trans*-AT PKS systems.<sup>20</sup> These systems are known for their ability to introduce unusual chain-branches during polyketide assembly, e.g. as observed in the biosynthesis of leinamycin<sup>21</sup>, mupirocin<sup>22</sup>, bacillaene<sup>23</sup> and myxovirescin<sup>24</sup>. Such so called “ $\beta$ -branching events” are directed by a set of enzymes usually including a CP, KS, HMG-CoA synthase (HCS), and two enoyl-CoA hydratases (ECHs).<sup>25</sup> The methyl group at C-21 in myxopyronin is introduced by such a  $\beta$ -branching cassette (MxC-MxG) (Fig. 2A). In  $\beta$ -branch-incorporation, the CP is loaded with a malonyl unit by an acyltransferase (AT) which is often also part of the  $\beta$ -branching cassette, followed by decarboxylation to generate acetyl-S-CP, catalyzed by KS. The key reaction is then performed by HCS, catalyzing the aldol attack of the acetyl enolate onto the assembly line-tethered  $\beta$ -keto thioester to generate an HMG-S-CP. The HMG-S-CP is then sequentially dehydrated and decarboxylated by the ECHs to obtain the  $\beta$ -methylated intermediate. A few *in vivo* studies showed that deletion of one of  $\beta$ -branching cassette genes result in production of novel metabolites. In mupirocin studies, the deletion of *mupH* (HCS) has resulted in derailment of the normal biosynthetic pathway and instead produced a truncated polyketide intermediate mupirocin H (Fig. 2B).<sup>26</sup> Another effect of HCS deletion

was observed during myxovirescin studies. In myxovirescin biosynthetic pathway, TaC and TaF are both annotated as HCSs which play role in introducing methyl group at C-12 and ethyl group at C-16, respectively. When TaF was deleted, surprisingly TaC rescues myxovirescin assembly by installing two acetate building blocks, one at C12 (which is further oxygenated and methylated) and another one at the C16  $\beta$ -keto positions of the respective intermediates. This results in a novel myxovirescin endowed with two methyl groups (Fig. 2C).<sup>24</sup>

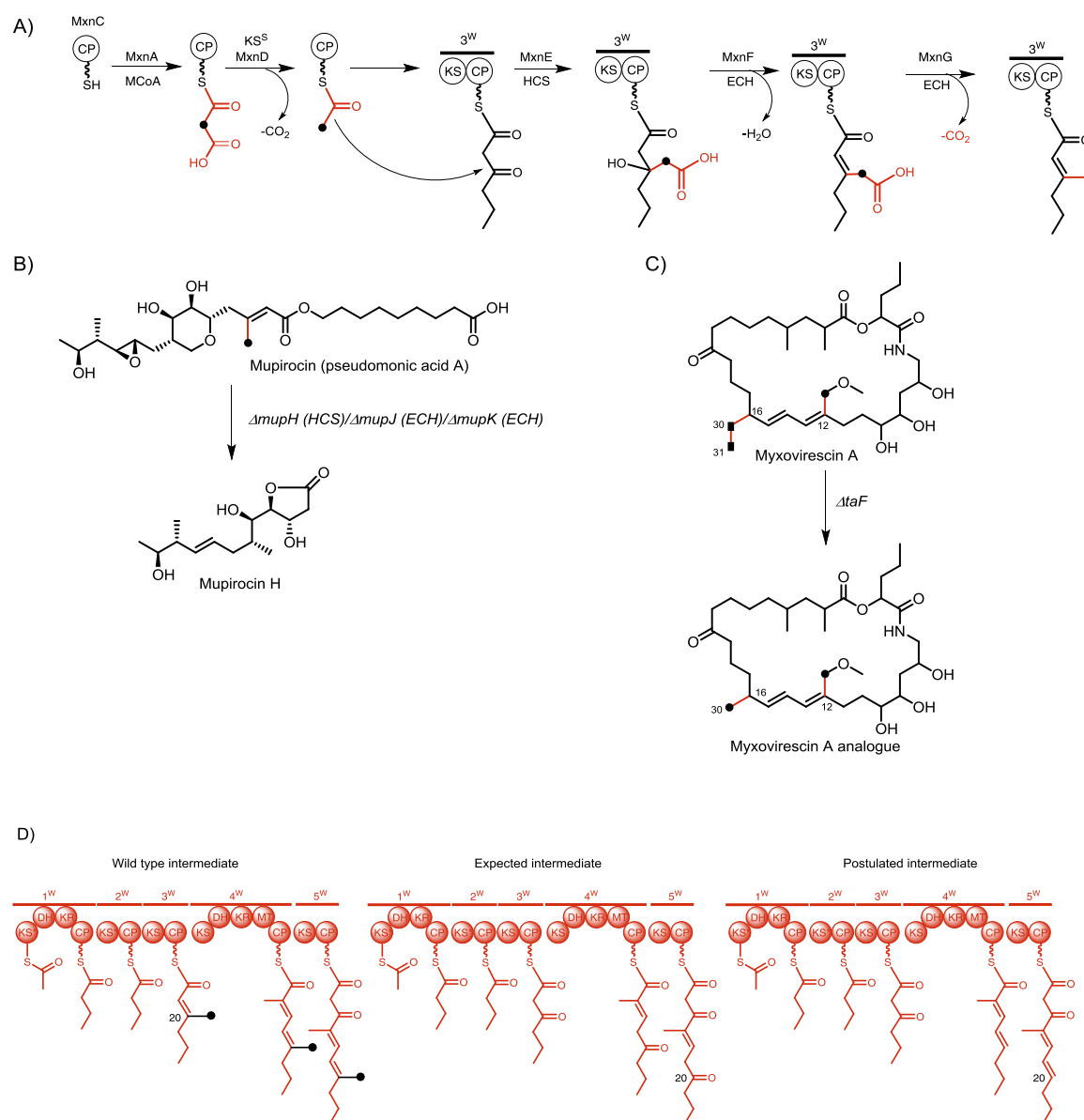


**Figure 2.** A) Possible reaction mechanism of MxnC-MxnG in myxopyronin A biosynthesis; B) Illustration of HCS deletion effect on mupirocin biosynthesis; C) Illustration of HCS deletion effect on myxovirescin biosynthesis; D) The intermediate in western chain assembly line for the wild type, the expected intermediate from the  $\Delta mxC-G$  mutant, and the postulated intermediate based on the isolated 21-desmethyl-myxopyronin A. The  $\beta$ -branches denotes by black circles (methylene group derived from the C2 portion of acetate) or boxes (the C2-C3 fragment derived from succinyl-CoA at carbon C16 for myxovirescin).

However, the reverse experiment where TaC was deleted did not show a similar complementary pattern by the existing TaF. This result might be due to the specificity of their

docking interactions with other enzymes comprising the megasynthase complex or incorporation of the larger ethyl group early in biosynthesis might result in the rejection of the modified intermediate at later biosynthetic steps.<sup>24</sup>

Based on the  $\beta$ -branching biochemistry illustrated in Fig. 2A, it was initially predicted that deletion of the  $\beta$ -branching cassette from myxopyronin biosynthetic gene cluster would result in the production of novel myxopyronin containing an unmodified C-20 carbonyl functionality (Fig 2D). Instead, the deletion mutant  $\Delta mxnC-G$  generated a myxopyronin analogue containing a  $\Delta^{19,20}$  double bond (21-desmethyl-myxopyronin A) with a yield that was fiftyfold lower than that of native myxopyronin in the wild-type strain (Fig. 2D).

The formation of this unexpected double bond can be explained by the downstream KR and DH activities at module 4<sup>W</sup>, which might act on both the C-18  $\beta$ -carbonyl and the C-20 O-carbonyl functionality of the biosynthetic intermediate (Fig. 2D). There are two proposed scenarios to explain this result: (1) the conjugated olefinic system might be essential for pyrone ring formation, and C-20 carbonyl intermediates bound to CP-5<sup>W</sup> are not processed, or (2) O-carbonyl reduction on module 4<sup>W</sup> is highly efficient, but because of the lack of the C-21  $\beta$ -branch, the overall productivity of the condensation step is significantly decreased. However, the mutasynthesis studies showed that only the  $\alpha$ -methyl group and  $\alpha$ -double bond are necessary for  $\alpha$ -pyrone ring formation (see Chapter 4).<sup>27</sup> These requirements would indirectly favour scenario (2) over scenario (1) since the olefinic system is apparently not compulsory for myxopyronin production. Future studies to investigate substrate specificity for this final condensation reaction can be performed using the established *in vitro* and mutasynthesis system presented in this thesis.

### 6.2.2 The importance of MxnH for O-methylation in myxopyronin biosynthesis

Methylation plays an important role on the functional output of many metabolic pathways such as bioavailability, bioactivity, and reactivity of acceptor molecules.<sup>28</sup> Natural products are often decorated with methyl groups and these methylation reactions are usually catalyzed by *S*-adenosyl-L-methionine (SAM)-dependent methyltransferases (MTs).<sup>28</sup> MTs are frequently integrated as domains within the PKS machinery, which act on the growing intermediate, or encoded by stand-alone genes to introduce methyl groups at different stages of the biosynthesis often as post-PKS modifications.<sup>29</sup> Myxopyronin and its closely related compound corallopyronin possess a unique terminal methyl ester moiety at their eastern chain which is also observed in other myxobacterial compounds such as melithiazol A and myxothiazol Z. (Fig. 1, Fig. 3). The eastern part of myxopyronin was shown to be important

for its bioactivity since initial structure activity relationship (SAR) studies show that slight variations in the eastern part of the molecule result in a dramatic loss of inhibitory activity.<sup>30</sup> Thus, investigation on biosynthesis detail of these  $\alpha$ -pyrone compounds will provide useful insights for structural modification *via* bioengineering.

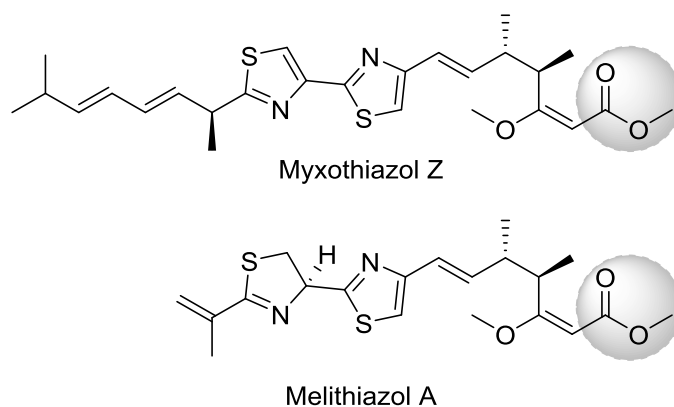


**Figure 3.** Structures of myxothiazol Z and melithiazol A. Methyl ester moiety is highlighted in grey.

Feeding studies on myxopyronin and coralopyronin suggested that the methyl ester moiety is derived from SAM, possibly carbonic acid which is methylated as free precursor or as assembly line intermediate.<sup>18,31</sup> In agreement, *in silico* analysis also proposed that this unusual *O*-methyl functionality is likely to be introduced by putative SAM-dependent-carboxy-methyltransferases (*O*-MTs) MxnH and CorH, respectively.<sup>18,19</sup> Indeed, Pfam analysis<sup>32</sup> showed that CorH/MxnH (86 % sequence identity) belong to the family of leucine carboxyl methyltransferase (LCMT). These enzymes methylate the carboxyl group of the C-terminal leucine residue of the protein phosphatase 2A catalytic subunit to form alpha-leucine ester residues.<sup>33</sup> BLAST search analysis of CorH/MxnH also revealed their sequence identity with MelK, putative *S*-adenosyl methionine (SAM)-dependent MT (identity ~28 %), from melithiazol biosynthesis. MelK has been biochemically characterized and is responsible for the rare methylation of carboxylic acid during myxothiazol/melithiazol biosynthesis to form a methyl ester moiety.<sup>34</sup>

As an attempt to elucidate the function of *mxnH* and to generate myxopyronin analogue, an in-frame deletion of *mxnH* was performed. However, myxopyronin production was completely abolished and the expected myxopyronin analogue containing a free carbamic acid moiety was not observed. The successful complementation experiment showed that the *mxn* biosynthetic genes are in principle functional in the *mxnH* deletion mutant, and implied that the formation of a methyl carbamate is essential for eastern chain biosynthesis.<sup>19</sup> Accordingly, *in vitro* assays performed by Schäberle and co-workers using heterologously

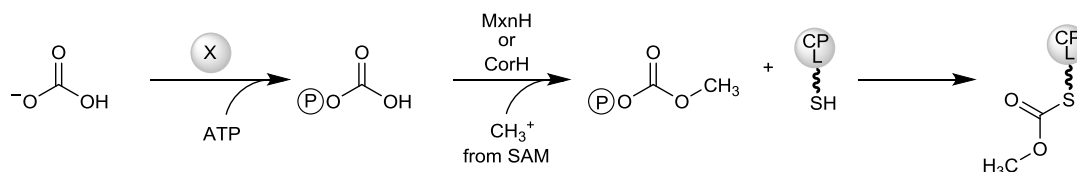
expressed CorH showed that CorH methylates  $\text{HCO}^{3-}$  through SAM consumption, indicating SAM as the methyl group donor.<sup>35</sup> The biochemical studies of CorH also indicated that the *O*-methylation reaction seems to precede the attachment of the starter unit to the PKS machinery.<sup>35</sup>

From the *in vivo* and *in vitro* experiments, a carbonic acid or a more stable monomethyl ester is likely the first building block loaded onto the PKS-NRPS eastern chain assembly line. However, building blocks are usually in the form of coenzyme A (CoA) esters before they are loaded by AT. Even though no such enzyme is encoded in the *mxn/cor* gene cluster, the existence of such an enzyme encoded somewhere in the producer genome cannot be excluded. The only AT (MxnA/CorA) present in the *mxn/cor* cluster is a malonyl-CoA-specific AT domain, which is unlikely to select another substrate to be loaded to the CPs. Moreover, the *trans*-ATs seem to have specific interactions with CPs in the assembly line in order to ensure loading of the correct substrate.<sup>36</sup> Therefore, MxnA/CorA do not seem to load foreign substrate and it is more likely that the substrate is self-loaded onto the CP-1<sup>E</sup> as already described for other CPs.<sup>37</sup>

While PKS substrates are usually activated by attachment of CoA, in NRPS the amino acid activation is achieved by reaction with ATP within the adenylation (A) domain to enable subsequent loading onto the NRPS CP domains.<sup>38,39</sup> Since the free hydrogen carbonate ( $\text{HCO}^{3-}$ ) will be in equilibrium with  $\text{CO}_2$  (which is volatile), a phosphate group from ATP might be transferred to  $\text{HCO}^{3-}$  to form the more stable intermediate carbonyl phosphate.  $\text{HCO}^{3-}$  connected with an activating group will be much more stable than its free form and will allow an *O*-methylation reaction to occur efficiently. In CorH studies, an experiment using purified CP<sub>L</sub> (loading module CP) and cell lysates demonstrated that the concentration and stability of the precursor is high enough to enable loading of the CP.<sup>35</sup> Whether the precursor is methylated hydrogen carbonate itself or its phosphate ester cannot be judged from this experiment. However, feeding studies in the myxopyronin producer using triethylmethylammonium methyl carbonate did not restore myxopyronin production.<sup>19</sup> This indicates that the activation through phosphate group attachment is likely to happen before *O*-methylation and subsequent transfer of the methoxycarbonyl moiety to CP<sub>L</sub>. Indeed, at the N-terminus of MxnI (not observed in CorI), there is an unknown domain (X domain) which exhibits weak similarity to a truncated phosphoglucomutase/phosphomannomutase, alpha, beta/alpha domain II (PGM PMM II). This domain might not only be involved in the activation of the proposed bicarbonate starter by phosphoryl group transfer but also mediated the loading of the methoxycarbonyl moiety to CP<sub>L</sub> (Fig. 4).

Taken together, the hydrogen carbonate is presumably phosphorylated to form carbonyl phosphate (Fig. 4, Route I). Subsequently, the hydroxyl group is methylated by CorH/MxnH to form methoxycarbonyl phosphate, which is transferred to the CP<sub>L</sub> as the first building block (Fig. 4, Route I). Further studies need to be conducted to clarify the reaction sequence for the proposed phosphorylation and methylation reactions (Fig. 3, Route I or Route II). For example, further *in vitro* studies using methoxycarbonyl phosphate instead of methyl carbonate as substrate would shed more light on the loading process of module CP<sub>L</sub>.

Route I



Route II

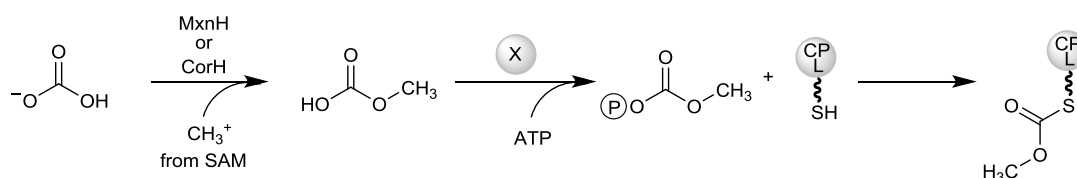


**Figure 4.** Proposed methylation step of CP<sub>L</sub> by MxnH or CorH. In Route I: the hydrogen carbonate is phosphorylated before methylation while in Route II the hydrogen carbonate is methylated before phosphorylation. Route I or Route II is then continued by the transfer of a methoxycarbonyl moiety to the CP<sub>L</sub>. CP<sub>L</sub>: CP loading, X : PGM PMM II.

In summary, the targeted knock-outs have provided insights into the function of the genes involved in myxopyronin biosynthesis. A thorough understanding of the mechanisms and specificity regarding all steps involved in natural product assembly will facilitate efforts to engineer and modify existing natural product biosynthetic pathways with a goal toward optimizing pharmacological properties or using natural products as a starting point for further synthetic modifications.

### 6.3 $\alpha$ -Pyrone ring formation during polyketide biosynthesis – in depth studies on myxopyronin

$\alpha$ -pyrones are found in a number of natural products isolated from plants, animals, bacteria, fungi, and insects that exhibit a broad range of biological activities, such as antifungal, antibiotic, cytotoxic, neurotoxic and phytotoxic.<sup>40</sup> However, there is not much information available regarding the biosynthetic strategies for  $\alpha$ -pyrone formation. Up to date, these  $\alpha$ -pyrone containing natural products are typically synthesized by type II and type III PKSs such as described for wailupemycin<sup>41</sup> and csypyronin,<sup>42–44</sup> respectively. Type II PKS multienzyme complexes carry a single set of iteratively acting activities and usually use CP to



activate the acyl CoA substrates and to channel the growing polyketide intermediates (Fig. 5).<sup>38</sup> Type III PKSs, also known as chalcone synthase (CHS) like PKSs, consist of homodimeric enzymes that basically are iteratively acting condensing enzymes using acyl CoA substrates (Fig. 4).<sup>38</sup> Nevertheless, type II and type III PKSs are essentially different systems compared to a type I PKS where multifunctional enzymes organized in modules responsible for non-iterative catalytic steps of one cycle of polyketide chain elongation.

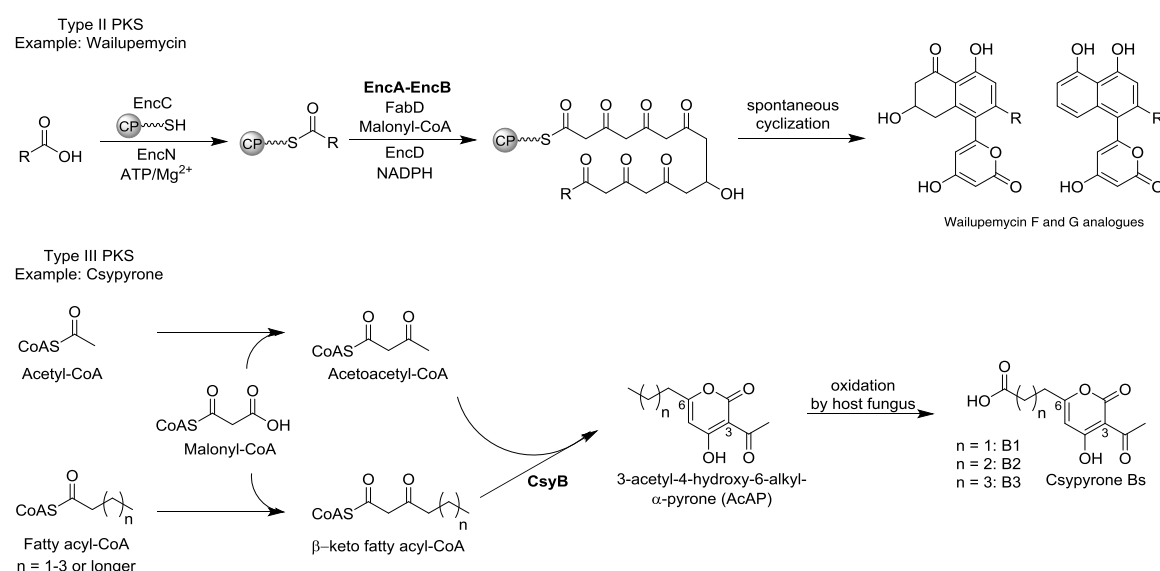


**Figure 5.** Biosynthesis of natural products biosynthesized by type II (wailupemycin)<sup>41</sup> and III (csyprone)<sup>43</sup> containing  $\alpha$ -pyrone rings. The protein marked in bold is the responsible ketosynthase catalyzing the ring formation.

Myxopyronin and corallopyronin, synthesized by NRPS/PKS (type I PKS) hybrid, are myxobacterial compounds that contain such a structural motif in their structures. In order to address the question how this  $\alpha$ -pyrone ring moiety is generated, a comprehensive *in vitro* study was performed. The key reaction in myxopyronin biosynthesis is the formation of the  $\alpha$ -pyrone ring from two PKS/NRPS derived chains, western and eastern chain (Fig. 6A). This reaction is catalyzed by a putative stand-alone ketosynthase (KS), MxnB. In the myxopyronin biosynthetic assembly line, the chains are presumably bound to the corresponding CPs - the western chain is tethered to the CP-5<sup>W</sup> and the eastern chain to CP-6<sup>E</sup> (hereafter referred to as CP-W and CP-E, respectively). In order to prove this hypothesis, a series of *in vitro* assays were performed and they showed that MxnB catalyzes this essential reaction step utilizing thioester substrates coupled to either *N*-acetylcysteamine (NAC) or a CP.<sup>45</sup> The reaction sequence of myxopyronin was determined by in-depth biochemical experiments including MxnB structural studies and detailed analysis of the identified novel myxopyronin congeners in the extract of the producer strain. Based on the crystal structure, MxnB possesses two binding tunnels (one for each substrate) namely red (for western chain) and blue (for eastern

chain) tunnels (Fig. 6B). By combining all of the data, we proposed that the western chain binds to the KS first, before the eastern chain. Further biochemical studies and discussion are described in **Chapter 3**.

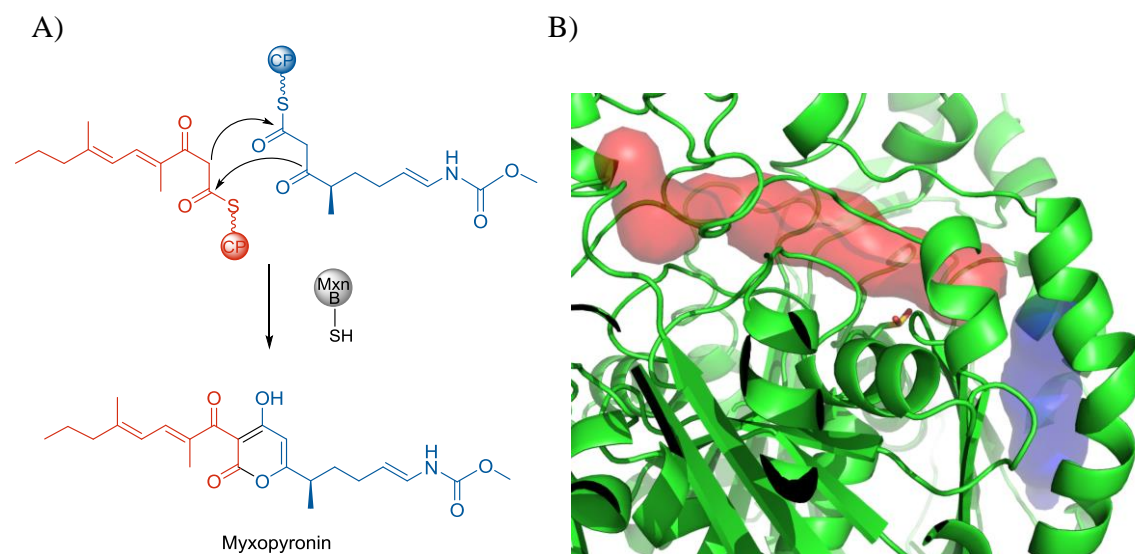


**Figure 6.** A) Proposed final step for myxopyronin formation. Red and blue define the western and eastern part of the molecule, respectively. B) Side view of the two proposed substrate-binding tunnels in MxnB, canonical tunnel (red) and additional tunnel (blue). The active site cysteines (C121) are shown as sticks. Tunnels were predicted using Mole 2.0.<sup>46</sup>

During the MxnB biochemical studies, the reaction involving CP-bound substrates had a 12-fold higher turnover rate than SNAC substrates. This finding indicates the importance of protein-protein interactions between KS and CP in multimodular PKSs.<sup>47,48</sup> The ability of CPs to conduct self-acylation has been previously reported.<sup>37,49</sup> In this study, CP-W and CP-E also show such capacities even though differences in the priming efficiency between the western and eastern SNAC substrates are observed. The differences in loading efficiency are expected to arise from the structural difference between the two chains.

In the present study, several KS mutations were conducted to investigate the residues responsible for accommodating the substrate in the tunnel. However, the performed KS mutations were not able to block the tunnels completely. Therefore, further mutation studies could be performed in the future to pinpoint residues that make contact with the substrate. Understanding the key residues responsible for substrate interaction within the tunnel will be an important milestone to modify substrate specificity and further the generation of myxopyronin analogues. Initial studies have indeed shown that several unnatural western substrates are accepted by MxnB to yield myxopyronin analogues. However, the product formation efficiency between different substrates has not yet been determined.

Furthermore, in order to gain further insights into the molecular basis of interactions between KS and CP-W or CP-E in myxopyronin biosynthesis, protein docking and

subsequent experimental studies remained to be conducted. Understanding the fundamental catalytic mechanisms and protein-protein interactions necessary for myxopyronin biosynthesis are necessary for further myxopyronin pathway engineering. The presented *in vitro* approach to form myxopyronin might be one of the routes to produce myxopyronin analogues with improved bioactivities. Although total synthesis of myxopyronin has been achieved,<sup>50</sup> the process is time-consuming and the yield is low. In addition to the isolation of main myxopyronin analogues (MxnWE), isolation of the other types (MxnEW, MxnEE and MxnWW) is also of interest. The bioactivity assays for all of the myxopyronin analogues would help us to better understand the structure-activity relationship (SAR) between myxopyronin and RNAP.

Before MxnB was characterized, there was only one example of 5-membered ring formation by a type I PKSs reported; the stand-alone KS (RkD) which condenses a CP-bound substrate, forming the tetronate ring during the biosynthesis of the phosphatase inhibitor RK-682 (Fig. 7).<sup>51</sup> MxnB becomes the first stand-alone KS described as catalyzing a 6-membered ring formation in a type I PKS pathway. Thus it is an important addition to the thiolase enzyme family (Fig. 7).

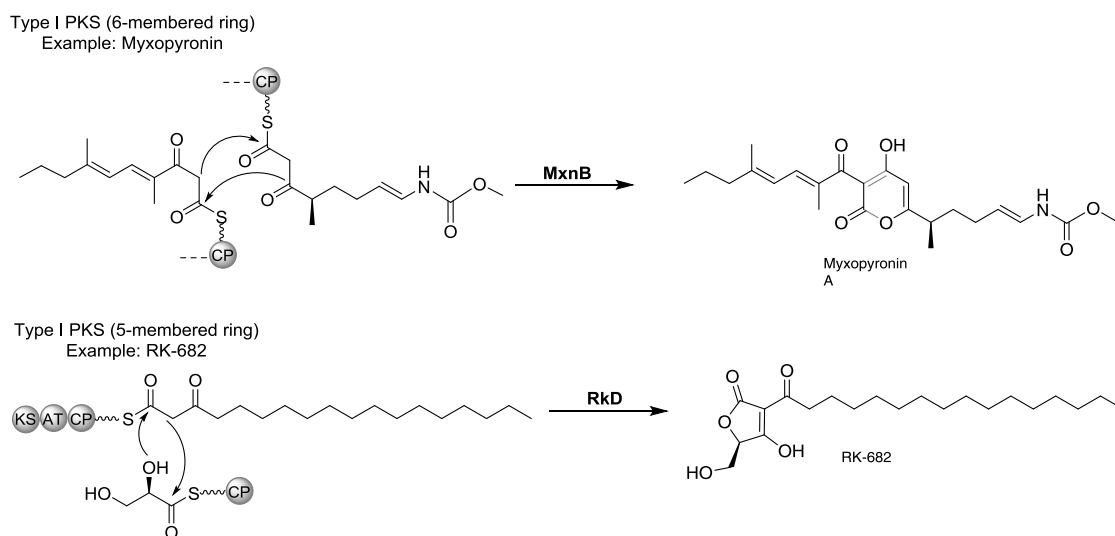


**Figure 7.** Biosynthesis of natural products biosynthesized by type I PKS (myxopyronin)<sup>19</sup> containing  $\alpha$ -pyrone ring and RK-682<sup>51</sup> which contains a tetronate ring. The protein marked in bold is the responsible ketosynthase catalyzing the ring formation.

This enzyme will not only provide novel opportunities to rationally engineer the structural diversity of natural products but also to generate antibiotics that are not easily accessible by synthetic methods. The established platform will allow us to fine-tune the structure of the analogues to achieve optimal balance of good drug parameters, e.g., physicochemical, ADME, and low toxicity properties.

## 6.4 Expanding the chemical space of $\alpha$ -pyrone antibiotics – Mutasythesis approach towards novel myxopyronin analogues

Genetic engineering has become a powerful tool for the generation of new structural variants of natural products. More chemical diversity can even be achieved when the genetic tools are combined with synthetic chemistry.<sup>52</sup> One implementation of these tool combinations is named mutasythesis: the biosynthesis of a natural product precursor is blocked by a relevant gene inactivation experiment. Subsequently synthetic analogues of this precursor (mutasythons) are added to the culture medium, giving rise to an incorporation of the foreign moiety into the natural product and thereby yielding new derivatives.<sup>52–54</sup> A prominent example for such a mutasythesis experiment is exemplified by the production of doramectin by the genetically modified avermectin producer *Streptomyces avermitilis* M1.<sup>55–57</sup> Doramectin was produced by feeding cyclohexane carbocyclic acid (CHC) to a mutant of *S. avermitilis* lacking a branched-chain ketoacid dehydrogenase (*bkd*) (Fig. 8).<sup>56</sup>

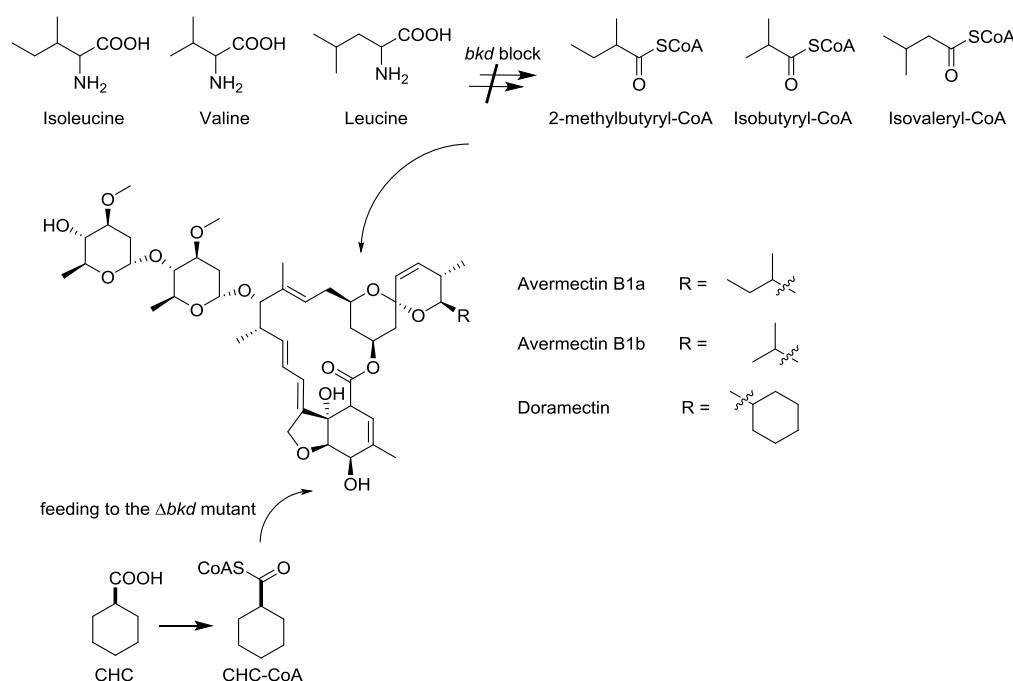


**Figure 8.** The role of precursors in the biosynthesis of avermectin and doramectin in *S. avermitilis*. Avermectin B1a and B1b are generated using the starter units 2-methylbutyryl-CoA and isobutyryl-CoA, respectively. In the *bkd* mutant, the formation of these starter units from branched-chain amino acid degradation is blocked. Doramectin is generated by feeding CHC to the *S. avermitilis*  $\Delta bkd$  mutant where the CHC is presumably activated by a non-selective acyl CoA ligase and loaded onto the avermectin biosynthetic pathway (Figure is adapted from Reference<sup>58</sup>)

In the  $\Delta bkd$  mutant, the biosynthesis of isobutyryl-CoA or 2-methylbutyryl-CoA is disrupted, which diminishes the supply of the original substrate of AT domain in the loading module for avermectin biosynthesis.<sup>56</sup> The generated avermectin analogue, doramectin, was found to possess a better bioactivity compared to avermectin.<sup>56</sup>

Despite its importance in drug discovery and lead optimization, mutasynthesis has three principal limitations<sup>59</sup>: (1) the range of the precursors that can be introduced into the final molecule is not only limited by the substrate specificity of the downstream biosynthetic enzymes but also the toxicity effect from the supplied mutasynthons and/or the generated natural product derivatives to the cells; (2) usually only structural features generated in early steps of the biosynthesis are addressed due to difficult or even unworkable experimental requirements for modifications at later stages; and (3) the range of precursors that can be taken up into the producing cells is limited. Nonetheless, even minor modifications can result in a significant impact on the bioactivity as exemplified by doramectin, a mutasynthesis product of the avermectin pathway (Fig. 8).<sup>56</sup>

In the present work, a mutasynthesis approach towards novel myxopyronin analogues was established resulting in 12 new derivatives (**Chapter 4**).<sup>27</sup> Our studies focused on the modifications in the myxopyronin western chain as it offers wider scope for structural variations according to the results from previous SAR studies.<sup>30,60,61</sup> Complete western chain biosynthesis was blocked by inactivation of the corresponding PKS MxnK resulting in a mutant ( $\Delta mxnK$ ; in-frame deletion of 5.6 kb internal fragment of *mxnK*) that is not able to produce myxopyronin. A series of  $\beta$ -keto SNACs were then introduced to  $\Delta mxnK$  and based on this experiment the essential part of the western chain required for pyrone ring formation was defined as the  $\alpha$ -methyl group and the  $\alpha$ -double bond (Fig. 9). Despite numerous attempts, the isolation of new derivatives was not successful due to the limited uptake of the  $\beta$ -keto SNAC and/or its fast degradation in the culture. In order to circumvent the fast degraded and unstable  $\beta$ -keto SNAC, simplified and more stable SNAC substrates were synthesized, which should be incorporated at earlier stages of the biosynthesis (Fig. 9). For this, two additional mutants were generated by site-directed mutagenesis to inactivate the carrier protein domains from module CP-1<sup>W</sup> and CP-4<sup>W</sup> resulting in  $\Delta CP-1^W$  and  $\Delta CP-4^W$ , respectively (Fig. 9).

The successful incorporation of the simplified SNAC substrates after feeding to the  $\Delta CP$  mutants indicates that all of the corresponding downstream KS domains possess a certain range of substrate flexibility. It has been proposed that the KS domains from *trans*-ATs developed through horizontal gene transfer, by assembly of substrate-specific KS domains.<sup>62</sup> In contrast, *cis*-AT KS domains evolved through duplication of entire modules in which KS domains are embedded.<sup>63,64</sup> Examination of the X-Cys active site motif in KS domains from *cis*- and *trans*-AT PKSs revealed interesting differences between the two types. This X residue appeared to affect the size of the KS binding pocket. For *trans*-AT PKSs, which accept  $\alpha$ - and  $\beta$ -carbon branched substrates, X is always a less sterically demanding

residue such as Ala, Gly, or Asn (exclusively for KSs that use amide-containing substrates). On the other hand, *cis*-AT PKSs might not go through the evolving process to create any variety of amino acids at this X position in order to develop a mechanism of specificity. This is supported by the data from all the fully assigned *cis*-PKSs in the literature that X is always Ala.<sup>65</sup>

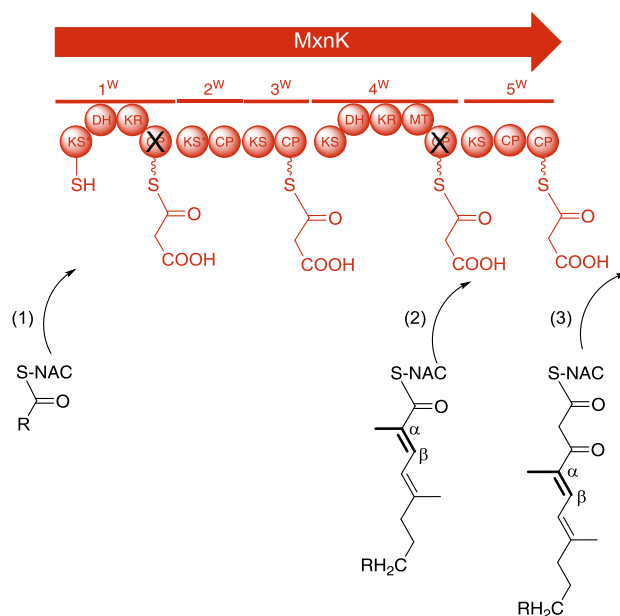


**Figure 9.** Illustration of the mutasynthesis experiment on (1)  $\Delta$ CP-1<sup>W</sup>, (2)  $\Delta$ CP-4<sup>W</sup>, (3)  $\Delta$ *mxnK* with the corresponding SNAC substrates. The essential structural parts for condensation reaction are marked in bold. R=alkyl chain or other functional groups.

In the myxopyronin PKS/NRPS assembly line, all of the KSs have X = Ala, except for KS-3<sup>E</sup> (X = Leu) (Fig. 10). These data may explain the incorporation of various SNAC substrates to the  $\Delta$ CP-1<sup>W</sup> and  $\Delta$ CP-4<sup>W</sup> and suggest future potential to introduce structurally more diverse substrates into the CP-engineered mutasynthesis system. Despite the successful CP-engineered mutasynthesis experiment, the yield of final products was still too low for product isolation (1-10  $\mu$ g/L) to allow for bioactivity testing. Detection of unconsumed substrates in the culture supernatant suggested that insufficient uptake into the cells is a limiting factor. Various trials to increase the yield were conducted but still not able to improve the yield so far.

As discussed above, during the initial mutasynthesis studies, the essential part of the native western chain to enable pyrone ring formation was determined as the  $\alpha$ -methyl group and the  $\alpha$ -double bond (Fig. 11, W1-W3). Interestingly, this requirement did not apply to the *in vitro* studies (see Chapter 3), which indicate that MxnB including the involved CPs are promiscuous enzymes able to utilize a broader range of substrates for pyrone ring formation (Fig. 11, W1-W5).

	X-Cys
KS-E1	SEAVDAACASSLVALH
KS-E2	SEAVDTACSSSLVAIH
KS-E3	SEPVDTLCSSSLVAIH
KS-E4	SEAIDTACSSSLVAIH
KS-E5	SFAVDSACASALTAIH
KS-E6	SEPVDTACSSSLIAVQ
KS-W1	SFTIDAACASSLVALH
KS-W2	SLAVDTACSSSLAAIH
KS-W3	SEPCDTACSSSLIAIH
KS-W4	AMQVDTACSSSLVAVH
KS-W5	SLMVDTACSSSLTALH

**Figure 10.** Alignment of the KS involved in myxopyronin biosynthetic pathway. X is the residue right before the active site Cys that confers substrate specificity for the KS.

However, the correlation between the enzymatic *in vitro* conversion and the subsequent yields of myxopyronin analogues from feeding experiments *in vivo* remain to be investigated. Different outcomes for *in vitro* and *in vivo* (mutasynthesis) approaches have been reported for other natural product biosynthetic pathways as well. In the studies of aminocoumarin biosynthesis, the *in vitro* experiments were used to determine the substrates used in the *in vivo* feeding experiments.<sup>66</sup> Aminocoumarin antibiotics contain amide bonds formed between an aminocoumarin ring and an aromatic acyl component (3-dimethylallyl-4-hydroxybenzoate = ring A). This amide bond formation is catalyzed by amide synthetases (CloL, NovL or CouL). *In vitro* assays using these amide synthetases were performed in order to identify which synthetic analogs of the prenylated 4-hydroxybenzoate moiety would be accepted in the *in vivo* feeding experiments using ring A defective mutants of the aminocoumarin antibiotic producers.<sup>66</sup>

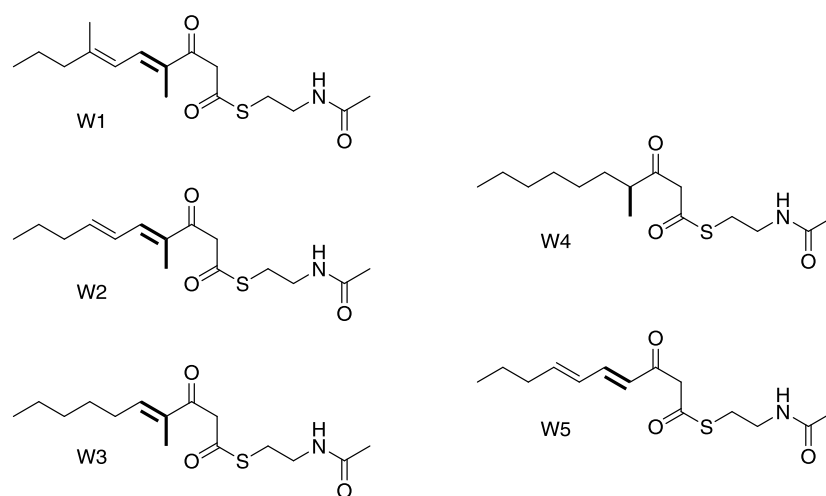


**Figure 11.** A few examples of synthetic western side-chain mimics that have been used in both of mutasynthesis and *in vitro* experiments. W1-W3 are accepted in the mutasynthesis experiments while W1-W5 are accepted in *in vitro* experiments.

Comparing both approaches established for characterizing and engineering myxopyronin biosynthesis, *in vitro* pyrone ring formation and *in vivo* mutasynthesis, reveals pros and cons relating to the generation of novel myxopyronin analogues (Table 1). Regarding the effort for substrate preparation, *in vitro* experiments need two substrates instead of only one substrate required for *in vivo* mutasynthesis experiments. Hereby, however, the *in vitro* approach in principle also allows for conversion of modified eastern chain substrates to access a larger chemical space, which is additionally favoured by a broader substrate tolerance observed in the performed enzyme assays. Moreover, the isolation process is probably less complicated from *in vitro* biotransformation compared to the complex medium and metabolite mixtures harvested from *in vivo* experiments. Despite all of the mentioned advantages and disadvantages of these two systems, both offer valuable insights into the biochemistry and architecture of key enzymes for myxopyronin biosynthesis and will enable more directed myxopyronin pathway engineering in the future.

In addition, parallel *in vitro* studies on MxnB homolog CorB from the highly related corallopyronin pathway (Schäberle and co-workers, unpublished results) have revealed that CorB fulfils the same function as MxnB in catalyzing the formation of  $\alpha$ -pyrone ring structures. However, a mutasynthesis system in the native corallopyronin producer *Corallocooccus coralloides* could not be established due to limitations in the genetic accessibility, which to our knowledge does not allow pathway engineering so far. Therefore, the established myxopyronin western chain mutasynthesis system in principle should also enable generation of corallopyronin-like analogues in the future.

**Table 1. Comparison between *in vitro* and *in vivo* approaches in producing myxopyronin analogues**

Parameter	<i>In Vitro</i>	<i>In Vivo</i>
Range of substrates	Broad	Narrow
Needed substrates	Eastern chain and western chain substrate	Only western chain substrate
Resulting analogues	Four different analogues can be obtained (MxnWE, EW, EE, WW)	Only one analogue (MxnWE)
Isolation process	Simpler process due to the less complex reaction mixture	More challenging process due to complex medium/metabolite mixture from bacterial culture
Cell permeability	N/A	A limiting factor

N/A: Not Applicable



## 6.5 Heterologous expression of complex natural product biosynthetic pathways –myxopyronin production in the myxobacterial model strain *M. xanthus*

The advances in cloning and characterization of natural product biosynthetic machineries have contributed to numerous opportunities for improving the production and diversification of natural products.<sup>46</sup> However, many natural products are still produced in low yields, which limit the downstream experiments such as pharmacokinetics/pharmacodynamics analysis and lead optimization. To overcome this limitation, heterologous expression of the engineered biosynthetic gene clusters in non-native host strains has been widely and effectively used.<sup>47,48</sup> Moreover, heterologous expression also represents a valuable tool to explore genome mining information, e.g. to exploit the biosynthetic potential of a certain strain by awakening its silent gene clusters, which are normally not expressed in the native producer under standard laboratory conditions.<sup>48</sup> Complete gene clusters for the natural products of interest can be transferred into a more suitable organism that grows faster, is genetically characterized and stable, and is amenable to manipulation. Achieving heterologous expression of natural products or their derivatives allows circumventing laborious strain optimization approaches and the development of fermentation procedures for the native producers. Especially for slow growing or difficult to grow microorganisms such as myxobacteria, symbionts, or sponge related bacteria, heterologous expression is a huge advantage. Myxobacteria are not only difficult to cultivate but also complicated to be genetically modified. In fact, it was so far necessary to establish mutagenesis procedure for each strain independently.<sup>67</sup> Genetic modification attempts are also hampered by the multi-resistance of myxobacteria to most antibiotics commonly used as selection markers, their unfavourable growth characteristics (e.g. strains grow in clumps), their overall susceptibility to various stress factors, and the lack of basic genetic tools (e.g. suicide vectors). Thus, these drawbacks have pointed out the importance of establishing heterologous expression systems for myxobacterial biosynthetic pathways.

Introduction of large biosynthetic gene clusters into heterologous hosts is still a challenging effort, which is limited not only by the biochemistry and genetics of the host organisms but also by the size of the DNA that is introduced. Up to date, only a few examples for successful expression of complete biosynthetic machineries for myxobacterial compounds in either phylogenetically related or distant hosts are known (Fig. 12 and Table 2). These examples are the production of epothilone in *M. xanthus* and in *Streptomyces coelicolor* (initial yields ~0.2 mg/L),<sup>68,69</sup> soraphen in *S. lividans* (yield 0.3 mg/L),<sup>70</sup> flaviolin in *Pseudomonas putida* (yield 6 mg/L),<sup>71</sup> myxochromide in *P. putida* (yield 40 mg/L),<sup>72,72</sup>

myxothiazol in *M. xanthus* (yield 20-60 mg/L),<sup>73</sup> pretubulysin in *P. putida* or *M. xanthus* (yield 0.0176 mg/L or 0.176 mg/L, respectively),<sup>74</sup> dawenol in *M. xanthus* (yield 0.05 mg/L),<sup>75</sup> polyunsaturated fatty acid (PUFA) in *M. xanthus* (yield 0.2-0.8 mg/g cell dry weight) (see more examples in Table 2).<sup>76</sup> In a few cases, time-consuming cloning procedures were used, and the biosynthetic gene clusters were transferred in several fragments such as epothilone<sup>68,77</sup> and soraphen<sup>70</sup>. In other cases, the biosynthetic genes are “stitched” together mainly from cosmid libraries *via* Red/ET recombineering to obtain the final construct for the gene cluster.<sup>72-74</sup>

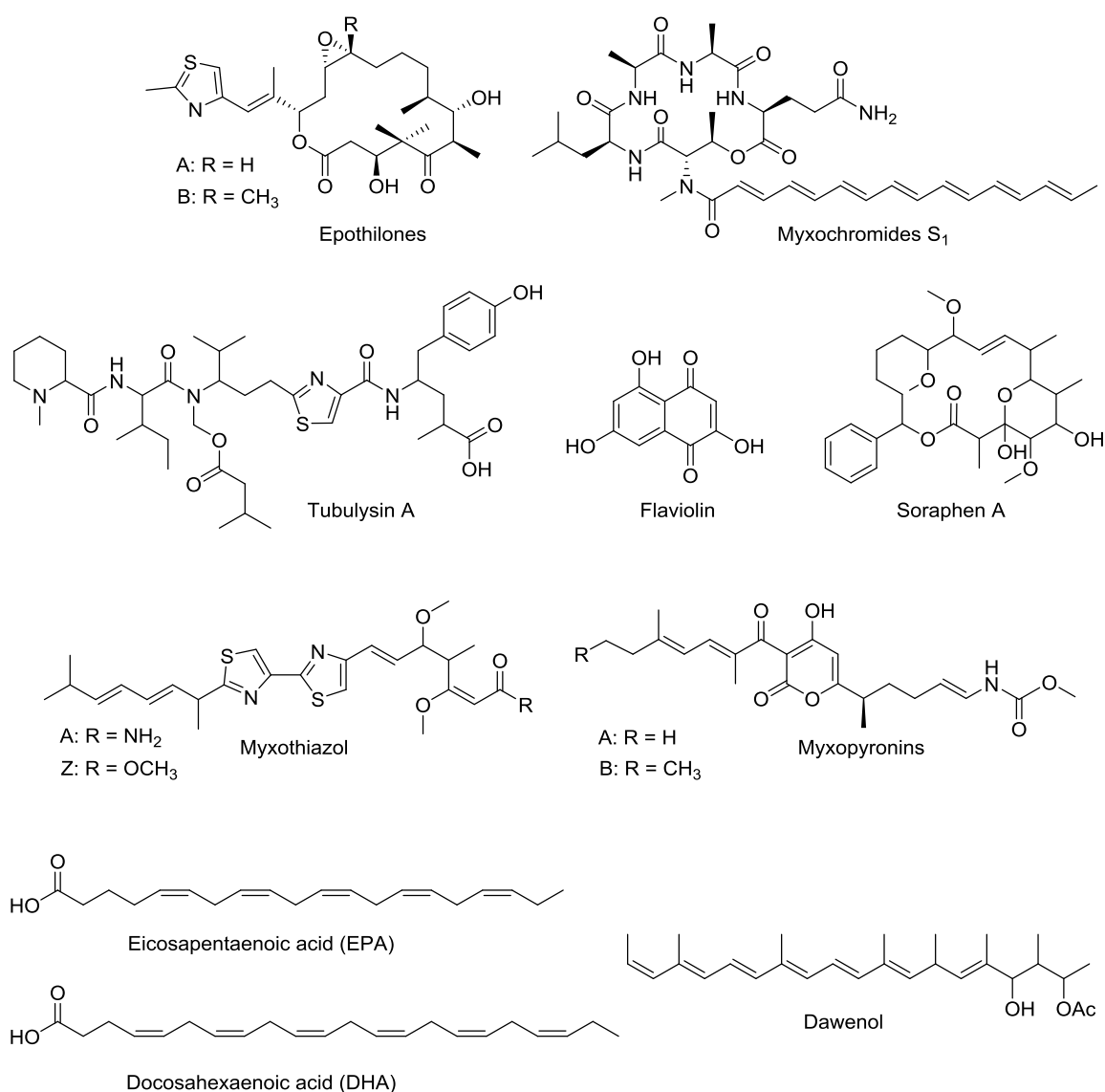


**Figure 12.** Heterologously expressed myxobacterial gene clusters in either phylogenetically related or distant hosts.

In order to improve the productivity of myxopyronin and facilitate its pathway engineering, a heterologous expression system for the entire biosynthetic pathway was established in the course of the present work (see **Chapter 5**). The myxopyronin biosynthetic

gene cluster was assembled into one entity through several rounds of directed mutagenesis, Red/ET recombineering, and conventional cloning technology under control of the Tn5 promoter employing the low copy number vector p15A *ori* with *tet<sup>R</sup>*. The plasmid was then used to integrate the gene cluster into the heterologous host chromosome, *M. xanthus* DK1622Δ*mchA::tet* (Wenzel, unpublished result). The obtained expression strain indeed started to produce myxopyronins with an initial yield of around 5 mg/L.

There are essentially two ways of introducing the foreign biosynthetic gene cluster to heterologous host: (1) plasmid-based expression and (2) chromosomal integration.<sup>78</sup> In plasmid-based expression, the biosynthetic gene clusters can be expressed from self-replicating plasmids, either from a single plasmid, containing the entire biosynthetic pathway, or from multiple plasmid individually expressing modules *in cis*. This system relies on the availability of plasmid replicons capable of functioning in the host. Although plasmid-based expression would be a convenient method, unfortunately there is no replicative expression plasmid yet available for introducing gene cluster to myxobacterial host, unless chromosomal modifications are performed to facilitate this purpose. Therefore, the introduction of the described myxobacterial biosynthetic pathways to the myxobacterial host usually depends on chromosomal integration which allows stable heterologous expression in the host.

Chromosomal integration is further classified to three main methods: (1) homologous recombination, (2) transposition, and (3) phage-derived systems.<sup>78</sup> In phage-derived systems, the recombination event is catalyzed by a phage integrase (*int*) that promotes recombination between two short DNA recognition sequences, the phage attachment site (*attP*) and a corresponding attachment site within the bacterial chromosome (*attB*) resulting in the integration of the entire plasmid at the bacterial attachment locus.<sup>79</sup> This method was almost exclusively applied to heterologous expression in *Streptomyces*, until recently it was applied to heterologously produce epothilone in *M. xanthus* using *mx8* and *mx9* as specific integration site in the host.<sup>77,80,81</sup>

For the integration of myxobacterial gene cluster into the heterologous host, homologous recombination and transposition have been widely utilized. Homologous recombination is a process of exchanging DNA between two regions of identical sequence. Endogenous recombinases from the heterologous host can promote integration through large regions of DNA sequence homology (normally 1 kb). The length of the homology region has shown positive influence in the recombination efficiency.<sup>82</sup> For chromosomal integration, a “suicide vector” that lacks the ability to replicate in the host, carries a sequence of DNA to be integrated along with a region of homology to the intended integration site. This results in the

gene of interest being integrated at the selected site. In the present study, homologous recombination has been effectively used in the gene knockouts, promoter and restriction sites insertion, and importantly in the integration of the complete myxopyronin biosynthetic gene cluster.

The complete myxopyronin biosynthetic pathway was introduced using *tet<sup>R</sup>* as homologous region. This integration site *tet<sup>R</sup>* is located at the locus of the deleted endogenous myxochromide A gene cluster (Wenzel, unpublished results). The deletion of the cluster is predicted to reduce the number of co-produced compounds as also observed in myxothiazol heterologous production. When the myxothiazol gene cluster was introduced to the inactivated endogenous myxovirescin gene cluster in *M. xanthus*, the production yield was found significantly higher (20 mg/L) compared to the yield from the native producer *S. aurantiaca* (10 mg/L). The questions whether integration site and method will have any significant effect on myxopyronin yield in *M. xanthus* remains to be investigated in the future. Previous studies have indeed shown that integration site for heterologous expression of a gene cluster also influences its expression and the production levels of the compound as seen in pretubulylin (20-fold lower compared to native producer),<sup>74</sup> epothilone (100-fold lower) and myxochromide S (75-125 fold higher) in *M. xanthus*.<sup>83</sup> In these cases, the gene clusters were introduced to *M. xanthus* by transposition method which proved to give high integration efficiency. In this method, transposable element or transposon itself is flanked by inverted terminal repeats that are recognized by a corresponding transposase, which facilitates the insertion of the transposon into a target site. They are usually used in genetics to create non-specific gene knock-outs for gene function analysis.<sup>84,85</sup> Since the integration site by transposon insertion is random, it is necessary to assess the compound titres from numerous clones, even though in pretubulylin<sup>74</sup> and epothilone<sup>83</sup> production in *M. xanthus* the difference between each clone was small.

As we have already learned from the previous examples (Table 1), *M. xanthus* appears to be a suitable and convenient expression host for myxobacterial pathways. *M. xanthus* is the best-characterized model organism in myxobacteria that has been extensively studied by many research groups providing comprehensive information such as its complete genome sequence,<sup>9</sup> transcriptional regulator of secondary metabolite clusters,<sup>86</sup> and predation.<sup>87</sup> The genetics and molecular techniques to engineer this organism has also been established since 20 years ago.<sup>88</sup> Importantly, *M. xanthus* offers similarly high GC content, preferential codon usage, presence of a broad-spectrum P-pant transferase required for the activity of PKS/NRPS megasynthetases, no additional metabolic engineering steps were required, growth in suspension, significantly shorter doubling time compared to other

myxobacteria. Thus, *M. xanthus* has become an alternative host for production of polyketides, especially those from other myxobacterial pathways.

On the other hand, *P. putida* eventually provides similar characteristics to *M. xanthus* regarding its ability to heterologously produce secondary metabolites such as myxochromides,<sup>72,83</sup> flaviolin,<sup>71</sup> and PUFAs (Gemperlein, unpublished result). However, additional metabolic engineering in *P. putida* is sometimes necessary when the introduced biosynthetic pathways require certain precursor supply for their biosynthesis, for example methylmalonyl-CoA (mm-CoA) which is not naturally produced by *P. putida*. This was exemplified in the production of myxothiazol where an mm-CoA biosynthetic pathway from *S. cellulosum* So ce56 was introduced to *P. putida* prior to the introduction of myxothiazol gene cluster.<sup>89</sup> Another well-established system is *Streptomyces* expression system which also has been developed for production of myxobacterial polyketides. However, the yields can be low as shown in epothilone, which was attributed to a bacteriostatic effect of these compounds to the host.

After considering the above-mentioned factors, especially the fact that myxopyronin producer *M. fulvus* is closely related to *M. xanthus*, it was chosen as the first host to heterologously express myxopyronin gene cluster. The initial myxopyronin yield was very promising (5-10 mg/L, as also in native producer) and comparable, although not to all, to other myxobacterial pathways that have also been expressed in *M. xanthus* (see Table 2). In addition to all of the other factors, another important factor for successful heterologous expression is transcription of the foreign genes by the host's RNA polymerase (RNAP). Transcription is an essential cellular process which plays important role in controlling bacterial gene expression and depends on the efficient interaction of the RNAP with the respective promoter DNA. As the recognition specificity for promoters seems to correlate with the genomic GC content of a species, the heterologous host might not recognize the native promoters present in a specific biosynthetic gene cluster. If closely related heterologous hosts are chosen, retaining the native promoters will likely circumvent this problem as readily observed in myxopyronin and other myxobacterial compounds production. However, there are examples in which the native promoters were replaced by other promoters compatible with the respective host (e.g., *act* promoters<sup>68,90,91</sup>, *ermE* promoter<sup>92</sup> or with certain characteristics such as inducibility (thiostrepton-inducible *tipA* promoter for *Streptomyces*<sup>93</sup> and the toluic-acid inducible  $P_m$  promoter for *Pseudomonas* strains<sup>72</sup>). Inducible expression is usually required in gene clusters whose encoded metabolites may be toxic to the hosts. Promoter exchange has proved to be crucial in the heterologous expression of myxochromide. When the promoter and the host are exchanged from  $P_m$  to  $P_{aphII}$  and from

*P. putida* to *Coralloccoccus coralloides* GT-2, the yield significantly increases from 40 mg/L to 600 mg/L.<sup>94</sup> Moreover, promoter exchange from *P<sub>m</sub>* to *Tn5* and host exchange to *M. xanthus* even increase the yield to 1 g/L.<sup>83</sup> These results illustrated that the compatibility between a promoter and a heterologous host needs to be considered before introducing a certain promoter to the biosynthetic gene cluster.

Once the heterologous expression is achieved and stably maintained within the chosen heterologous host, further optimization of production can be achieved by classical strain improvement and improving growth conditions. The production of myxothiazol was increased from 20 mg/L to 60 mg/L through classical strain improvement and a careful bioprocess optimization enabling also production of epothilone up to 23 mg/L. Fermentation conditions are usually optimized by different media trials that can provide all the nutrients needed not only to ensure sufficient growth of the respective recombinant microorganism but also to enable the efficient biosynthesis of the expected natural product. In the current study, growth media improvement has resulted in the increase of myxopyronin production from 5 mg/L to 100 mg/L (in collaboration with Acies Bio, Slovenia). Further studies to improve the heterologous strain for example by random mutagenesis are currently on going. This improved productivity will open up many opportunities for further pathway engineering to generate novel myxopyronin analogues, e.g. via mutasynthesis which was not efficient in the natural producer strain. In summary, there is no exact formulation so far to guarantee successful heterologous expression of biosynthetic gene clusters. There are many factors that need to be considered such as the host, size of the gene cluster, integration method, promoter selection, growth optimization, and so forth. One of these factors might work perfectly for one case but it might not give the same effect for another case. Nevertheless, the heterologous expression technique is continuously being researched and developed, thus in the future there might be a better design to produce a good heterologous expression system.

## 6.6 Concluding Remarks and Future Directions

This thesis focused on the RNAP inhibitor myxopyronin produced by *M. fulvus* Mx f50. The genetically accessible bacterium *M. fulvus* Mx f50 has greatly facilitated the identification of myxopyronin gene cluster including clarification of several gene functions in myxopyronin biosynthesis. The knowledge obtained from this part of the study has then become the basis of *in vitro*, mutasynthesis, and heterologous expression studies. The significant improvement of the heterologous expression production yields achieved here is now intended to be employed to overcome the production issues in mutasynthesis experiments. Mutasynthesis and *in vitro* systems with their advantages and disadvantages offer various ways to generate

novel myxopyronin analogues. These approaches will hopefully lead to the successful production of biologically more active myxopyronin derivatives in the future. This project has contributed to establishing a platform to produce myxopyronin analogues, which could also be applied for engineering other anti-infectives from myxobacteria and other organisms.

Table 2. Myxobacterial compounds produced in heterologous hosts

Compound	Class	Producing organism	Size of cluster	Vector used	Strategy to ensure production (i.e., promoters, regulator, etc).	Host strain	Production medium (host)	Yield WT (Yield Host)	Ref. cluster/ Ref. het. exp.
Epothilone	PKS/ NRPS	<i>Sorangium cellulosum</i> SMP44	56 kb	SCP2* based plasmid (replicative) and pSET152 based plasmid (integrative)	<i>actI</i> promoter (in both plasmids)	<i>S. coelicolor</i> CH999	R2YE	20 mg/L (50-100 µg/L)	68/68
		<i>S. cellulosum</i> So ce90	56 kb	Cloning vectors (2x integrated by homologous recombination)	-	<i>M. xanthus</i>	CMM	(1-23 mg/L)	68/69,95
		<i>S. cellulosum</i> So ce90	56 kb	2x <i>E. coli</i> - <i>Streptomyces</i> shuttle vector	<i>pikAI</i> promoter (in both plasmids)	<i>S. venezuelae</i> DHS2001	R2YE	(0.1 µg/L EpoB) (0.4 µg/L EpoD)	68/96
		<i>S. cellulosum</i>	54 kb	pBR322 <i>ori</i> , RSF1030 <i>ori</i> , CloDF13 <i>ori</i>	P <sub>BAD</sub> promoter	<i>E. coli</i>	2xYT	(1 µg/L)	68/97
		<i>S. cellulosum</i> So ce90	58 kb	pUC <i>ori</i>	<i>Tn5</i> promoter	<i>M. xanthus</i> DK1622	CTT	(100 µg/L)	68/77
Soraphen A	PKS	<i>S. cellulosum</i> So ce26	67.5 kb	pTBK (integrative) pTBBH (integrative) pTUE (replicative)	<i>tipA</i> promoter, addition of precursor cinnamic acid enriched the titer	<i>Streptomyces lividans</i> ZX7	YEME	150-1000 mg/L (0.3 mg/L)	98/70
Flaviolin	PKS	<i>S. cellulosum</i> So ce56	1.1 kb	pJB861 (replicative)	P <sub>m</sub> promoter	<i>P. putida</i> KT2440	LB	- (6 mg/L)	71/71
						<i>P. syringae</i> pv. <i>tomato</i>		trace amount	71/71
Myxochromide S	PKS/	<i>Stigmatella</i>	30 kb	SuperCos 1 derivative	P <sub>m</sub> promoter	<i>P. putida</i>	LB	8 mg/L	99/72



	NRPS	<i>aurantiaca</i> DW4/3-1			<i>Tn5</i> promoter	KT2440		(40 mg/L)	
					<i>P<sub>aphII</sub></i> promoter	<i>P. putida</i> KT2440	LB	(0.1 mg/L)	99/83
					<i>Tn5</i> promoter	<i>C. macrosporus</i> GT-2	M medium based	(600 mg/L)	99/94
						<i>M. xanthus</i> DK1622	CTT	(1 g/L)	99/83
Myxothiazol	PKS/ NRPS	<i>S. aurantiaca</i> DW4/3-1	57 kb	p15A <i>ori</i>	<i>P<sub>m</sub></i> promoter	<i>M. xanthus</i> DZF1	CTT	10 mg/L (20-60 mg/L)	100/73
		<i>S. aurantiaca</i> DW4/3-1	57 kb	p15A <i>ori</i>	<i>P<sub>m</sub></i> promoter	<i>P. putida</i> FG2005	LB	10 mg/L (0.005-0.6 mg/L)	100/89
Pretubulyisin	PKS/ NRPS	<i>Cystobacter</i> sp. BCb004	40 kb	p15A <i>ori</i>	<i>P<sub>tet</sub></i> promoter	<i>P. putida</i>	LB	1-4 mg/L (1.76 µg/L)	101,102/74
						<i>M. xanthus</i> DK1622	CTT	(0.19 mg/L)	
Dawenol	PKS	<i>S. aurantiaca</i> DW4/3-1	21 kb	ColE1 <i>ori</i>	-	<i>M. xanthus</i> DK1622	CTT	N/A (0.05 mg/L)	75/75
PUFA DHA/EPA	PKS	<i>Aetherobacter</i> <i>rufus</i> SBSr002	16.2 kb	p15A <i>ori</i>	<i>Tn5</i> promoter	<i>M. xanthus</i> DK1622	CTT	Both native strains producing DHA and EPA	Gemperlein et.al. Unpublished results
	PKS	<i>Aetherobacter</i> sp. SBSr008	16.2 kb	p15A <i>ori</i>	<i>Tn5</i> promoter	<i>M. xanthus</i> DK1622	CTT	DHA: 3.8 mg/g (0.2 mg/g)*  EPA: 4.7-6.2 mg/g (0.8 mg/g)*	
Myxopyronin	PKS/ NRPS	<i>Myxococcus</i> <i>fulvus</i> Mx f50	53 kb	p15A <i>ori-tet<sup>R</sup></i>	<i>Tn5</i> promoter	<i>M. xanthus</i> DK1622ΔmchA ::tet	CTT  M7s/6a	5-10 mg/L  (5-100 mg/L)	19/ Sucipto, et.al. unpublished results

Het. Exp.: Heterologous expression; CMM: Citrate minimal medium; CTT: Casitone Tris medium LB: Lysogeny Broth; NRPS: Nonribosomal peptide synthetase; PKS: Polyketide synthase; WT: Wild type; \*: cell dry weight; p15 *ori*: a vector containing minimal backbone with p15 *ori* as origin or replication

## 6.7 References

1. Bode, H. B. & Müller, R. The impact of bacterial genomics on natural product research, *Angew. Chem. Int. Ed. Engl.* **44**, 6828–6846 (2005).
2. Zerikly, M. & Challis, G. L. Strategies for the discovery of new natural products by genome mining, *ChemBioChem* **10**, 625–632 (2009).
3. Wilkinson, B. & Micklefield, J. Mining and engineering natural-product biosynthetic pathways, *Nat. Chem. Biol.* **3**, 379–386 (2007).
4. Blin, K. *et al.* antiSMASH 2.0 - a versatile platform for genome mining of secondary metabolite producers, *Nucleic Acids Res.* **41**, W204-W212 (2013).
5. Starcevic, A. *et al.* ClustScan: an integrated program package for the semi-automatic annotation of modular biosynthetic gene clusters and in silico prediction of novel chemical structures. *Nucleic Acids Res.* **36** , 6882–6892 (2008).
6. Weber, T. *et al.* CLUSEAN: a computer-based framework for the automated analysis of bacterial secondary metabolite biosynthetic gene clusters, *J. Biotechnol.* **140**, 13–17 (2009).
7. Anand, S. *et al.* SBSPKS: structure based sequence analysis of polyketide synthases. *Nucleic Acids Res.* **38** , W487–W496 (2010).
8. Khaldi, N. *et al.* SMURF: Genomic mapping of fungal secondary metabolite clusters. *Fungal Genet. Biol.* **47**, 736–41 (2010).
9. Goldman, B. S. *et al.* Evolution of sensory complexity recorded in a myxobacterial genome, *P. Natl. Acad. Sci. USA* **103**, 15200–15205 (2006).
10. Huntley, S. *et al.* Comparative genomic analysis of fruiting body formation in myxococcales, *Mol. Biol. Evol.* **28**, 1083–1097 (2011).
11. Schneiker, S. *et al.* Complete genome sequence of the myxobacterium *Sorangium cellulosum*, *Nat. Biotechnol.* **25**, 1281–1289 (2007).
12. Ivanova, N. *et al.* Complete genome sequence of *Haliangium ochraceum* type strain (SMP-2(T)), *Standards in Genomic Sciences* **2**, 96–106 (2010).
13. Bode, H. B. & Müller, R. in *Myxobacteria: Multicellularity and differentiation*, edited by D. Whitworth (ASM Press, Chicago, 2007), pp. 259–282.
14. Meiser, P. *et al.* DKxanthene biosynthesis -- understanding the basis for diversity-oriented synthesis in myxobacterial secondary metabolism, *Chem. Biol.* **15**, 771–781 (2008).
15. Meiser, P. Bode, H. B. & Müller, R. The unique DKxanthene secondary metabolite family from the myxobacterium *Myxococcus xanthus* is required for developmental sporulation, *P. Natl. Acad. Sci. USA* **103**, 19128–19133 (2006).
16. Bode, H. B. *et al.* Mutasynthesis-derived myxalamids and origin of the isobutyryl-CoA starter unit of myxalamid B, *ChemBioChem* **8**, 2139–2144 (2007).
17. Schley, C., Altmeyer, M. O., Swart, R., Müller, R. & Huber, C. G. Proteome Analysis of *Myxococcus xanthus* by Off-Line Two-Dimensional Chromatographic Separation Using Monolithic Poly-(styrene-

- divinylbenzene) Columns Combined with Ion-Trap Tandem Mass Spectrometry. *J. Proteome Res.* **5**, 2760–2768 (2006).
18. Erol, Ö. *et al.* Biosynthesis of the myxobacterial antibiotic coralopyronin A, *ChemBioChem* **11**, 1235–1265 (2010).
  19. Sucipto, H. Wenzel, S. C. & Müller, R. Exploring chemical diversity of  $\alpha$ -pyrone antibiotics: molecular basis of myxopyronin biosynthesis, *ChemBioChem* **14**, 1581–1589 (2013).
  20. Piel, J. Biosynthesis of polyketides by trans-AT polyketide synthases, *Nat. Prod. Rep.* **27**, 996–1047 (2010).
  21. Tang, G. L. Cheng, Y. Q. & Shen, B. Leinamycin biosynthesis revealing unprecedented architectural complexity for a hybrid polyketide synthase and nonribosomal peptide synthetase, *Chem. Biol.* **11**, 33–45 (2004).
  22. El-Sayed, A. K. *et al.* Characterization of the mupirocin biosynthesis gene cluster from *Pseudomonas fluorescens* NCIMB 10586, *Chem. Biol.* **10**, 419–430 (2003).
  23. Calderone, C. T. Kowtoniuk, W. E. Kelleher, N. L. Walsh, C. T. & Dorrestein, P. C. Convergence of isoprene and polyketide biosynthetic machinery: isoprenyl-S-carrier proteins in the pksX pathway of *Bacillus subtilis*, *P. Natl. Acad. Sci. USA* **103**, 8977–8982 (2006).
  24. Simunovic, V. & Müller, R. 3-Hydroxy-3-methylglutaryl-CoA-like synthases direct the formation of methyl and ethyl side groups in the biosynthesis of the antibiotic myxovirescin A, *ChemBioChem* **8**, 497–500 (2007).
  25. Calderone, C. T. Isoprenoid-like alkylations in polyketide biosynthesis, *Nat. Prod. Rep.* **25**, 845–853 (2008).
  26. Wu, J. *et al.* Mupirocin H, a novel metabolite resulting from mutation of the HMG-CoA synthase analogue, mupH in *Pseudomonas fluorescens*, *Chem. Commun. (Camb.)*, 2040–2042 (2007).
  27. Sahnner, J. H. *et al.* Advanced mutasynthesis studies on the natural  $\alpha$ -pyrone antibiotic myxopyronin from *Myxococcus fulvus*, *ChemBioChem* **16**, 946–953 (2015).
  28. Liscombe, D. K. Louie, G. V. & Noel, J. P. Architectures, mechanisms and molecular evolution of natural product methyltransferases, *Nat. Prod. Rep.* **29**, 1238–1250 (2012).
  29. Rix, U. Fischer, C. Remsing, L. L. & Rohr, J. Modification of post-PKS tailoring steps through combinatorial biosynthesis, *Nat. Prod. Rep.* **19**, 542–580 (2002).
  30. Doundoulakis, T. *et al.* Myxopyronin B analogs as inhibitors of RNA polymerase, synthesis and biological evaluation, *Bioorg. Med. Chem. Lett.* **14**, 5667–5672 (2004).
  31. Kohl, W. Irschik, H. Reichenbach, H. & Höfle, G. Antibiotics from gliding bacteria. XXII. The biosynthesis of myxopyronin A, an antibiotic from *Myxococcus fulvus* strain Mx f50, *Liebigs Ann. Chem.* 1088–1093 (1984).
  32. Finn, R. D. *et al.* Pfam: the protein families database, *Nucleic Acids Res.* **42**, D222 (2014).
  33. Baere, I. de *et al.* Purification of porcine brain protein phosphatase 2A leucine carboxyl methyltransferase and cloning of the human homologue, *Biochemistry* **38**, 16539–16547 (1999).

34. Müller, I. & Müller, R. Biochemical characterization of MelJ and MelK - myxobacterial enzymes that transform an amide into a methyl ester, *FEBS J.* **273**, 3768–3778 (2006).
35. Schäberle, T. F. Mohseni, M. M. Lohr, F. Schmitz, A. & König, G. M. Function of the loading module in CorI and of the O-methyltransferase CorH in vinyl carbamate biosynthesis of the antibiotic coralopyronin A, *Antimicrob. Agents Chemother.* **58**, 950–956 (2014).
36. Musiol, E. M. *et al.* Supramolecular Templating in Kirromycin Biosynthesis: The Acyltransferase KirCII Loads Ethylmalonyl-CoA Extender onto a Specific ACP of the trans-AT PKS, *Chem. Biol.* **18**, 438–444 (2011).
37. Hitchman, T. S. Crosby, J. Byrom, K. J. Cox, R. J. & Simpson, T. J. Catalytic self-acylation of type II polyketide synthase acyl carrier proteins, *Chem. Biol.* **5**, 35–47 (1998).
38. Hertweck, C. The biosynthetic logic of polyketide diversity, *Angew. Chem. Int. Ed. Engl.* **48**, 4688–4716 (2009).
39. Lautru, S. & Challis, G. L. Substrate recognition by nonribosomal peptide synthetase multi-enzymes, *Microbiology* **150**, 1629–1636 (2004).
40. McGlacken, G. P. & Fairlamb, I. J. S. 2-Pyrone natural products and mimetics: isolation, characterisation and biological activity. *Nat. Prod. Rep.* **22**, 369–385 (2005).
41. Kalaitzis, J. A., Cheng, Q., Thomas, P. M., Kelleher, N. L. & Moore, B. S. In Vitro Biosynthesis of Unnatural Enterocin and Wailupemycin Polyketides. *J. Nat. Prod.* **72**, 469–472 (2009).
42. Seshime, Y., Juvvadi, P. R., Kitamoto, K., Ebizuka, Y. & Fujii, I. Identification of csypyrone B1 as the novel product of *Aspergillus oryzae* type III polyketide synthase CsyB. *Bioorg. Med. Chem.* **18**, 4542–4546 (2010).
43. Hashimoto, M. *et al.* *Aspergillus oryzae* CsyB Catalyzes the Condensation of Two  $\beta$ -Ketoacyl-CoAs to Form 3-Acetyl-4-hydroxy-6-alkyl- $\alpha$ -pyrone. *J. Biol. Chem.* **289**, 19976–19984 (2014).
44. Mori, T. *et al.* Structural Basis for the Formation of Acylalkylpyrones from Two  $\beta$ -Ketoacyl Units by the Fungal Type III Polyketide Synthase CsyB. *J. Biol. Chem.* **290**, 5214–5225 (2015).
45. Sucipto, H. *et al.* In Vitro reconstitution of  $\alpha$ -Pyrone ring formation in myxopyronin biosynthesis, *Chem. Sci.* **6**, 5076–5085 (2015).
46. Sehnal, D. *et al.* MOLE 2.0: advanced approach for analysis of biomacromolecular channels. *J. Cheminform.* **5**, 39 (2013)..
47. Wu, N. Cane, D. E. & Khosla, C. Quantitative analysis of the relative contributions of donor acyl carrier proteins, acceptor ketosynthases, and linker regions to intermodular transfer of intermediates in hybrid polyketide synthases, *Biochemistry* **41**, 5056–5066 (2002).
48. Meier, J. L. & Burkart, M. D. The chemical biology of modular biosynthetic enzymes, *Chem Soc.Rev.* **38**, 2012–2045 (2009).
49. Arthur, C. J. *et al.* Self-malonylation is an intrinsic property of a chemically synthesized type II polyketide synthase acyl carrier protein, *Biochemistry* **44**, 15414–15421 (2005).

50. Rentsch, A. & Kalesse, M. The total synthesis of corallopyronin A and myxopyronin B. *Angew. Chem. Int. Ed. Engl.* **51**, 11381–11384 (2012).
51. Sun, Y. H. *et al.* In vitro reconstruction of tetronate RK-682 biosynthesis, *Nat. Chem. Biol.* **6**, 99–101 (2010).
52. Kennedy, J. Mutasynthesis, chemobiosynthesis, and back to semi-synthesis: combining synthetic chemistry and biosynthetic engineering for diversifying natural products, *Nat. Prod. Rep.* **25**, 25–34 (2008).
53. Rinehart, K. L. Mutasynthesis of new antibiotics, *Pure Appl. Chem.* **49**, 1361–1384 (1977).
54. Kirschning, A. & Hahn, F. Merging chemical synthesis and biosynthesis: A new chapter in the total synthesis of natural products and natural product libraries, *Angew. Chem. Int. Ed. Engl.* **51**, 4012–4022 (2012).
55. Hafner, E. W. *et al.* Branched-chain fatty acid requirement for avermectin production by a mutant of *Streptomyces avermitilis* lacking branched-chain 2-oxo acid dehydrogenase activity, *J. Antibiot.* **44**, 349–356 (1991).
56. McArthur, H. A. I. A novel avermectin, doramectin—a successful application of mutasynthesis. In *Developments in industrial microbiology—BMP '97* (eds Hutchinson, C.R. & McAlpine, J.) 43–48 (Society for Industrial Microbiology, Fairfax, VA, 1998).
57. Dutton, C. J. *et al.* Novel avermectins produced by mutational biosynthesis, *J. Antibiot.* **44**, 357–365 (1991).
58. Cropp, T. A. *et al.* Recent Developments in the Production of Novel Polyketides by Combinatorial Biosynthesis. *Biotechnol. Genet. Eng. Rev.* **19**, 159–174 (2002).
59. Weissman, K. J. Mutasynthesis - uniting chemistry and genetics for drug discovery, *Trends Biotechnol.* **25**, 139–142 (2007).
60. Lira, R. *et al.* Syntheses of novel myxopyronin B analogs as potential inhibitors of bacterial RNA polymerase, *Bioorg. Med. Chem. Lett.* **17**, 6797–6800 (2007).
61. Mukhopadhyay, J. *et al.* The RNA polymerase "switch region" is a target of inhibitors, *Cell* **135**, 295–307 (2008).
62. Nguyen, T. *et al.* Exploiting the mosaic structure of trans-acyltransferase polyketide synthases for natural product discovery and pathway dissection, *Nat. Biotechnol.* **26**, 225–233 (2008).
63. Jenke-Kodama, H. Sandmann, A. Müller, R. & Dittmann, E. Evolutionary implications of bacterial polyketide synthases, *Mol. Biol. Evol.* **22**, 2027–2039 (2005).
64. Ginolhac, A. *et al.* Type I polyketide synthases may have evolved through horizontal gene transfer, *J. Mol. Evol.* **60**, 716–725 (2005).
65. Jenner, M. *et al.* Substrate Specificity in Ketosynthase Domains from trans-AT Polyketide Synthases, *Angew. Chem. Int. Ed. Engl.* **52**, 1143–1147 (2013).
66. Galm, U. Desso, M. A. Schmidt, J. Wessjohann, L. A. & Heide, L. In vitro and in vivo production of new aminocoumarins by a combined biochemical, genetic, and synthetic approach, *Chem. Biol.* **11**, 173–183 (2004).

67. Silakowski, B. Kunze, B. & Müller, R. Multiple hybrid polyketide synthase/non-ribosomal peptide synthetase gene clusters in the myxobacterium *Stigmatella aurantiaca*, *Gene* **275**, 233–240 (2001).
68. Tang, L. *et al.* Cloning and heterologous expression of the epothilone gene cluster, *Science* **287**, 640–642 (2000).
69. Julien, B. & Shah, S. Heterologous expression of epothilone biosynthetic genes in *Myxococcus xanthus*, *Antimicrob. Agents Chemother.* **46**, 2772–2778 (2002).
70. Zirkle, R. Ligon, J. M. & Molnar, I. Heterologous production of the antifungal polyketide antibiotic soraphen A of *Sorangium cellulosum* So ce26 in *Streptomyces lividans*, *Microbiology* **150**, 2761–2774 (2004).
71. Gross, F. *et al.* Bacterial type III polyketide synthases: Phylogenetic analysis and potential for the production of novel secondary metabolites by heterologous expression in pseudomonads, *Arch. Microbiol.* **185**, 28–38 (2006).
72. Wenzel, S. C. *et al.* Heterologous expression of a myxobacterial natural products assembly line in pseudomonads via red/ET recombineering, *Chem. Biol.* **12**, 349–356 (2005).
73. Perlova, O. *et al.* Reconstitution of myxothiazol biosynthetic gene cluster by Red/ET recombination and heterologous expression in *Myxococcus xanthus*, *Appl. Environ. Microbiol.* **72**, 7485–7494 (2006).
74. Chai, Y. *et al.* Heterologous expression and genetic engineering of the tubulysin biosynthetic gene cluster using Red/ET recombineering and inactivation mutagenesis, *Chem. Biol.* **19**, 361–371 (2012).
75. Oßwald, C. *et al.* A highly unusual polyketide synthase directs dawenol polyene biosynthesis in *Stigmatella aurantiaca*. *J. Biotechnol.* **191**, 54–63 (2014).
76. Gemperlein, K., Rachid, S., Garcia, R. O., Wenzel, S. C. & Muller, R. Polyunsaturated fatty acid biosynthesis in myxobacteria: different PUFA synthases and their product diversity. *Chem. Sci.* **5**, 1733–1741 (2014).
77. Oßwald, C. *et al.* Modular Construction of a Functional Artificial Epothilone Polyketide Pathway. *ACS Synth. Biol.* **3**, 759–772 (2014).
78. Ongley, S. Bian, X. Neilan, B. A. & Müller, R. Recent advances in the heterologous expression of microbial natural product biosynthetic pathways, *Nat. Prod. Rep.* **30**, 1121–1138 (2013).
79. Groth, A. C. & Calos, M. P. Phage integrases: Biology and applications. *J. Mol. Biol.* **335**, 667–678 (2004).
80. Magrini, V. Creighton, C. & Youderian, P. Site-specific recombination of temperate *Myxococcus xanthus* phage Mx8: Genetic elements required for integration, *J. Bacteriol.* **181**, 4050–4061 (1999).
81. Julien, B. Characterization of the integrase gene and attachment site for the *Myxococcus xanthus* bacteriophage Mx9, *J. Bacteriol.* **185**, 6325–6330 (2003).
82. Fujitani, Y., Yamamoto, K. & Kobayashi, I. Dependence of frequency of homologous recombination on the homology length. *Genet.* **140**, 797–809 (1995).
83. Fu, J. *et al.* Efficient transfer of two large secondary metabolite pathway gene clusters into heterologous hosts by transposition, *Nucleic Acids Res.* **36**, e113 (2008).

84. Hayes, F. Transposon-based strategies for microbial functional genomics and proteomics. *Annu. Rev. Genet.* **37**, 3–29 (2003).
85. Reznikoff, W. S. & Winterberg, K. M. Transposon-based strategies for the identification of essential bacterial genes. *Methods Mol. Biol.* **416**, 13–26 (2008).
86. Volz, C. Kegler, C. & Müller, R. Enhancer binding proteins act as hetero-oligomers and link secondary metabolite production to myxococcal development, motility and predation, *Chem. Biol.* **19**, 1447–1459 (2012).
87. Reichenbach, H. in *Myxobacteria II*, edited by M. Dworkin & D. Kaiser (ASM Press, Washington, D.C. 1993), pp. 13–62.
88. Ueki, T. Inouye, S. & Inouye, M. Positive-negative KG cassettes for construction of multi-gene deletions using a single drug marker, *Gene* **183**, 153–157 (1996).
89. Gross, F. *et al.* Metabolic engineering of *Pseudomonas putida* for methylmalonyl-CoA biosynthesis to enable complex heterologous secondary metabolite formation, *Chem. Biol.* **13**, 1253–1264 (2006).
90. Xue, Q. Ashley, G. Hutchinson, C. R. & Santi, D. V. A multiplasmid approach to preparing large libraries of polyketides, *P. Natl. Acad. Sci. USA* **96**, 11740–11745 (1999).
91. Wohlert, S. *et al.* Insights about the biosynthesis of the avermectin deoxysugar L-oleandrose through heterologous expression of *Streptomyces avermitilis* deoxysugar genes in *Streptomyces lividans*, *Chem. Biol.* **8**, 681–700 (2001).
92. Sanchez, C. *et al.* The biosynthetic gene cluster for the antitumor rebeccamycin: Characterization and generation of indolocarbazole derivatives, *Chem. Biol.* **9**, 519–531 (2002).
93. Otsuka, M. Ichinose, K. Fujii, I. & Ebizuka, Y. Cloning, sequencing, and functional analysis of an iterative type I polyketide synthase gene cluster for biosynthesis of the antitumor chlorinated polyenone neocarzinil in "*Streptomyces carzinostaticus*", *Antimicrob. Agents Chemother.* **48**, 3468–3476 (2004).
94. Perlova, O. Gerth, K. Kuhlmann, S. Zhang, Y. & Müller, R. Novel expression hosts for complex secondary metabolite megasynthetases: Production of myxochromide in the thermophilic isolate *Corallocccus macrosporus* GT-2, *Microbial Cell Factories* **8** (2009).
95. Lau, J. *et al.* Optimizing the heterologous production of epothilone D in *Myxococcus xanthus*, *Biotechnol. Bioeng* **78**, 280–288 (2002).
96. Park, S. R. *et al.* Heterologous production of epothilones B and D in *Streptomyces venezuelae*, *Appl. Microbiol. Biotechnol.* **81**, 109–117 (2008).
97. Mutka, S. C. Carney, J. R. Liu, Y. & Kennedy, J. Heterologous production of epothilone C and D in *Escherichia coli*, *Biochemistry* **45**, 1321–1330 (2006).
98. Ligon, J. *et al.* Characterization of the biosynthetic gene cluster for the antifungal polyketide soraphen A from *Sorangium cellulosum* So ce26, *Gene* **285**, 257–267 (2002).
99. Wenzel, S. C. *et al.* Structure and biosynthesis of myxochromides S1-3 in *Stigmatella aurantiaca*: evidence for an iterative bacterial type I polyketide synthase and for module skipping in nonribosomal peptide biosynthesis, *ChemBioChem* **6**, 375–385 (2005).

100. Silakowski, B. *et al.* New lessons for combinatorial biosynthesis from myxobacteria: the myxothiazol biosynthetic gene cluster of *Stigmatella aurantiaca* DW4/3-1, *J. Biol. Chem.* **274**, 37391–37399 (1999).
101. Sandmann, A. Sasse, F. & Müller, R. Identification and analysis of the core biosynthetic machinery of tubulysin, a potent cytotoxin with potential anticancer activity, *Chem. Biol.* **11**, 1071–1079 (2004).
102. Chai, Y. *et al.* Discovery of 23 natural tubulysins from *Angiococcus disciformis* An d48 and *Cystobacter* SBCb004, *Chem. Biol.* **17**, 296–309 (2010).